Design of FRP and Steel Plated RC Structures

Retrofitting Beams and Slabs for Strength, Stiffness and Ductility

Deric John Oehlers and Rudolf Seracino

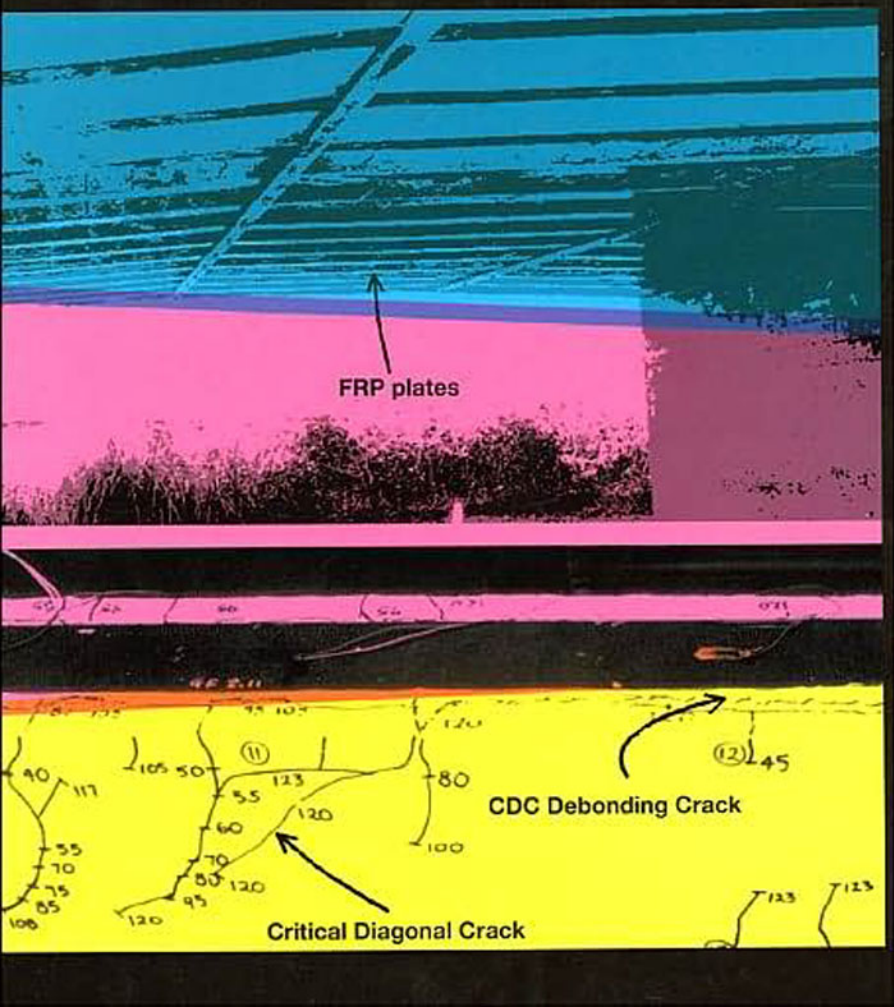

Design of FRP and Steel Plated RC Structures

Retrofitting Beams and Slabs for Strength, Stiffness and Ductility

Elsevier Internet Homepage - http://www.elsevier.com
Consult the Elsevier homepage for full catalogue information on all books, journals and electronic products and services.

Elsevier Titles of Related Interest

ANSON *et al.*
Advances in Building Technology (ABT2002)
ISBN: 008 044100 9

CHAN *et al.*
Advances in Steel Structures (ICASS '02)
ISBN: 008 044017 7

FRANGOPOL *et al.*
Reliability and Optimization of Structural Systems
ISBN: 008 042826 6

HOLLAWAY & HEAD
Advanced Polymer Composites and Polymers in the Civil Infrastructure
ISBN: 008 043661 7

OEHLERS & BRADFORD
Composite Steel and Concrete Structural Members
ISBN: 008 041919 4

TENG
FRP Composites in Civil Engineering
ISBN: 008 043945 4

WANG *et al.*
Shear Deformable Beams and Plates
ISBN: 008 043784 2

Related Journals/Products
Free specimen copy gladly sent on request. Elsevier Ltd, The Boulevard, Langford Lane, Kidlington, Oxford, OX5 1GB,UK

CAD
Composites Part A: Applied Science and Manufacturing
Composites Part B: Engineering
Composite Structures
Computer Methods in Applied Mechanics and Engineering
Computers and Structures
Construction and Building Materials
Engineering Failure Analysis
Engineering Structures
International Journal of Solids and Structures
Journal of Constructional Steel Research
Mechanics of Materials

To Contact the Publisher
Elsevier welcomes enquiries concerning publishing proposals: books, journal special issues, conference proceedings, etc. All formats and media can be considered. Should you have a publishing proposal you wish to discuss, please contact, without obligation, the publisher responsible for Elsevier's civil and structural engineering programme:

Keith Lambert
Materials Science and Engineering
Elsevier Ltd
The Boulevard, Langford Lane
Kidlington, Oxford
OX5 1GB, UK

Phone: +44 1865 843411
Fax: +44 1865 843920
E-mail: k.lambert@elsevier.com

General enquiries, including placing orders, should be directed to Elsevier's Regional Sales Offices – please access the Elsevier homepage for full contact details (homepage details at the top of this page).

Design of FRP and Steel Plated RC Structures

Retrofitting Beams and Slabs for Strength, Stiffness and Ductility

by

DERIC JOHN OEHLERS and RUDOLF SERACINO

School of Civil and Environmental Engineering,
The University of Adelaide, Australia

ELSEVIER

2004

Amsterdam - Boston - Heidelberg - London - New York - Oxford - Paris
San Diego - San Francisco - Singapore - Sydney - Tokyo

ELSEVIER B.V.
Sara Burgerhartstraat 25
P.O. Box 211, 1000 AE
Amsterdam, The Netherlands

ELSEVIER Inc.
525 B Street
Suite 1900, San Diego
CA 92101-4495, USA

ELSEVIER Ltd.
The Boulevard
Langford Lane, Kidlington,
Oxford OX5 1GB, UK

ELSEVIER Ltd.
84 Theobalds Road
London WC1X 8RR
UK

First edition 2004

Library of Congress Cataloging in Publication Data
A catalog record is available from the Library of Congress.

British Library Cataloguing in Publication Data
A catalogue record is available from the British Library.

ISBN: 0-08-044548-9

♾ The paper used in this publication meets the requirements of ANSI/NISO Z39.48-1992 (Permanence of Paper).
Printed in The Netherlands.

Preface

Retrofitting is a major growth area in civil engineering simply because the infrastructure is forever expanding and aging and more of the available resources are being used to maintain it. Hence, it is imperative to develop inexpensive and efficient retrofitting techniques, and tests have shown that bonding longitudinal plates to the surfaces of reinforced concrete structures can be economical, efficient and unobtrusive. However, these tests have also shown that the plates can debond prematurely so that much high quality research has been done around the world on identifying and quantifying these debonding mechanics. It may be worth noting that because plated structures exhibit unique forms of failure, they should be treated as a new form of structure.

This book covers all forms of longitudinal plating reinforced concrete beams and slabs. The plates can be either adhesively bonded or bolted, they can be flat plates or of any shape and size and they can be made from any material such as steel, aluminium or any type of fibre reinforced polymer (FRP). Furthermore, the issues of premature failure and the ultimate strength and ductility which includes moment redistribution are fully addressed. The aim of this book is to provide engineers with a deep understanding of the fundamental behaviour of externally plated structures and, in particular, to provide the design tools so that they can develop their own forms of this retrofitting technique or to develop safe and efficient forms for their specific structural problem.

Chapter 1 describes the numerous forms of longitudinal plating that can be applied, and in particular the unique failure mechanisms associated with all plate materials that have to be designed against and how this affects the choice of plate and form of bonding. Intermediate crack (IC) debonding of adhesively bonded plates is the dominant form of debonding as it directly affects the choice of plate, directly affects the flexural capacity and ductility of the beam and indirectly affects the shear capacity. Hence, it is the starting point of the design procedure and is covered in Chapter 2. Having quantified the IC debonding resistance, it is used in Chapter 3 to quantify both the flexural strength and ductility of adhesively plated beams and slabs. The analysis for the flexural capacity of bolted plated beams is also covered in this chapter as well as the ability to redistribute moment. IC debonding may be considered the dominant form of debonding, but an analysis of published test results has shown that it is not the most common form of debonding which is that due to the formation of critical diagonal cracks (CDC). CDC debonding is covered in both Chapters 4 and 5 where it is shown that the addition of longitudinal plates can substantially increase the shear capacity of beams or slabs without stirrups. However, it is also shown how CDC debonding may prevent the use of adhesively bonded plates in some regions of a beam. In which case bolted plates may have to be used as this is a ductile form of retrofitting that is not affected by the formation of CDCs. The final major debonding mode, that of plate end (PE) debonding, is covered in Chapter 6. This form of debonding rarely controls or limits the design as it can be easily prevented by terminating the plate in regions of low moment. However, it does allow the designer to determine the minimum length of plate required and hence optimise the cost. Finally, comprehensive and detailed design examples are given in Chapter 7 covering virtually all forms of longitudinal plating beams and slabs. Of interest, it is shown how combinations of plating techniques often provide the best solutions, can provide

substantial increases in strength, and how moment redistribution can substantially affect the choice of plating.

It is not the object of this book to prescribe one form of plating or plating material as it is felt that this approach limits the use of plating. For example, the calculations in Chapter 7 clearly show that if the designer is restricted to using adhesively bonded FRP plates then this can severely limit the increase in strength. Whereas, combining adhesively bonded FRP plates with adhesively bonded steel plates or with bolted FRP plates can allow large increases in strength and in turn a much larger use of FRP plates. The authors feel that adhesive bonding FRP plates should typically be the first choice because of its durability and ease of application. However, adhesively bonding FRP whilst having many benefits also has some limitations. For example metal plates can be designed to yield prior to debonding which is not an option available for FRP material which is an elastic brittle material. Hence, FRP plates may have to be restricted to regions of continuous beams where moment redistribution does not occur whilst metal plates can be used in regions where moment redistribution is required. As another example, it may be determined by calculations that it is not be possible to adhesively bond plates in negative moment regions of continuous beams where the vertical shear is large and hence where stirrups are required. In which case, metal or FRP plates can be bolted in these negative regions and used in conjunction with adhesively bonded FRP plates in the positive moment regions where the vertical shear is lower. It can now be seen why the object of this book is to provide generic design rules that cover all forms of longitudinal plating so that designers can choose and develop their own unique plating systems.

This book is not meant to be a code or standard; nor has it attempted to summarise the research on plating which has already been done in numerous papers and books; nor has it covered the design of the plate material as it is assumed that the plates are supplied by the manufacturers with guarantees such as against delamination within the FRP plate and durability. Instead, this book is meant to be a design guide that covers all of the major aspects of the mechanical design of plated beams and slabs. It covers the fundamental principles that govern: the major aspects of plate debonding; the shear capacity and flexural capacity of plated beams; and moment redistribution in plated beams. Furthermore, these fundamental principles are described in a form that can be applied to plates of any material, shape or position and have been described in a way that can be applied to new forms of plating such as near surface mounted plates. Near surface mounted plates have the potential to rapidly expand the use of plating due to their large strain capacities which not only provide a more efficient use of the material but more importantly provide much greater ductility. In order to try and cover all of the major aspects of design, we have had to introduce research concepts that are relatively new and in their early stages of development; in particular moment redistribution where we felt that ductility, which is often considered by structural engineers to be as important as strength and often more important, had to be covered from the fundamental principles. Having described the overall governing fundamental principles, we have developed design approaches based on advanced work on IC debonding published by others. However, we have used our own research on PE and CDC debonding as these are generic rules as they can be applied to any plate material, plate shape and plate position.

The first author has been studying plating since the mid eighties during which time he has had the privilege and enjoyment of working with and supervising some outstanding researchers, in particular Dr. M.S. Mohamed Ali Sahib and Dr. Ninh T. Nguyen whose contribution to the fundamental understanding of this field of research

has allowed this book to be written. We would also like to acknowledge with thanks the facilities made available at our University of Adelaide for the writing of this book and the invaluable support provided by Professor Kitipornchai at Hong Kong City University where the first author wrote his portion of the book whilst on study leave. Thanks also to Professor Jin-Guang Teng at Hong Kong Polytechnic University for his close collaboration and providing information and photographs, and above all and in particular the support and encouragement by our wives Bernie and Joanne.

This page is intentionally left blank

Notation

The following notation is used in this book and is first defined where first used in the text. Hence, although in general only one meaning is assigned to each symbol, in cases where more than one meaning is given then the correct one will be evident from the context in which it is used.

A_{int} = surface area of plate/concrete interface
A_p = cross-sectional area of plate
A_{rect} = area of a rectangular section of plate
$(A_{rect})_{sp}$ = A_{rect} of side plate
$(A_{rect})_{tfp}$ = A_{rect} of tension face plate
A_s = cross-sectional area of reinforcing bar; cross-sectional area of all the longitudinal reinforcing bars crossing the CDC
A_{sc} = cross-sectional area of the compression reinforcing bars
A_{st} = cross-sectional area of tension reinforcing bars
AUST = Australian
BRIT = British
$(b_{bnd})_{ang}$ = width of the bonded region in an angle bonded to the tension face
b_c = width of concrete element; effective width of concrete element; width of RC beam; width of slab; width of web of RC beam
b_p = width of plate
b_{sp} = width of side plate
b_{tfp} = width of tension face plate
CDC = critical diagonal crack
CDC_{plated} = CDC in plated beam
$CDC_{unplated}$ = CDC in unplated beam
CFRP = carbon fibre reinforced polymer
c = distance from tension reinforcing bars to tension face; reinforcing bar cover
d = effective depth of RC beam measured from compression face
d_{ang} = distance between angle centroid and neutral axis of cracked plated section
de = depth of the position of the maximum strain in plate from the compression face
d_{na} = depth to neutral axis from compression face
d_p = distance of individual plate centroid from the neutral axis of the composite plated beam
d_{ps} = perpendicular distance of prestressing tendon from focal point; lever arm of prestressing force from the compression face
d_{sp} = distance of side plate centroid from neutral axis of plated beam
d_{tfp} = distance of tension face plate centroid from neutral axis of plated beam
d_{ufp} = distance of underside plate centroid from neutral axis of plated beam
d_y = depth of the pseudo plastic concrete zone
E = Young's modulus; material stiffness
E_a = Young's modulus of adhesive
E_{al} = Young's modulus of aluminium
E_{CFRP} = Young's modulus of carbon FRP plate
E_c = Young's modulus of concrete
$(E_c)_{long}$ = long term Young's modulus of concrete
$(E_c)_{short}$ = short term Young's modulus of concrete
E_{GFRP} = Young's modulus of glass FRP plate

E_p = Young's modulus of plate
E_s = Young's modulus of steel
$(EA)_p$ = axial rigidity of plate
EI = flexural rigidity of a beam
$EI_{constant}$ = results when flexural rigidity is assumed constant along beam
EI_{cr} = flexural rigidity of cracked section
$(EI)_{cr.pl}$ = flexural rigidity of cracked plated section
EI_{crack} = results allowing for variations of elastic flexural rigidities EI_{scr} and EI_{hcr}
$(EI_{cracked})_{long}$ = long term cracked flexural rigidity of unplated section
$(EI_{cracked})_{short}$ = short term cracked flexural rigidity of unplated section
$(EI)_{creep}$ = long term flexural rigidity of cracked plated section
EI_h = flexural rigidity of hogging region
EI_{hcr} = flexural rigidity of elastic cracked plated section in hogging region
EI_{hdeb} = flexural rigidity of hogging region at plate debonding
$(EI)_{hog}$ = flexural rigidity of hogging region
$(EI)_{min}$ = minimum secant flexural rigidity
$(EI)_p$ = flexural rigidity of plate
EI_s = flexural rigidity of sagging region
$(EI)_{sag}$ = flexural rigidity of sagging region
EI_{scr} = flexural rigidity of elastic cracked sagging region; flexural rigidity of cracked plated section in sagging region
EI_{sdeb} = flexural rigidity of sagging region at plate debonding
$(EI)_{short}$ = short term flexural rigidity of cracked plated section
EI_{sit} = flexural rigidity in sagging region for iterative analysis
$EI_{\varepsilon p}$ = flexural rigidity at plate strain ε_p
$EI_{\varepsilon c}$ = flexural rigidity at concrete crushing
EUR = European
e = distance of $(W_{dat})_{cr}$ from focal point
F = force; resultant force
F_c = axial force in concrete element
F_n = resultant force normal to plate in tensile or compressive zone
F_p = axial tensile force in plate element
$(F_{plate})_{cr}$ = force in plate resisting formation of diagonal crack
F_{ps} = prestressing force
F_s = axial force in steel reinforcing bars
$(F_{sp})_{cr}$ = force in side plate resisting formation of diagonal crack
F_t = total axial tensile force
$(F_{tfp})_{cr}$ = force in tension face plate resisting formation of diagonal crack
FRP = fibre reinforced polymer
f_c = concrete compressive cylinder strength
f_{cb} = Brazilian tensile strength of concrete; split tensile strength of concrete; $0.53\sqrt{f_c}$
f_{CFRP} = carbon FRP fracture stress
f_{FRP} = FRP fracture stress
f_{GFRP} = glass FRP fracture stress
f_s = serviceability plate stress
f_t = tensile strength of concrete; $0.4\sqrt{f_c}$
f_{tef} = effective tensile strength of concrete in CDC analysis
f_y = metal yield stress; yield strength of reinforcing bars
f_{yp} = yield strength of metal plate

GFRP = glass fibre reinforced polymer
HK = Hong Kong
h = depth of beam
$(h_{bnd})_{ang}$ = depth of portion of angle web adhesively bonded to the beam side
$(h_{bnd})_{sp}$ = depth of bonded side plate
I = second moment of area about centroid
I_{ang} = second moment of area of angle about angle centroid and about axis parallel to bending axis
$(I_{cracked})_{long}$ = long term second moment of area of unplated cracked section transformed to concrete
$(I_{cracked})_{short}$ = short term second moment of area of unplated cracked section transformed to concrete
$I_{cr.pl}$ = second moment or area of cracked plated section
I_p = second moment of area of plate about centroid
IC = intermediate crack
K = coefficient in PE debonding equations
K_M = parameter of stress resultants at datum point in CDC analysis; moment factor M_{dat}/V_{dat}
K_W = parameter for applied loads in CDC analysis; load factor W_{dat}/V_{dat}
$(K_W)_{sag})_{udl}$ = K_W for sagging region in encastre beam with uniformly distributed load with datum at point of contraflexure
$(K_W)_{hog})_{udl}$ = K_W for hogging region in encastre beam with uniformly distributed load with datum at point of contraflexure
k_u = neutral axis depth factor; d_{na}/d
L = beam span; length of hogging or sagging region; lever arm
L_{anch} = length of plate required for anchorage approach
L_{CDC} = length of plate required from CDC analysis
L_e = effective length; minimum length of plate required for full anchorage; minimum anchorage length l_p to achieve maximum debonding axial force $(P_{IC})_{max}$; full anchorage length
L_{flex} = length of plate required for flexure
L_h = length of hogging region
L_{hinge} = hinge length
L_{hog} = length of hogging region
L_o = length of shear span in CDC analysis; length of free body in CDC analysis
L_p = anchorage length of plate from CDC
L_{pl} = length of plate per half span
$(L_p)_{tfp}$ = anchorage length of tension face plate
L_{PE} = length of plate required for PE debonding analysis
L_{poc} = distance of point of contraflexure from nearest support
L_{rect} = lever arm from the centroid of the rectangular section to the compression face
$(L_{rect})_{sp}$ = L_{rect} side plate
$(L_{rect})_{tfp}$ = L_{rect} tension face plate
L_s = length of sagging region
L_{sag} = length of sagging region
$L_{sh\text{-}sp}$ = length of plate in shear span
l_b = bonded length of plate
M = moment
M_{beam} = constant moment in beam
M_{cap} = moment capacity; maximum moment that can be obtained

$(M_{cap})_{fi}$ = moment capacity from a full interaction analysis
$(M_{cap})_{pi}$ = moment capacity allowing for partial interaction
M_{creep} = moment due to long term loads and sustained live loads that induce creep
M_{dat} = moment at datum point
$(M_{dat})_{applied}$ = applied moment at datum point
$(M_{dat})_{cr}$ = moment at datum point when a diagonal crack forms and when $(V_{dat})_{cr}$ is acting
$(M_{dat})_{h}$ = moment at datum point in the hogging region
$(M_{dat})_{hog}$ = moment at datum point in the hogging region
$(M_{dat})_{s}$ = moment at datum point in the sagging region
$(M_{dat})_{sag}$ = moment at datum point in the sagging region
$M_{elastic}$ = elastic moment based on constant EI
M_{h} = hogging moment; maximum hogging moment; hogging moment at the support
$(M_{h})_{EIcracked}$ = hogging moment based on a beam with varying elastic EI of EI_{scr} and EI_{hcr}
$(M_{h})_{el}$ = elastic hogging moment
$(M_{h})_{test}$ = hogging moment in test
$(M_{h})_{pl}$ = hogging moment capacity of plated section
$(M_{h})_{u}$ = ultimate strength of hogging section; ultimate strength of unplated hogging section
M_{hu} = ultimate strength of hogging section; ultimate strength of plated hogging section
$(M_{h})_{un}$ = maximum hogging moment capacity of unplated section
$(M_{h})_{u\text{-}max}$ = maximum possible hogging moment based on moment redistribution
$(M_{h})_{u\text{-}plated}$ = moment capacity of plated hogging section
M_{hog} = moment at supports; maximum hogging moment
$(M_{hog})_{res}$ = support moment to cause residual strains
$(M_{hog})_{u}$ = hogging moment capacity
M_{max} = maximum applied moment in beam
M_{p} = moment in plate
M_{PE} = PE debonding capacity
$(M_{PE})_{ang.sp}$ = PE debonding capacity for angle plate beam bonded to the side face of the beam
$(M_{PE})_{ang.tfp}$ = PE debonding capacity for angle plate beam bonded to the tension face of the beam
$(M_{PE})_{cfp}$ = PE debonding capacity for compression face plates
$(M_{PE})_{sp}$ = PE debonding capacity for a side plate beam
$(M_{PE})_{tfp}$ = PE debonding capacity for a tension face plated beam
$(M_{PE})_{ufp}$ = PE debonding capacity for underside of flange plates
M_{plate} = moment in plate
M_{s} = sagging moment; maximum sagging moment
$(M_{s})_{el}$ = elastic sagging moment
$(M_{s})_{pl}$ = sagging moment capacity of plated section
M_{sag} = moment at mid-span; maximum sagging moment
$(M_{sag})_{u}$ = sagging moment capacity
M_{short} = moment at plate end due to short term loads; moment due to short term loads
M_{static} = static moment
$(M_{static})_{plated}$ = static moment capacity of plated beam
$(M_{static})_{res}$ = static moment to cause residual strains

$(M_{static})_u$ = theoretical maximum static moment when hogging and sagging sectional capacities achieved
$(M_{static})_{unplated}$ = static moment capacity of unplated beam
$(M_{st})_{pl}$ = static moment capacity of plated beam
$(M_{st})_{un}$ = static moment capacity of unplated beam
$(M_s)_{test}$ = sagging moment in test
M_{su} = ultimate strength of sagging section; ultimate strength of unplated sagging section
$(M_s)_{un}$ = maximum sagging moment capacity of unplated section
$(M_s)_{u\text{-}max}$ = maximum possible sagging moment based on moment redistribution
$(M_s)_{u\text{-}plated}$ = moment capacity of plated sagging section
$(M_s)_{un}$ = sectional strength of unplated sagging region
M_{sp} = moment in side plate
$(M_s)_{pl}$ = moment capacity of plated section in sagging region
M_{tfp} = moment in tension face plate
M_u = ultimate moment capacity
$(M_u)_{pl}$ = flexural capacity of plated section
M_x = variation of applied moment along length of beam
ΔM = percentage increase in moment capacity due to plating
ΔM_{cap} = increase in flexural capacity due to plating
ΔM_{st} = increase in static moment due to plating
m_{long} = long term modular ratio E_s/E_c
m_p = modular ration of the plate material stiffness to that of the concrete; E_p/E_c
m_s = modular ratio E_s/E_c
m_{short} = short term modular ratio E_s/E_c
%MR = percentage moment redistribution
N_{long} = number of bolts in a shear span to resist P_{plate}
N_{vert} = number of bolts in a shear span to resist the vertical forces induced by M_{plate}
$(n_{crack})_{long}$ = long term elastic neutral axis depth of unplated cracked section
$(n_{crack})_{short}$ = short term elastic neutral axis depth of unplated cracked section
P = applied load
P_{bar} = tensile axial force in reinforcing bar
P_{dowel} = shear transferred by dowel action
P_{IC} = IC debonding resistance of plate; IC debonding force; $A_p\sigma_{IC}$
$(P_{IC})_{max}$ = maximum IC debonding resistance of fully anchored plate
$P_{IC\text{-}tooth}$ = contribution to plate force from an individual concrete tooth
P_{inter} = compressive force across crack interface; passive normal force; passive compressive interface force
P_p = axial force in plate
$(P_p)_{max}$ = maximum IC debonding resistance
P_{plate} = axial force in plate in a beam to cause IC debonding; axial force in plate; maximum force in plate in CDC analysis
$(P_{plate})_{cfp}$ = axial force in compression face plate
$(P_{plate})_{sp}$ = axial force in side plate
$(P_{plate})_{tfp}$ = axial force in tension face plate
$P_{pull\text{-}test}$ = IC debonding resistance measured from a pull-push test
P_{sh} = shear capacity of a single bolt in a bolted plated joint
P_{sp} = axial force in side plate
$P_{stirrup}$ = axial force in internal steel stirrup
P_{tfp} = axial force in tension face plate

P_u = fracture capacity of FRP plate; $A_p f_{FRP}$
P_y = yield capacity of metal plate; $A_p f_{yp}$
PE = plate end
RC = reinforced concrete
t_a = thickness of adhesive layer
t_{cfp} = thickness of compression face plate
t_p = plate thickness
t_{sp} = side plate thickness
t_{tfp} = tension face plate thickness
$(t_{tfp})_{ang}$ = plate thickness of angle flange attached to tension face
t_{ufp} = thickness of plate at underside of flange
udl = uniformly distributed load
V = vertical shear force
$V_{applied}$ = applied shear load
VAy/Ib = elastic interface shear stress; VQ/It
V_c = shear capacity of unplated beam or slab without stirrups; concrete component of the shear capacity
$(V_c)_{code}$ = concrete component of the shear capacity of unplated beams from national standards
V_{conc} = resistance to shear across diagonal crack
$(V_{conc})_{code}$ = resistance to shear across critical diagonal crack in a plated beam based on code concrete shear resistance
$(V_{conc})_{pl}$ = shear capacity at the weakest or critical diagonal crack in a plated beam
$(V_{conc})_{sp}$ = shear capacity of side plated beam
$(V_{conc})_{tfp}$ = shear capacity of tension face plated beam
$(V_{conc})_{un}$ = shear capacity at the weakest or critical diagonal crack in an unplated beam; concrete component of the shear capacity V_c
$V_{c\text{-}plate}$ = shear capacity of plated beam or slab without stirrups; V_c enhanced by plating; shear load to cause CDC debonding
V_{cr} = shear load to cause cracking
$V_{c\text{-}unpl}$ = concrete shear capacity of unplated beam
V_{dat} = shear load at any convenient datum point
$(V_{dat})_{applied}$ = design applied shear load at datum point; shear at datum point due to applied loads
$(V_{dat})_c$ = shear load at datum point to cause shear failure in a beam without stirrups; shear load at datum point to cause the critical diagonal crack
$(V_{dat})_{c\text{-}mean}$ = shear load at datum point to cause the critical diagonal crack in an unplated beam based on mean approach
$(V_{dat})_{c\text{-}plate}$ = shear load at datum point to cause shear failure in a plated beam without stirrups; shear load at datum point to cause CDC debonding
$((V_{dat})_{c\text{-}plate})_{full}$ = shear load at datum point to cause shear failure in a fully plated beam without stirrups; shear load at datum point to cause CDC debonding in a fully plated anchored beam
$(V_{dat})_{c\text{-}plate\text{-}mean}$ = shear load at datum point to cause the critical diagonal crack in a plated beam based on mean approach
$(V_{dat})_{c\text{-}unpl}$ = shear load at datum point to cause shear failure in an unplated beam
$(V_{dat})_{cr}$ = vertical shear load at datum point when diagonal crack forms; shear at datum point to cause cracking in unplated beam
$(V_{dat})_{crack}$ = shear load at the datum point to cause a diagonal crack
$[(V_{dat})_{crack}]_{mean}$ = shear load at datum point to cause a diagonal crack based on mean approach
$[(V_{dat})_{crack}]_{pl}$ = shear load at the datum point to cause a diagonal crack in a plated beam

$[(V_{dat})_{crack}]_{un}$ = shear load at the datum point to cause a diagonal crack in an unplated beam

$(V_{dat})_{crit}$ = shear load at datum point to cause crack sliding in the critical, that is weakest, diagonal crack

$[(V_{dat})_{crit}]_{mean}$ = shear load at the datum point to cause a critical diagonal crack in a plated beam based on the mean approach

$([(V_{dat})_{crit}]_{mean})_{pl}$ = shear load at the datum point to cause crack sliding in a fully plate fully anchored beam based on the mean approach

$([(V_{dat})_{crit}]_{mean})_{un}$ = shear load at the datum point to cause crack sliding in an unplated beam based on the mean approach

$[(V_{dat})_{crit}]_{pl}$ = shear load at the datum point to cause a critical diagonal crack in a plated beam; shear load at datum point to cause CDC debonding

$[(V_{dat})_{crit}]_{un}$ = shear load at the datum point to cause a critical diagonal crack in an unplated beam; shear load at datum point to cause the concrete component of shear failure

$(V_{dat})_{cr\text{-}plate}$ = shear load at the datum point to cause cracking in the plated beam

$((V_{dat})_{cr\text{-}plate})_{hog}$ = shear load at the datum point to cause cracking in the plated beam in the hogging region

$((V_{dat})_{cr\text{-}plate})_{sag}$ = shear load at the datum point to cause cracking in the plated beam in the sagging region

$(V_{dat})_{h}$ = shear load at datum point in hogging region

$(V_{dat})_{hog}$ = shear load at datum point in hogging region

$(V_{dat})_{mean}$ = mean of $(V_{dat})_{cr\text{-}plate}$ and $(V_{dat})_{u\text{-}pres/metal}$

$((V_{dat})_{poc})_{udl}$ = shear load at point of contraflexure for uniformly distributed load in encastre beam

$(V_{dat})_{s}$ = shear load at datum point in sagging region

$(V_{dat})_{sag}$ = shear load at datum point in sagging region

$(V_{dat})_{slide}$ = shear at datum point to cause crack sliding

$[(V_{dat})_{slide}]_{mean}$ = shear load at the datum point to cause crack sliding in a plated beam based on mean approach

$[(V_{dat})_{slide}]_{pl}$ = shear load at the datum point to cause crack sliding in a plated beam

$[(V_{dat})_{slide}]_{un}$ = shear load at the datum point to cause crack sliding in an un plated beam

$(V_{dat})_{strength}$ = shear at datum point to cause failure

$(V_{dat})_{u}$ = shear load at datum point to cause shear failure across a diagonal crack; shear load at the datum point to cause crack sliding across a diagonal crack; shear load at datum point to cause crack sliding in unplated beam

$(V_{dat})_{u\text{-}metal}$ = shear load at datum point to cause shear failure across a diagonal crack based on longitudinal reinforcement approach

$((V_{dat})_{u\text{-}metal})_{sag}$ = shear load at datum point to cause crack sliding in a metal tension face plated beam in the sagging region based on the longitudinal reinforcement approach

$((V_{dat})_{u\text{-}metal})_{hog}$ = shear load at datum point to cause crack sliding in a metal tension face plated beam in the hogging region based on the longitudinal reinforcement approach

$(V_{dat})_{u\text{-}plate}$ = shear load at datum point to cause crack sliding in a plated beam

$(V_{dat})_{u\text{-}pres}$ = shear load at datum point to cause shear failure across a diagonal crack based on passive prestress approach

$(V_{dat})_{u\text{-}pres/metal}$ = refers to both $(V_{dat})_{u\text{-}pres}$ and $(V_{dat})_{u\text{-}metal}$

$((V_{dat})_{u\text{-}pres})_{hog}$ = shear load at datum point to cause crack sliding in the hogging region based on the passive prestress approach

$((V_{dat})_{u\text{-}pres})_{sag}$ = shear load at datum point to cause crack sliding in the sagging region based on the passive prestress approach

$(V_{incr})_{pp}$ = increase in the shear capacity due to passive prestress

V_{max} = maximum applied shear in a beam

$(V_{max})_{Lo}$ = maximum applied shear force at the focal point; distribution of shear due to the applied load

V_p = volume of plate

V_{plate} = vertical force in couple to resist M_{plate}

$(V_{pp})_{ACI}$ = concrete component of the shear capacity in a prestressed beam based on ACI approach

$(V_{pp})_{Euro}$ = concrete component of the shear capacity in a prestressed beam based on the Eurocode

V_s = shear resisted by the internal steel stirrups

$(V_{stirrup})_{transverse}$ = shear resisted by external transverse plates

$(V_{stirrups})_{pl}$ = total shear resisted by internal and external stirrups

V_u = shear capacity across a diagonal crack; equal to V_c for the CDC in an unplated beam

$V_{u\text{-}plate}$ = shear capacity across a diagonal crack in a plated beam

ΔV_{conc} = increase in the concrete component of the shear capacity due to plating

$(\Delta V_{conc})_{pl}$ = increase in the concrete component of the shear capacity due to plating

$\Delta V_{c\text{-}plate}$ = increase in V_c due to plating; increase in the concrete component of the shear capacity due to plating

-ve = negative; hogging

+ve = positive; sagging

W_{dat} = applied load acting on free body in CDC analysis; portion of the applied load, that induces V_{dat}, that is acting on the free body

$(W_{dat})_{cr}$ = resultant of applied loads acting on free body when $(V_{dat})_{cr}$ is acting in deriving the load to cause cracking

$(W_{dat})_h$ = applied load acting on free body in hogging region in CDC analysis

$(W_{dat})_{h\&s}$ = applied load acting on free body that crosses both the hogging and sagging regions in CDC analysis

$(W_{dat})_s$ = applied load acting on free body in sagging region in CDC analysis

$(W_{dat})_u$ = resultant of applied loads acting on free body when $(V_{dat})_u$ is acting in deriving the load to cause crack sliding

w = uniformly distributed load

w_{fail} = uniformly distributed load to cause failure

x = distance from free edge of pull-push specimen; distance from loaded end of concrete prism; horizontal projection of CDC; distance from nearest support

y = distance from axial force to compression face

z = distance of focal point from point of contraflexure

α = coefficient of IC debonding resistance equation

β = parameter defining position of transition strain ε_e

β_p = plate width parameter $f(b_p/b_c)$

β_L = plate length parameter $f(l_b/L_e)$

χ = curvature

χ_{add} = additional curvature applied after plating adjacent to plate end

χ_c = curvature at concrete crushing

χ_{cap} = curvature capacity

$(\chi_c)_{max}$ = maximum curvature when concrete crushing controls

χ_{creep} = additional curvature applied after plating adjacent to plate end due to concrete creep due to long term loads

$(\chi_{creep})_{plate}$ = creep curvature that occurs after plating

χ_{deb} = curvature at plate debonding

χ_{max} = maximum curvature; curvature capacity

χ_{PE} = curvature to cause PE debonding in an individual plate; PE debonding curvature capacity

χ_{plate} = curvature in plate

$(\chi_p)_{max}$ = maximum curvature when plate failure controls

χ_{RC} = curvature in RC beam

χ_{short} = additional curvature applied after plating adjacent to plate end due to short term loads

$(\chi_{short})_{plate}$ = short term curvature that occurs after plating

χ_{shrink} = additional curvature applied after plating adjacent to plate end due to concrete shrinkage

$(\chi_{shrink})_{code}$ = shrinkage curvature from national standards

$(\chi_{shrink})_{plate}$ = shrinkage curvature that occurs after plating

χ_u = curvature at end of plastic plateau; ultimate curvature capacity

χ_y = curvature at onset of plastic plateau

δ = deflection

δ_f = interface slip when τ_{int} reduces to zero

δ_{IC} = end slip between concrete and plate at loaded end of concrete prism in pull-push specimen; interface slip at intermediate crack

δ_{int} = interface slip

ε = strain

ε_b = maximum strain in tension reinforcing bar

ε_{bar} = strain in reinforcing bar; strain in reinforcing bars at plate debonding

$(\varepsilon_{bar})_{propped}$ = strain in tension reinforcing bar in a propped analysis

$(\varepsilon_{bar})_{unpropped}$ = strain in tension reinforcing bar in unpropped analysis

$(\varepsilon_{bar})_{res}$ = residual strain in tension reinforcing bar in an unpropped analysis; strain in bar prior to plating

ε_c = concrete crushing strain

$(\varepsilon_c)_{max}$ = maximum strain in the concrete at plate debonding; maximum strain in concrete

$(\varepsilon_{comp.edge})_{res}$ = residual strain in the concrete adjacent to the compression edge of the plate

ε_{CFRP} = strain at which carbon FRP material fractures

ε_{db} = plate IC debonding strain; IC debonding strain capacity of plate

$(\varepsilon_{db})_{anch}$ = IC debonding strain in anchorage approach

ε_{deb} = experimental plate IC debonding strain

ε_e = strain in concrete at transition from elastic to plastic zone

ε_f = maximum plate strain; strain capacity of plate

ε_{fract} = plate fracture strain

ε_{FRP} = FRP strain capacity; strain at which FRP material fractures

ε_{GFRP} = strain at which glass FRP material fractures

ε_{IC} = axial strain in plate at IC debonding

ε_p = plate strain

$\varepsilon_{p\text{-}bot}$ = strain at bottom edge of plate

$\varepsilon_{p\text{-}top}$ = strain at top edge of plate

ε_{pivot} = pivotal strain

$(\varepsilon_{pivot})_{RC}$ = pivotal strain in the reinforced concrete; pivotal strain in RC beam adjacent to plate that debonds

$(\varepsilon_{pivot})_{res}$ = residual strain in the concrete prior to plating at the level of the future pivotal point

ε_{pmax} = maximum strain in plate

ε_{rebar} = fracture strain of reinforcing bar

ε_{res} = residual strain at tension face

ε_s = strain in tension reinforcing bars
ε_{sh} = concrete shrinkage strain; concrete shrinkage strain after plating
ε_{sp} = strain at centroid of side plate
ε_{tfp} = strain at centroid in tension face plate
ε_y = yield strain of steel; yield strain of reinforcing bar
γ = depth of rectangular stress block factor
γ_O = cohesive effectiveness factor in shear to resist crack sliding
λ = coefficient in cohesive effectiveness factor γ_O; 1.6
θ = inclination of the CDC
θ_{hinge} = hinge rotation
θ_{mean} = inclination of CDC crack used in mean approach
ρ = area of all the longitudinal reinforcing bars as a proportion of the cross-sectional area of the concrete element; % longitudinal reinforcing bars; longitudinal reinforcing bar function
ρ_{eq} = equivalent area of longitudinal reinforcing bar in Blaschko's approach
ρ_{plate} = longitudinal reinforcement approach function
σ = stress
σ_{db} = axial stress at IC debonding
σ_{IC} = axial stress in plate at IC debonding
σ_n = stress at interface normal or perpendicular to interface
$\sigma_{p.IC}$ = stress in plate at intermediate crack
σ_{ps} = mean stress in concrete element due to prestress F_{ps}
σ_{pp} = mean stress in concrete due to passive prestress of plate
τ = interface shear stress
τ_f = peak interface shear stress
τ_{int} = interface shear stress between plate and concrete
τ_{Rd} = basic design shear strength in Eurocode

subscripts:
ang = angle
conc = shear capacity at formation of weakest or critical diagonal crack
crack = formation of a diagonal crack
crit = weakest critical diagonal crack relative to applied shear
cfp = compression face plate
dat = datum point
p = plate
pl = plated
slide = rigid body displacement; crack sliding
sp = side plate
tfp = tension face plate; tension face plated
un = unplated

Contents

Chapter 1: Introduction

1.1 Introduction

Existing reinforced concrete structures are often in need of strengthening, stiffening, improving the ductility or repair. A common form of retrofitting is to adhesively bond plates or sheets to the surfaces. However, tests have shown that these plates are prone to premature debonding, as has occurred to the tension face plate in Fig.1.1, which can inhibit the use of this retrofitting technique. The aims of this book are to:

- provide a comprehensive overview of all types and forms of plating
- provide an insight into the various plate debonding or peeling mechanisms
- compare, comment and apply the numerous design procedures or guidelines that are currently available in Australia, Europe, Hong Kong and the USA
- show where adhesively bonded plates can be safely applied, where they should not be applied and where bolted plates should be used instead of adhesively bonded plates
- clearly distinguish between the behaviours of metal and FRP plated sections
- provide comprehensive information so that retrofitting by plating can be used with safety and confidence and, hence, extend the use of all types of plating
- provide engineers with the design tools to develop their own unique plating systems and to decide on appropriate techniques specific to their retrofitting problems

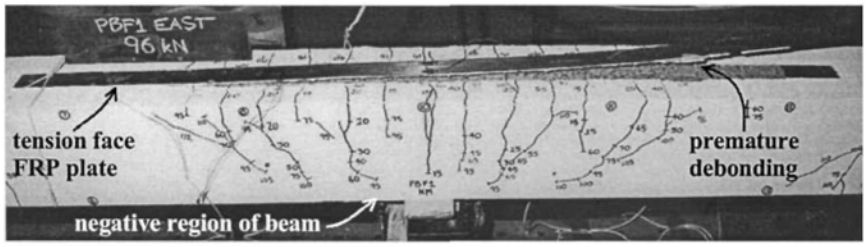

Figure 1.1 Premature failure of adhesively bonded plate

This book covers the mechanics of retrofitting reinforced concrete (RC) beams and slabs using externally bonded longitudinal plates. The plates can be made of FRP, steel, aluminium or any metal; they can have any shape such as flat plates, channels or angle sections; they can be bonded to any surface such as the tension face, sides or compression face; and they can be either adhesively bonded or bolted. Methods of analysis are illustrated and applied to determine the strength, stiffness and ductility of plated structures and design procedures for preventing premature debonding are compared.

In this chapter, the large variety of forms of longitudinal plating available to the designer is first described. This is then followed by a description of the premature failure mechanisms that can occur and have to be designed for, and how these failure mechanisms can affect the choice of plate material and size. Design guides are then compared which shows that there is general agreement on the failure mechanisms.

1.2 Forms of plating beams and slabs

Forces can be transmitted to the external plates from the RC structure through an adhesive bond, through bolts or through wrapping. Plates can be placed on any surface of the beam or slab and they can have any shape such as flat plates, channels or angle sections.

1.2.1 Bonding or joining techniques

1.2.1.1 Bolted and adhesively bonded plates

It is common practice to adhesively bond plates to the tension faces of slab structures as in Fig.1.2(a). Plates can also be adhesively bonded to the sides of beams as in Section A-A in Fig.1.3. However, if a ductile connection is required or if the adhesively bonded plate is prone to premature debonding or peeling, then the plate can be bolted as shown in Figs. 1.2(b) and 1.3. Although plates can be bolted to the tension face as in Fig.1.3, this may be difficult in beams due to congestion of the longitudinal tension reinforcement, in which case the plates can be bolted to the sides of the beam where only the stirrups have to be avoided.

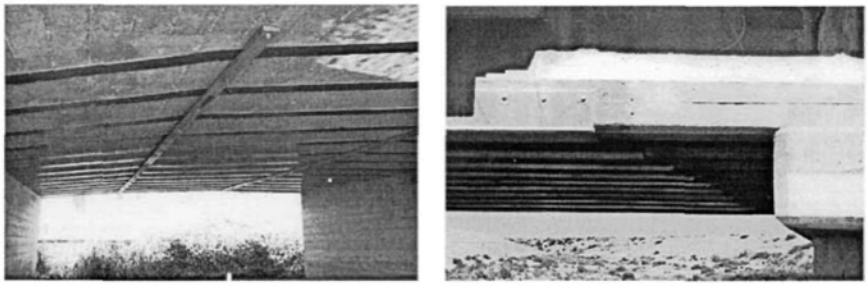

(a) adhesively bonded FRP plates (b) bolted steel plates

Figure 1.2 Retrofitting bridges

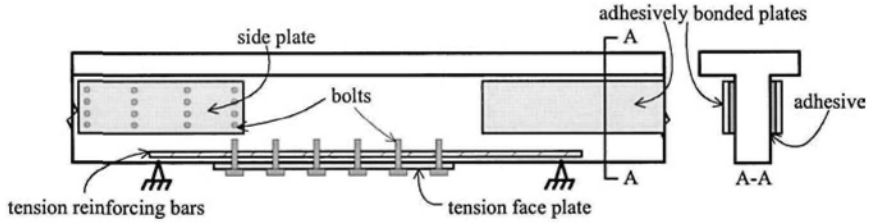

Figure 1.3 Bonding plates by adhesion and/or bolting

Plates can be both bolted and adhesively bonded but it should be remembered that each bonding technique works independently of the other; they do not enhance each other as bolts form a ductile connection that requires slip, whereas, adhesion forms a stiff but brittle connection. For additional safety, a plate can be designed as both bolted and adhesively bonded so that the bolts take over should the adhesive deteriorate. Bolts act as shear connectors in the composite plated structure so that they can be designed using the principles applied to stud shear connectors in composite steel and concrete beams (Oehlers and Bradford 1995, 1999) that are available in

national standards. A bolted FRP plate is probably more expensive to install than an adhesively bonded FRP plate, but bolting does allow the full strength of the plate to be achieved, whereas, adhesively bonded FRP plates often debond at strains between one-quarter to one-third of their fracture strain.

1.2.1.2 Wrapping and mechanical end anchorage

An alternative technique to bolting and/or adhesion for transferring the force into the plate is wrapping as shown in Fig.1.4 where the plate is both adhesively bonded and vertically wrapped around a rounded corner. The most efficient form is to fully wrap the cross-section as shown in A-A. This is a common practice in columns. The vertical wrap neither prevents nor inhibits the plate from debonding but takes over transferring the force, such as at C, after debonding. It is a very efficient system for increasing the vertical shear capacity of a beam with stirrups, as the fully wrapped section has sufficient ductility to allow the stirrups to yield or at least get significantly stressed whilst the wrap is still resisting vertical shear force. However, it is a difficult system to apply as the plate has to penetrate the flange of the beam. An alternative approach is to partially wrap as in B-B but, in this case, the resistance to the force D is generally low and the system is also brittle so that it is likely that the plate will debond before there is any significant stressing of the stirrups. A good compromise is shown at E-E where the plate is bonded within the flange on both surfaces providing a relatively strong joint and a ductile system that may allow some stressing of the stirrups prior to debonding.

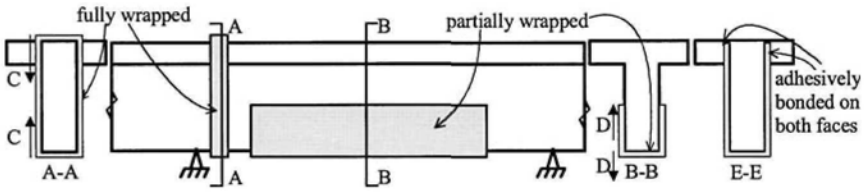

Figure 1.4 Vertically wrapped plates

An example of longitudinal wrapping is shown in Figs.1.5 and 1.6 where the bends in the plate at the ends at positions *A* in Fig. 1.5 act as an anchorage after the adhesively bonded plate has debonded. Anchorage failure can be clearly seen in Fig. 1.6 which was preceded by IC debonding. If possible, wrapping and clamping the plates at the supports such as at *C* in Fig. 1.5 provides an even stronger anchorage after debonding. Bolting the plates at the ends *B* has the same effect as wrapping as the bolts provide anchorage after debonding. It may be worth noting that an adhesively bonded plate or a plate bolted along its length such as in Fig.1.3 can accommodate a variation in longitudinal stress along the plate whereas in end anchored plates as in Fig.1.5 the plates are uniformly stressed along their length which will require a different analysis procedure.

Wrapping and adhesive bonding were applied to strengthening the bridge corbels in Fig.1.7(a) where the plate is adhesively bonded to the top of the corbel and wrapped around the sides. Full size specimens were tested to failure up-side-down in Fig.1.7(b). The *intermediate crack* caused the plate to debond after which the stress in the plate was maintained by the anchorage effect of the wrap until this also failed as shown in Fig.1.8(a). The end anchorage was enhanced with the addition of bolts to the wrap, as in Fig.1.8(b), as an additional safety measure should the adhesive deteriorate

prematurely. These tests clearly showed that the anchorage effect of the wrap was not effective until after debonding and did not affect the load at which debonding occurred.

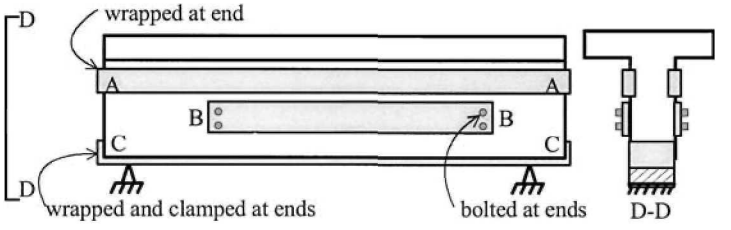

Figure 1.5 Longitudinally wrapped plates

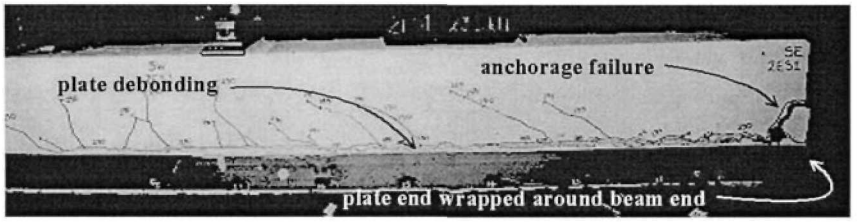

Figure 1.6 Longitudinally wrapped plate after debonding

(a) plating corbel (b) failure of wrapped plate

Figure 1.7 Bridge corbel strengthened by wrapping

1.2.2 Plate position

1.2.2.1 Tension face plates

The most commonly used plate position is the tension face, as in Figs.1.2(a) and 1.9, as it maximises the flexural lever arm and, hence, maximises the increase in the flexural capacity due to plating. However, the debonding stress concentrations in the tension face plate tend to interact with those in the adjacent tension reinforcing bars making the tension face plates more susceptible to premature debonding. It is also

worth remembering that the addition of tension reinforcement reduces the ductility of the RC cross-section which may limit the increase in strength that can be achieved with tension face plates. An alternative would be to plate the sides of the beam.

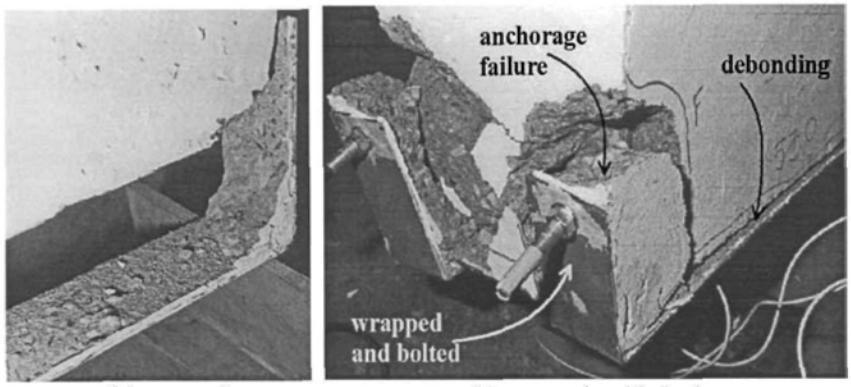

(a) wrapped (b) wrapped and bolted

Figure 1.8 End anchorage failure

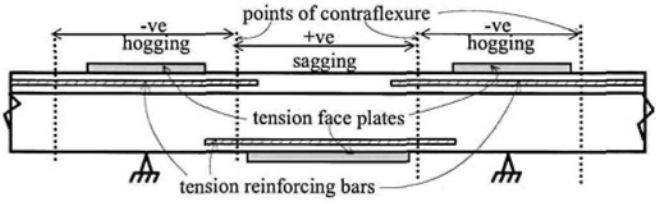

Figure 1.9 Tension face plated beam

1.2.2.2 Side plates

Examples of side plated beams are shown in Figs. 1.2(b) and 1.10. For a given area of plate, side plates are less efficient in increasing the flexural capacity than tension face plates due to the reduced lever arm. However, it may be possible to bond a greater area of plate to the sides than the tension face of the beam; side plated beams tend to be more ductile than tension face plated beams particularly if the plate is extended into the compression region of the web as in plate A in Fig.1.10; adhesively bonded side plates have been found to be less susceptible to debonding as there is little interaction between the debonding stresses and the stresses surrounding the tension reinforcing bars; and adhesively bonded side plates can substantially increase the concrete component of the vertical shear capacity and can substantially increase the total shear capacity when bolted.

1.2.2.3 Compression face plates

Plates can also be bonded to the compression face as in Fig.1.11. Compression face plates such as at position A can be used to increase both the ductility and vertical shear resistance of beams. It is also common practice to extend tension face plates such as at B into the compression faces as this inhibits but does not necessarily prevent debonding. Compression face plates are less susceptible to premature

debonding than tension face plates as there is no interaction between the debonding stresses and those surrounding compression reinforcing bars.

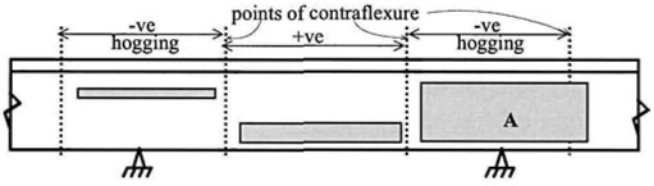

Figure 1.10 Side plated beam

1.2.3 Plate shapes

As well as flat plates, channel or U sections can be used as in Fig.1.12; these shapes are easily formed using the wet lay-up procedure with FRP sheets. Combinations of shapes can also be used as in Fig.1.13 where the U section and side plate are bonded adjacent to the ends of the tension face plate specifically to inhibit debonding of the tension face plate.

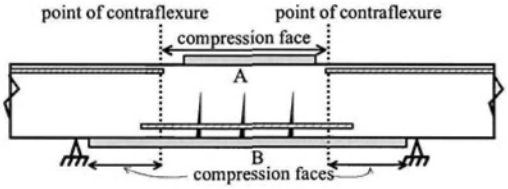

Figure 1.11 Compression face plated beams

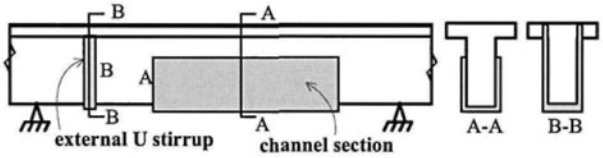

Figure 1.12 Channel or U sections

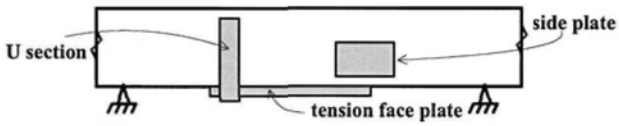

Figure 1.13 Combinations of plates

1.3 Major debonding mechanisms in adhesively bonded plates

In general practice, the adhesive used to bond a plate to a concrete element is much stronger than the tensile strength of the concrete so that debonding or peeling

invariably occurs within the concrete element as shown in Fig.1.8(a). Any crack that intercepts a plate will induce some amount of debonding to relieve the stress concentrations at the intercept. This will be referred to as intermediate crack (IC) interface cracking and generally has little or no effect on the overall strength of the structure. If this IC interface cracking spreads sufficiently to reduce the strains in the plate then this will be referred to as IC debonding. The formation of a critical diagonal crack (CDC), the type of crack commonly associated with the shear capacity of a beam or slab without stirrups V_c, also induces debonding and is referred to as CDC debonding. Furthermore, the curvature in a beam can also cause the plate to debond from the plate ends (PE) inwards and this is referred to as PE debonding. Although not a common debonding mechanism in most retrofitted RC beams or slabs, it is good practice to ensure that the interface shear stresses between the plate and concrete do not cause tensile failure of the concrete and this is referred to as *VAy/Ib* debonding.

In summary, IC debonding is associated with the strains in the plate, CDC debonding is associated with the rigid body shear displacement across a diagonal crack, and PE debonding is associated with the curvature in a beam. All the forms of adhesively bonded plates described in Section 1.2 are susceptible to the following debonding mechanisms in Sections 1.3.1 to 1.3.4.

1.3.1 Intermediate crack (IC) debonding

When an intermediate crack at A-A in Fig.1.14 intercepts a plate, compatibility requires that the plate is subjected to infinite strains across the crack width B-B which of course cannot occur. The accommodation of the intermediate crack is accomplished through some shear straining across the adhesive layer but primarily by the formation of the horizontal interface crack in Fig.1.14 (IC interface crack) such that the deformation in the plate over the length C-C is equal to that in the concrete that incorporates the width of the intermediate crack. As the applied load is increased opening the intermediate crack and increasing the longitudinal strain in the plate, the IC interface crack propagates due to the combination of shear and normal stresses at the crack tip.

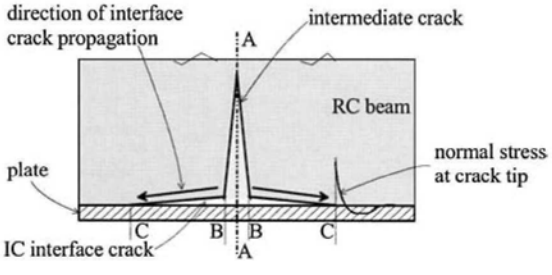

Figure 1.14 IC interface cracking mechanism

The intermediate crack in Fig.1.14 can be any kind of crack such as the flexural crack and flexural/shear cracks in Fig.1.15 or the diagonal cracks in Fig.1.16. It can be seen in both Figs. 1.15 and 1.16 that IC interface cracks initiate at the crack/plate intercept and propagate towards the plate end. They can occur at very low loads and are initially of no significance, as in Figs. 1.15 and 1.16, until they have spread sufficiently to join together and reduce the strains in the plate, in which case IC debonding can be considered to occur. It can be seen that IC debonding is primarily

concerned with the strains in the plate that are required to accommodate the intermediate crack and it is a gradual failure with plenty of warning.

1.3.2 Critical diagonal crack (CDC) debonding

The critical diagonal crack (CDC) debonding mechanism is illustrated in Fig.1.17. The critical diagonal crack is not an inclined shear/flexural crack as in Fig.1.15, nor a diagonal crack as in Fig.1.16, but it is a single inclined crack in a shear span across which rigid body shear displacement occurs. It is the critical diagonal crack associated with the shear failure of beams or slabs without stirrups, that is the CDC associated with the concrete shear capacity of a beam or slab V_c. It is the rigid body sliding action and rotation across the CDC in Fig.1.17 that causes the plate to debond from the root of the crack at B towards the plate end at C as shown. As with all shear failures, failure is very rapid and explosive with virtually no prior warning. Numerous tests have clearly shown that stirrups do not prevent nor inhibit this form of debonding as the plate debonds before the stirrups are stretched to yield.

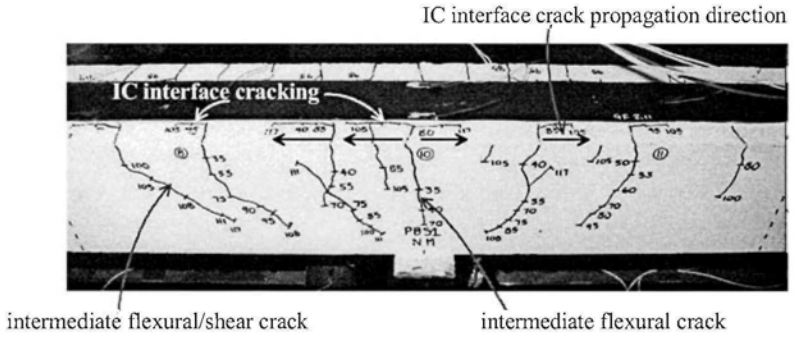

Figure 1.15 IC interface cracking induced by flexural and flexural/shear cracks

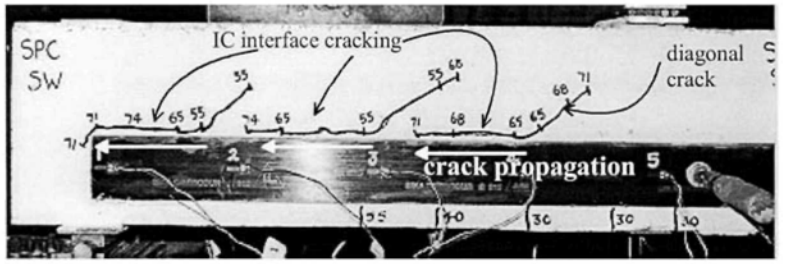

Figure 1.16 IC interface cracking induced by diagonal cracks

Figure 1.18 is a further illustration of the important difference between IC debonding induced by flexural/shear cracks and CDC debonding due to the rigid body displacement across a CDC. As the applied load was being gradually increased in the beam in Fig.1.18, the IC interface cracks induced by the intermediate flexural and shear cracks were gradually propagating in the region over the support. However, suddenly and without any prior warning the critical diagonal crack formed and the

plate debonded from the root of the diagonal crack to the plate end in a region which was uncracked prior to the formation of the critical diagonal crack.

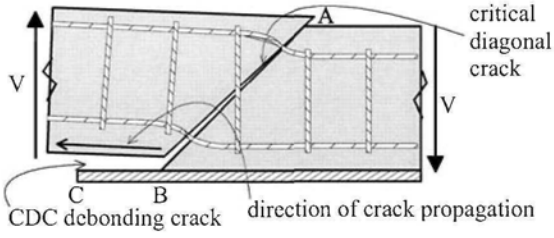

Figure 1.17 Critical diagonal crack (CDC) debonding mechanism

A further example of the rapid and catastrophic nature of CDC debonding is illustrated in Fig.1.19 for a beam with a tension face plate that was terminated near a support. A diagonal crack occurred at an applied load of 100 kN. Virtually nothing happened after that but then at a substantially higher load of 188 kN the critical diagonal crack formed in a previously uncracked region and the rigid body displacement across this crack caused the plate to debond. It can be seen that the critical diagonal crack occurred within the plated region and because of this it caused debonding and also that debonding occurred near to the plate end. In summary, critical diagonal crack debonding is associated with the rigid body shear displacement across a critical diagonal crack and it is a catastrophic failure that occurs without warning.

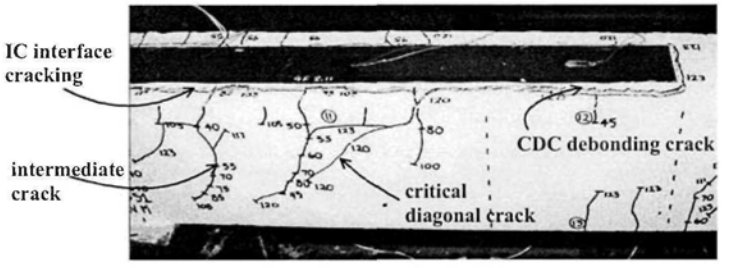

Figure 1.18 Critical diagonal crack debonding amongst flexural/shear cracks

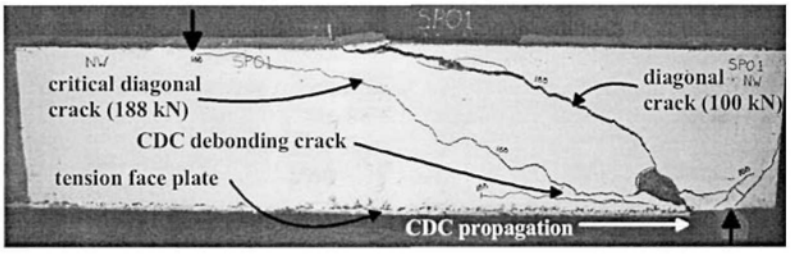

Figure 1.19 Sudden occurrence of critical diagonal crack

1.3.3 Plate end (PE) debonding

Plate end (PE) debonding is considered the easiest form of debonding to visualise as illustrated in Fig.1.20. As curvature is applied to the beam, the plate tries to remain straight which causes debonding cracks to start at the plate ends and propagate inwards, this is referred to as plate end debonding. Unlike IC and CDC debonding where the debonding cracks start within the plated region and propagate outwards towards the plate ends, for PE debonding the debonding cracks initiate at the plate ends and propagate inwards.

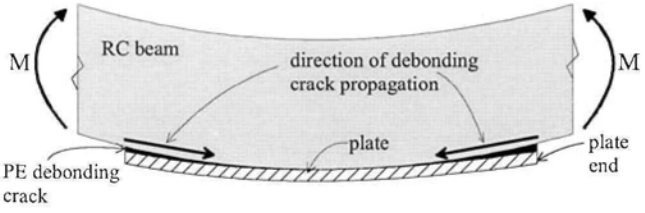

Figure 1.20 Plate end (PE) debonding mechanism

An example of plate end debonding is shown in Fig.1.21 for a beam with a side plate. The debonding crack first gradually propagated from the plate end inwards as the load was increased, and then rapidly, causing the strains in the plate to reduce upon which debonding was assumed to have occurred. In summary, plate end (PE) debonding is a gradual form of failure and is induced by curvatures in the beam.

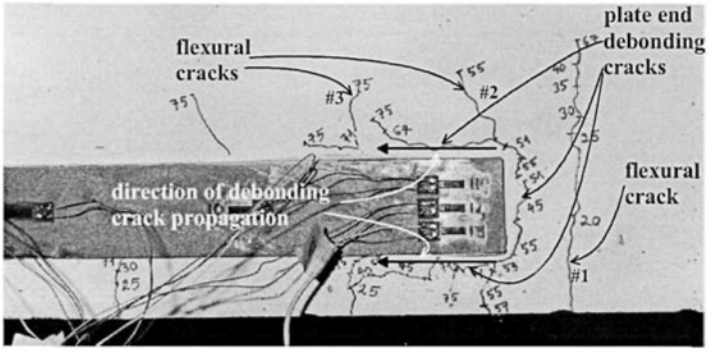

Figure 1.21 Plate end (PE) debonding in a side plated beam

1.3.4 Interface shear stress (VAy/Ib) debonding

The interface shear stress between the plate and the RC beam can be derived from elementary structural mechanics using the well known VAy/Ib or equations that depend on the vertical shear force V at a section of a beam. The first author has tested hundreds of plated beams and none would appear to have failed by this mechanism of failure. However, there is a possibility that the interface shear stress VAy/Ib might cause debonding when thick plates are used, such as might occur if plating is used at serviceability to reduce deflections. Furthermore, the VAy/Ib shear stress may be more likely to cause debonding in plated prestressed beams as the prestress will inhibit the formation of the intermediate and critical diagonal cracks and hence delay

both IC and CDC debonding. Hence, it is good practice to check the VAy/Ib shear stress and if necessary restrict it to less than the tensile strength of the concrete.

Figure 1.22 shows IC debonding of a tension face plate in a constant moment region and Fig.1.23 shows PE debonding also in a constant moment region where obviously in both cases the vertical shear force V is zero. Hence it can be seen that as the VAy/Ib shear stress depends on the vertical shear force V, restricting the VAy/Ib shear stress will not prevent either IC or PE debonding. Furthermore, as CDC debonding is due to a rigid body shear displacement as shown in Fig.1.19, limiting the VAy/Ib shear stress cannot be used to design against CDC debonding. In summary, the VAy/Ib shear stress should not be used to design against IC, CDC and PE debonding. The VAy/Ib shear stress should be considered as the fourth major mode of debonding and restricted to less than the tensile strength of the concrete.

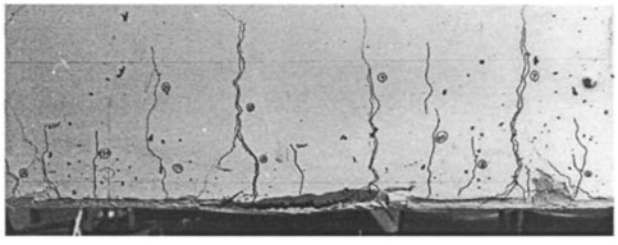

Figure 1.22 IC debonding of a tension face plate in a constant moment region

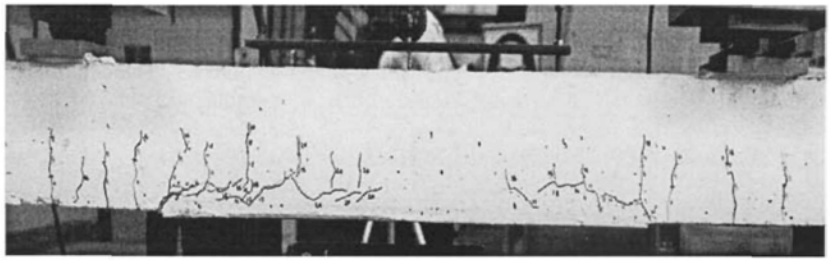

Figure 1.23 PE debonding of a tension face plate in a constant moment region

1.3.5 Desired form of flexural failure

Figures 1.24 and 1.25 show examples of side and tension face plated beams in which concrete crushing occurred prior to debonding of the plates. Small amounts of IC interface cracking can be seen along the edges of the plates but this was not sufficient to reduce the stresses in the plates so that the beams achieved their theoretical flexural capacities based on the material properties. This may be considered as the desired form of failure as most reinforced concrete beams and slabs are designed to fail due to concrete crushing whether they are under-reinforced or over-reinforced.

The desired concrete crushing failures shown in Figs. 1.24 and 1.25 can only be achieved if IC, CDC and PE debonding can be prevented from occurring before the design load to cause concrete crushing. However, this may not always be possible; in which case, it may be necessary to design for either IC or CDC debonding to occur at the design load so that concrete crushing will not occur. Rarely will PE debonding

control the design capacity as this mode of failure can be easily prevented by terminating the plate at a point of contraflexure or at least in a low moment region.

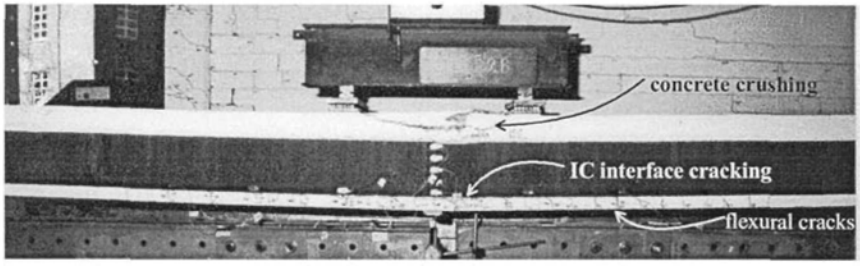

Figure 1.24 Flexural failure of a side plated beam

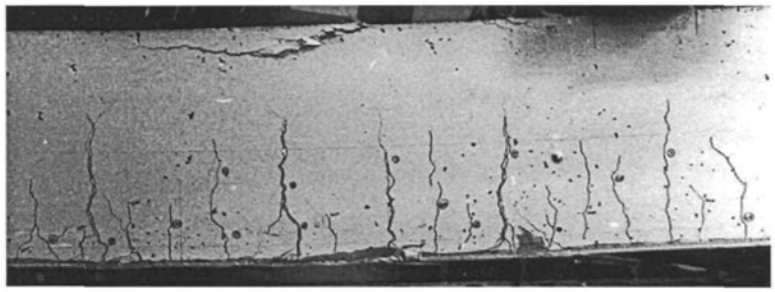

Figure 1.25 Flexural failure of a tension face plated beam

It may be worth noting that even if it is possible to design a plated beam or slab so that the concrete crushes prior to debonding, numerous tests by the authors have shown that there is a very good chance that the plates will still debond after the maximum flexural capacity has been reached. Hence, debonding may still affect the ductility of the section and the ability to redistribute moment within a continuous beam. However, this restricted ductility can be designed for and is an illustration of the advanced analysis procedures that have to be applied in designing plated structures, particularly if ductility is required to redistribute moments, to resist seismic loads or to absorb dynamic loads.

1.3.6 Summary of common debonding mechanisms

The three common major debonding mechanisms, that is intermediate crack (IC), critical diagonal crack (CDC) and plate end (PE) debonding, apply to all forms of plating and for all types of plate material. Longitudinal tension face plates as in Fig.1.26 are probably the most common form of plating and are susceptible to IC, CDC and PE debonding in both the positive and negative moment regions as shown. Exactly the same mechanisms apply to side plated beams as shown in Fig.1.27.

Plates can be bonded to the compression face as in the upper plate in Fig.1.28, or tension face plates can be extended into the compression faces, as in the lower plate, to try to inhibit debonding. However, these compression face plates are also susceptible to CDC and PE debonding as shown, but obviously not to IC debonding as

the intermediate crack which is a requirement for IC debonding will not occur in the compression zone.

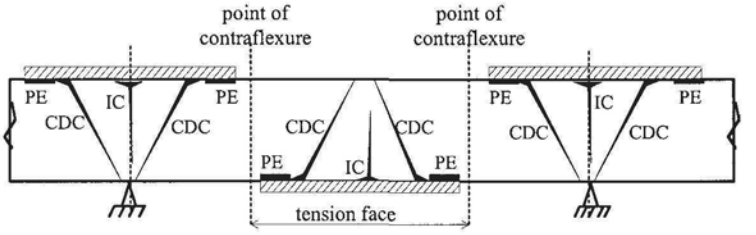

Figure 1.26 Longitudinal tension face plates

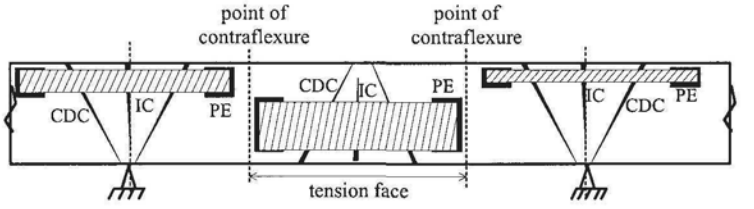

Figure 1.27 Longitudinal side plates

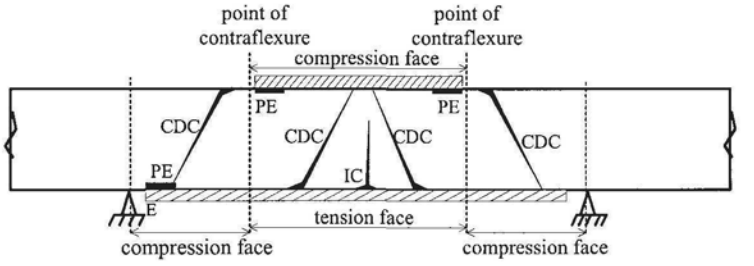

Figure 1.28 Longitudinal compression face plates

It may be worth noting that transverse plates such as A and B in Fig.1.29, although not the subject of this book, are also susceptible to IC debonding as shown.

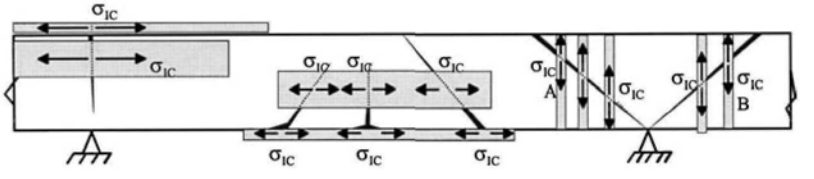

Figure 1.29 IC debonding in transverse plates

1.4 Failure of bolted plates

In Fig.1.30, thick FRP plates have been bolted to the sides of an RC beam. The behaviour of this beam is similar to the behaviour of commonly used composite steel and concrete beams. It can be seen that the concrete has crushed and the beam has attained its desired theoretical ultimate strength.

The bolts or bolt shear connectors in Fig.1.30 are analogous to mechanical stud shear connectors in composite steel and concrete beams and require slip to transmit the shear forces. Compared with an adhesive bond which is brittle, bolt shear connectors are ductile and, unlike adhesively bonded plates, can easily accommodate any critical diagonal crack. Hence this system can be used in regions of a continuous beam where CDC debonding or ductility requirements prevent the plates from being adhesively bonded.

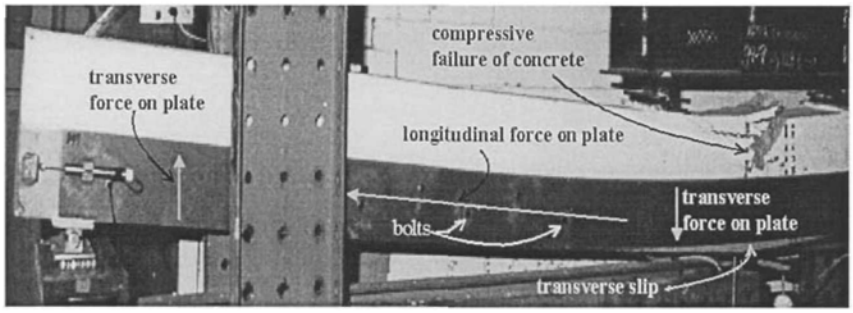

Figure 1.30 Flexural failure of a bolted plated beam

As with stud shear connectors in composite steel and concrete beams, bolt shear connectors can fail by fracturing due to excessive slip as shown in Fig.1.31(a), but this can be easily prevented by designing for full shear connection. Placing the side plate partly in the compression region can increase the ductility of the beam but the plate is then susceptible to buckling as shown in Fig.1.31(b). Comprehensive design rules (Smith, Bradford and Oehlers 1999a, 1999b, 2000, 2001) are available for quantifying the plate buckling load and for distributing the bolts so that buckling does not occur. However, a simple solution is to prevent plate buckling by restricting the plates to the tension zones as in Figs.1.30 and 1.31(a).

1.5 Plate material and geometry

The type of plate material used may often be governed by durability requirements as well as the intended form of bonding.

1.5.1 Adhesively bonded plates

A comparison of the mechanical properties of materials that are frequently bonded to concrete structures is shown in Fig.1.32. The strength, stiffness and ductility of adhesively bonded plated sections depends on all the properties shown in Fig.1.32; it depends on the material stiffness E, the FRP fracture stress f_{FRP} or the metal yield

stress f_y, the FRP strain capacity ε_{FRP} as well as the extent of the metal yield plateau that is the metal ductility.

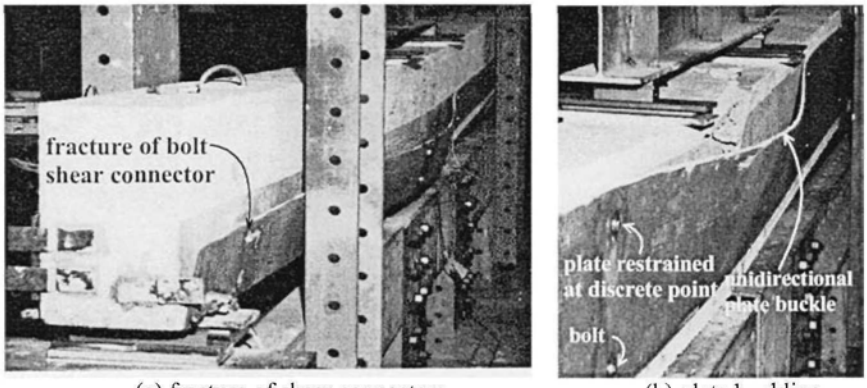

(a) fracture of shear connectors (b) plate buckling

Figure 1.31 Premature failure of bolted plated beams

Steel can be considered as stiff and ductile having a relatively high Young's modulus (E_s) and, hence, high material stiffness followed by a large yield plateau which signifies a high material ductility. Aluminium tends to be less stiff (E_{al}) than steel and is also ductile. In contrast to metal plates, fibre reinforced polymer plates are totally brittle, that is without a ductile plateau, and fracture at a strain ε_{CFRP} and ε_{GFRP} that depends on the fibres being used. The stiffness of fibre reinforced polymer (FRP) plates E_{CFRP} and E_{GFRP} depends primarily on the type and concentration of the fibre. For example, carbon fibre reinforced polymer (CFRP) plates can be made with sufficient fibres so that the plate is stiffer than steel as shown and reducing the density of the fibre will obviously reduce the Young's modulus. Glass fibre reinforced polymer (GFRP) plates tend to fracture at a higher strain than carbon fibre plates but are less stiff and both generally fracture at strains well below the fracture strain of steel but at much higher stresses.

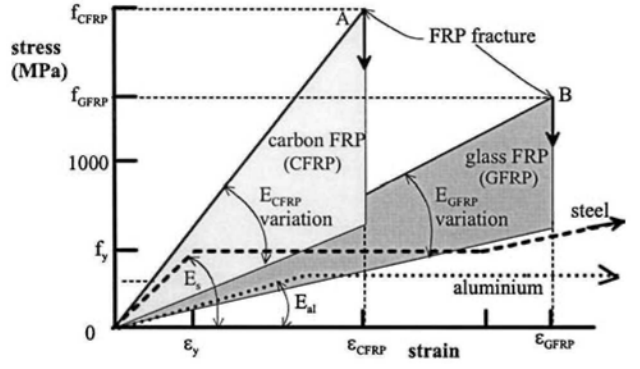

Figure 1.32 Adhesively bonded plate materials

Whilst the plate material remains linear elastic, the dependence of the plate debonding stress σ_{IC} is given by the following empirically derived rule (Teng et al 2002).

$$\sigma_{IC} \propto \sqrt{\frac{E_p \sqrt{f_c}}{t_p}} \qquad 1.1$$

where E_p = Young's modulus of the plate, f_c = compressive cylinder strength of the concrete and t_p = plate thickness. It can be seen in Eq.1.1 that the concrete term has a minimal effect on the debonding stress as, for example, doubling the concrete strength will only increase the debonding stress by 19%. Rearranging Eq.1.1 gives the following debonding strain ε_{IC}.

$$\varepsilon_{IC} \propto \sqrt{\frac{\sqrt{f_c}}{E_p t_p}} \qquad 1.2$$

FRP plates are commonly chosen to maximise the debonding stress in order to maximise the increase in the flexural capacity. Hence from Eq.1.1 thin stiff plates are suitable, and from Fig.1.32 carbon FRP would be the best choice. As an example, pultruded carbon FRP plates are usually supplied in thicknesses $t_p \approx 1.2$ mm with a Young's modulus $E_p > 150$ GPa which gives debonding stresses σ_{IC} of about 450 MPa, which can be compared with the ultimate fracture stress $f_{CFRP} > 1500$ MPa. It can be seen that the debonding stress is little more than that of high yield steel and well below the ultimate tensile strength of the FRP. However, if ductility is a requirement, then Eq.1.2 suggests that thin plates with a low Young's modulus would be the preferred option such as that provided by glass FRP as shown in Fig.1.32. Several layers of FRP plates can be used, however from Eqs. 1.1 and 1.2 both the strains and stresses at debonding reduce making the system mechanically even less efficient, although generally the force in the plate increases as the thickness increases. This could be an option for reducing deflections at serviceability where the working stresses are lower than at ultimate which will allow thicker plates. Pultruded plates tend to have unidirectional fibres whilst those plates manufactured from FRP sheets using the wet lay-up process tend to be bi-directional.

Metal plates can be designed using Eq.1.1 to remain linear elastic prior to debonding; this may be a suitable approach for plating at serviceability stresses as it would allow thick plates. However at the ultimate limit, metal plates have one advantage over FRP plates in that they can be designed to yield prior to debonding which can ensure a reasonable amount of ductility if required. Typically, steel plates of thickness $t_p < 4$ mm will yield before debonding although plated beam tests show that debonding will eventually occur but at relatively high strains.

1.5.2 Bolted plates

The criteria for choosing plates for bolting are totally different from those for adhesive bonding. Debonding is now no longer an issue so thick plates can be used. Thick plates are also required so that they do not buckle if placed in the compression zone as in Fig.1.31(b) and in order to transmit the bearing force from the bolts. Typical examples of materials used in bolted plates are shown in Fig.1.33.

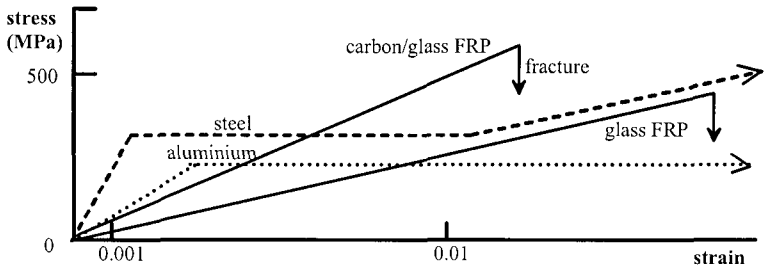

Figure 1.33 Bolted plate materials

As thick plates can be used and are in fact beneficial, plates can be made not only from metals but also from glass fibre which is less expensive than carbon fibre or from a combination of carbon and glass; these plates range from 5 mm to 15 mm thick. The FRP fibres have to be in at least two directions to resist the splitting forces from the bolts. The ultimate fracture strength of these FRP plates is of the same order as steel so that a much larger proportion of the ultimate strength can be used in design as compared to adhesively bonded FRP plates where the debonding stress is usually much lower than the fracture stress.

1.6 Commentary of design guides for longitudinal plating

1.6.1 Scope of comparison

Numerous papers have been published on adhesive bonding external plates and most manufacturers give or refer to guidelines. However, this comparison is restricted to the approaches listed in Table 1.1 which consist of the Australian research brought together and documented in this book as a design guide, as well as the Hong Kong research and design guide also issued as a book, and the British, European and American guidelines, as it is felt that these are fairly comprehensive and reasonably independent.

Table 1.1 FRP plating guidelines

Australian	Oehlers and Seracino (2004) Design of FRP and steel plated RC structures
British	Canakya et al Concrete Society Technical Report No. 55 (2000) Design guidance for strengthening structures using fibre composite materials
European	Triantafillou et al fib bulletin 14 (2001) Externally bonded FRP reinforcement for RC structures
Hong Kong	Teng, Chen, Smith and Lam FRP Strengthened RC structures (2002)
USA	Rizkalla et al ACI 440.2R-02 (2002) Guide for the design and construction of externally bonded FRP systems for strengthening concrete structures

In the following comparison and discussion of the guidelines in Table 1.1, it may be worth bearing in mind that these guidelines were issued as early as the year 2000 and during this intervening period there has been very rapid improvements in the understanding of plated structures and in the development of design rules. Hence, when these guidelines were first issued, they were the state-of-the-art and provided design guidelines for a new and very complex subject which was, and still is, evolving rapidly. To help in a systematic comparison of these guidelines, the Australian design approach will be described first as it covers all forms of plating, after which the comparison will be restricted to adhesively bonded FRP tension face plated structures as all the guidelines apply to this form of plating.

1.6.2 Australian approach

The scope of the Australian approach is summarised in Fig.1.34. The designer first requires the distribution of the envelopes of applied vertical shear and bending moment. These are shown schematically in Fig.1.34(a). They are a reminder that the stress resultants can vary at a design point particularly if designing for moving loads, as in a bridge, where there may not be a convenient position of zero moment. The design approach then consists of the follow steps:

- Choose the type of plate material at a given hogging or sagging region by considering durability, ductility, moment redistribution requirements and ease of application. Combinations of plate materials can be considered for example steel plates may be required in the hogging regions for ductility whilst carbon FRP plates can be used in the sagging regions.
- Decide on the plate position, such as side or tension face plates, for convenience or for mechanical considerations such as strength or ductility. For example, it may not be convenient to plate the tension faces of the hogging regions in which case the underside of the flanges or the sides of the webs could be plated.
- Choose a plate thickness and hence plate stress and plate strain, as governed by *IC debonding,* at positions of maximum moment. In some cases, it may be ineffective to adhesively bond FRP plates to the tension faces, as the plates may debond before the tension reinforcing bars yield. In which case, it may be more appropriate to plate regions closer to the neutral axis such as the underside of the flanges in the hogging regions so that the reinforcing bars yield before the plates debond. The plate thickness will also depend on the limit state, as for example at serviceability lower stresses occur so that thicker plates can be used.
- Determine the cross-sectional area of plate for flexural requirements of strength or serviceability.
- Assume the plate extends to the points of contraflexure or where the moment is low, that is the shear span is fully plated. Determine the *CDC resistance and the position of the critical diagonal crack.* Where the CDC resistance is too low, either try to add plates to increase the resistance or if this is not sufficent change to *bolting plates* in this region.
- If the CDC resistance of the fully plated region is sufficient, determine the extent of plating which is governed by the *position of the CDC and by PE debonding.*

It can be seen in the design steps listed above that IC debonding is the dominant debonding mechanism as it controls the type, size and position of the plate. However, CDC debonding may prevent the use of adhesively bonded plates in some shear spans, in which case bolted plates can be substituted. CDC debonding also

controls the extent of plating as the plate has to extend beyond the critical diagonal crack. PE debonding also governs the extent of plating but rarely, if ever, prevents plating as it can be designed against by simply terminating the plate at a point of contraflexure or where the curvature is low.

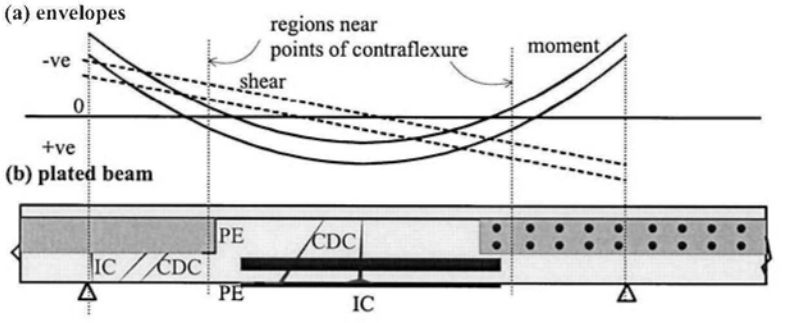

Figure 1.34 Australian approach

1.6.3 Adhesively bonded FRP tension face plated structures

As all of the design guidelines in Table 1.1 cover plating using FRP tension face plates as shown in Fig.1.35, this form of plating will be used to compare the different guidelines. The design rules cover both the hogging (-ve) and sagging (+ve) regions of the beam. For convenience, we will consider the sagging region in Fig.1.35 which is represented as a simply supported beam in Fig.1.36.

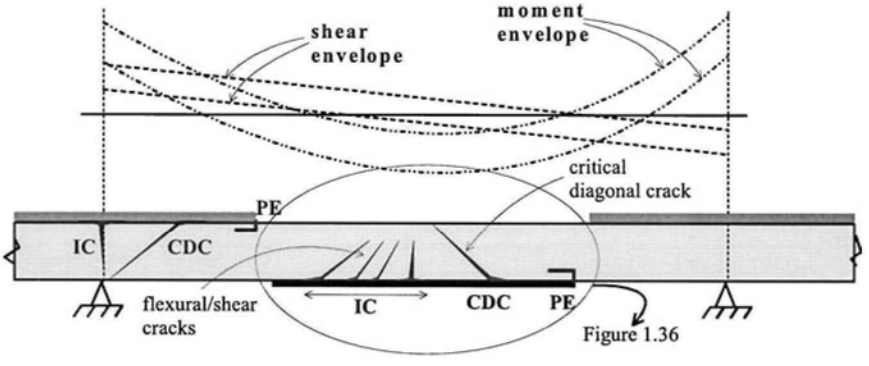

Figure 1.35 Tension face plates

The different debonding failure mechanisms, which have already been described in Section 1.3, are shown again in Fig.1.36. The 5 mechanisms encircled in Fig.1.36 were extracted from the five guidelines in Table 1.1. The names used for each mechanism, as listed in the boxes in Fig.1.36, may differ between the guidelines but there appears to be an almost unanimous agreement on the mechanisms of debonding which is a very important first stage in the development of design rules. The USA guidelines do not describe the failure modes directly but do refer to three conference papers which clearly describe failure Mechanisms 1-4; this has been referred to as *referenced* in the boxes in Fig.1.36. Similarly, the British guideline also

refers to a conference paper for Mechanism 4. Much of the agreement shown in Fig.1.36 would appear to ensue from an excellent conference paper by Blaschko et al (1998). The European approach makes the distinction between the cracked region of a beam and the uncracked region as shown in Fig.1.36 and it is a requirement that the plate is anchored in the uncracked region. This leads to the three IC debonding failure regions: at the anchorage zone (Mechanism 1); at the position of maximum moment (Mechanism 3); and at flexural/shear cracks (Mechanism 2).

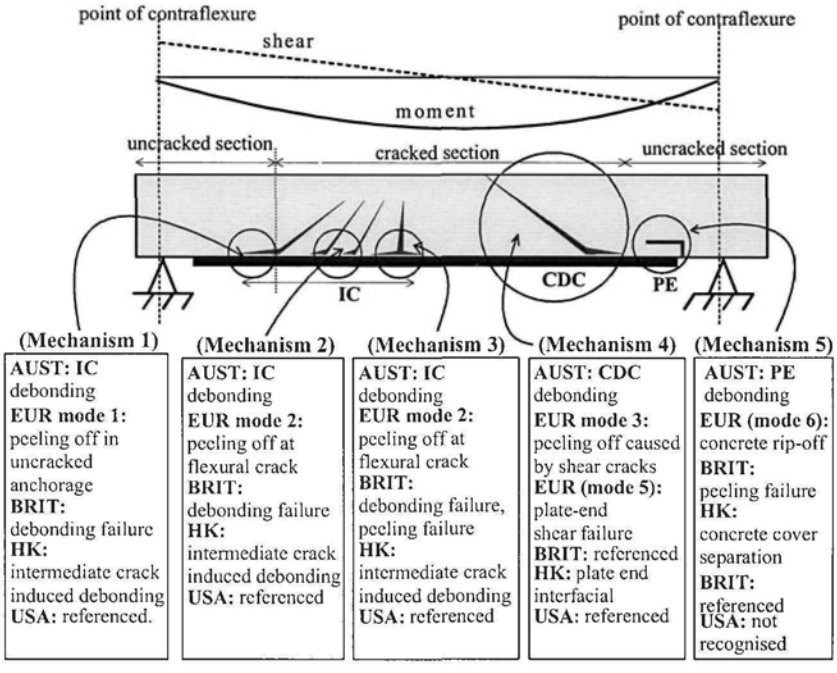

Figure 1.36 Comparison of debonding failure mechanisms

For Mechanism 1 in Fig.1.36, there is a general agreement in calculating the axial force in the plate allowing for the bond length. There is also general agreement for Mechanisms 2 and 3, although in the latter there is a slight confusion with the British approach which first refers to it as *debonding failure* but then suggests using the equation for *peeling failure* in this region. For Mechanism 5, there is also general agreement. However, the European approach describes the failure, identified as mode 6 in the box, but does not give design rules. This is probably because plate end debonding is very unlikely to control design when using FRP plates as they are usually very thin and also because of the necessity for terminating the plate in an uncracked region which by definition will be at or close to a point of contraflexure.

Finally, there is further general agreement for Mechanism 4 where design rules originating from the concrete shear capacity V_c are proposed. However, there is slight confusion with the European approach which gives it two labels and describes *plate-end shear failure* (identified as mode 5) using Fig.1.37. This figure shows a simply supported beam with plates terminating almost at the supports and with a horizontal debonding crack on the right hand side and a diagonal crack on the left

hand side. The authors are familiar with plate end debonding as in Fig.1.23 which looks familiar to the debonding crack on the right side of Fig.1.37, but this only occurs when the plate is terminated in a region of high curvature which does not exist at the supports.

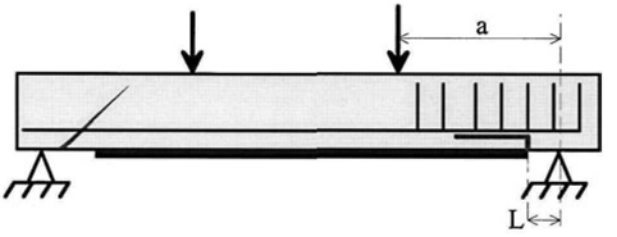

Figure 1.37 fib 14 diagram for '*FRP plate-end shear failure*'

Combining the two cracks in Fig.1.37, resembles the CDC debonding failure in Fig.1.19 and which is also shown in Fig.1.38 for a plated beam without stirrups and in Fig.1.39 for a plated beam with stirrups. Whether or not this is the *plate-end shear failure* described in the European guideline, these failed beams show that it may be difficult to find an uncracked region of a beam within which to anchor the plate end as required in the European guideline simply because shear cracks can occur near points of contraflexure.

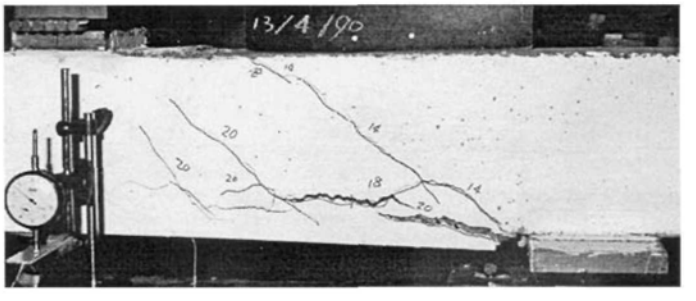

Figure 1.38 '*plate-end shear failure*' of beam without stirrups (CDC debonding)

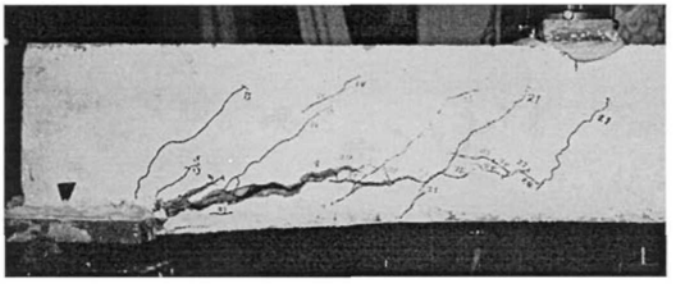

Figure 1.39 '*plate-end shear failure*' of beam with stirrups (CDC debonding)

1.7 Conclusions

It has been shown that there is a very wide variety of forms of plating available to designers in order to develop a retrofitting solution for their problems. Plates of any material or of any shape and size can be adhesively bonded or bolted to any surface of the reinforced concrete structure. The designer can choose or design a plating system for durability, flexural strength, stiffness or ductility, and shear strength. It has also been shown, that there is a general consensus on the debonding mechanisms.

Design rules are now available for all the different forms and for all the debonding mechanisms described in this chapter. Chapter 2 describes IC debonding, which is the dominant mode of debonding as it controls the choice of plate material, size, shape and position. A comparison is also made of the different guidelines for the IC debonding resistance as well as the emerging design philosophies based on the European and Australian approaches. Having chosen the plate size, the analyses for the flexural strength and ductility are described in Chapter 3, where it is shown that the ability or requirement for moment redistribution can have a major effect on the choice and effectiveness of the plating system.

Having now designed for IC debonding, the beam must be checked for CDC debonding. This is first done in Chapter 4 for tension face plates in order to compare the different guidelines directly, and then in Chapter 5 for other forms of plating in which the Australian approach is used as the other approaches are not applicable. Having now designed for CDC debonding and determined the extent of plating required to encompass the critical diagonal crack, the plate is extended further in Chapter 6, if need be, to ensure that PE debonding does not occur. At this stage, all the design rules have been described and implemented, and Chapter 7 is used to illustrate the full extent of the analyses and in particular how combining different forms of plating can often achieve the best results. The European and Australian design philosophies are implemented. However, most of the analysis techniques used in following the design philosophies apply the Australian approach only because this covers all forms of plating.

1.8 References

ACI 440.2R-02 (2002). Emerging Technology Series. *Guide for the Design and Construction of Externally Bonded FRP Systems for Strengthening Concrete Structures.* Reported by ACI Committee 440. American Concrete Institute, Farmington Hills, Michigan, USA.

Blaschko, M., Nierdermeier, R., and Zilch, K. (1998). "Bond failure modes of flexural members strengthened with FRP". *Proceedings of Second International Conference on Composites in Infrastructures*, Saadatmanesh, H. and Ehsani, M. R., eds., Tucson, Arizona, 315-327.

Concrete Society Technical Report No. 55 (2000). *Design guidance for strengthening concrete structures using fibre composite materials.* The Concrete Society. Century House, Telford Avenue, Crowthorne, Berkshire, UK.

fib bulletin 14 (2001). *Externally bonded FRP reinforcement for RC structures. Design and use of externally bonded fibre reinforced polymer reinforcement (FRP EBR) for reinforced concrete structures.* Task Group 9.3 FRP reinforcement for concrete structures. Lausanne, Switzerland.

Oehlers, D. J. and Bradford, M. A. (1995). "Composite Steel and Concrete Structural Members: Fundamental Behaviour". *Pergamon Press,* Oxford.

Oehlers, D.J. and Bradford, M.A. (1999). "Elementary behaviour of Composite Steel and Concrete Structural Members". *Butterworth Heinemann,* Oxford, September.

Oehlers, D.J. and Seracino, R. (2004). "Design of FRP and steel plated RC structures: retrofitting of beams and slabs for strength, stiffness and ductility". Elsevier.

Smith, S.T., Bradford, M.A. and Oehlers, D.J. (1999) "Local buckling of side-plated reinforced concrete beams. Part 1: Theoretical study". *ASCE Structural division, Journal of Structural Engineering,* June, 622-634.

Smith, S.T., Bradford, M.A. and Oehlers, D.J. (1999). "Local buckling side-plated reinforced concrete beams. Part 2: Experimental study". *ASCE Structural division, Journal of Structural Engineering,* June, 635-643.

Smith, S.T., Bradford M.A. and Oehlers, D.J. (2000). "Unilateral buckling of elastically restrained rectangular mild steel plates". *Journal of Computational Mechanics,* Vol.26, No.4, 317-324.

Smith, S.T., Bradford, M.A., and Oehlers, D.J. (2001). "Buckling tests on steel plates restrained at discrete points in the retrofit of reinforced concrete beams", *Proc. ICE, Structs. & Bldgs,* 146(2), 115-127, May.

Teng, J.G., Chen, J.F,. Smith, S.T., and Lam, L. (2002). "FRP Strengthened RC Structures". *John Wiley and Sons.* Ltd. Chichester, England.

Chapter 2: Intermediate Crack (IC) Debonding

2.1 Introduction

The intermediate crack debonding mechanism has been described in Section 1.3.1. It was shown that a crack that intercepts a plate must induce some debonding in the vicinity of the crack to relieve the strain concentrations. This was referred to as IC interface cracking and is of little consequence unless it propagates sufficiently to cause substantial separation of the plate from the concrete which then reduces the strains in the plate. At this stage it is referred to as IC debonding.

Intermediate crack (IC) debonding can be considered the dominant mode of debonding as it affects both the flexural strength and ductility of the beam and, as will be shown in Chapters 4 and 5, it affects indirectly the CDC debonding resistance. The fact that it is referred to as the dominant mode of failure does not necessarily mean that it is the most common mode of failure as analyses of published test data suggest that CDC debonding occurs more often. As IC debonding is a plate strain related debonding mechanism, it generally initiates at the position of maximum moment, as in Fig. 2.1, where the flexural crack intercepts the plate and where the strains in the plate are at their maximum.

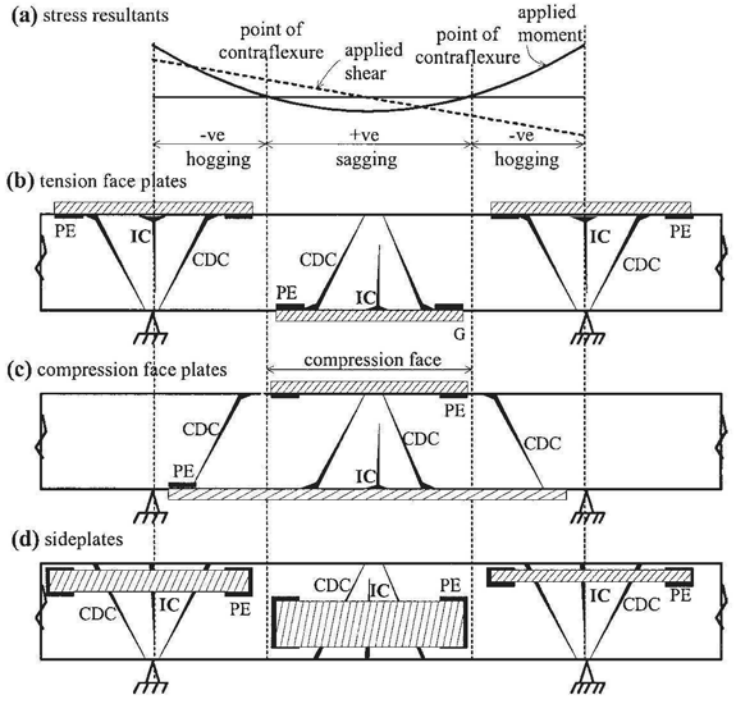

Figure 2.1 Occurrence of IC debonding

Before the flexural strength, flexural stiffness or flexural ductility can be assessed, the strain and stress at IC debonding needs to be determined for plates in

any of the positions shown in Fig. 2.1, which is the subject of this chapter. Examples of IC debonding are first described in this chapter, which is then followed by a description of the IC debonding mechanism in pull tests and in beam tests. From a comparison of the IC debonding resistances, there would appear to be emerging two distinct design philosophies both of which are correct but which are based on significantly differing premises.

2.2 Examples of IC debonding

2.2.1 Adhesively bonded longitudinal plates predominantly in flexure

2.2.1.1 Tension face plates

The IC interface cracks initiate within the region of maximum moment as shown in the tension face plated beam in Fig. 2.2, and then the individual IC interface cracks gradually propagate, from their associated flexural and flexural/shear intermediate cracks, towards the plate ends as can also be seen in Fig. 1.15. Eventually these cracks join up or merge as shown in Fig. 2.3 where only the ends of the plate are attached or anchored.

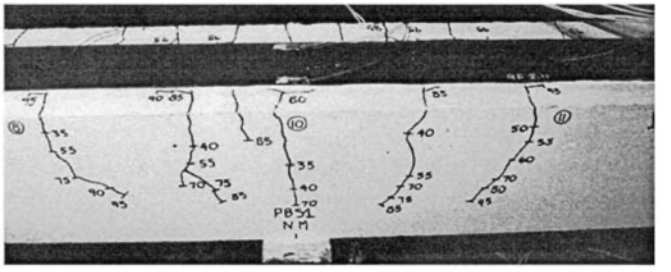

Figure 2.2 IC interface cracking

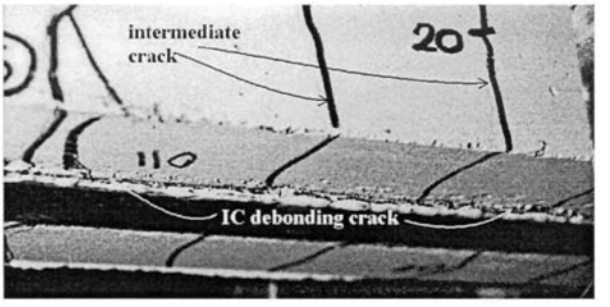

Figure 2.3 IC debonding

At the stage of IC interface cracking shown in Fig. 2.3, where only the plate ends are attached, the plate is acting like an external prestressing rod with uniform strain between the end anchorages so that standard beam theory cannot be applied. This behaviour may be sufficient to cause the strains in the plate to reduce, even though the ends of the plate are still anchored, in which case IC debonding has

occurred. Alternatively, soon after the IC interface cracks merge the debonding cracks spread rapidly to the plate ends causing IC debonding as shown in Fig. 1.1. Tests have shown that the spread of IC interface cracking prior to IC debonding can vary from as little as 10% of the plate length to about 40%, so that the extent of the spread of IC interface cracking is not a reliable guide to eventual IC debonding.

Unlike interface shear stress (VAy/Ib) debonding described in Section 1.3.4, IC debonding is not directly related to the vertical shear force V as it can occur in a constant moment region as shown in Fig. 2.4. The behaviour of IC debonding is more akin to the partial-interaction behaviour of embedded reinforcing bars between flexural cracks or the partial-interaction behaviour of stud shear connectors in composite steel and concrete beams.

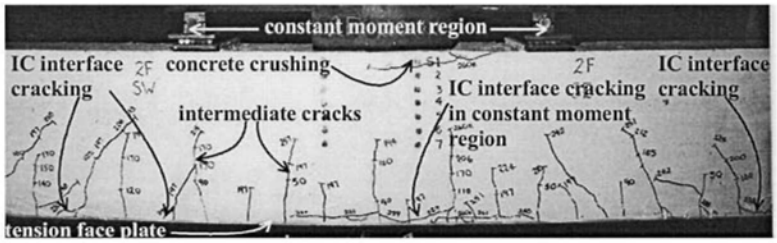

Figure 2.4 IC interface cracking in a constant moment region

2.2.1.2 Side plates

Figure 2.5 shows the hogging (-ve) region of a two span continuous beam in which longitudinal side plates have been adhesively bonded to the tension region of the side of the beam. The side plates have been deliberately extended past the points of contraflexure into what may be termed flexurally uncracked regions. Under the hogging region plate, the ends of the side plates for the sagging regions can be seen, which have also been extended past the point of contraflexure into the uncracked regions. It can be seen that IC debonding and its associated IC interface cracking also occurs in side plated beams. As would be expected, the intermediate cracks mainly consist of inclined flexural/shear cracks that are concentrated in the region of maximum moment. It can also be seen that where these intermediate cracks intercept the longitudinal side plate they induce IC interface cracks at the top and bottom edges of the longitudinal plate that propagate away from the position of maximum moment towards the plate ends. The IC interface cracks on the right hand side have reached the point of contraflexure after which the strains in the strain gauges, which can be seen at the mid-depth of the plate, reduced significantly indicating IC debonding was complete even though the anchorage zones were still attached.

Figure 2.6 shows IC debonding in a steel side plate in which the plate ends were still anchored, which is the same behaviour as the tension face plate in Fig. 2.3. In contrast, Fig. 2.7 shows how IC debonding has caused the end anchorages to debond in all of the longitudinal plates in the two span continuous beam with carbon FRP side plates that were attached to the tension zones.

It is the experience of the authors that the vast majority of plates in adhesively bonded plated beams will debond at some stage of their loading cycle. This is because IC debonding is not solely dependent on the strain in the plate but also depends on the width of the intermediate crack that has to be accommodated by the plate. Hence, even when the applied load is reducing causing the strains in the plate also to reduce,

the plate will still usually debond at some stage of the loading cycle because of the widening of the intermediate cracks. It is, therefore, necessary to design for ductility for which design procedures are available.

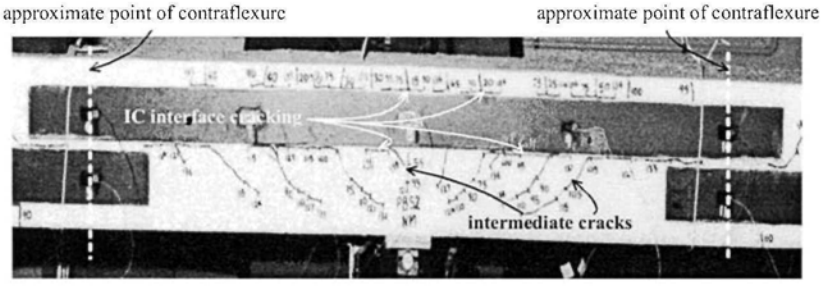

Figure 2.5 IC interface cracking and IC debonding of steel plates

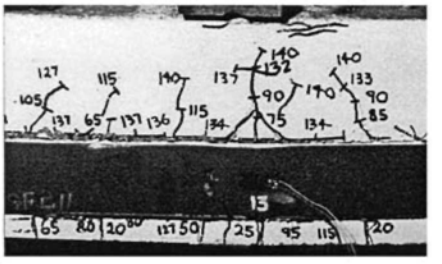

Figure 2.6 IC debonding with plate ends still anchored

Figure 2.7 IC debonding throughout longitudinal carbon FRP side plates

2.2.2 Adhesively-bonded and bolted longitudinal plates predominantly in flexure

Unlike adhesively-bonded plates, bolted plates can exhibit a large amount of ductility as shown in Fig. 2.8. Figure 2.8 is an example of a tension face plate that has been both adhesively-bonded and bolted. Bolts form a ductile connection that requires significant slip in the order of millimeters to transfer the interface shear forces. In contrast, an adhesive bond is a stiff brittle joint that requires slips of the order of micrometers prior to IC interface cracking and only tenths of millimeters after IC interface cracking to resist shear. Hence, the adhesively-bonded and bolted plate in Fig. 2.8 first acts purely as an adhesively bonded plate where it can be seen that the intermediate cracks induce IC interface cracking.

Eventually the IC interface cracks in Fig. 2.8 merge and allow the plate to substantially slip relative to the RC beam. This then allows the bolts to slip to resist the longitudinal shear, as can just be seen in Fig. 2.9(a) by the distance between the bolt head and its original position to the left. This form of plate retrofitting, that is

both adhesively-bonded and bolted was found to be extremely ductile as can be seen in Fig. 2.9(b) where the strains in the plate were sufficient to cause it to fracture.

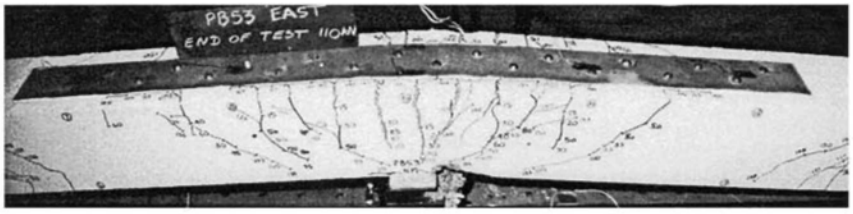

Figure 2.8 Adhesively-bonded and bolted plated beam at failure

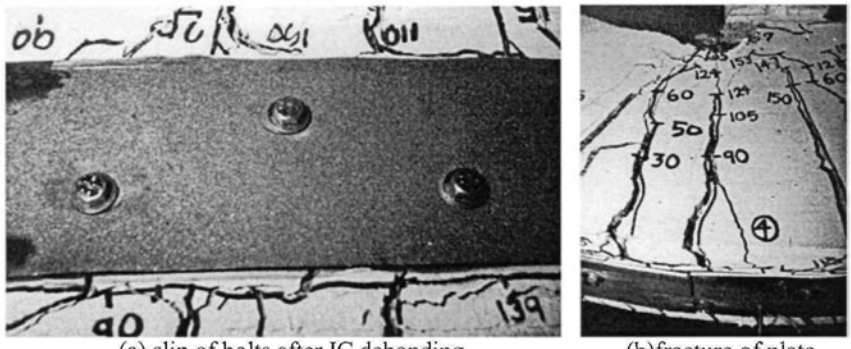

(a) slip of bolts after IC debonding (b)fracture of plate

Figure 2.9 Ductility of a bolted plated beam

As a matter of interest, these tests showed that adhesively-bonded and bolted plated beams behave better than either adhesively plated beams or bolted plated beams. This is probably because after IC debonding the bolts not only resist longitudinal shear but by holding the plate/concrete interface together allow longitudinal shear to be transferred by aggregate interlock. Hence bolting plates or bolting and adhesively-bonding plates are an ideal choice if ductility is required. However, bolting does not affect IC debonding unless the bolts are deliberately pretensioned to impose interface compression; it is felt that this should not be relied upon. It is suggested that bolted and adhesively-bonded plates should be designed as separate bolted and adhesively-bonded structures.

2.2.3 IC debonding resistance contribution to vertical shear

Another example of IC interface cracking which may lead to IC debonding is shown in Fig. 1.16 where it can be seen that the intermediate diagonal cracks have induced IC interface cracking. In this example, IC debonding has not yet occurred. However, Fig. 1.16 does illustrate how the IC debonding resistance indirectly increases the shear resistance of the beam V_c. This is because the longitudinal plate spans the diagonal crack. Should this diagonal crack then try to open up or slip to resist the vertical shear, then the IC debonding resistance of the plate will prevent this shear displacement and help increase the shear capacity, in much the same way as longitudinal reinforcing bars or prestressing increases the concrete shear capacity of a beam or slab V_c.

A further example of the importance of the IC debonding resistance and why it is the dominant debonding mechanism is shown in Fig. 2.10 where external FRP stirrups that span a diagonal crack have detached due to IC debonding as also illustrated in Fig. 1.29; these external stirrups can also rupture if thin enough as when produced by the wet lay up process. Furthermore, if FRP stirrups can be wrapped or anchored in the flange of a T-section then failure can also be by rupture.

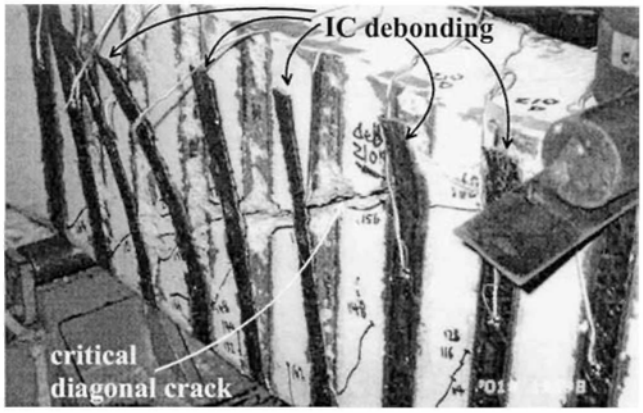

Figure 2.10 IC debonding in vertical FRP stirrups (Jin-Guang Teng)

2.3 IC debonding behaviour

2.3.1 IC debonding in pull-push tests

2.3.1.1 Pull-push tests

The resistance to IC debonding is often determined directly from simple single-lap pull-push tests of a plate-to-concrete joint such as that shown in Fig. 2.11(a). The plate is adhesively bonded to the concrete prism, the concrete is restrained and the plate pulled along its axis until failure occurs either by plate fracture or debonding. Typically, a wedge of concrete is pulled away at the loaded end of the concrete prism as can be seen in Figs. 2.11(b) and (c) and debonding occurs adjacent to the adhesive-concrete interface within the concrete adherend as can be seen in Figs. 2.12 and 1.8(a).

The pull-push specimen in Fig. 2.11(a) is a convenient and inexpensive way of estimating the IC debonding resistance in beams in much the same way as push tests are often used to estimate the shear resistance of new types of shear connectors in composite steel and concrete beams. The pull-push specimen may be considered to represent a beam such as that in Fig. 1.1 but with only a single flexural crack over the support. It is recognised that pull-push tests do not fully represent the behaviour in beams as they do not allow for the curvature in the beam, which may affect the interface normal stress distribution, nor do they allow for the interaction of interface shear stress distributions between closely spaced intermediate cracks. However, pull-push tests are a very convenient and inexpensive way of at least determining the parameters that affect IC debonding. Furthermore, it will be shown later, in Section 2.4.4, that the IC debonding resistances derived from pull-push tests give a lower bound to those derived from plated beams and slabs and, hence, can be used as a safe design option.

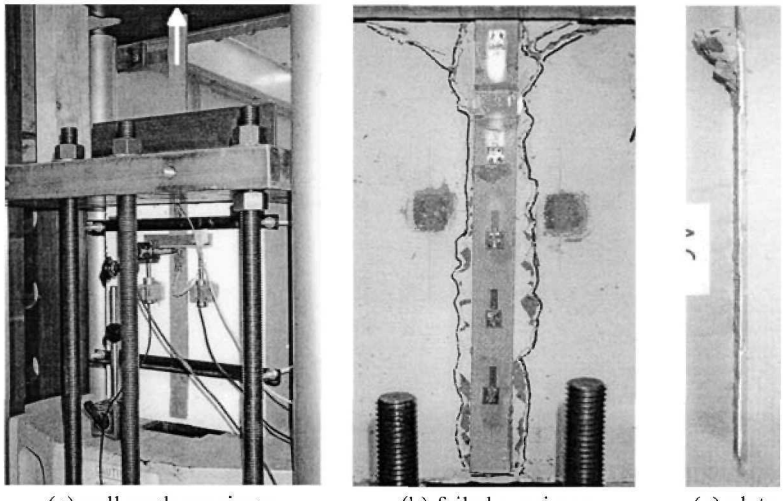

(a) pull-push specimen (b) failed specimen (c) plate

Figure 2.11 IC debonding pull-push specimens

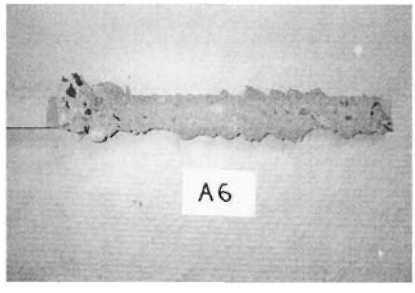

Figure 2.12 IC debonding within concrete

2.3.1.2 Global interface behaviour

The global distribution of the interface shear stress τ_{int} along the length of an adhesively-bonded plate in a pull-push test is shown in Figs. 2.13.

Figure 2.13 is the experimental interface shear stress τ_{int} distribution along the length of a 1.2 mm thick CFRP plate with an average adhesive layer thickness of 2 mm as the axial load in the plate is increased. The origin of the graph is at the loaded end (top) of the concrete prism in Fig. 2.11(b) which represents the position of an intermediate crack. Up to an applied load of 9.8 kN, the plate-to-concrete joint is uncracked and the shape of the shear stress distribution is that given by classical linear elastic theory. As the load is further increased to 42.8 kN, a softening branch develops from the loaded end of the plate indicating the propagation of IC interface micro-cracks which are typically not visible by the naked eye. At this load, the extent of IC interface micro-cracking is approximately 100 mm which is determined by the location of the peak shear stress as it moves towards the end (bottom) of the plate. As the load is increased to the peak load of 51.5 kN, a region of IC interface macro-

cracking develops from the loaded end of the plate and the elastic-softening region of the distribution moves towards the end of the plate. The extent of IC interface macro-cracking, identified by the length of plate from the loaded-end (or intermediate crack) and the start of the softening branch which is approximately 120 mm in Fig. 2.13, is the IC interface debonding crack that is visible as in Fig. 2.2. Under displacement control, a portion of the post-peak response can be observed prior to complete debonding as can be seen by the shear stress distribution at a load of 47.1 kN where the IC interface debonding crack has propagated approximately 150 mm from the loaded-end of the concrete prism.

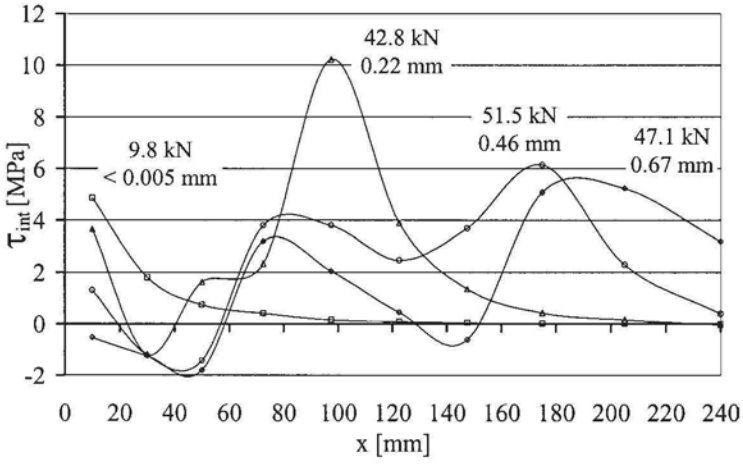

Figure 2.13 Distribution of interface shear stress τ_{int} with applied load and δ_{IC}

The variation in the shear stress distribution observed in Fig. 2.13 within the region of IC interface macro-cracking is a result of local bending of the plate due to the roughness along the IC interface crack. The negative shear stresses within the first 50 mm of the bonded joint after IC interface macro-cracking is an aberration due to the distortion of the strain in the vicinity of the concrete wedge attached to the plate such as at the top of the plate in Fig. 2.11(c).

Also given in Fig. 2.13 is the value of end slip δ_{IC} between the concrete and plate at the loaded end (top) of the concrete prism for the interface shear stress distributions shown. As the top of the concrete prism is equivalent to the position of an intermediate crack (IC), this slip has been referred to as δ_{IC}. It can be seen that very small changes in δ_{IC} cause very large changes in the distribution of τ_{int}.

2.3.1.3 Local and fundamental partial-interaction interface behaviour

(a) Shear-stress/slip

Of special significance is the variation of the interface shear stress τ_{int} with the interface slip δ_{int} at a specific position x along the plate as shown in Fig. 2.14. This variation is very important as it controls the propagation of the IC interface crack and ultimately the IC debonding mechanism and resistance. The τ_{int}/δ_{int} relationship is equivalent to a material property, such as the stress/strain relationship of a material, and if known could theoretically be input into numerical simulations of plated beams to determine IC debonding resistances. The τ_{int}/δ_{int} relationship is the fundamental property that controls IC debonding.

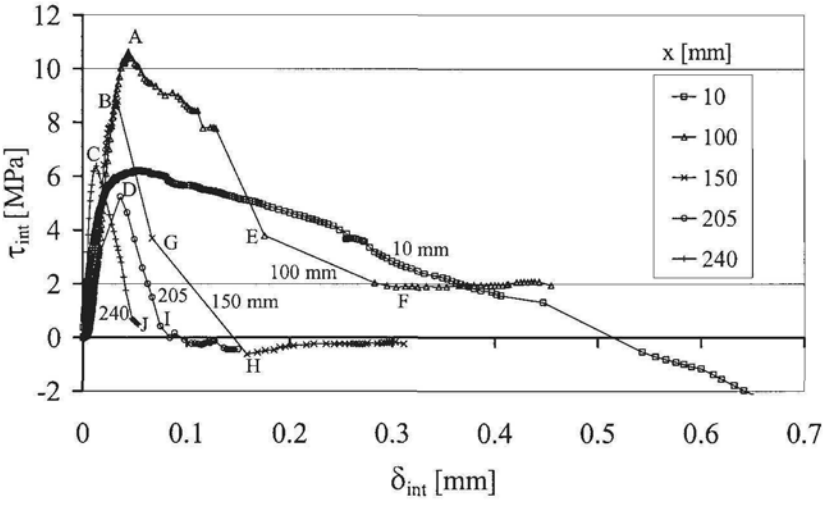

Figure 2.14 Variation of interface shear stess τ_{int} with interface slip δ_{int}

The best analytical solutions of the IC debonding mechanism in pull-push tests have used bilinear local τ_{int}/δ_{int} models such as those shown in Fig. 2.15. Bilinear models consist of an initial linearly ascending branch up to a peak interface shear stress τ_f followed by a linearly descending branch representing interface softening, or micro-cracking, until the interface shear stress reaches zero at which time macro-cracking, or IC interface debonding, is assumed to occur at a slip of δ_f. The absence of any residual shear strength after debonding in the bilinear models imply that friction and aggregate interlock over the debonded length is ignored.

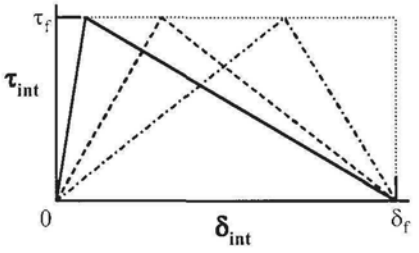

Figure 2.15 Idealised local shear stress slip relationship

Although the local τ_{int}/δ_{int} distributions shown in Fig. 2.14 can be idealised as bi-linear, it is clear that the distribution varies considerably along the length of the bonded joint. With the exception of the local τ_{int}/δ_{int} distribution 10 mm from the loaded-end of the concrete prism, which is affected by the concrete wedge attached to the plate as discussed in the previous section, two trends in the variation can be observed. One is that the peak shear stress, such as A, B, C and D in Fig. 2.14, prior to softening reduces further from the loaded-end, or as interface cracking propagates. Note that the maximum peak interface shear stress occurs locally at a distance of

about 100 mm (line x = 100 mm in Fig. 2.14) which corresponds to the location of the peak stress when a load of 42.8 kN in Fig. 2.13 was applied to the plate; this is the initiation of macro-cracking as described in Fig. 2.13. The second trend is the transition from a bilinear descending or interface softening branch, A-E-F and B-G-A in Fig. 2.14, near the loaded-end of the plate to a linear descending branch, D-I and C-J, towards the end of the plate. The softening response stiffness, the rate of reduction in shear in Fig. 2.14 after the peak shear, is less near the loaded-end of the plate which can be attributed to aggregate interlock and friction along the debonding crack as the interface slip increases. The frictional component is of course a function of the normal stress distribution across the bonded joint which in pull-push tests is highest near the loaded-end of the plate. Once softening begins near the end of the plate for longer bonded lengths the IC interface crack propagates rapidly and hence, there is no stiffening of the softening branch. However, as expected, one similarity between the local τ_{int}/δ_{int} distribution is the slope of the initial ascending branch as the interface is linear elastic within this region.

Factors that affect the local τ_{int}/δ_{int} distribution in pull-push tests include the material properties of the adherends E_p and E_c, the concrete strength, and geometric properties t_p and b_p/b_c. The influence of these factors on the IC debonding resistance is discussed in Section 2.4. Another factor that as of yet has not been adequately considered is the stiffness of the adhesive layer E_at_a.

The τ_{int}/δ_{int} relationships for both the IC interface cracking of an adhesively bonded plate and that for an embedded reinforcing bar are compared in Fig. 2.16. It can be seen that embedded reinforcing bars have a ductility that is an order of magnitude greater than that of the plate, that is the slip capacity is much greater and the bond strength over this slip is fairly constant. Hence, the design principles applied to the anchorage of reinforcing bars cannot be applied to the anchorage of adhesively bonded plates. Because the bond/slip characteristics of embedded reinforcing bars is characteristically ductile, it is a standard design procedure to assume the bond strength is constant over the anchor zone in calculating the anchorage length required. This same principle cannot be applied to adhesively bonded plates as the bond characteristics are brittle.

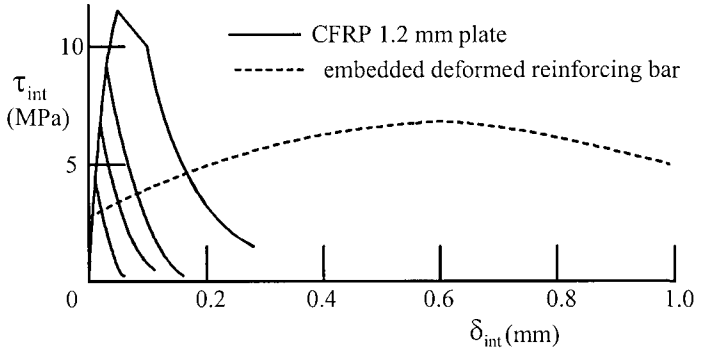

Figure 2.16 Comparison of plate and reinforcing bar τ_{int}/δ_{int} relationship

(b) Plate-axial-stress/slip

Finally, the variation of the plate stress at the intermediate crack $\sigma_{p,IC}$ with the slip at the same position δ_{IC} is shown in Fig. 2.17. This local behaviour at the intermediate

crack is a function of the global variation of τ_{int}/δ_{int} between intermediate cracks, that is the local variation σ_{IC}/δ_{IC} at an intermediate crack represents the behaviour between cracks. The $\sigma_{p.IC}/\delta_{IC}$ relationship for adhesively plated structures is equivalent to the load/slip relationship of shear connectors in composite steel and concrete beams. Stud shear connectors in composite steel and concrete beams can fail prematurely due to excessive slip and this is the situation with plated beams. This analogy helps to illustrate the similarity between these two systems and the fact that it is a partial interaction problem, that is there is a step change in the strain profile between the plate and the RC beam due to the slip, which was first solved for linear elastic composite beams by Newmark (1951).

The variation of plate stress with end slip is easily obtained from pull-push tests and can be used to identify the initiation of micro-cracking and macro-cracking as indicated in Fig. 2.17 by the abrupt changes in the response of the bonded joint. It has been shown (Yuan et al 2003) how these points on the $\sigma_{p.IC}/\delta_{IC}$ response can be used to define the bilinear local τ_{int}/δ_{int} model discussed in the previous section. Furthermore, experimental and parametric studies have shown that by increasing the bond length the ductility of the bonded joint can be increased and increasing the stiffness of the plate per unit width (E_pt_p) increases σ_{IC} at IC debonding at the expense of a reduced ductility.

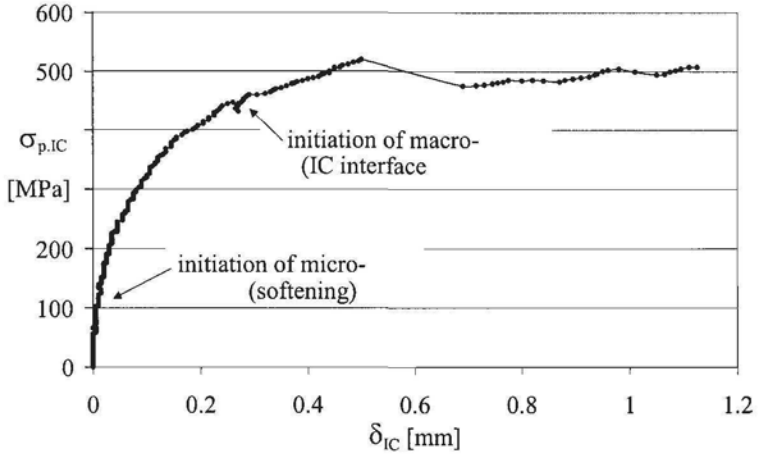

Figure 2.17 Variation of plate stress $\sigma_{p.IC}$ with end slip δ_{IC}

2.3.2 *IC debonding in beams*

2.3.2.1 IC interface crack propagation

The two span continuous beam in Fig. 2.18 is plated over its hogging region. The plates are terminated well past the points of contraflexure and close to the applied loads so that it can safely be said that the plates are anchored in an uncracked region.

IC debonding of a steel tension face plate is shown in Fig. 2.19. These beams were specifically designed so that IC debonding would precede PE debonding as well as precede CDC debonding and, hence, the absence of any critical diagonal cracks in the beam. The point of contraflexure can be estimated to lie approximately midway along the flexurally uncracked region E-D and so it can be seen that the plate was terminated well into the compression face and, hence, anchored in an uncracked

region. As designed for, PE debonding which propagates from the plate ends inwards, did not occur so that the only mechanism of debonding which occurred in this beam was IC debonding.

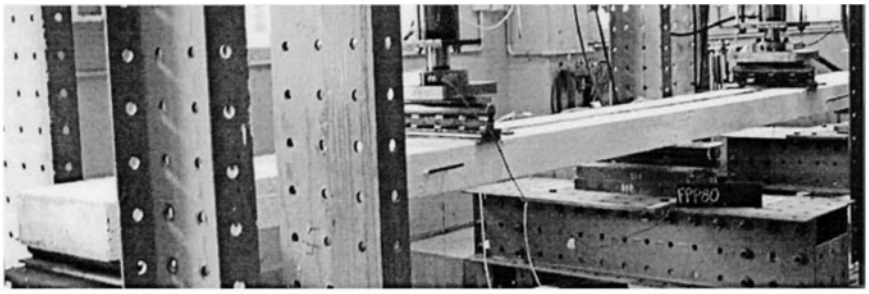

Figure 2.18 Two span continuous beam plated in hogging region

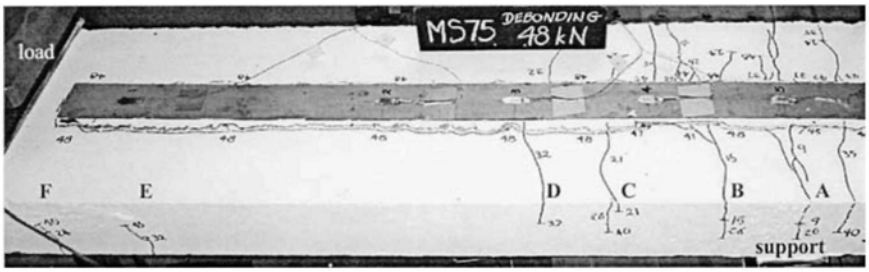

Figure 2.19 IC debonding failure of a steel tension face plated beam

The sequence of cracking is illustrated in Figs. 2.20 and 2.21 for a CFRP plate of the same length and width as the steel plate in Figs. 2.18 and 2.19. A flexural crack first formed over the support at a load that is marked 9 in Fig. 2.20(a) and from this intermediate crack, interface cracks propagated in both directions toward the plate ends. Further flexural cracks then occurred as the load was increased from 24 kN to 35 kN in Fig. 2.20(b) and from each emanated an IC interface crack which propagated towards the nearest plate end, that is away from the internal support. Hence in general, except for the flexural crack at the position of maximum moment where the IC interface crack propagated in both directions, the IC interface crack propagates in one direction towards a region of lower moment. At the load of 35 kN, the IC interface cracks are still concentrated close to the position of maximum moment. A further increase in load from 35 kN to 45 kN in Fig. 2.21 caused IC debonding as the IC interface crack propagated more rapidly to the point of contraflexure, and then at 45 kN it continued very rapidly towards the plate end in the anchorage zone although the plate end still remained attached.

Figure 2.19 illustrates the difference between IC debonding in a beam and IC debonding in a pull-push test as in Fig. 2.11(b). In Fig. 2.19, the force in the plate is transmitted from the concrete in the *uncracked* zone E-D which is equivalent to the pull-push specimen in Fig. 2.11(b), plus the force in the concrete between what is sometimes termed the concrete teeth D-C, C-B and B-A. Hence in this example, there are 4 zones in the shear span, bordered by the intermediate cracks, through which

shear forces can transmit the axial forces in the plate. These four zones pull the plate but may not necessarily achieve their maximum force at the same time which adds to the complexity of the problem. These concrete teeth are equivalent to the shear connectors in composite steel and concrete beams and their individual $\sigma p_{.IC}/\delta_{IC}$ behaviours (as described for pull-push tests in Section 2.3.1.3 and in Fig. 2.17) control the axial force in the plate. It is an irony of this mechanism that intermediate cracking may actually help to increase the force in the plate above that achieved from pull-push tests. It must be emphasised that this is a simplistic description of the shear force mechanism which it is felt is much more complex as it is also affected by the curvature in the beam.

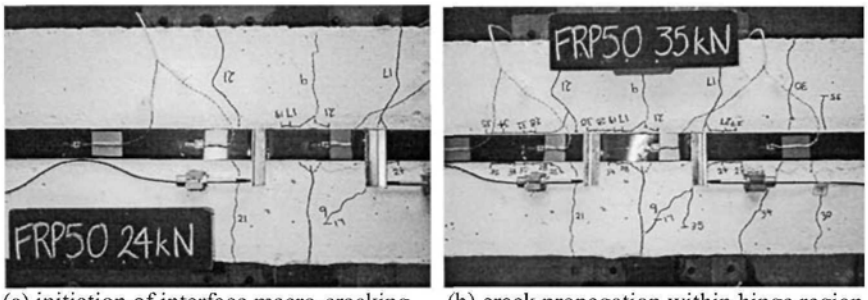

(a) initiation of interface macro-cracking (b) crack propagation within hinge region

Figure 2.20 IC interface cracking

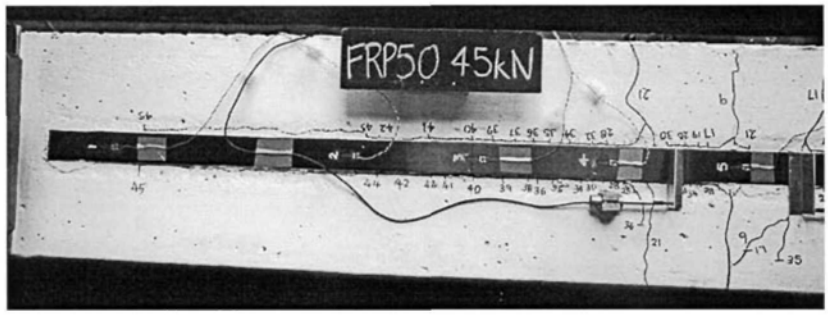

Figure 2.21 IC debonding crack propagation to uncracked anchorage zone

2.3.2.2 IC interface crack propagation simulations

Much research is still required to develop practical models that can adequately quantify the IC debonding stress of plates bonded within cracked regions of beams or slabs. However, several researchers (Monti et al 2003, Niu and Wu 2003) have developed fully non-linear finite element models to determine the influence of intermediate cracks on the interface shear stress distribution and IC debonding stress.

Except for the effect of curvature, it is generally accepted that pull-push tests are a good approximation of the behaviour in flexural members where IC debonding is controlled by a single dominant intermediate crack as may be the case in cantilever slabs, or where intermediate cracks are spaced far apart as in lightly reinforced members or strengthened plain concrete members. However, the IC debonding stress

obtained from pull-push tests is a lower bound to the IC debonding stress in flexural members where intermediate cracks are spaced closer than two times the effective length of the plate. The effective length of an adhesively bonded plate is commonly defined as the bond length under linear elastic deformation over which the interface shear stresses resist a minimum of 97% of the applied load for a joint with an infinite bond length. For example, for the pull-push test results shown in Fig. 2.13, the effective length at the linear elastic load limit of 9.8 kN is approximately 100 mm. When intermediate cracks are spaced closer than twice the effective length there is an interaction of the interface shear stress distribution between cracks. Within an uncracked block between intermediate cracks the interface shear stresses are in opposite directions and the resultant distribution may be simply obtained by superposition. The end result is that a larger force in the plate is required to propagate the IC interface debonding crack. In other words, the propagation of the debonding crack in one direction is hindered by the interface shear stresses acting in the opposing direction from the adjacent crack which must first be overcome before propagation continues towards the plate ends, eventually leading to complete IC debonding.

2.4 Comparison of IC debonding rules

2.4.1 Effective length or anchorage length concept

The axial force to cause debonding in a pull-push test, such as that shown in Fig. 2.11, depends on the length of plate bonded to the concrete. The typical variation obtained from pull-push tests in Fig. 2.22(a) is illustrated in Fig. 2.22(b). As the bonded length of the plate l_b is increased, the force in the plate to cause debonding P_{IC} also increases as shown. However, beyond a certain length L_e, the force to cause debonding remains constant at $(P_{IC})_{max}$; of course $(P_{IC})_{max}$ is limited by the force to fracture an FRP plate or yield a metal plate. As discussed in Section 2.3.1.1, this maximum resistance $(P_{IC})_{max}$ is because the IC interface crack bond behaviour is predominantly brittle as illustrated in Fig. 2.15. The minimum anchorage length of plate required to achieve the maximum axial force in the plate $(P_{IC})_{max}$ is often referred to as the effective length L_e. This anchorage length is typically 50 to 100 times the plate thickness t_p. As an example, for a 1.2 mm thick pultruded CFRP plate L_e may only be about 100 mm which is very short whereas for 7 mm steel plates it may be in the order of about half a meter.

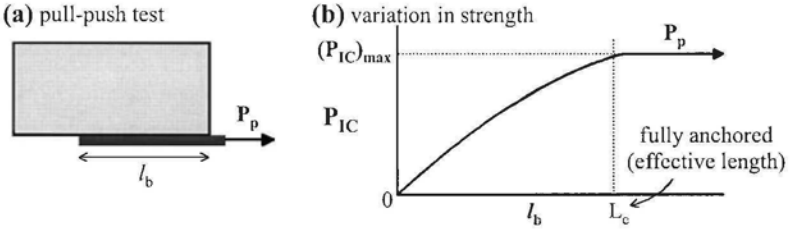

Figure 2.22 Effective length (anchorage length)

2.4.2 Effective width concept

Tests have also shown that the width of a plate b_p as a proportion of the width of the concrete element b_c, that is the parameter b_p/b_c as illustrated in the symmetrically

plated beam in Fig. 2.23(a), can also affect the debonding strength. This is a result of the interaction of the stress field in the disturbed region surrounding individual plates when they are placed close together, as shown in the top plates in Fig. 2.23(b). Placing the plate close to the edge of a concrete element, as in the bottom plate in Fig. 2.23(b), will also have the same effect by reducing the width of the debonding plane.

It is not always clear what width of the concrete element should be used in the parameter b_p/b_c when the plate is placed eccentric to the overall width of the concrete element as shown in Fig. 2.23(c). It is suggested that the principles used in national standards in determining the effective width of a beam allowing for shear lag or the principles used in determining the effective width of the concrete element resisting the anchorage forces in a post-tensioned beam can be used (Oehlers and Bradford 1999). Examples of these effective widths are shown in Fig. 2.23(c) in terms of the half effective widths $b_c/2$ where the smaller of the half widths $(b_c/2)_1$ and $(b_c/2)_2$ should be used in determining b_c. A similar approach can be used for interacting plates as in Fig. 2.23(d) where the mid-distance between plates is used as one boundary.

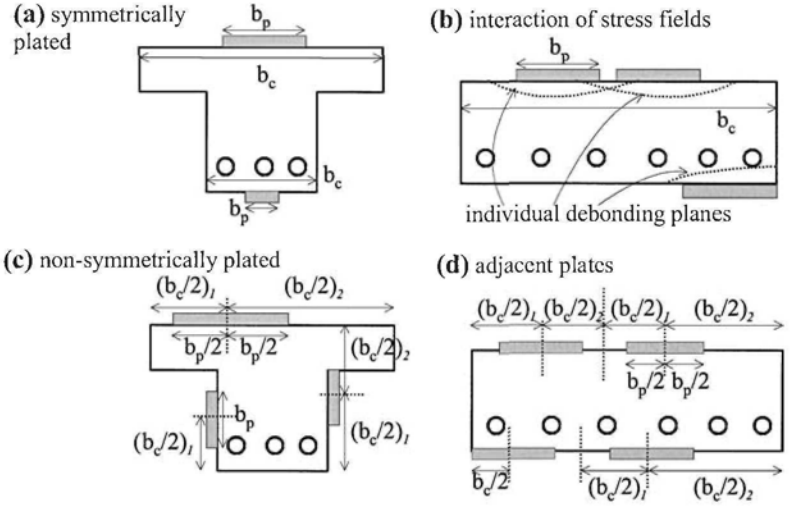

Figure 2.23 Effective widths

2.4.3 IC debonding resistances

Teng et al (2001) have published a comprehensive and excellent analysis of the IC debonding resistances of FRP and steel plated tests as well as a comparison of published debonding equations. They recommended the following form of equation for the IC debonding resistance for fully anchored plates based on fracture mechanics and experimental data.

$$\sigma_{IC} = \alpha\, \beta_p \beta_L \sqrt{\frac{E_p \sqrt{f_c}}{t_p}} \qquad \text{N and mm} \qquad 2.1$$

The parameter β_p allows for the width of the plate relative to the width of the concrete element as explained in Section 2.4.2 and is given by the following expression.

$$\beta_p = \sqrt{\frac{2 - b_p/b_c}{1 + b_p/b_c}} \qquad 2.2$$

Although a limit was not placed on the parameter b_p/b_c, it is recommended that $b_p/b_c \geq 0.33$ as recommended in the European guidelines (Table 1.1).

The full anchorage length or effective length of a plate in a pull-push test or in an uncracked zone is given by

$$L_e = \sqrt{\frac{E_p t_p}{\sqrt{f_c}}} \qquad \text{N and mm} \qquad 2.3$$

Tests have shown that when the bonded length l_b is less than L_e in Fig. 2.22, the strength varies according to the following function as shown in Fig. 2.22(b).

$$\beta_L = \begin{cases} 1 & \text{if } l_b \geq L_e \\ \sin[\pi L/2L_e] & \text{if } l_b < L_e \end{cases} \qquad 2.4$$

However, it is suggested that where possible all plates should be designed as fully anchored ($l_b > L_e$) and hence $\beta_L = 1.0$, if not then for a safe design and to simplify the analysis, the variation could be considered linear between $l_b = 0$ to $l_b = L_e$.

The α coefficient in Eq.2.1 was calibrated using a large number of tests that included steel plates, FRP plates, pull-push tests, slab tests and beam tests and the results are summarised in Table 2.1. Within these tests the plate thickness t_p varied from 0.11 mm to 3 mm, the Young's modulus E_p from 29 GPa to 230 GPa, and the concrete cylinder compressive strength f_c from 20 MPa to 48 MPa. The mean value of the α coefficient is given in row 1 and the 95% characteristic value in row 2.

Table 2.1 IC debonding coefficient α

α	pull tests			slabs	beams	slabs & beams
(1)	(2)	(3)	(4)	(5)	(6)	(7)
	FRP	Steel	Steel & FRP	-	-	-
(1) mean	0.448	0.401	0.427	0.720	1.100	0.887
(2) 95%	0.322	0.324	0.315	0.478	0.544	0.379

The α coefficient of 0.427 corresponding to the mean strength in Table 2.1 for all the pull-push tests in column 4 is less than that in slabs and beams of 0.887 in column 7. This suggests that the IC debonding mechanism in flexural members, described in Section 2.3.2, in which the *concrete teeth* created by the intermediate cracks, and which act as shear connectors can significantly increase the axial force in the plate (in this case allow the axial stress to be doubled). Possibly of more significance is that doubling the α coefficient in Eq.2.1 will allow the plate thickness to be quadrupled. However, the scatter of results, as represented by the 95% characteristic values in row 2 of Table. 2.1, is very large suggesting much more research is required to identify and quantify the parameters that control IC debonding.

2.4.4 Comparison of IC debonding resistances

A comparison of recommendations for IC debonding resistances is given in Table 2.2. To help in the comparison, the properties of the FRP plate used in Table 2.2 were assumed to be: E_p = 160 GPa; f_c = 30 MPa, t_p = 1.2 mm unless shown otherwise; and b_p/b_c = 0.5. In the first four rows in Table 2.2, the Chen and Teng results are based on the Hong Kong approach, Neubauer and Rostasy from the European approach, and both the Concrete Society and the German Institution of Construction from the British approach, as listed in Table 1.1. The remaining rows from 5 to 9 are the results from plated beam tests from The University of Adelaide. Rows 5 and 6 are the results from FRP plated tests with 1.2 mm plates which were increased to 2.4 mm thick in row 7. The results of 3 mm thick steel plated beam tests are included in rows 8 and 9 for comparison. The strains at debonding are listed in columns 1 for the 95% characteristic value and in row 2 for the mean value where given. Where columns 1 and 2 are combined, these are recommendations or test results. The stresses at debonding are listed in rows 3 and 4 and where combined are also the recommended or test results.

Table 2.2 FRP IC debonding resistances

Source	ε_{IC} **95%** (1)	ε_{IC} **mean** (2)	σ_{IC} **[MPa] 95%** (3)	σ_{IC} **[MPa] mean** (4)
1) Chen and Teng	0.0027	0.0053	427	854
2) Neubauer and Rostasy	0.0026			
3) Concrete Society	0.0060 - 0.0080		960 - 1,280	
4) German Inst. of construction	0.0065 - 0.0085		1,040 - 1,360	
5) Adelaide FRP beam tests 1999	0.0046 - 0.0052		782 - 884	
6) Adelaide FRP beam tests 2002	0.0025 - 0.0027		425 - 459	
7) Adelaide FRP beam tests 2002 (2.4 mm)	0.0015		255	
8) *Adelaide Steel beam tests 1999 (3 mm)*	*0.0201 - 0.0213*			
9) *Adelaide Steel beam tests 20002 (3 mm)*	*0.0045*			

The effective length of the 1.2 mm FRP plates in Table 2.2 was derived as 187 mm from Chen and Teng's model and 189 mm from Neubauer and Rostasy which shows a good agreement. By convention, the characteristic debonding strains in column 1 are the strains which would be used in design with an appropriate strength reduction factor. In column 1, Chen and Teng's characteristic debonding strain of 0.0027 is in close agreement with Neubauer and Rostasy's 0.0026, is significantly less than the test results in row 5 and is about the same as the test results in row 6. Chen and Teng's mean value of 0.0053 is in agreement with the test results in row 5. Chen and Teng's mean and characteristic results, Neubauer and Rostasy's characteristic result, and the tests results in rows 5 and 6 are well below the range of recommendations by the Concrete Society and the German Institution of Construction in rows 3 and 4 which should therefore be used with extreme caution. In row 7, the plate thickness was doubled and as would be expected the debonding strains reduced.

In row 8 in Table 2.2, the steel plated beams first yielded and then debonded at strains that were an order of magnitude greater than in the FRP tests in rows 5 and 6. This illustrates how, unlike FRP plates which are elastic/brittle, metal plates can be designed to yield prior to debonding and also how debonding still occurs after yielding as explained previously in Section 2.2.1.2. Also included in row 9 are the results of more recent tests in which the steel plates also yielded prior to debonding

but then debonded at much lower strains than those in row 8. The variations between test results illustrate the complexity of the problem. For example, another parameter in addition to intermediate crack spacing and curvature that may affect the IC debonding behaviour is adhesive stiffness $E_a t_a$ which is not considered by existing models as discussed in Section 2.3.1.3.

In Table 2.3, are listed the plate thicknesses in columns 3 and 4 at which the IC debonding resistance of a fully anchored metal plate is equal to its yield capacity. Hence, plate thicknesses below these values will yield prior to debonding. A mild steel plate, of E_s = 200 GPa and f_y = 300 MPa, and two aluminium plates, with E_{al} = 63 GPa and with different yield capacities of 125 MPa and 215 MPa, as listed in rows 1 to 3 and are used in this comparison. The results based on the characteristic debonding resistances are given in column 3. For steel plates the maximum thickness is about 3 mm. As the aluminium has a Young's modulus about one-third that of steel, it is more likely to debond as shown in Eq.2.1. Hence, for high yield capacity aluminium only very thin plates of about 2 mm can be used but thicker plates of 5 mm can be used if the aluminium has a low yield strength. It is worth comparing the plate thicknesses in column 3 that are based on the characteristic resistances with those in column 4 which are based on the mean resistances. It can be seen that if the mean values could be used, then the plate sizes could be quadrupled.

Table 2.3 IC debonding of metal plates

Metal	E [GPa] (1)	Ultimate			Serviceability	
		f_y [MPa]	$t_{p\_95\%}$ [mm]	t_{p_mean} [mm]	f_s [MPa]	$t_{p\_95\%}$ [mm]
		(2)	(3)	(4)	(5)	(6)
1) Steel	200	300	**3.0**	12.1	150	**12**
2) Aluminium	63	125	**5.6**	22.0	63	**22**
3) Aluminium	63	215	**1.9**	7.5	107	**8**

Not only are adhesively bonded plates used to increase the strength of a structure, but they are often used to improve their serviceability behaviour such as to reduce deflections or vibrations. For convenience, it has been assumed that the serviceability stresses listed in column 5 are half the yield stresses in column 2 in Table 2.3. The maximum plate thicknesses for these serviceability stresses are listed in column 6. These can be compared with those for the ultimate strength limits in column 3. As the plate stresses have been halved, the plate thicknesses have quadrupled. This illustrates how thick metal plates can be used at serviceability. However, the thicknesses given in column 6 should be viewed with caution as it is doubtful whether Teng's model (Eq.2.1) was calibrated with plates of these thicknesses.

2.5 IC debonding design philosophies

From the design guidelines listed in Table 1.1, there would appear to be two distinct design philosophies that are emerging. The Australian and Hong Kong approaches restrict IC interface cracks to a region around the position of maximum moment and this will be referred to as the *hinge approach*. Alternatively, in the European approach, the plate ends are anchored in an uncracked region where the IC interface

cracks are allowed to propagate and this will be referred to as the *anchorage* approach.

2.5.1 Anchorage design philosophy

The anchorage design philosophy developed in Europe (Table 1.1), which is only applicable to tension face plates, is illustrated in Fig. 2.24. In order to design for IC debonding at the positions of maximum moment, the tension face plates in both the hogging and sagging regions have to be terminated in uncracked regions indicated by the hatched areas. This suggests that the plates should be extended at least up to the points of contraflexure as shown. The axial force in the plate is, therefore, the sum of the forces imposed by each concrete tooth, formed by the intermediate cracks as shown, over half a region (that is half the hogging or half the sagging region) that is ΣP_{IC_tooth}. Plus the anchorage force in the uncracked region which is assumed to be the pull-push test strength P_{pull_test}. Hence the axial force in the plate P_p is given by

$$P_p = \sum P_{IC-tooth} + P_{pull-test} \qquad 2.5$$

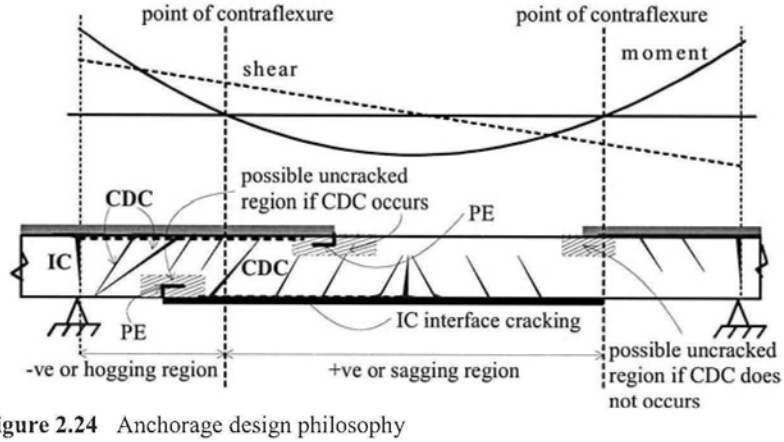

Figure 2.24 Anchorage design philosophy

One design difficulty that might occur on occasions is identifying an uncracked region with which to anchor the plates. For example, the anchorage design approach requires that the sagging region plate in Fig. 2.24 is extended towards the points of contraflexure. Hence, the plate ends are being extended into regions where the vertical shear force is increasing. There is, therefore, the possibility that the plates are being extended in regions where critical diagonal cracks will occur. If we are dealing with a beam with stirrups, then there may be a chance that the sagging region plates cannot be anchored in a region void of shear cracks. In contrast, if we are dealing with a slab, then there is a good chance that the plate can be anchored in a region void of critical diagonal cracks, as slabs are usually designed for only the concrete component of the vertical shear capacity V_c, that is they are usually designed without stirrups so that critical diagonal cracks do not occur. The hogging region plates in Fig. 2.24 are less of a problem, as the plates are being extended into regions where the vertical shear force is reducing. Hence, it should be possible to find an uncracked region.

Having designed for IC debonding in Fig. 2.24, CDC debonding still has to be checked in each region. Although, because of the distribution of vertical shear, the plate is more likely to fail by CDC debonding in the hogging region than in the sagging region. PE debonding still has to be checked but this is unlikely to be a problem as the plates having to be anchored in an uncracked region will probably be terminated near the points of contraflexure where the curvature is low. However, it should be remembered that PE debonding can occur in plates terminated in compression faces but they are less likely to debond than tension face plates.

In summary, it can be seen that the anchorage approach allows high stresses in the plate. This is because the axial force in the plate is contributed by both the ΣP_{IC_tooth} and P_{pull_test} components. Hence relatively small but highly stressed cross-sections of plate are required, however, the plate has to be extended over the whole hogging or sagging region. It is very important to recognise the fact that the anchorage design approach prevents IC debonding from interacting with PE debonding. The authors do not know of any research that has studied this interaction and feel that the best solution is to prevent this interaction as this approach does.

2.5.2 *Hinge design philosophy*

The hinge design philosophy proposed by the Hong Kong (Table 1.1) and Australian (Table 1.1) approaches is summarised in Fig. 2.25. In this approach, the axial force in the hogging and sagging region plates at the positions of maximum moment are restricted to the IC debonding resistance in pull-push tests.

$$P_p = P_{pull-test} \tag{2.6}$$

As shown in Eq.2.5, the force required to debond a fully plated beam is $\Sigma P_{IC\text{-}tooth}$ + $P_{pull\text{-}test}$, hence, restricting the plate force to $P_{pull\text{-}test}$ will limit the IC interface cracks to the region near the position of maximum moment where a plastic hinge may occur indicated by the hatched areas in Fig. 2.25. As the plates in the hogging and sagging regions in Fig. 2.25 do not have to be anchored in uncracked regions, the extent of these plates is determined by CDC and PE debonding and, hence, the plates can be terminated short of the points of contraflexure.

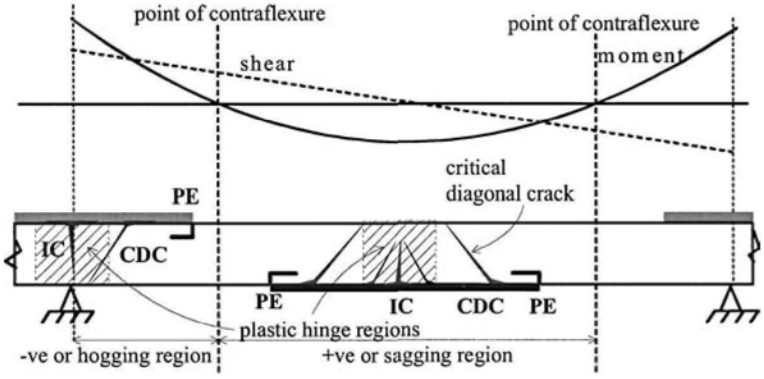

Figure 2.25 Hinge design philosophy

In the hinge approach, the plate is only allowed to carry a smaller force than in the anchorage approach so that a larger cross-section of plate is required for the same increase in strength. However, a shorter plate than in the anchorage approach can be used. As the anchorage approach allows higher strains in the plate than in the hinge approach, the anchorage approach will allow greater curvatures and hence may be more suitable where ductility is required. The hinge approach has the advantage that the IC debonding resistance can be determined directly from pull-push tests. As with the anchorage approach, it is very important to realise that the hinge approach prevents any interaction between IC and PE debonding as it restricts IC interface cracking to within the hinge region.

Both design philosophies are correct; they just approach the problem in different ways. An analogy can be made with earthquake design where the structure can be made very strong to directly resist the earthquake forces, or the structure can deliberately be made ductile to absorb the earthquake energy as it becomes non-linear. Both design philosophies are correct and the engineer can choose the appropriate one. However, the design philosophies should only be combined with care. For example, restricting the axial force in the plate to P_{pull_test} and anchoring the ends in uncracked regions is very safe. However, designing for the maximum theoretical force $\Sigma P_{IC\_tooth} + P_{pull\_test}$ and then terminating the plate short of an uncracked region is very unsafe. In comparison, the anchorage approach requires small cross-sections of highly stressed plates over long lengths, whereas the hinge approach requires large cross-sections of low stressed plates over short lengths.

2.6 Conclusions

If nothing more, this chapter has illustrated the complexities of IC debonding. It has been shown how IC debonding can be considered as a partial interaction problem as the progression of the IC interface crack allows slip between the plate and the concrete. However, and more importantly, there is also partial interaction because of the creation of plated concrete teeth between the intermediate cracks which act in a similar fashion to shear connectors in partial interaction composite steel and concrete beams. It should be recognised that this unique and highly original approach is proposed by both Niedermeier and Matthy in the European guideline (Table 1.1).

It has also been shown why IC debonding cannot be dealt with using the VAy/Ib approach, how bonded plates cannot be treated as reinforcing bars, and how bolting adhesively bonded plates can produce a highly ductile section. The very advanced work on the IC debonding resistance of Neubauer and Rostasy in the European guideline (Table 1.1) and that of Chen and Teng in the Hong Kong approach (Table 1.1) has given designers a comprehensive and safe tool to use in IC debonding design. In particular, the work of Chen and Teng in showing the difference in the IC debonding resistances in pull-push tests and beam tests should be recognised as it independently confirms the work of Niedermeier and Matthy.

Because of the work of Niedermeier and Matthy, Neubauer and Rostasy, and Chen and Teng, there would appear to be two emerging design philosophies. The *anchorage approach* extracts as much as possible from the plate by allowing for partial interaction but requires the entire hogging or sagging region to be fully plated. Hence, this approach leads to the minimum cross-sectional area of a highly stressed plate but over the longest length. In contrast, the *hinge approach* restricts the IC interface cracking to a small hinge area by limiting the strains in the plate. Hence, this

approach leads to a larger cross-sectional area of plate than in the anchorage approach, that is less stressed and required over a shorter length. Both approaches are correct and it is up to the designer to choose the most appropriate one. The anchorage approach does allow higher strains and hence higher ductility and the hinge approach allows the IC debonding resistance to be determined directly from pull-push tests. In both design philosophies, metal plates can be designed to yield prior to IC debonding to allow increases in ductility.

This chapter has not only qualitatively described the fundamental behaviour of IC debonding, but also provided quantitative design rules for determining the IC debonding resistance at the positions of maximum moment in the hogging and sagging regions in Fig. 2.1. In chapter 3, this will be used to quantify the flexural capacities, flexural stiffnesses and flexural ductilities.

2.7 References

Monti, G., Renzelli, M. and Luciani, P. (2003) "FRP adhesion in uncracked and cracked concrete zones." *Proceedings of the 6th International Symposium on FRP Reinforcement for Concrete Structures* (FRPRCS-6), World Scientific Publishing Company, Edited by: K.H. Tan, Singapore, 8-10 July, pp 183-192.

Newmark, N.M.., Siess C.P. and Viest I.M. (1951). "Tests and analysis of composite beams with incomplete interaction." *Proceedings Society for Experimental Stress Analysis*, 9, No.1, pp.75-92.

Niu, H.D. and Wu, Z.S. (2003) "Debonding and failure mechanisms of FRP-strengthened R/C beams influenced by flexural cracks." Submitted to *Journal of Composites for Construction, ASCE.*

Oehlers, D.J. and Bradford, M.A. (1999). *Elementary behaviour of Composite Steel and Concrete Structural Members.* Butterworth Heinemann, Oxford, September.

Teng, J.G., Chen, J.F,. Smith, S.T., and Lam, L. (2002). *FRP Strengthened RC Structures.* John Wiley and Sons. Ltd. Chichester, England.

Yuan, H., Teng, J.G., Seracino, R., Wu, Z.S. and Yao, J. (2003) "Full-range behavior of FRP-to-concrete bonded joints: A closed-form analytical solution." Submitted to *Engineering Structures.*

Chapter 3: Flexural Strength and Ductility

3.1 Introduction

The strains at which IC debonding occurs have been quantified in Chapter 2. These IC debonding strains are now used in this chapter to determine the flexural capacities and flexural ductilities at sections of maximum moment, such as those shown in Fig. 2.1, and also the ability of the beam to redistribute moment between hogging and sagging regions for any form of plated beam with any type of plate material.

Adhesively bonded plated structures will probably debond at some stage of their load cycle; for example, debonding can occur prior to the tension reinforcing bars yielding, whilst the concrete is still elastic or while the flexural strength is reducing in the falling branch. Hence, the problem of ductility is very important in plated structures. The elementary concepts of ductility are first described and may cover basic ideas already familiar to the reader. This is followed by a section on moment redistribution, because it will be shown that often the choice of the plating material and technique is governed by the ability to redistribute moment. In fact, it will be shown through worked examples in Chapter 7 that, in some cases, if moment redistribution is not allowed or cannot be allowed then the increase in strength due to plating may be minimal and the structure not worth plating.

Having allowed for moment redistribution, the designer now knows the required moment capacities at the positions of maximum moment to resist the applied load and in particular the type of plate material or bonding technique that can be used. The derivation of the flexural capacities of plated structures is now covered and the chapter is concluded with worked examples.

3.2 Ductility

The ductility of a structure is as important as its strength. Often in basic design, the design procedure directly addresses the flexural strength and indirectly addresses the flexural ductility by providing provisos such as requiring the section to be *under-reinforced* or placing limits on the neutral axis depth. This approach is fine when dealing with RC structures with steel reinforcing bars that have a high strain capacity and are fully anchored, but is not sufficient when dealing with brittle materials such as FRP or brittle failure mechanisms such as plate debonding.

There are many forms of ductility that affect the behaviour of a structure. The basic concepts of material ductility as represented by the stress/strain relationship are first covered. From the stress/strain relationships, can be derived the moment/curvature relationship for a given section which represents the sectional ductility which is then covered. The integration of the curvature along the beam can be used to derive the beam ductility which is finally covered.

3.2.1 Material ductility

The concept of material ductility has already been discussed in Section 1.5.1. The material ductility of steel, as illustrated in Fig. 1.32, can be considered as stiff, as it has a high Young's modulus E, and ductile because of the large yield plateau where strain hardening occurs at about ten times the yield strain and fracture after strain

hardening at a strain of about one hundred times the yield strain. For all intents and purposes, the strain capacity of most steels is usually considered in design as infinite as the concrete crushes in an RC beam well before the steel fractures and, hence, rarely is the fracture strain incorporated into the design procedure. Aluminium is also a ductile material, however it is also flexible as it has a Young's modulus about one-third of that of steel, and it has a large strain capacity. The FRP materials represented in Fig. 1.32 have a range of stiffnesses depending on the density of the fibre. The carbon FRP in Fig. 1.32 can be made as stiff as steel, however it is a totally brittle material as there is no ductile plateau and, furthermore, the strain at fracture is relatively small. The glass FRP is generally flexible with a low Young's modulus, brittle and with a higher strain capacity than carbon FRP but less that that in metals.

In conclusion, steel can be classified as a stiff ductile material with a high strain capacity. Aluminium is flexible and ductile with a high strain capacity. Carbon FRP can be stiff or flexible, depending on the density of the fibre, also brittle and has relatively low strain capacity. And finally glass FRP is flexible, brittle, with a moderate strain capacity. The stiffness, the ductility and the strain capacity can affect the sectional ductility.

3.2.2 Sectional ductility

3.2.2.1 Moment/curvature

The sectional ductility is usually represented by the moment/curvature relationship (M/χ). In Fig. 3.1 are typical examples of the sectional M/χ relationships derived from numerical simulations, for an unplated RC beam at A, for the same RC beam with a 3 mm thick by 80 mm wide adhesively bonded steel plate at B, for adhesively bonded carbon FRP plates of various thicknesses and widths, for FRP plated beams in which fracture of the FRP controlled the strength such as at E, and for FRP plated beams in which plate debonding controlled the strength such as those in the region C.

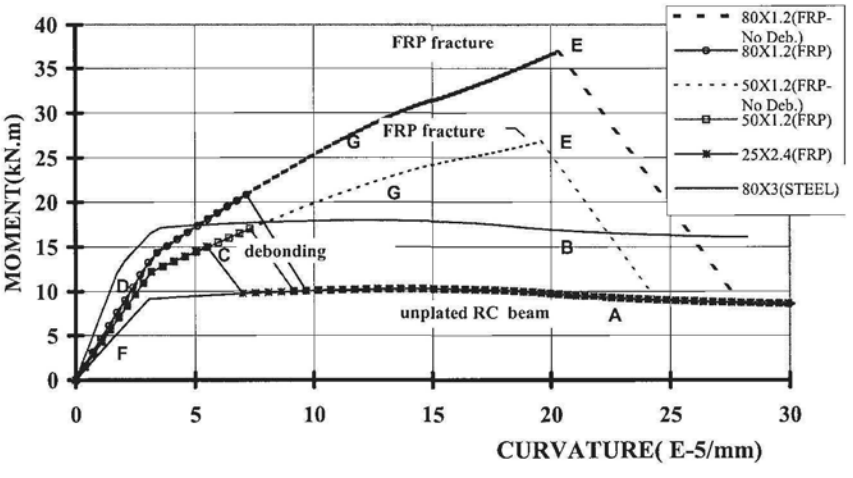

Figure 3.1 Moment/curvature relationships

The unplated RC beam shown as line A in Fig. 3.1 exhibits the classical M/χ relationship with an initial linear part at F, the slope of which is the flexural rigidity of the beam EI. After the tension reinforcing bars have yielded in the region D, there is a

near horizontal ductile plateau at A, the extent of which is limited by the concrete crushing. The effect of adding a 3 mm steel plate which was designed to yield before debonding is shown as line B. As the steel plate was assumed not to debond in this simulation, the characteristics or shape of the M/χ relationship are the same as that of the unplated beam at A, except that the initial flexural rigidity EI in region D has now two changes in slope, when the plate yields and when the reinforcing bars yields; this is of course ignoring the initial softening when concrete first cracks. However, it should be remembered that even when metal plates are designed so that the IC debonding strain is greater than the yield strain, that is they are designed to yield before debonding, tests have shown that debonding may still occur before the concrete crushes, as indicated by the debonding strains at rows 8 and 9 in Table 2.2 which are much greater than the yield strain of steel. When debonding does occur, the M/χ relationship simply reverts back to that of the unplated beam.

In contrast to the steel plated beam at B in Fig. 3.1, an FRP plated beam does not have a horizontal plateau. Instead, the moment keeps increasing, after the tension reinforcement has yielded, but at a more gradual rate as at G. This is because the FRP plate, being an elastic material that does not yield, keeps atttracting more force until either the force in the plate causes IC debonding, such as at region C, or the plates fracture in region E, after which the behaviour of the beam reverts to that of the unplated structure at A. Generally for FRP plates and in particular pultruded plates, the plate debonds well before the plate fractures as shown in the simulation in Fig. 3.1 and which is also indicated by the IC debonding strains in Table 2.2 that are much smaller than typical fracture strains of 0.01 or greater. Both the short inclined region after the reinforcing bars yield around D and prior to debonding at C, and the fact that the plated hinge keeps attracting moment, inhibit the ability of FRP plated joints to redistribute moment.

3.2.2.2 Maximum curvatures

Of importance are the curvatures at the maximum moments in Fig. 3.1 as they directly affect the ability of a beam to redistribute moment. These curvatures can be derived from a commonly used standard sectional analysis as illustrated in Fig. 3.2 for a side plated beam. The maximum curvature χ_{max} at the maximum moment capacity M_{cap} depends on one of the following criteria: the concrete crushing strain ε_c; the plate IC debonding strain ε_{db}; or the plate fracture strain ε_{fract}.

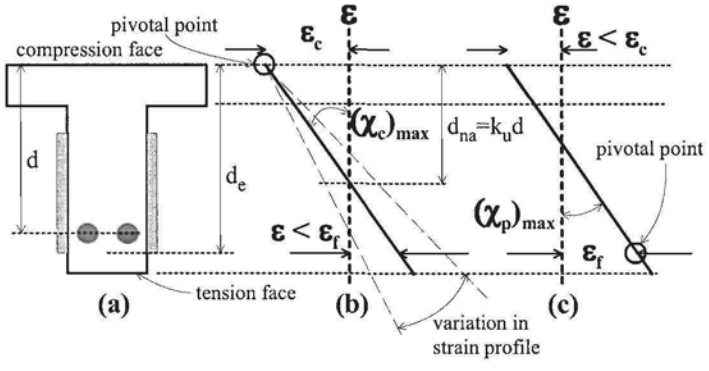

Figure 3.2 Pivotal points in strain profiles

The derivation of the maximum curvature when concrete crushing at a strain ε_c is assumed to control the analysis is illustrated in Fig. 3.2(b); this represents the standard analysis used for RC beams with steel reinforcing bars. As the concrete is assumed to crush first, the strain at the top compressive surface at failure is known and, therefore, fixed at the concrete crushing strain ε_c which is usually around 0.003 or 0.004 depending on the national standard being used. This point on the strain profile will be referred to as the pivotal point and is identified by the circle in Fig. 3.2(b). It is referred to as the pivotal point as the linear strain profile can then be swung around this pivotal point like a pendulum as shown, until a strain profile is reached which from the ensuing stress profile the forces in the cross-section sum to zero; this procedure will be explained in detail in Section 3.4. From the strain profile at longitudinal equilibrium, can be derived the maximum curvature when concrete crushing controls the design $(\chi_c)_{max}$. Also from the strain profile at equilibrium can be derived the maximum strain in the plate, which in the example in Fig. 3.2(a) will occur at the bottom edge of the plate at distance d_e from the compression face. The strain capacity of this plate is the lesser of either the IC debonding strain ε_{db} or the plate fracture strain ε_{fract} which is shown as ε_f in Fig. 3.2(b). If the maximum strain in the plate is less than ε_f, as shown in Fig. 3.2(b), then the initial assumption that concrete crushing controls the analysis is correct and $(\chi_c)_{max}$ is the maximum curvature.

If the initial assumption of ε_c controlling the design was found to be incorrect in the preceding paragraph, a further analysis has to be done where the pivotal point is moved to the level of the maximum strain in the plate as shown in Fig. 3.2(c). In this case, the pivotal strain ε_f is the lesser of ε_{db} or ε_{fract} and the strain profile is pivoted about this new point until longitudinal equilibrium is achieved whence $(\chi_p)_{max}$ and also the moment capacity at plate debonding M_{cap}. It is also worth noting at this stage that the minimum secant flexural rigidity that the section can attain is also given $(EI)_{min} = M_{cap}/\chi_{max}$ as it will be shown later in Section 3.3.2 that this controls the amount of moment redistribution that can occur.

3.2.2.3 Moment/strains

It is often very difficult to directly measure the moment/curvature relationship in RC beams due to concrete cracking and crushing. However, a good indication of the M/χ relationship of a plated beam is the moment/plate-strain (M/ε_p) relationships, as the curvature would be expected to be in proportion to the plate strain as indicated in Fig. 3.2. The following moment/plate-strain relationships were derived from tests on two span continuous beams in which the RC beams and test set up were identical so that the only variation was the plate and bonding technique.

The moment/plate-strain relationship for a beam with an adhesively bonded 3 mm thick and 100 mm wide steel tension face plate is shown in Fig. 3.3. In this test, all the plates yielded at an early stage of loading and before the maximum moment capacity was reached. This was to be expected as the plates were mild steel as compared to the high yield tension reinforcing bars; furthermore, being tension face plates and, therefore, further from the neutral axis than the tension reinforcing bars, they were always subjected to higher strains. The hogging region plate failed prematurely due to CDC debonding, after the plate had yielded but before the tension reinforcing bars had yielded; compared with the sagging region plates which failed through IC debonding, it can be seen that CDC debonding is extremely brittle and should be avoided at all cost. The sagging region plates remained adhered to the beam well after yielding of the tension reinforcing bars and attained very high strains at

virtually a constant moment before eventually debonding occurred at strains of about 0.02, which is an order of magnitude greater than the crushing strain of concrete or the yield strain of the reinforcing bars. Even though IC debonding did occur, it is suggested that this plated section is ductile.

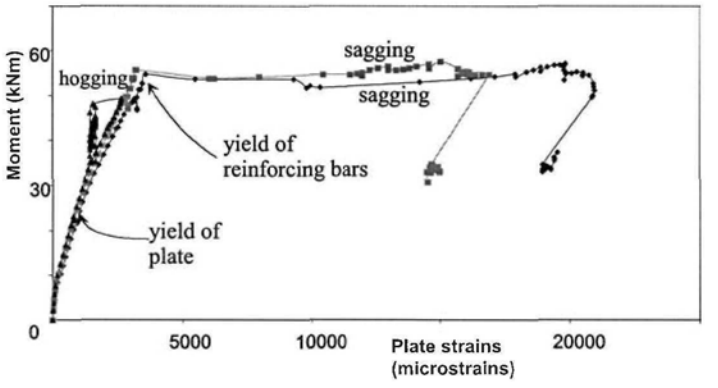

Figure 3.3 M/ε_p relationship of an adhesively bonded steel tension face plated beam

The moment/plate-strain relationship for a carbon FRP tension face plated beam is shown in Fig. 3.4; the plate thickness was 1.2 mm and the plate width 50 mm. The plates remained adhered to the beam after the tension reinforcing bars had yielded and eventually failed through IC debonding at a strain of about 0.005. This is a relatively large debonding strain for FRP plates as it is close to Chen and Teng's mean value of 0.0053 in row 1 of Table 2.2 and well above the characteristic values of Chen and Teng's and Neubauer and Rostasy's in rows 1 and 2 of about 0.0026. Even though these tension face plates were further from the neutral axis than the tension reinforcing bars, these debonding strains were sufficiently large to allow the tension reinforcing bars to yield. It may be worth noting that if these plates had debonded at the characteristic value of 0.0026 in Table 2.2, then it can be seen from Fig. 3.4 that the reinforcing bars would not have yielded prior to debonding so that this would have been a very inefficient form of rehabilitation or strengthening. It can be seen in Fig. 3.4 that after the tension reinforcing bars had yielded, the moment capacity still increased gradually because the plates, being elastic, kept attracting load as explained in Section 3.2.1.2. From a comparison of the steel plate results in Fig. 3.3 in which debonding occurred at plate strains of about 0.02, with the FRP plate results in Fig. 3.4 in which debonding occurred at plate strains of about 0.005, it is suggested that FRP plated sections can be considered as on the brittle side but with some ductility.

In Fig. 3.5 are the results from a test in which the steel plates were both bolted and adhesively bonded. The same 3 mm thick steel plates, as were used in the adhesively bonded plate in Fig. 3.3, were used in this test; the hogging region of the tested beam is shown in Fig. 2.8. The thin 3 mm thick steel plates are probably not ideally suited to bolting as, because of their thinness, there is only a small area of plate bearing against the bolt. Hence, the main advantage in bolting this adhesively bonded plate is probably the additional passive clamping action across the plate/beam interface that the bolts provide, that allows more shear to be transferred by aggregate interlock once IC debonding has occurred, as described in Section 2.2.2. However, as

can be seen in Fig. 3.5 when compared with Fig. 3.3, the adhesively bonded and bolted plates performed well. Plate strains of about 0.04 were achieved compared with those of 0.02 in the adhesively bonded steel plate which suggests a very ductile behaviour. The increase in strength between the bolted plates in Fig. 3.3 and the adhesively-bonded and bolted plates in Fig. 3.5 was not due to the addition of bolts but because the bolted plates had a slightly higher yield capacity than the adhesively bonded plates.

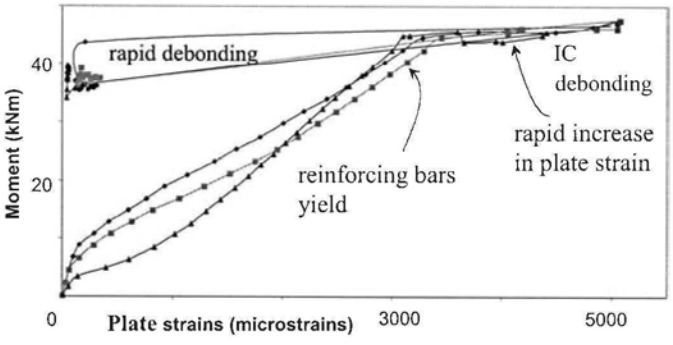

Figure 3.4 M/ε_p relationship of an adhesively bonded FRP tension face plated beam

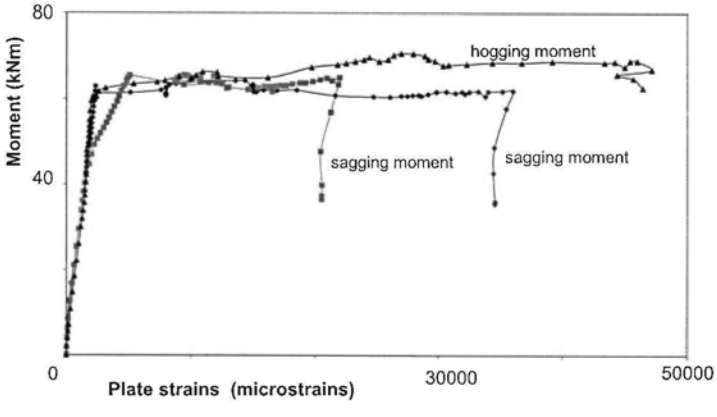

Figure 3.5 M/ε_p relationship of a bolted and adhesively bonded steel tension face plated beam

In summary, the adhesively bonded and bolted steel plated sections showed very good sectional ductility reaching strains of 0.04, the adhesively bonded steel plated section showed good ductility with strains of 0.02 and importantly, the adhesively bonded FRP plated section showed some ductility at strains of 0.005.

3.2.3 Beam ductility

There are numerous ways of measuring the beam ductility. In this section, we will be looking at the non-linear deflection as it is a good indication of the ability of the beam

to absorb energy. Furthermore, the ability of a *joint* in a beam to maintain a moment as the beam deflects and loads up other *joints* is also an indication of the ability to redistribute moment in a statically indeterminate beam. The term *joint* will be used loosely to represent any position of maximum hogging or sagging moment where ductility or a reduction in flexural rigidity is required to redistribute moment; a *plastic hinge* being a special case of a joint.

3.2.3.1 Moment/deflection

The moment/deflection (M/δ) plots for tension face plated beams are given in Fig. 3.6 for a beam with adhesively bonded steel plates, in Fig. 3.7 for a beam with adhesively bonded FRP plates and in Fig. 3.8 for a beam with steel plates that were both bolted and adhesively bonded; these are the same beams as in Section 3.2.2.3 where the M/ε_p behaviours were described.

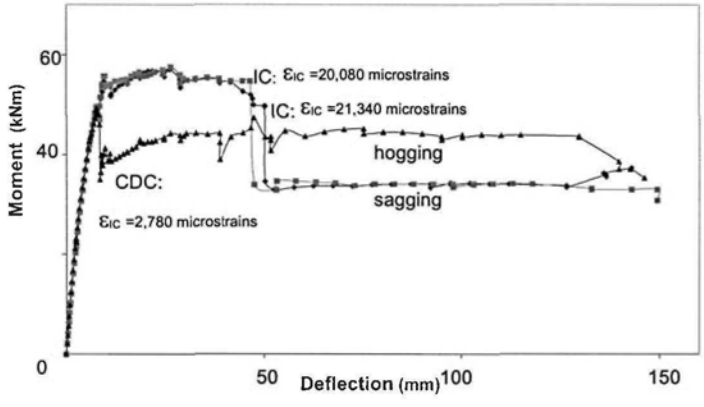

Figure 3.6 M/δ relationship of an adhesively bonded steel tension face plated beam

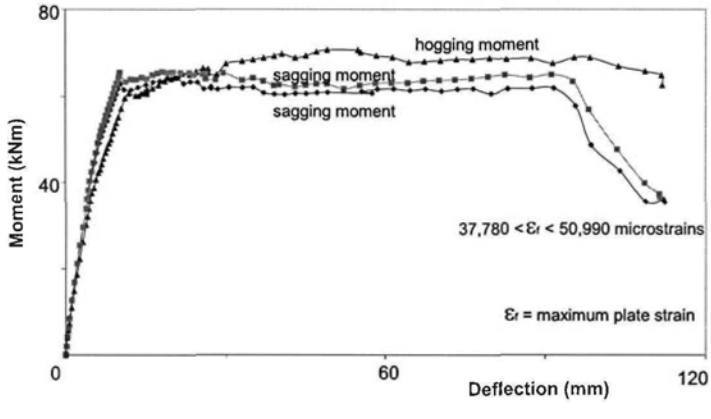

Figure 3.7 M/δ relationship of a bolted and adhesively bonded steel tension face plated beam

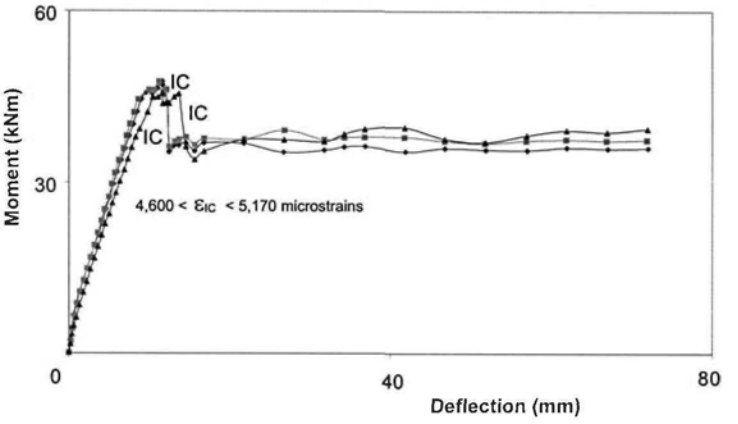

Figure 3.8 M/δ relationship of an adhesively bonded FRP tension face plated beam

Apart from the hogging region plate in Fig. 3.6 in which CDC debonding occurred, the adhesively bonded steel plated sections in the sagging regions in Fig. 3.6 had substantial ductile plateaus that extended through a deflection of about 38 mm whilst maintaining their moment capacities, afterwhich the behaviour reverted back to that of the unplated section. The adhesively bonded and bolted steel plated beam in Fig. 3.7 had an excellent ductile plateau and was able to maintain its moment capacity over a deflection of 85 mm. The results from the adhesively bonded FRP plated beam is shown in Fig. 3.8, where it can be seen that there is hardly any ductile plateau. The same RC beam with FRP side plates is shown in Fig. 3.9. In this case, a softened but still increasing moment M/δ response after yield of the tension reinforcing bars at point A is observed over a deflection of about 8 mm.

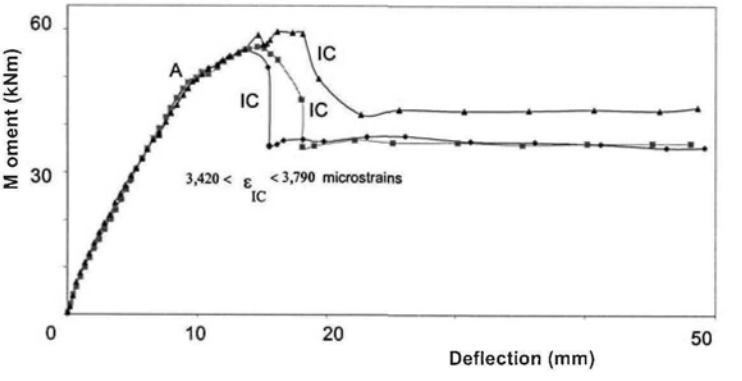

Figure 3.9 M/δ relationship of an adhesively bonded FRP side plated beam

3.2.3.2 Moment redistribution concept

In order to illustrate the phenomenon of moment redistribution, that is the ability of statically indeterminate beams to redistribute moment, let us consider the *encastre* or

built in beam of length L in Fig. 3.10(c), which can also be considered to represent an internal span of a continuous beam. For convenience, let us assume that the same longitudinal reinforcing bars are in the top and bottom of the beam. Hence, the hogging and sagging regions have the same moment/curvature relationships as shown in Fig. 3.10(a), where the idealised perfectly elastic portion has a flexural rigidity of EI up to an ultimate moment capacity of M_u at a curvature χ_y, after which there is a perfectly plastic ductile plateau up to an ultimate curvature of χ_u at which failure occurs. Let us also assume that the beam is only subjected to a uniformly distributed load w kN/m, as shown in Fig. 3.10(c), so that whilst elastic, that is whilst the flexural rigidity of the whole beam remains at EI, the moment at the supports M_{hog} is twice that at mid-span M_{sag}. Hence for this specific beam, there is no moment redistribution whilst the maximum hogging moment M_{hog} is equal to twice the maximum sagging moment M_{sag}. However, when $M_{hog} \neq 2M_{sag}$, then moment redistribution is assumed to be occurring. We will, therefore, define moment redistribution as occurring when the distribution of moment within a beam is not given by elastic analyses that assume EI is constant within the beam. We will use this simple definition for convenience, as designers generally assume in their elementary analyses that EI is constant within a beam in determining the initial distribution of moment which can then be redistributed.

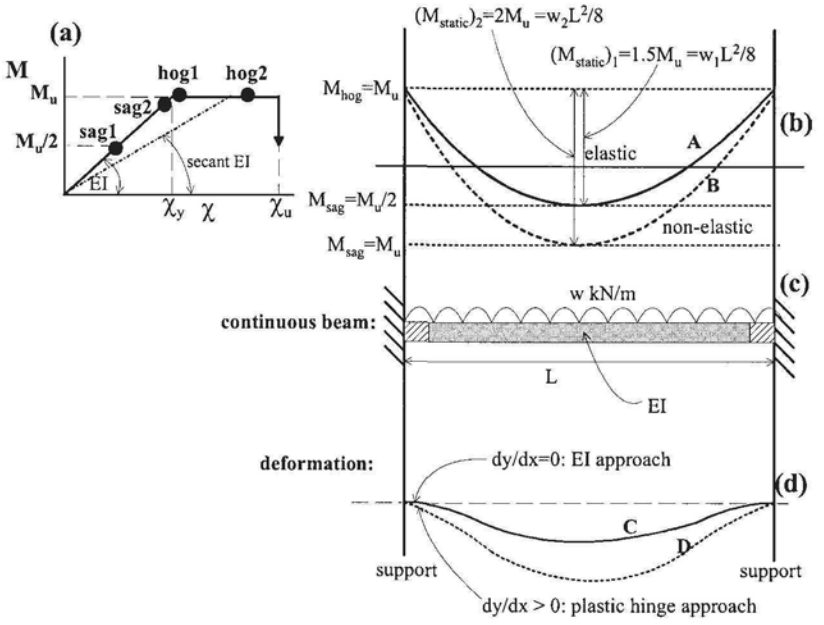

Figure 3.10 Moment redistribution concept

As the uniformly distributed load w is gradually applied to the beam in Fig. 3.10(c), the beam is initially elastic so that $M_{hog} = 2M_{sag}$ so that there is no moment redistribution. When the support moment first reaches its moment capacity M_u as shown as the point *hog1* in Fig. 3.10(a), then the mid-span moment is at $M_u/2$ which is shown as *sag1*. At this stage, the total or static moment is $(M_{static})_1 = 1.5M_u = w_1L^2/8$

as shown in Fig. 3.10(b) and labeled *elastic,* and the distribution of moment is given by line A. Up to this point, the beam remains linear elastic. As the load is further increased, the beam deflects further increasing M_{sag} above $M_u/2$ in Fig. 3.10(b) but the moment at the support remains at M_u. The only way the increased deflection or deformation due to the increased load can be accommodated is for the curvature at the supports to increase from *hog1* to *hog2* in Fig. 3.10(a) and the hogging curvature will keep increasing until the sagging curvature *sag1* reaches *sag2* in Fig. 3.10(a), that is the mid-span moment has reached its capacity M_u whilst the behaviour of the hogging region is no longer elastic. The total or static moment has now reached $(M_{static})_2 = 2M_u = w_2L^2/8$ in Fig. 3.10(b), which is the maximum static moment and, hence, the maximum load w_2 that can be applied as all the joints have reached their moment capacities and a collapse mechanism has formed. The distribution of moment within the beam is now given by line B which has been labeled *non-elastic.*

It can be seen, in the example in Fig. 3.10, that it is the hogging joints that are required to maintain the moment whilst their curvature is increasing. Hence in this example, it is the hogging joints that have to redistribute moment and it is their ductility that governs the amount of moment redistribution that can occur. If for example, it was necessary for *hog2* in Fig. 3.10(a) to exceed the curvature capacity of the section χ_u, to achieve the static moment $(M_{static})_2$ in Fig. 3.10(b), as may occur when there is a large amount of tension reinforcement or debonding occurs in the hogging section, then *sag2* in Fig. 3.10(a) cannot achieve M_u and the continuous beam fails before its theoretical plastic capacity can be achieved. It can be seen in this example that the sagging moment joint has only to reach its moment capacity, that is its curvature has only to reach χ_y, hence its ductility, that is its capacity to extend along the plateau in Fig. 3.10(a), is of no consequence. Unless of course the beam is required to absorb energy such as under seismic loads, in which case it may be a requirement that *sag2* also extends into the plastic zone to allow the beam to deflect further and absorb energy but with no increase in load.

Figure 3.10 is concerned with redistribution of moment from the hogging region to the sagging region. However, moment redistribution can occur either way. Consider, for example the beam in Fig. 3.11(b). Let us assume that the design loads induced the elastic distribution of moment line B in Fig. 3.11(a); in which case, the maximum hogging moment is two-thirds the static moment as shown and the maximum sagging moment one-third. The continuous beam can be designed for a smaller hogging moment capacity and a corresponding larger sagging moment capacity as shown by line C which has the same static moment capacity M_{static} as line B. In this case when the beam is gradually loaded, as initially $M_{hog} = 2M_{sag}$ but the capacity $(M_{hog})_u < 2(M_{sag})_u$, the support moment capacity is reached first and we have the situation described in Fig. 3.10 where ductility is required in the hogging region. If instead, it is decided to make the hogging regions stronger as shown by line A, then as the beam is gradually loaded, the moment capacity at mid-span is reached first. In which case, the sagging region has to be ductile as moment is being redistributed from the sagging region to the hogging region.

3.2.3.3 Moment redistribution capacity

To determine whether a beam is ductile enough to redistribute moment is an extremely complex problem and there is much good ongoing research to try to find a comprehensive and simple solution. The problem is to find out how the beam can deform to accommodate the non-elastic distribution of moment line B in Fig. 3.10(b) and then to determine whether the deformation capacity of the beam can

accommodate this required deformation. There would appear to be two approaches: we can either assume that there is a discontinuity of the slope at the supports as shown in line D in Fig. 3.10(d) and this will be referred to as the *hinge approach*; or it can be assumed that there is no discontinuity, such as at line C, and this will be referred to as the *flexural rigidity approach*. In many ways, these approaches can be combined and they are illustrated in Fig. 3.12.

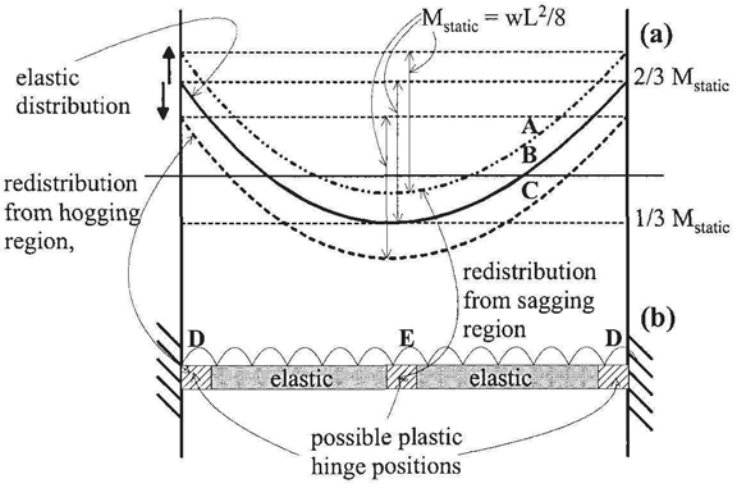

Figure 3.11 Moment redistribution

(a) Hinge approach

In the hinge approach, it is assumed that most of the beam of length L remains linear elastic at a flexural rigidity EI as shown in Fig. 3.12(c), and that there are small hinge regions at the joints of length L_{hinge} where moment redistribution requires ductility as explained in Fig. 3.10. The hinge length $L_{hinge} << L$, being the order of magnitude of the depth of the beam. It is assumed that the hinge, often referred to as the *plastic hinge*, accommodates the discontinuity of slope at the supports in line D in Fig. 3.12(f). This discontinuity is caused by the non-elastic moment distribution, line B in Fig. 3.12(a), where there are support moments M_u and an applied load w_2 kN/m that induces at static moment $(M_{static})_2$. The discontinuity of slope can be determined from the analyses depicted in Figs. 3.12(d) and (e). In Fig. 3.12(d), the redundant support moments are removed so we are dealing with a statically determinant simply supported beam with a uniformly distributed load w_2 of flexural rigidity EI; the slope at the supports $(dy/dx)_{static}$ can be derived by integration of the curvature along the length of the beam. The simply supported beam is now subject to only the end moments M_u as in Fig. 3.12(e). Also from integration of the curvature, can be derived the slope at the supports $(dy/dx)_{support}$. Hence the discontinuity of the slope in line D in Fig. 3.12(f) is equal to the difference between $(dy/dx)_{static}$ and $(dy/dx)_{support}$ and which is accommodated by the plastic hinge. As the length of the hinge is very small, it is often assumed that the curvature within the hinge is constant so that the rotation capacity of the hinge is simply $\chi_u L_{hinge}$ where χ_u is the curvature capacity of the section as illustrated in Fig. 3.10(a). It can be shown for the very simple case of an encastre beam with a uniform load that for design

$$\frac{L}{2EI}\left[\frac{2}{3}M_{static} - M_u\right] \leq \chi_u L_{hinge} \qquad 3.1$$

where the left hand side of Eq. 3.1 is the discontinuity in the slope in line D in Fig. 3.12(f) and the right hand side is the rotation capacity of the hinge. The main problem in this approach is in deciding what to use for the length of the hinge.

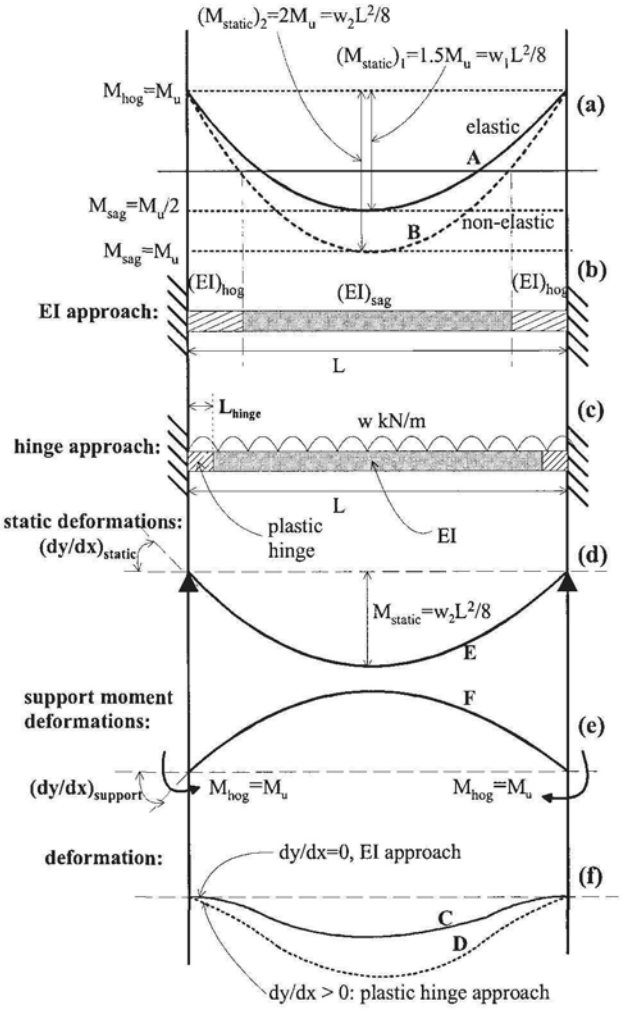

Figure 3. 12 Compatibility in moment redistribution

(b) Flexural rigidity approach

In contrast to the *plastic hinge* approach, the *flexural rigidity* approach (Oehlers et al 2003(a) and (b)) assumes that the slope at the supports is zero as shown in line C in Fig. 3.12(f). This can only be accommodated by allowing variations in the flexural

rigidity along the length of the beam as shown in Fig. 3.12(b), where $(EI)_{hog}$ represents the flexural rigidity of the hogging region and $(EI)_{sag}$ that of the sagging region. It is not the magnitudes of these flexural rigidities that controls redistribution but their relative values or proportions, that is $(EI)_{hog}/(EI)_{sag}$. For example when $(EI)_{hog} = (EI)_{sag}$, that is $(EI)_{hog}/(EI)_{sag} = 1$, then, in this example, the elastic distribution of moment is achieved so that $M_{hog} = 2M_{sag}$ so that there is no moment redistribution. Even if we were to double both flexural rigidities, $(EI)_{hog}/(EI)_{sag}$ remains at unity and, therefore, M_{hog} remains at $2M_{sag}$ so there is still no moment redistribution. However, if the secant $(EI)_{hog}$ is taken, it reduces as χ increases along the plateau in Fig. 3.10(a), then $(EI)_{hog}/(EI)_{sag}$ also reduces and as M_{hog} is constant whilst M_{sag} is increasing $M_{hog} < 2M_{sag}$, that is moment redistribution is occurring. The minimum flexural rigidity of M_{hog} depends on the sectional curvature capacity χ_u in Fig. 3.10(a).

Another way of visualising the flexural rigidity approach is that as the flexural rigidity at the supports $(EI)_{hog}$ in Fig. 3.12(b) reduces relative to $(EI)_{sag}$, the support attracts less moment. For example, when $(EI)_{hog} \rightarrow 0$, the continuous beam in Fig. 3.12(b) reverts to a simply supported beam, so that all of the hogging moment has been redistributed to the sagging region. On occasions in the remainder of this book, we will refer to the regions where the flexural rigidity is reducing, such the hogging region in Fig. 3.12(b), as the *plastic hinge* even though we are dealing with the *flexural rigidity* approach. This is just to emphasise that it is this region that exhibits ductility in order to achieve moment redistribution. It may be worth noting at this stage that for the *flexural rigidity* approach, the length of the *hinge* is the length of the hogging region bound by the points of contraflexure as shown in Fig. 3.12(b); the reason for this is explained later in Section 3.3.2 and 3.3.3.

(c) Test example of moment redistribution

A typical test result of moment redistribution from two span continuous beams such as that shown in Fig. 2.18 is given in Fig. 3.13. The beams were plated over their hogging region as shown in Fig. 2.18 with a 50 mm wide 1.2 mm thick carbon FRP plate, and designed and loaded to achieve their moment capacity in the hogging regions first so that moment redistribution occurred from the hogging region to the unplated sagging region. The loading arrangement was such that in an elastic analysis in which EI was assumed constant, the hogging moment would be 75% of the static moment as shown by the horizontal line in Fig. 3.13. Hence, if the beam remained elastic the hogging moment should remain at 75% of the static load. It can be seen that up to applied loads of 15 kN the beam does behave elastically (the line from the origin should be ignored as the graph should start at the first load point), after which the hogging moment reduced in proportion to the static moment indicating that moment redistribution occurred in this FRP plated beam.

3.3 Moment redistribution capacities

3.3.1 *Neutral axis depth approach*

Most national codes use the neutral axis factor $k_u = d_{na}/d$ in Fig. 3.2, where d is the effective depth of the beam and d_{na} the depth to the neutral axis both measured from the compression face, to ensure sufficient sectional ductility at a *joint* for moment redistribution in unplated reinforced concrete beams. As defined previously, the term *joint* will be used to represent any position or region of maximum hogging or sagging moment where a *hinge* may have to occur to redistribute moment such as the hatched

regions D and E in Fig. 3.11 as well as the hatched regions in Figs. 3.12(b) and (c). A *hinge* will be defined loosely as a region where the curvature has to follow the plateau in Fig. 3.10(a) such as at *hog2*. Hence, the term *hinge* will be used where a plastic hinge is required such as in the hatched regions in the hinge approach in Fig. 3.12(c) or where the flexural rigidity has to reduce as in the hatched region in the EI approach in Fig. 3.12(b).

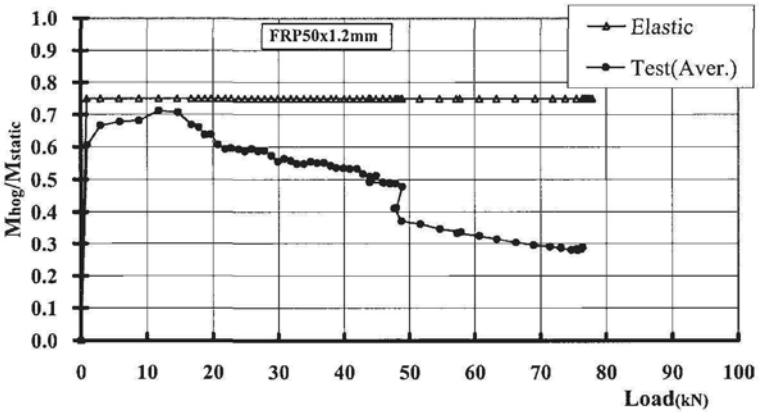

Figure 3.13 Moment redistribution in a two span continuous beam test

The range of moment redistributions allowed in national codes is illustrated in Fig. 3.14. Most codes allow up to 30% redistribution for k_u values that range from zero to 0.3, and zero redistribution for k_u values that range from 0.2 to 0.6. As an example of the application of k_u values, let us assume that the design load has been applied to a beam and from an elastic analysis, based on EI being constant along the length of the beam, the moment at one joint is $M_{elastic}$. The Australian code suggests that if $k_u < 0.2$ at that joint then that joint can form a hinge and redistribute 30% of its elastic moment $M_{elastic}$. Hence the joint can be designed for 70% of $M_{elastic}$, just as long as the other joints in the beam are increased in strength to allow the same total or static moment in the beam. The Australian code also suggests that if $k_u > 0.4$ at that joint then moment redistribution is not allowed to occur at that joint; which means that that joint cannot reach its moment capacity prior to the total design load being applied (that is it cannot form a hinge) but is allowed to just reach its moment capacity when the full design load is reached.

How the neutral axis depth factor k_u affects the ductility is illustrated in Fig. 3.15 for the values used in the Australian Code. It is assumed in this analysis that concrete crushing causes failure (that is the strength reduces after the concrete starts to fail) and that this occurs at a strain $\varepsilon_c = 0.003$. Hence $\varepsilon_c = 0.003$ is the pivotal point, as described in Fig. 3.2, of the analysis as shown in Fig. 3.15. As the pivotal point is fixed at $\varepsilon_c = 0.003$, the k_u factor controls the strain in the tension face. For example, when $k_u = 0.2d$ in Fig. 3.15, then the tension face strain is $\varepsilon_{0.2d} = 0.012$, as shown, and when $k_u = 0.4d$ then the tension face strain is $\varepsilon_{0.4d} = 0.0045$ (this assumes that the effective depth d of the beam is close to the depth of the beam h as shown). The k_u factor does not control the curvature which is given by $\varepsilon_c/k_u d$ as this depends on the effective depth of the section d. However, the k_u factor does control the rotation of the

plastic hinge θ_{hinge} as this is given by $\chi_u L_{hinge} = (\varepsilon_c/k_u d)\, L_{hinge}$ and if $L_{hinge} \approx d$ then the rotation, that is the change in slope within the hinge, is given by $\theta_{hinge} \approx \varepsilon_c/k_u$.

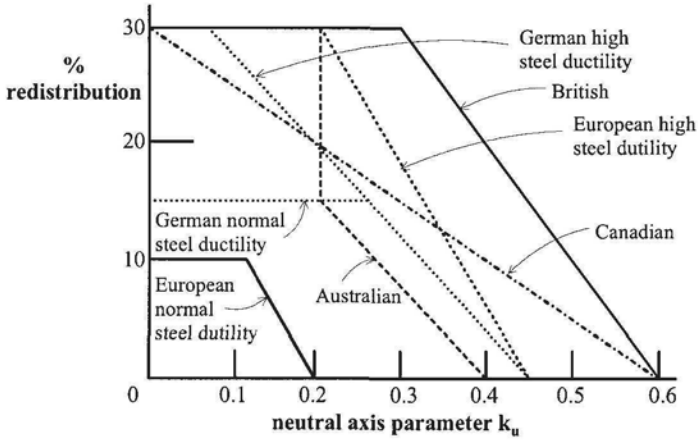

Figure 3.14 Moment redistribution code requirements

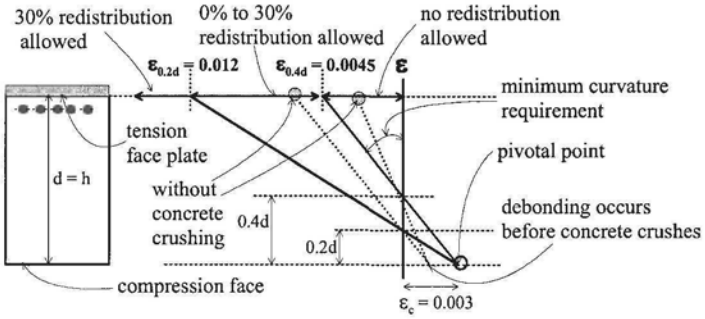

Figure 3.15 Plate strain requirements for moment redistribution

The Australian code requires that $k_u < 0.2d$ to allow 30% redistribution and, as shown in Fig. 3.15, this requires a tension face strain of 0.012 which means that if a plate were attached to the tension face then the IC debonding strain would have to be greater than 0.012. It can be seen in Table 2.2 that this strain of 0.012 is much greater than all the recommendations for FRP plates in rows 1 to 4. It is even much greater than the upper limit to the Concrete Society and German recommendations in rows 3 and 4. Even if the upper bound limit of the British recommendation of $k_u = 0.3$ for 30% redistribution, as shown in Fig. 3.14, is used, the strain required of $\varepsilon_{0.3d} = 0.007$ is still only within the Concrete Society and German recommendations and well above those determined from beam tests, in rows 5 to 6 of Table 2.2, and above the mean values for pull tests in row 1. Hence it would appear that a 30% redistribution or more is very unlikely to be achieved in FRP plated structures. However, the steel debonding strains of 0.0201 – 0.0213, in row 8 of Table 2.2, are well above the

required strain of 0.012, which would suggest that some steel plated beam joints can redistribute 30% or more of their elastic moment.

At the other extremity of redistribution in Fig. 3.14, the Australian, German and European codes require that no redistribution is allowed when k_u is greater than about 0.4. As shown in Fig. 3.15, this neutral axis depth factor requires a strain on the tension face of $\varepsilon_{0.4d}$ = 0.0045. This is still above the characteristic FRP values proposed by Chen and Teng, and Neubauer and Rostasy in rows 1 and 2 in Table 2.2 and only just achievable in the FRP plated beams in rows 5 and 6. Hence it would appear that redistribution should not be allowed for FRP plated beams as suggested in the European guidelines (2001) in Table 1.1. However, the steel plated specimens in rows 8 and 9 in Table 2.2 can achieve these strains and hence are capable of at least some moment redistribution; this is because steel or other metal plates can be designed to yield before IC debonding.

It could be argued and it is true that the plates will probably debond before the concrete crushes, and hence the pivotal point moves to the left as shown in Fig. 3.15. This shift of the pivotal point would change the strain profiles to the broken lines and would require smaller tension face strains to achieve the required k_u factors as shown. However as can be seen, from the difference in slope between the broken and solid lines, the required curvatures reduce and, hence, also their sectional ductility and, therefore, the ability of a joint to redistribute moment. Hence, it is suggested that the k_u factor should not be used to control moment redistribution in plated structures where concrete crushing does not control failure as the rotation of the plastic hinge is no longer proportional to ε_c/k_u. The British guidelines (2000) recommend using the k_u factor to control ductility in flexural calculations that are based on concrete crushing, which is fine for plated structures where IC debonding does not precede concrete crushing.

In conclusion, it is suggested that the k_u factor should not be used to control ductility in plated structures, that FRP plated joints should in general not be allowed to redistribute moment, and that metal plated joints have the ability to redistribute as the plate can be designed to yield before debonding.

3.3.2 *Flexural rigidity approach*

Tests on two span continuous plated beams (Oehlers et al 2003(a) and (b)), such as in Fig. 2.18, have shown that the *flexural rigidity* approach described in Section 3.2.3.3 can be used to predict the amount of moment redistribution that plated structures can withstand. Of the different approaches described in Section 3.2.3.3, the *flexural rigidity* approach probably works best because plated structures tend to debond before the concrete crushes.

To illustrate the analysis, let us consider the propped cantilever in Fig. 3.16(a), which is an analysis of the two span beam in Fig. 2.18. It will be assumed that metal plates are used in the hogging region and the sagging region remains unplated. The M/χ relationship for the hogging region is shown as the hogging joint in Fig. 3.17; the elastic part is that of the cracked plated section of flexural rigidity EI_{hcr} which can be derived from transformed sections and by assuming that the tensile strength of the concrete is zero. The ultimate strength of this plated section M_{hu} is the strength when both the metal plate and the tension reinforcing bars have yielded. The length of the ductile plate from point B_h onwards is governed by either the concrete crushing at χ_c or the plate debonding at χ_{deb} and the curvatures and strains at which this occurs can be derived from the analyses illustrated in Fig. 3.2. The same approach can be applied

to determining the M/χ relationship for the sagging region which is shown as the sagging joint in Fig. 3.17 and which in this example is assumed to be unplated.

Let us first assume that the hinge occurs at the hogging joint in Fig. 3.16(a), that is the plated hogging section has to exhibit ductility whilst the sagging region only has to achieve its ultimate strength at point C_s in Fig. 3.17. Hence at debonding, the hogging joint has a flexural rigidity of EI_{hdeb} as shown in Fig. 3.17, and the sagging joint has a flexural rigidity EI_{scr}. The flexural rigidity approach is very simple. It assumes that the whole of the hogging region of length L_h in Fig. 3.16(b) and (c) has a flexural rigidity of $EI_h = EI_{hdeb}$ and the whole sagging region of length L_s has a flexural rigidity of EI_{scr}. The reason that this approach works is that moment redistribution does not depend on the magnitude of the flexural rigidities but on their proportions as explained in Section 3.2.3.3. Hence, just as long as the relative stiffnesses between the two regions is correct, it does not matter what the actual stiffnesses are.

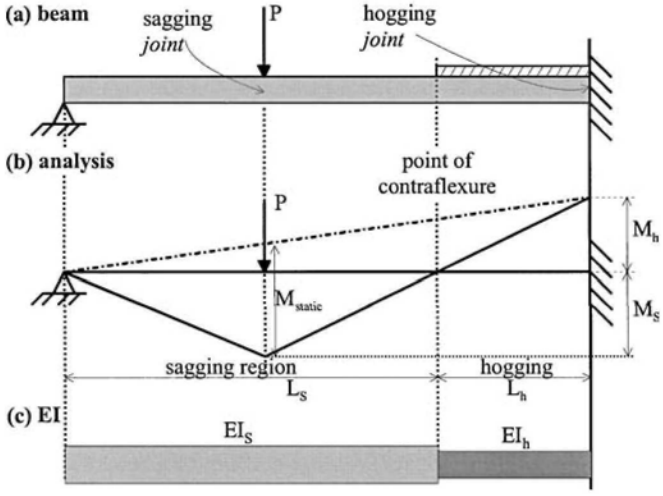

Figure 3.16 Flexural rigidity analysis

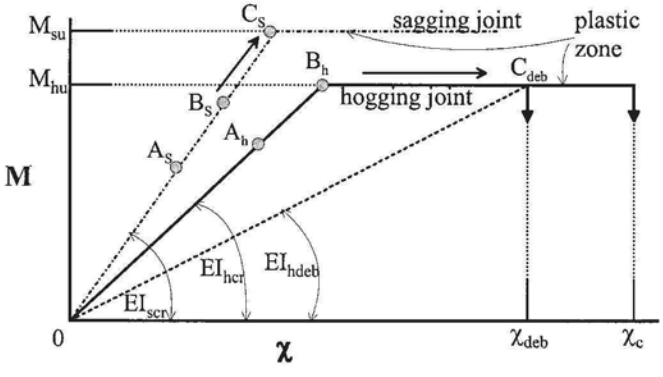

Figure 3.17 M/χ response with horizontal plateau

There are closed form solutions for simple load configurations and simple restraints. However, an elementary beam stiffness computer program is ideal for the analysis. Let us consider the beam in Fig. 3.16(a) and we wish to determine the applied load to cause debonding, the distribution of moment at failure, and hence determine whether the amount of moment redistribution that the indeterminate beam was designed for can be accommodated. As described in the previous paragraph, the flexural rigidity of the hogging region is $EI_h = EI_{hdeb}$ and that of the sagging region $EI_s = EI_{scr}$. The problem is that the point of contraflexure is not known, because it depends on the variation in EI along the length of the beam, so that the position of the point of the point of contraflexure L_h has to be initially guessed. The beam is then loaded to determine whether the point of contraflexure coincides with the guessed value of L_h and iterated until it does. As this is an elastic analysis, the point of contraflexure is independent of the magnitude of the load so that any load can be applied just as long as the distribution is correct. Once the correct spread of the flexural rigidities has been found, that is L_h corresponds with the point of contraflexure, the analysis will give the proportion M_h/M_s in Fig. 3.16(b). This proportion can then be compared with the capacity proportion M_{hu}/M_{su} from Fig. 3.17, to ensure that debonding occurred before the sagging capacity was achieved as was assumed in this analysis.

An alternative approach is to first assume that both of the zones L_s and L_h in Fig. 3.16(b) and (c) are initially elastic, that is they have flexural rigidities EI_{scr} and EI_{hcr}, then repeat the iterative approach described in the previous paragraph to find M_h/M_s, and compare this with the capacities M_{hu}/M_{su} to determine which region reaches its capacity first. For example, let us assume that a load P in Fig. 3.16(b) is applied, and from the iterative analysis we derive that the moment in the sagging region is A_s and that in the hogging region is A_h as in Fig. 3.17. Increasing these moments in the same proportion would give B_s and B_h which shows that the hogging joint reaches its capacity first. Hence, by applying further load and going from B_s to C_s and from B_h to C_{deb}, it now needs to be determined whether the ultimate strength M_{su} at C_s or debonding at C_{deb} first occurs. The flexural rigidity in the hogging region gradually reduces between B_h and C_{deb} along the plastic zone. The simplest solution is to go straight to C_{deb} by using EI_{hdeb} in the hogging region whilst maintaining EI_{scr} in the sagging region as described in the previous analysis in the previous paragraph. From a comparison between M_h/M_s and M_{hu}/M_{su} can be determined whether debonding first occurs at C_{deb} or whether the sagging capacity M_{su} is first reached. If the sagging capacity is first reached, then both capacities M_{hu} and M_{su} are achieved prior to debonding. If the sagging capacity is not reached, then the moment in the sagging region at debonding in the hogging region will have been derived already from the analyses using EI_{scr} and EI_{hdeb} which is the moment that occurs on debonding.

The analysis of FRP plated sections will follow the same procedure as with metal plates. In this case, for the M/χ relationship for the FRP section in the hogging region, there will be softening after yielding of the tension reinforcement, which will be referred to as the plastic zone, with a reduced (non-zero) positive tangent stiffness, instead of a horizontal plateau as shown in Fig. 3.18. If the sagging joint is unplated or has a metal plate, it will have a horizontal plateau (plastic zone), as shown, so that the moment capacity does not increase; that is the analysis is stopped when point B_s is reached, so that the analysis procedure described in the previous paragraph can be applied. However, if the sagging region has an FRP plate, the capacity can gradually

increase as shown, in which case the softened branch (plastic zone) of the sagging joint will have to be followed. Ignoring the plastic zone will give a safe design. Alternatively, using EI_{sdeb} and EI_{hdeb} for the sagging and hogging regions will first determine which plate debonds first. The plate that does not debond will lie somewhere in the plastic zone such as at A_s in the sagging joint, so that this flexural rigidity of EI_{sit} can be varied to iterate towards the correct solution when $M_{hu}/M_s = M_h/M_s$.

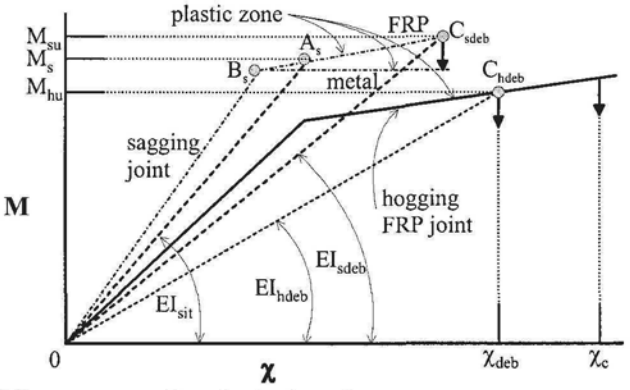

Figure 3.18 M/χ response with softening branch

3.3.3 *Examples of moment redistribution capacities*

In order to illustrate moment redistribution in plated beams, two span continuous beams were tested as shown in Fig. 2.18. Only the hogging regions were plated as shown in Fig. 3.19. The beams were deliberately designed so that the moment capacity would be reached first in the plated hogging region. Hence the ductility of this section, that is its ability to redistribute moment, could be measured. To ensure that the hinge formed in the hogging region and that there was ample scope for moment redistribution, there were only two 12 mm diameter tension reinforcing bars in the hogging region compared with four 16 mm tension reinforcing bars in the sagging regions so that the flexural capacity of the hogging region M_{hu} was much greater than that of the sagging region M_{su}. However, this difference in the longitudinal tension reinforcing bars also meant that there was a large difference in the flexural rigidities of the cracked sections EI_{cr} which by itself would affect moment redistribution as described in Section 3.3.2.

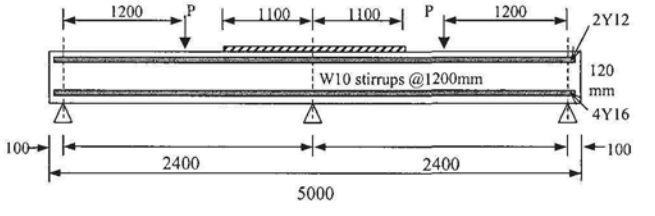

Figure 3.19 Moment redistribution test specimen

The test beam in Fig. 3.19 is symmetrical and hence acts as a propped cantilever as shown in Figs. 3.16 and 3.20. The broken line in Fig. 3.20 represents an elastic analysis in which EI is constant along a span. For the loading arrangement in Fig. 3.19, this gives a hogging moment $(M_h)_{el}$ that is 20% greater than the sagging moment $(M_s)_{el}$. Hence whilst the beam remains linear elastic and exhibits constant EI, it would be expected that $(M_h)_{el}/(M_s)_{el} = 1.2$. If in the tests $(M_h)_{test}/(M_s)_{test} < 1.2$ as represented by the unbroken line in Fig. 3.20 then this represents moment redistribution.

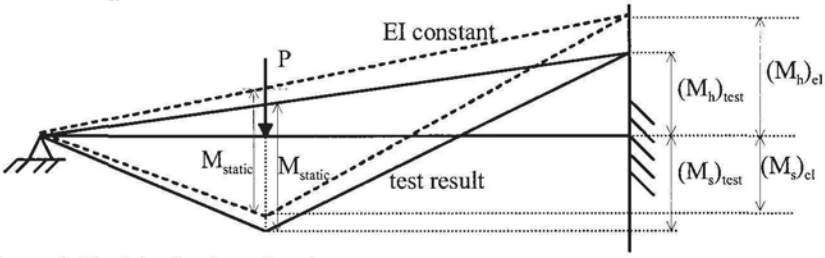

Figure 3.20 Distribution of static moment

The test results for a beam with a 2 mm thick mild steel plate is shown in Fig. 3.21. The ordinate gives the measured hogging moment in the test M_h as a proportion of the measured sagging moment M_s and the abscissa gives the measured static moment M_{static}, as shown in Fig. 3.20, as a proportion of the theoretical maximum static moment $(M_{static})_u$. The theoretical maximum static moment occurs when both the hogging and sagging joints reach their theoretical maximum sectional capacities M_{hu} and M_{su} in Figs. 3.17 and 3.18; this is the maximum static moment that can occur when there is sufficient ductility in the continuous beam to redistribute moment so that all the joints reach their ultimate capacity. The line marked *elastic (EI constant)* in Fig. 3.21 is the variation if EI is constant along the length of the beam which for this test is at 1.2. The line marked *EI approach* is based on a flexural rigidity analysis for moment redistribution as described in Section 3.3.2. The line marked *max moment redistribution prior to plate debond* signifies the amount of moment redistribution that can occur if the flexural capacities of both the plated hogging region and unplated sagging region are achieved which would be the aim in design. Finally, the line marked *max moment redistribution of unplated RC beam* represents the amount of redistribution that could occur after the plate has debonded and the beam is acting as totally unplated.

It can be seen in Fig. 3.21 that at the start of loading M_h/M_s is close to 120% which signifies that EI is constant along the length of the beam; the beam at these early stages of loading is uncracked under flexure, hence the flexural rigidities of the cross-sections are barely affected by the longitudinal reinforcement so that EI is constant. The divergence around the line $M_h/M_s = 1.2$ is simply the beam bedding down at very low loads. The hogging moment as a proportion of the sagging M_h/M_s then reduces gradually. Soon after the first flexural crack is visible the first IC interface crack can be seen when the hogging moment has reduced to about 90% of the sagging moment and the applied load is about 45% of the load that eventually caused IC debonding; the occurrence of the IC interface crack at such a small proportion of the load to cause IC debonding further reinforces the fact that IC interface cracking by itself is no problem and is also little indication of when IC debonding will occur. IC debonding then occurred at the maximum plate strain and

close to the value predicted by the flexural rigidity approach, where the hogging moment is now 66% of the sagging moment but short of the theoretical maximum redistribution at a hogging moment of 50% of the sagging moment. Hence, the beam has just failed prematurely, that is debonding of the hogging plate has occurred before the maximum capacity of the sagging region could be achieved. However, there has been a significant amount of moment redistribution as the hogging moment has reduced from 120% to 66% of the sagging moment and the continuous beam has achieved 79 % of its theoretical maximum capacity of $(M_{static})_u$.

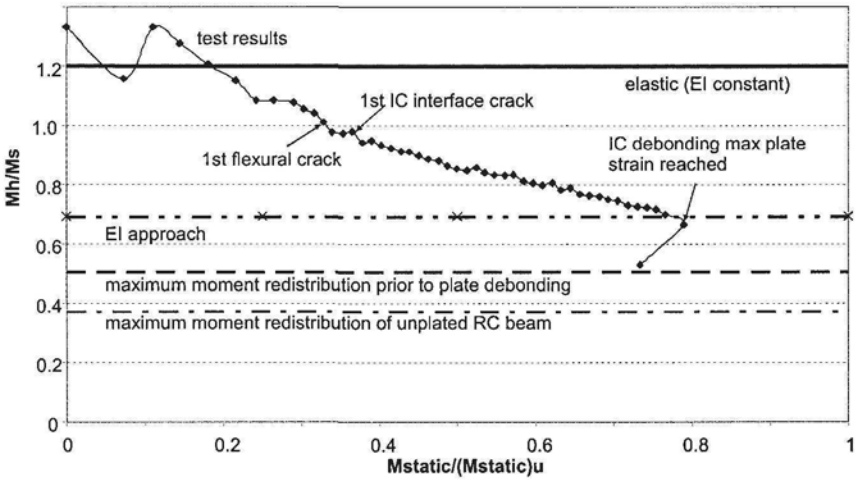

Figure 3.21 Moment redistribution in steel plated beam; $t_p = 2mm$

The test results from a carbon FRP plated beam with a 1.2 mm thick plate are shown in Fig. 3.22. The initial divergence from $M_h/M_s = 1.2$ at very low loads is simply due to bedding down of the beam. As with the steel plated beam in Fig. 3.21, M_h/M_s reduced gradually from a low load indicating moment redistribution started at an early stage. The first IC interface crack was also visible at an early load at about 35% of the load to cause IC debonding which further reinforces the point that the appearance of IC interface cracks is of little consequence. The maximum plate strain occurred at a redistribution close to that predicted by the flexural rigidity approach where the hogging moment was 72% of the sagging moment. After which, the plate strains reduced and debonding occurred at a hogging moment of 65% of the sagging moment and at an applied load of 58% of the theoretical maximum. The beam then reverted to the behaviour of an unplated beam. It is interesting to note that unlike the steel plated beam in Fig. 3.21, IC debonding occurred after the plate strains had reduced and not at the maximum plate strain.

The results from a series of tests with steel and carbon FRP plates are given in Table 3.1. In these tests, the steel plate thicknesses in column 1 were varied from 1 mm to 3 mm, and the FRP plates from very thin plates using the wet lay up procedure to quite thick plates for FRP at 2.4 mm. The maximum plate strains in column 3 just prior to debonding are in line with those already reported in Table 2.2; the steel plates having yielded prior to debonding and the FRP debonding strains are close to the characteristic values in Table 2.2.

The percentage moment redistribution in column 4 of Table 3.1 is derived from Eq. 3.2 with the moments in Fig. 3.20. It is the difference in the hogging moment between the theoretical elastic value based on EI being constant $(M_h)_{el}$ and the test result $(M_h)_{test}$ for the same static load as shown in Fig. 3.20.

$$\%MR1 = \frac{(M_h)_{el} - (M_h)_{test}}{(M_h)_{el}} \times 100 \qquad 3.2$$

Hence, %MR1 in Table 3.1 is the percentage redistribution for a beam originally analysed using standard linear elastic theory where EI is assumed to be constant; as in standard design practice. It can be seen in column 4 that there has been a reasonable amount of moment redistribution; that for the steel plates varies from 22% to 48% and for the FRP plates from 28% to 35%. However, part of this moment redistribution is directly due to the difference in flexural rigidities of the hogging and sagging regions, EI_{hcr} and EI_{scr} in Fig. 3.17, because of the difference in their tension reinforcing bars as shown in Fig. 3.19. The hogging region has much less tension reinforcing bars than the sagging region. Hence the flexural rigidity of its cracked section EI_{hcr} in Fig. 3.17 would be expected to be much less that that of the sagging region EI_{scr}, and this difference by itself would account for a part of the moment redistribution, even if none of the joints reached and entered their plastic zones in Figs. 3.17 and 3.18 where the EI values would then start to reduce.

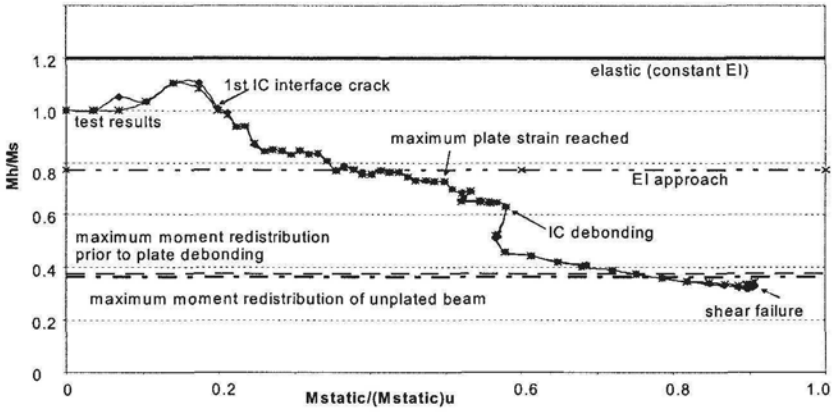

Figure 3.22 Moment redistribution in carbon FRP plated beam; t_p = 1.2mm

Let us determine how much of the moment redistribution in column 4 in Table 3.1 can be attributed to the difference between the elastic stiffnesses EI_{scr} and EI_{hcr} in Fig. 3.17 and how much is due to following the plastic zones. To do this, $(M_h)_{el}$ and $(M_s)_{el}$ in Fig. 3.20 needs to be derived from an analysis in which the stiffness of the beam is now EI_{scr} in the sagging region and EI_{hcr} in the hogging region, instead of being assumed constant at EI as in column 4 in Table 3.1. Hence the moment redistribution for the difference between EI_{scr} and EI_{hcr} is now accounted for in the analysis, so that any redistribution would now be due to following the plastic zones in Figs 3.17 and 3.18. Hence the percentage redistribution in column 5 in Table 3.1 is given by

$$\%MR2 = \frac{(M_h)_{EI\ cracked} - (M_h)_{test}}{(M_h)_{EI\ cracked}} \times 100 \qquad 3.3$$

For the steel plates in Table 3.1, the percentage redistribution due to following the plastic zones, which is given in column 5, is only slightly less than the total moment redistribution in column 4. In contrast for the FRP plated specimens, the moment redistribution due to following the plastic zones in column 5 is very small compared to the total redistribution in column 4. These results are to be expected as the sectional ductility of FRP plated sections, as shown by the plastic zones in Figs 3.1 and 3.4, is relatively small compared with the plastic zones of steel plated sections in Figs 3.1 and 3.3.

Table 3.1 Percentage moment redistribution

t_p (mm) (1)	plate material (2)	ε_{deb} (3)	%MR1 ($EI_{constant}$) (4)	%MR2 (EI_{crack}) (5)
3	steel	0.0044	22	16
2	steel	0.0059	33	28
1	steel	0.0149	48	43
2.4	CFRP	0.0020	30	5
1.2	CFRP	0.0029	29	4
1.2	CFRP	0.0025	28	7
wet lay up	CFRP	0.0041	35	6

In conclusion, FRP plated specimens can redistribute moment if this is a function of the elastic cross sectional stiffnesses but the plastic zone component of moment redistribution is negligible. On the other hand, metal plated specimens can redistribute due to both their initial cracked stiffness component as well as their plastic zone component.

3.3.4 Plating design considerations

To illustrate the concept of moment redistribution and in particular how it affects the choice and positioning of plates for rehabilitation, we will consider an internal bay of a continuous beam with uniformly distributed loads, which will be represented as an encastre beam. We will use the term *plastic hinge* to loosely refer to a region of a beam that requires ductility in order to redistribute moment, that is any region that has to follow the plastic zones as shown in Figs. 3.17 and 3.18. The plastic hinge will be shown as a circle in the diagram even though the region of the beam following the plastic zone or diverging from the elastic cracked section EI may be quite large. We will also use the word *rotate* to loosely to describe the act of moving along the plastic zone as this requires increases in the deflection but not necessarily a discontinuity in the slope as shown in Fig. 3.10(d). We will also assume that EI_{scr} and EI_{hcr} in Fig. 3.17 are roughly equal so that we can ignore moment redistribution due to their difference.

The basic design for moment redistribution will be first revised for an unplated beam, and then it will be presented in a form specifically for plated structures to illustrate how moment redistribution can affect the choice of the plating technique and can limit the increase in strength that can be achieved. As it was shown in the previous Section that carbon FRP plates can only achieve a small amount of moment

redistribution that is associated with the plastic zone, it will be assumed that FRP plated joints cannot redistribute moment whereas metal plated joints can.

3.3.4.1 Moment redistribution in unplated beams

(a) Plastic hinges at supports

Let us consider the beam in Fig. 3.23 which has been designed for a moment capacity of $(M_h)_u$ at the hogging joint and $(M_s)_u$ at the sagging joint. Hence, the curve marked A will be the distribution of moment at failure and the beam has been designed for the following static moment

$$M_{static} = (M_h)_u + (M_s)_u = \frac{w_{fail} L^2}{8} \qquad 3.4$$

where w_{fail} is the uniformly distributed load to cause failure. The elastic distribution of this static moment based on a constant EI value is shown as line B, where for this case of an internal bay with a uniformly distributed load

$$(M_h)_{el} = \frac{2}{3} M_{static} \quad \text{and} \quad (M_s)_{el} = \frac{1}{3} M_{static} \qquad 3.5$$

so that $(M_h)_{el} = 2(M_s)_{el}$. It can be seen in Fig. 3.23 that the designers have reduced the capacity of the hogging joint and increased that of the sagging joint from the elastic analysis. Therefore, the hogging region has to redistribute the moment, that is maintain its moment capacity and rotate until the sagging region reaches its moment capacity. The ability of the unplated hogging region to rotate depends on the neutral axis factor k_u as described in Section 3.3.1. It can be seen that the sagging region only needs to achieve its moment capacity and hence does not have to rotate and hence its neutral axis factor k_u is irrelevant.

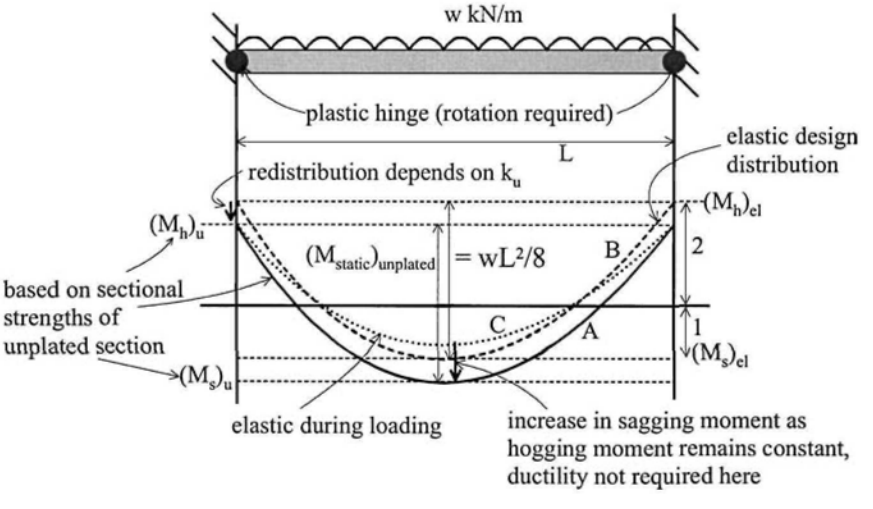

Figure 3.23 Moment redistribution in unplated beam - hogging hinges

Another way of viewing the moment redistribution in Fig. 3.23 is to consider the changes in the distribution of moment as the load is gradually increased from zero. Initially everything is elastic so that $M_h = 2M_s$. Therefore as the load is increased, the hogging joint will first reach its moment capacity as shown by the dotted line C. The hogging hinges shown now have to maintain their moment capacities and rotate until the sagging region reaches its moment capacity. Hence k_u of the hogging region determines the ability to redistribute moment in the case shown above. The thick arrow at the hogging joint in Fig. 3.23 indicates that the hogging moment is being reduced so that moment is being redistributed from the hogging region to the sagging region. Similarly for the sagging region, the thick arrow indicates that the moment is being increased.

(b) Plastic hinge in the sagging region

An example of redistribution from the sagging region to the hogging region is shown in Fig. 3.24. In this case, the designers have reduced the capacity of the sagging region and increased the capacity of the hogging region to maintain M_{static}. Hence on loading, the moment capacity of the sagging region will first be reached, as shown by the dotted line C, so that the plastic hinge at the sagging region needs to maintain its moment capacity whilst rotating to allow the moment capacities at the supports to be reached. Hence k_u at mid-span now determines the ability to rotate.

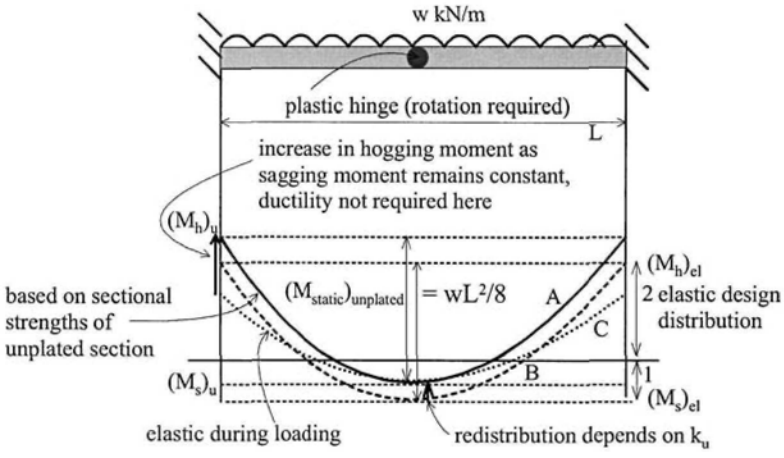

Figure 3.24 Moment redistribution in unplated beam – sagging hinge

As an example, if the mid-span was strengthened by plating so that $(M_s)_u$ in Fig. 3.24 is now the strength of the plated section, then metal plates would have to be used as FRP plated sections are too brittle to allow moment redistribution. However, FRP plates could have been used at the supports as moment redistribution is not required there. A similar argument applies to the hogging regions in Fig. 3.23. If the strength distribution line A was that of the plated beam, then metal plates would have had to be used at the supports to allow for moment redistribution, whereas, FRP plates could have been used at mid-span. It must be emphasised that the k_u factor for moment redistribution can only be applied directly to metal plated sections if it can be shown that concrete crushing controls the strength, that is at concrete crushing the strain in the plate is less than that required to cause debonding.

3.3.4.2 Moment redistribution in plated beams

Continuous beams plated with metal plates that are designed to yield before debonding and in which the concrete crushes prior to debonding can be designed directly as unplated beams, that is the moment redistribution can be based on the k_u factor. However, if the metal plates debond prior to the concrete crushing strain being achieved or if FRP plates are to be used, then moment redistribution may restrict the regions where plating can be used and control the type of plate used at a section.

(a) FRP plating sagging and hogging regions

It may be necessary to FRP plate both the hogging and sagging regions due to strength or serviceability requirements as shown in Fig.3.25. The use of FRP will preclude any moment redistribution so that the strengthened structure must have an elastic distribution of moment, which for this beam's restraints and loading configuration requires that the moment capacity of the hogging region is twice that of the sagging region as shown by the dotted line B. Hence, if it is necessary to increase the static moment capacity from that of the original unplated beam of $(M_{static})_{unplated}$ to $(M_{static})_{plated}$ as shown, then the amount of strengthening in each region is specifically defined as shown in Fig. 3.25. Theoretically this approach allows 'unlimited' strengthening or strengthening 'unlimited' by moment redistribution.

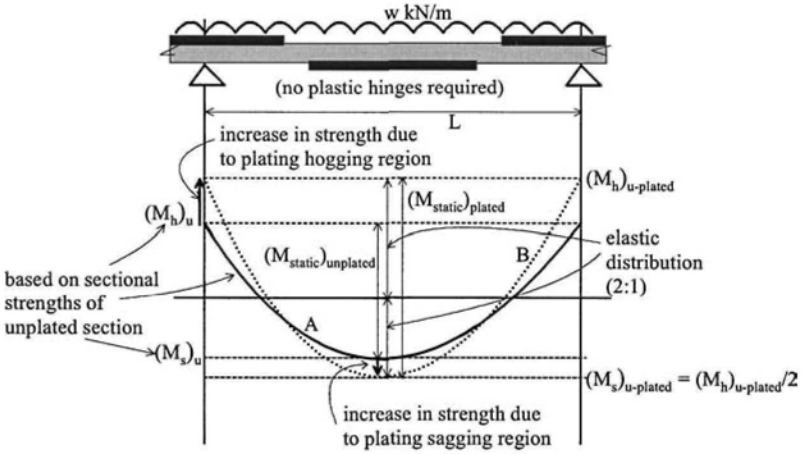

Figure 3.25 FRP plating all joints

(b) FRP plating hogging regions

As the hogging regions are to be plated with FRP in Fig. 3.26, plastic hinges are not allowed to form in the hogging regions and can only form in the sagging region as shown. Hence, it is necessary for the sagging region to remain unplated or plated with a metal plate that has been designed to allow the concrete to crush prior to debonding. The strength of the beam prior to plating is given by line A in Fig. 3.26; that is the distribution of moment at failure. The unplated beam can withstand a static moment of $(M_h)_u + (M_s)_u$ as shown and, hence, the uniformly distributed load at failure is given by Eq. 3.4. The problem is to determine how much the beam can be strengthened by only using FRP plates in the hogging regions; that is how much can the static moment $(M_h)_u + (M_s)_u$ be increased.

Let us first consider the option of not plating the sagging region but just using FRP plates in the hogging regions. Let us also assume that the ductility of the sagging region (as indicated by its neutral axis depth factor k_u as it is unplated) allows 30% moment redistribution, and as the hogging regions will have FRP plates, no redistribution is allowed there. The greatest increase in strength can be achieved by using the full moment redistribution capacity of the unplated sagging region. We are trying to find line C in Fig. 3.26, which is the distribution of moment of the plated structure at failure.

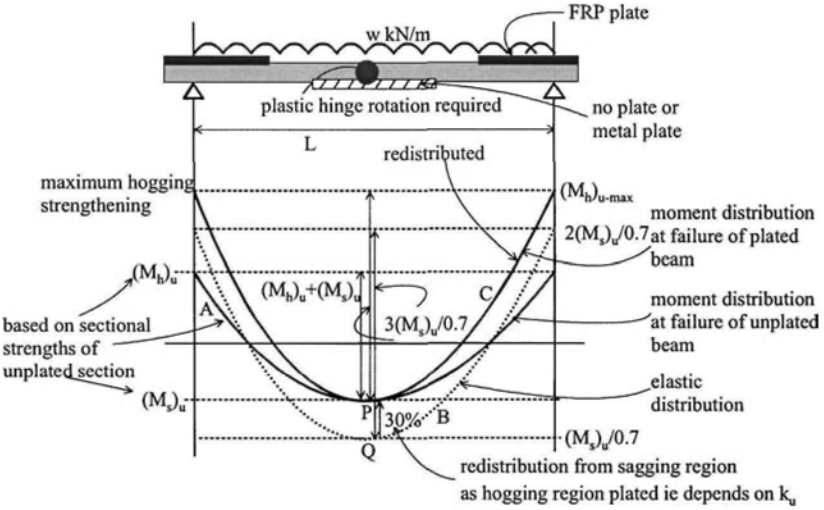

Figure 3.26 FRP plating hogging regions – 30% redistribution from sagging region

As the sagging region in Fig. 3.26 remains unplated, all we know is that line C, the strength of the plated beam, coincides with line A, the strength of the unplated beam, at point P at $(M_s)_u$ as shown. We do know that the sagging region can redistribute moment by 30%, which means that on applying the load to the elastic beam prior to moment redistribution, the moment at mid-span is greater than P and at point Q. The ductility of the sagging region allows part of this peak moment at Q to be redistributed to the hogging regions. As we know that 30% redistribution is allowed, the peak moment at Q is $(M_s)_u/0.7$, so that when 30% of this moment is redistributed then the moment becomes that at P of $(M_s)_u$. So we now have the magnitude of point Q of $(M_s)_u/0.7$. This is the moment prior to moment redistribution and, hence, it is just one point on the elastic distribution of moment on the beam; that is the distribution of moment based on EI being constant. As point Q, of magnitude $(M_s)_u/0.7$, is on the elastic distribution of moment, then the peak hogging moments must be twice this amount as shown, that is $2(M_s)_u/0.7$. Hence, the maximum elastic distribution of moment, line B, has been determined which has a static moment capacity of $3(M_s)_u/0.7$ as shown. This elastic distribution of moment can be redistributed by 30% of the sagging moment at Q to shift the whole curve upwards, as shown, to line C which is the redistributed moment at failure. From this redistributed moment can be derived the maximum possible hogging moment $(M_h)_{u\text{-}max} = 3(M_s)_u/0.7 - (M_s)_u$ which is the maximum hogging strength that can be attained when only the hogging regions are FRP plated. The increase in the static moment is given

by $3(M_s)_u/0.7 - [(M_s)_u + (M_h)_u]$ from which can be determined the increase in the applied load.

The rehabilitation procedure developed for plating is in many ways the inverse of a standard design procedure. Hence as a check to ensure our rehabilitation procedure is correct, we can apply the reverse design philosophy which is the standard design procedure. Line C in Fig. 3.26 is now the distribution of moment at failure of the plated structure which represents the strength of the structure and which we know the values of; we also know the value of the static moment for this distribution. Line B is the elastic distribution of line C; that is it has the same static moment and is distributed such that the maximum hogging moment is twice the maximum sagging moment. As we first apply and then gradually increase the load, such that the hogging moment is twice the sagging moment, the sagging moment capacity at point P is first reached. Hence, the sagging joint has to maintain this moment and keep rotating until the hogging moment capacities have been reached. If the capacity at point P is 30% (depending on the k_u value of the cross-section) less than that at point Q, then our retrofitting design procedure is correct.

If the sagging region, in Fig. 3.26, was plated with metal plates which were designed so that not only did the plates yield but that the concrete crushed before the plate debonded, then $(M_s)_u$ in Fig. 3.26 is simply that of the plated section and the above analysis can be used.

(c) FRP plating sagging regions

An example of FRP plating the sagging region is shown in Fig. 3.27. Exactly the same procedure as described in the previous Section on *FRP plating hogging regions* can be applied for this sagging region, except, of course, that the plastic hinges now occur in the hogging regions so that only the sagging regions can be FRP plated. It will be assumed that the hogging regions are unplated or that there are metal plates that allow the concrete to crush prior to debonding so that the ability to redistribute depends on the k_u factor which will be assumed allows 30% redistribution.

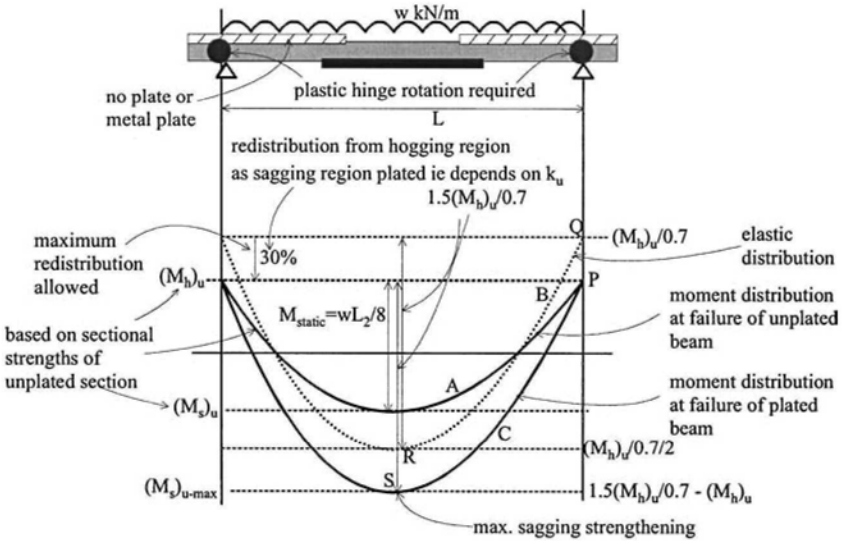

Figure 3.27 FRP plating sagging region – 30% redistribution from hogging regions

Line A in Fig. 3.27 depicts the strength of the beam without FRP plates; that is the distribution of moment at failure. Because the hogging regions can redistribute moment, one point on the elastic distribution prior to moment redistribution is given by point Q, such that a 30% reduction in Q, due to moment redistribution, gives point P. Having now fixed point Q, which is one point on the elastic distribution, point R is now fixed as it is half of the moment at Q, that is for this beam configuration. Hence, the whole elastic configuration of line B is now known. The moment distribution of line B can now be redistributed down by 30% of the hogging moment to give point S, which is the maximum strength that the plated sagging region can achieve based on moment redistribution.

Applying the converse of the rehabilitation approach to determine whether our analysis is correct. Line C in Fig. 3.27 is the strength of the plated structure. Line B is the elastic distribution. On applying the load gradually, the hogging capacity is reached first. Hence it is this joint that redistributed the moment and it is this joint that allows 30% redistribution. Hence if point P is 30% less than point Q then the original rehabilitation design is correct.

We have now reached the stage that for the beam in Fig. 3.27 we know, from moment redistribution considerations, that the most the sagging strength can be increased using FRP plates is $1.5(M_h)_u/0.7 - [(M_h)_u + (M_s)_u]$. Similarly, for the beam in Fig. 3.26, the maximum increase in the hogging region, that depends on moment redistribution, that can be achieved using FRP plates is $3(M_s)_u/0.7 - [(M_s)_u + (M_h)_u]$. The next step in the design procedure is to determine: whether these capacities can be achieved; if metal plates that have been used in other sections will allow the concrete to crush; and what is the maximum increase that can be obtained when moment redistribution is not required. This is the subject of the next section.

3.4 Sectional flexural strength and ductility capacity

The following analyses determine the flexural capacity of adhesively bonded plated sections in which failure is controlled by either concrete crushing, IC plate debonding or plate fracture. These analyses also derive the moment/curvature relationships, such as those in Figs. 3.17 and 3.18, that are required for the moment redistribution flexural rigidity approach in Section 3.3.2. These analyses also determine whether the IC debonding strain capacities in metal plated structures are sufficient to allow the concrete to crush and hence allow the k_u factor to be used for the plated section as discussed in Section 3.3.4.

The analyses are separated into propped structures, that is structures that are propped to remove the stresses within the structure prior to plating. This may be a useful technique for reducing deflections and crack widths at serviceability but the procedure can induce earlier debonding which can occur before the tension reinforcing bars have yielded. However, it is a useful starting point in the analysis as it is simpler than that for the ensuing section on unpropped construction. In unpropped construction, the beam or slab is plated whilst still carrying its self weight and some superimposed dead and live load. Hence the residual stresses in the RC section prior to debonding have to be taken into account. The residual stresses in the tension reinforcing bars are beneficial as they can ensure that the reinforcing bars yield before the plate debonds. This may be a major consideration when adhesively bonding FRP plates to the tension faces as FRP plates can debond at relatively low strains as shown

in Table 2.2. In fact, pre-loading beams prior to adhesive bonding can be very beneficial by ensuring yielding of the reinforcing bars prior to debonding.

3.4.1 *Propped structure*

The elementary flexural analysis of an unplated RC beam or slab is first revised. Then this standard approach is adapted to allow for the analysis of adhesively bonded metal and FRP plated structures where the plate is attached to a beam without any residual stresses, that is propped. The adhesively bonded approach is then adapted to allow for bolting.

3.4.1.1 Unplated section

A standard flexural analysis of an ordinary reinforced concrete beam is illustrated in Fig. 3.28. The beam cross-section is shown in Fig. 3.28(a) where the longitudinal reinforcement can be placed anywhere. Figures 3.28(b) to (d) depict the behaviour along the longitudinal axis of the beam at a specific section of the beam. Figure 3.28(b) is the distribution of longitudinal strain and will be referred to as the strain profile, Fig. 3.28(c) is the profile of the longitudinal stress, and that in Fig. 3.28(d) the longitudinal forces.

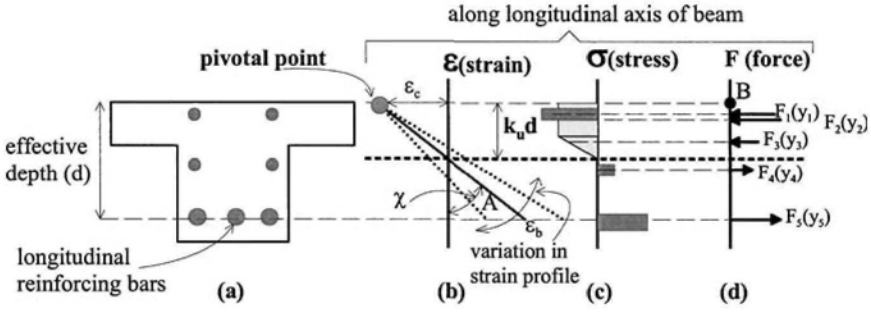

Figure 3.28 Standard flexural analysis of an RC beam

It is fairly standard practice to assume that the strain capacity of the longitudinal reinforcing bars is very large compared with the strain capacity of the concrete and, hence, does not cause failure; although this assumption can be easily checked. In which case, whether the longitudinal reinforcing bars have yielded or not, eventual failure of the beam is caused by the concrete crushing at a strain ε_c. This strain is given in national codes and is usually around 0.003 or 0.004. As concrete crushing at a strain ε_c causes failure, it is the one point on the strain profile that we know and it will be referred to as the pivotal point as shown in the strain profile in Fig. 3.28(b). The correct strain profile can be any strain profile that pivots about ε_c as shown in Fig. 3.28(b); that is the strain profile rotates about the pivotal point like a pendulum. An iterative procedure can be used to find the correct strain profile and spreadsheets are an ideal tool for doing these analyses.

A neutral axis depth $k_u d$ has to be guessed to fix the strain profile about the pivotal point, such as the profile A in Fig. 3.28(b). For the fixed strain profile A and from the known material stress/strain relationships, or their idealised relationship, can be derived the stress profile as shown in Fig. 3.28(c). The concrete stress profile is often considered as rectangular when the concrete has reached the crushing strain ε_c, however any shape according to the national code can be used; it is common practice

to ignore the tensile strength of the concrete in ultimate strength analyses due to the very large strains associated with failure but this can be easily incorporated if thought necessary. Integrating the stresses over the areas in which they act gives the resultant forces F and their positions y in the force profile in Fig. 3.28(d). The position y can be measured from any level in the cross-section and is often measured from the extreme compression fibre at B for convenience. If the longitudinal forces F sum to zero, for this beam with no externally applied axial load which is often the case, then there is longitudinal equilibrium and the guess for the neutral axis position and hence the strain profile is correct. Otherwise the strain profile can be swung around the pivotal point as shown in Fig. 3.28(b) to find a strain profile in which there is longitudinal equilibrium.

Let us assume that the profile A in Fig. 3.28(b) is the correct strain profile at failure as it is in longitudinal equilibrium; that is the longitudinal forces in Fig. 3.28(d) sum to zero. The moment capacity can be derived from the force distribution in Fig. 3.28(d) by taking moments about some convenient point such as the extreme compressive fibre at point B; however for a beam with no externally applied axial load taking moments at any level will give the same answer. Furthermore, the curvature at failure χ can be determined from Fig. 3.28(b) and even the maximum strain in the tension reinforcing ε_b in Fig. 3.28(b) at concrete failure.

As a matter of interest, if the strain in the tension reinforcing ε_b in Fig. 3.28(b) is greater than the fracture strain of the bar ε_{rebar}, which is unlikely but may occur particularly with the introduction of higher-strength/lower-ductility reinforcing steel in RC structures, then the assumption that concrete crushing at ε_c causes failure has been proved to be incorrect and the analysis has to be repeated, but this time with the pivotal point at ε_b which is now the fracture strain of the reinforcing steel. However, in this case the idealised rectangular stress block distribution for the concrete cannot be used as it only applies when ε_c is achieved so that the 'true' stress distribution should be used. The procedure can also be used to determine the behaviour at first yield, in which case the pivotal point is at ε_b which is now equal to the yield strain of the bar ε_y. Hence this procedure can be used to derive the whole moment/curvature relationship of an RC beam such as those shown in Figs 3.17 and 3.18 and which are required for the flexural rigidity approach for moment redistribution.

3.4.1.2 Adhesively bonded tension face plated beams

The flexural analysis for a tension face plated beam is shown in Fig. 3.29. As shown by the possible pivotal strains in Fig. 3.29(b), failure of the beam can be caused by either the concrete crushing at a strain ε_c, the plate IC debonding at a strain ε_{db}, the plate fracturing at ε_{frac}, or the reinforcing bars fracturing at ε_{rebar}. Hence, the pivotal point in the analysis can occur at either ε_c, ε_{db}, ε_{frac} or ε_{rebar}, whichever occurs first. It is simply a question of guessing which of these strains is reached first and pivoting about this strain. If the results show that the other strains have not been reached then the initial assumption is correct, otherwise, the analysis has to be repeated by pivoting about the strain that has been exceeded.

For pultruded carbon FRP plates, the IC debonding strain ε_{IC}, as listed in Table 2.2, is generally much smaller than the plate fracture strain ε_{frac}, and certainly much smaller than the reinforcing bar fracture strain ε_{rebar}. Hence in the region of the tension face, the first strain to be reached is generally the IC debonding strain, although this may not be the case with very thin wet lay up plates or if glass FRP plates are used. Experience has shown that with carbon FRP plates, the concrete rarely reaches its

failure strain of ε_c and quite often remains in the pseudo elastic range. Hence for carbon FRP plates, a good initial assumption for the pivotal point is the IC debonding strain $\varepsilon_{IC} = \varepsilon_{db}$ as shown in Fig. 3.29(c). It needs to be emphasised that even if the pivotal point is incorrectly chosen, the ensuing analyses will show this to be the case so that the pivotal point can be eventually changed to the correct value.

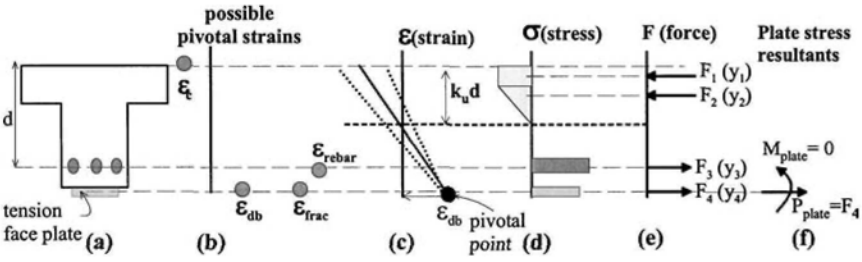

Figure 3.29 Flexural analysis of a tension face plated beam

Having chosen the pivotal point in Fig. 3.29(c), the analysis follows the standard procedure described in Section 3.4.1.1. For a given strain profile in Fig. 3.29(c), can be derived the stress profile in Fig. 3.29(d). The concrete stress has been shown as elastic/plastic in Fig. 3.29(d); however, any national variation will do, just as long as it allows for low stresses in the pseudo elastic range as IC debonding can occur when the concrete stresses at the compression face are very low. From the stress profile can be derived the force profile in Fig. 3.29(e), and if these forces are in longitudinal equilibrium, that is they sum to zero for a beam with no externally applied axial load, then the strain profile is correct. The strain profile in Fig. 3.29(c) is now known and can be used to see if any of the other possible pivotal points in Fig. 3.29(b) have been exceeded. If a possible pivotal point strain has been exceeded, then the position of the pivotal point should be changed to that pivotal strain and the process continued until no possible pivotal point strains are exceeded. Once the correct strain profile in Fig. 3.29(c) has been found, then the curvature at failure is given by the slope of the strain profile in Fig. 3.29(c), and the moment capacity by taking moments of the longitudinal forces in Fig. 3.29(e). These results will give the end of the plastic zone in Fig. 3.18.

The analysis procedure described in Fig. 3.29 can be used to find the whole moment/curvature relationship such as that shown in Fig. 3.18. However it may be more straightforward to find the flexural rigidity of the cracked section and possibly the moment at first yield of the reinforcing bars from elementary linear elastic analyses. If not, the start of the plastic zone such as B_s in Fig. 3.18 can be derived from Fig. 3.29 by this time pivoting about the yield strain of the reinforcing bars ε_y at the level of the reinforcing bars.

Also of interest are the stress resultants in the plate, as shown in Fig. 3.29(f), as it is these stress resultants that have to be transferred across the plate/beam interface. For example, it may have been decided to bolt the plates as well as adhesively bond the plates, as in Figs. 2.8 and 2.9, so that the bolts will take over if the adhesive bond deteriorated such as might occur in a fire or due to rusting at the interface in steel plated structures. In which case, the bolts would have to be designed to resist the stress resultants in Fig. 3.29(f). For tension face plates, the major stress resultant is the axial force $P_{plate} = F_4$, so that the bolts would have to be designed to

resist this axial force as described in Section 3.4.1.5. The moment in the plate M_{plate} is not actually zero as shown in Fig. 3.29(f) because the strain through the plate is inclined as shown in Fig. 3.29(c). However, because the plate is very thin compared with the depth of the beam, the moment in the plate is considerably smaller than the moment in the beam and usually ignored; that is the inclination of the strain in the plate is usually ignored.

Exactly the same procedure as outlined in Fig. 3.29 can be applied to metal plates. However, if they have been designed to yield before debonding, then a better starting position for the pivotal point may be at the concrete crushing strain ε_c, as shown in Fig. 3.28(b), and then check to ensure that IC debonding has not preceded concrete crushing. If this is the case, then the ductility of the metal plated section can be assumed to be governed by the neutral axis depth factor k_u as described in Section 3.3.1, otherwise, the flexural rigidity approach in Section 3.3.2 may have to be applied if moment redistribution is required.

3.4.1.3 Adhesively bonded shallow FRP side plated beams

The flexural analysis of a fairly shallow FRP side plated beam, in which the plate has been placed in the tension zone of the beam, is shown in Fig. 3.30. IC debonding occurs at the level of the largest tensile strain in the plate, that is at the level of the plate furthest from the neutral axis; which is where the pivotal point is shown in Fig. 3.30(b). The usual iterative procedure is applied to determine longitudinal equilibrium and to then check that the choice of the pivotal point is correct. The strain profile in Fig. 3.30(b) also gives the strain in the reinforcing bars ε_{bar}. If the reinforcing bars have not yielded, this may be considered to be very inefficient, as far as the strengthening procedure is concerned, and it also leads to a brittle section which is undesirable. If debonding prior to bar yielding does occur, then a solution would be to move the plate upwards towards the compression zone. For example, having the bottom of the plate above the level of the reinforcing bars will ensure that the reinforcing bar strains are always larger than the plate strains and, hence, the reinforcing bars are more likely to yield before the plates debond.

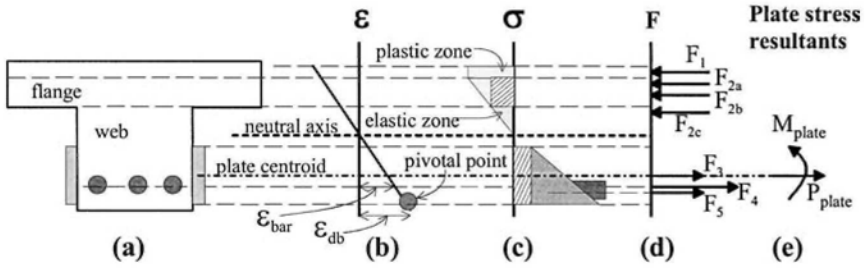

Figure 3.30 Flexural analysis of an FRP side plated beam

From the strain profile in Fig. 3.30(b), can be derived the stress profile in Fig. 3.30(c); the tensile strength of the concrete can be easily incorporated if desired. Invariably for carbon FRP plated specimens, much of the concrete in compression is within the elastic or pseudo elastic zone as shown in Fig. 3.30(c). This is because the IC debonding strains of carbon FRP pultruded plates are quite small as shown in Table 2.2. This can also be deduced from Eq. 1.2 which shows that the debonding strain is inversely proportional to the stiffness of the plate material, which for carbon

FRP is generally quite large. As FRP is a linear elastic material, the stresses within the plate are linearly distributed as shown in Fig. 3.30(c). The forces in Fig. 3.30(d) can be derived from both the stress distributions in Fig. 3.30(c) and the cross-sectional areas over which they act in Fig. 3.30(a); bearing in mind that, in this example, the plate forces F_3 and F_5 are the forces in both of the plates shown in Fig. 3.30(a). It is convenient to divide the stress profiles into distributions that can be conveniently integrated over the cross-sectional area such as triangular and rectangular components. For example, the concrete stress distribution in Fig. 3.30(c) has been separated into: the plastic zone in the flange to give the force F_1 at the mid-depth of the plastic zone; the elastic zone in the web which has a stress resultant of F_{2c} acting a third the way down the triangular stress distribution in the web; and the elastic zone in the flange which has been broken down into a rectangular stress and triangular stress distributions with the resultant forces F_{2a} and F_{2b}. Similarly, the FRP plate stress distribution has been divided into the rectangular portion shown hatched that acts over the whole of the plate area and whose force F_3 acts through the plate centroid, and the triangular distribution that also acts over the whole of the plate area but the resultant F_5 acts one-third the way up the plate.

In Fig. 3.30(e) is the resultant axial force in the plate P_{plate} and the moment in the plate about the plate centroid M_{plate}. These stress resultants are not required in the design of adhesively bonded plates but would be required if it was decided to bolt the adhesively bonded plate as an additional safeguard. It must be emphasised that the adhesive bonded system should be considered to act independently of the bolted system and, hence, the two systems should be designed independently of each other; it is suggested that the bolts should not be considered to enhance the adhesively bonded system and vice versa, as an adhesive bond is brittle whilst a bolted bond is ductile as it needs interface slip. The resultant axial force in the plate P_{plate} is simply the sum of the plate forces F_3 and F_5 in Fig. 3.30(d), and the resultant moment M_{plate} is simply determined by taking moments of the plate forces F_3 and F_5 about the plate centroid. The bolts have to resist these stress resultants as explained in Section 3.4.1.5.

3.4.1.4 Adhesively bonded deep metal side plated beams

It is well known that the addition of tension reinforcement such as the tension face plate in Fig. 3.29(a) will always reduce the sectional ductility, and it is often this reduction in ductility that limits the increase in flexural strength that can be achieved by plating. Extending the adhesively bonded side plates in Fig. 3.30(a) into the compression zone as shown in Fig. 3.31(a) can increase the flexural capacity whilst maintaining and sometimes even increasing the ductility.

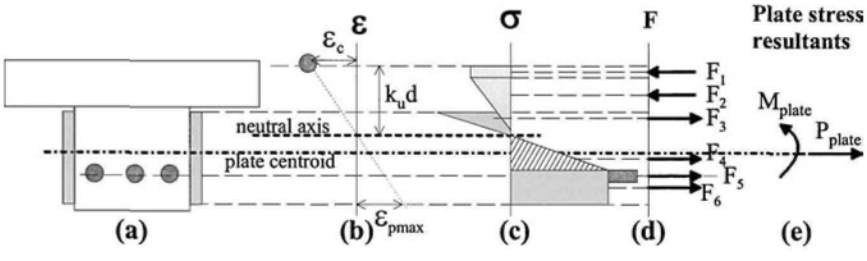

Figure 3.31 Flexural analysis of a deep metal side plated beam

For an ultimate limit strength analysis, the metal side plates in Fig. 3.31 would probably be designed to yield before debonding. In which case, the assumption that the pivotal point is at the concrete crushing strain ε_c, as shown in Fig. 3.31(b), would be a reasonable start to the analysis, with the usual checks for debonding after the analysis is complete. If the concrete crushing strain ε_c did control the analysis at ultimate, then the neutral axis depth factor k_u in Fig. 3.31(b) would control moment redistribution. For a serviceability analysis, thick plates would probably have been used to increase the flexural rigidity and reduce deflections and crack widths and would have been designed not to yield at the low serviceability loads. In this case, the debonding strain would control the analysis, that is ε_{pmax} in Fig. 3.31(b) would be ε_{db} and the pivotal point would be at this position.

The stress resultants in the plate are shown in Fig. 3.31(e) and as mentioned previously, if the plates were bolted so that the bolts took over totally if the adhesive bond deteriorated, then the bolts would have to be designed to resist these stress resultants. It is worth comparing the stress resultants in Figs. 3.29(f) for the tension face plate which occupies a small vertical dimension, with Fig. 3.30(e) for the shallow side plate, and with Fig. 3.31(e) for the deep side plate which occupies a large vertical dimension. It is worth noting that as a general rule that as the vertical dimension of the plate increases, the axial force in the plate P_{plate} reduces and the moment in the plate M_{plate} increases. Let us consider an FRP plated beam as an example, when the vertical dimension of the plate is simply the plate thickness as in the tension face plate in Fig. 3.29(a), then $M_{plate} \rightarrow 0$ and P_{plate} is at its maximum which is the product of the cross-sectional area of the plate and the debonding stress. As the vertical height of the plate increases as in Fig. 3.31(a), the tensile component in the plate, that is F_3 increases reducing the overall axial force P_{plate} and increasing the moment M_{plate}. Hence for shallow plates the bolt forces tend to be governed by P_{plate} whereas for deep plates they tend to be governed by M_{plate}.

3.4.1.5 Bolted side plated beams

The analysis for bolting a metal or FRP plate to the sides of a beam is illustrated in Fig. 3.32; the analysis follows the same general procedure that was used for adhesively bonded plates. Unlike adhesively bonded connections, bolted connections are highly ductile and are unlikely to fail in a brittle fashion. Hence, a standard analysis for RC structures can be followed by pivoting about ε_c, as shown in Fig. 3.32(b); after which for an FRP plate, the strain in the plate can be checked to ensure that it has not fractured.

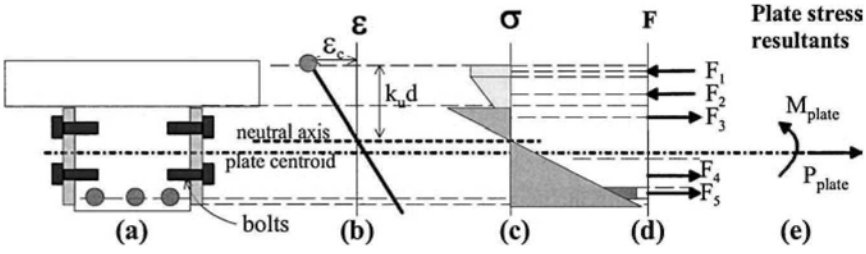

Figure 3.32 Bolted FRP side plate

Consider the forces in the plates in Fig. 3.32(d); from the forces F_3 and F_4, can be derived the axial force in the two plates P_{plate} and the moment about the plate

centroid M_{plate} for the two plates. Similar analyses have already been illustrated in Figs 3.29 to 3.31. These stress resultants in the plates are transferred from the RC beam to the plate through the bolt shear connectors shown in Figs 3.32(a) and 3.33(a).

Figure 3.33 is a longitudinal view of the beam over either the hogging region or the sagging region of length L; that is, between the points of contraflexure which also represent the supports of a simple supported beam. This portion of a beam will be referred to as a *region*, as it refers to either the hogging region or the sagging region. This region can be considered to consist of two parts on either side of the position of maximum moment, which will be referred to as the left and right *shear spans* and which have plates of length $(L_{sh\text{-}sp})_{left}$ and $(L_{sh\text{-}sp})_{right}$. It is important to realise that the plates in each shear span resists both P_{plate} and M_{plate}; that is, both the plate and the bolts in each shear span resist P_{plate} and M_{plate}. It is also worth noting that if P_{plate} and M_{plate} represent the forces in two plates as would be the case in the side plate analyses in Figs.3.30 to 3.32, then the number of bolts required is the total number of bolts in a shear span and should be spread equally between the plates on either side of a beam as in Fig. 3.32(a) and uniformly along a shear span as in Fig. 3.33.

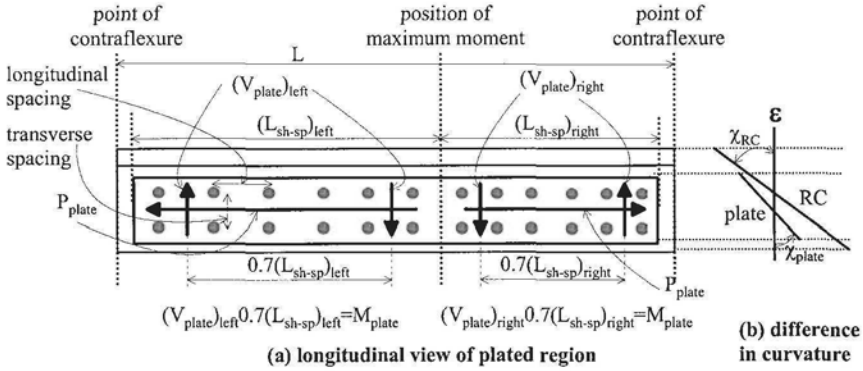

Figure 3.33 Design forces in bolted plates

On either side of the position of maximum moment in Fig. 3.33(a), the bolts have to resist the stress resultants in the plate, that is M_{plate} and P_{plate} as shown in Fig. 3.32(e) (similarly in Figs 3.29(f), 3.30(e), and 3.31(e)). It is a safe design to simply determine the number of bolts that are required to resist the longitudinal force P_{plate} by itself (N_{long}) and then add the number of bolts required to resist the vertical force in the bolts induced by M_{plate} (N_{vert}) as shown in Fig. 3.33(a). Let us assume that the shear capacity of a single bolt in a bolted plated joint is P_{sh}, which can, if need be, be determined directly from push tests in the same way as the capacity of shear connectors for composite steel and concrete beams is determined.

The number of bolts required to resist the longitudinal force P_{plate} in each shear span $L_{sh\text{-}sp}$ in Fig. 3.33(a) is $N_{long} = P_{plate}/P_{sh}$. Tests and numerical simulations (Oehlers et al 2000) have found that the moment M_{plate} is resisted by a vertical force couple V_{plate} in Fig. 3.33(a) that have a lever arm of $0.7L_{sh\text{-}sp}$ where $L_{sh\text{-}sp}$ is the length of the plate in a shear span. Hence $V_{plate} = M_{plate}/0.7L_{sh\text{-}sp}$, so that the number of bolts required to resist both vertical forces in a shear span is $N_{vert} = 2(M_{plate}/0.7L_{sh\text{-}sp})/P_{sh}$. Therefore, the number of bolts required in a shear span is $N_{long} + N_{vert} = P_{plate}/P_{sh} + 2(M_{plate}/0.7L_{sh\text{-}sp})/P_{sh}$. Mechanical shear connectors, such as bolt shear connectors, are ductile connections and, hence, they can be spread uniformly along a shear span as

shown in Fig. 3.33(a); that is the longitudinal and lateral spacings are the same throughout a shear span. If the shear span plates are of equal length, $(L_{sh\text{-}sp})_{left} = (L_{sh\text{-}sp})_{right}$, then the number of bolts and their distribution in each shear span will be the same, so that the total number of bolts in a region will be twice that in a shear span. If the shear span plates are of different lengths, then the number of bolts in each shear span will be different due to the difference in V_{plate} between shear spans and their spacings will also be different; the shorter right shear span plate in Fig. 3.33(a) will require more bolts than in the left and will, therefore, require a closer longitudinal spacing of the bolts.

It is worth bearing in mind that the analyses shown in Figs. 3.29 to 3.33 assume full interaction between the plate and the beam which occurs in adhesively bonded plates as an adhesive bond is a very rigid joint. However, for bolted connections to work, slip is required between the plate and the beam to induce the shear forces in the bolts. Hence, a bolted joint is a partial interaction joint in which there is longitudinal and vertical slip between the plate and the beam and, therefore, the curvature in the plate χ_{plate} is less than that in the beam χ_{RC} as shown in Fig. 3.33(b). The strains in the plate, therefore, lag behind those in the beam, so that this difference in curvature can reduce the strength slightly. Tests on bolted plated beams have shown (Oehlers et al 2000) that, in general, the reduction in the increase in strength due to plating is about 8% with one beam recording a 15% reduction. This is the reduction in the *increase in strength due to plating* and not the reduction of the total strength. It is, therefore, recommended that a safe design, to allow for partial interaction, would be to reduce *the increase in strength due to plating* derived from a full interaction analysis by 15%.

It is also worth bearing in mind that the analysis in Fig. 3.32 is a full shear connection analysis which means that sufficient bolts are provided to resist P_{plate} and M_{plate}. Fewer bolts can be provided, in which case the stress resultants P_{plate} and M_{plate} are now governed by the number of bolts provided, and this is referred to as a partial shear connection analysis and details of this analysis can be found elsewhere (Oehlers and Bradford 1995). However, when a partial shear connection analysis is used, the ductility of the shear connectors now becomes very important in order to prevent the bolt shear connectors from fracturing due to excessive slip as shown in Fig. 1.31(a). Hence, it is recommended that a full shear connection analysis is applied as depicted in Fig. 3.32.

Bolted plates when placed in the compression zone such as in Figs 3.32 and 1.31(b) can buckle and there are guidelines for positioning the bolts to prevent buckling for steel plated members (Smith et al 1999, 2000 and 2001). However, restricting the bolted plates to the tension zones such as in Figs 3.29 and 3.30 will overcome this problem. Buckling is not a problem with adhesively bonded plates. It is also worth bearing in mind that bolted FRP plates are not susceptible to premature debonding or premature failure so that they can generally be designed to attain a high stress in the FRP, whereas, the maximum stress in adhesively bonded FRP plates is generally quite small and may only be 20% to 30% of their fracture stress.

The design of the bolt shear connectors is illustrated in Fig. 3.34. Bolt shear connectors behave in a similar fashion to stud shear connectors in composite steel and concrete design. Hence, it is recommended that rules for the design of stud shear connectors (Oehlers and Bradford 1995, 1999) can be applied directly and which are given in national codes for composite steel and concrete beams. The bolts act as dowels in transferring the shear from the RC member to the plate; the top bolt marked as *bolt shear connector* in Fig. 3.35 has broken by dowel action with the characteristic

small zone of crushed concrete just visible adjacent to the bolt on the left side. A minimum length of bolt embedded in the concrete in Fig. 3.34 is required to prevent embedment failure (that is to prevent the bolts from pulling out). The stirrups act as transverse reinforcement. The shear planes in the RC beam have to be able to resist the imposed dowel forces. There must be sufficient cover to the bolt to prevent the dowel forces from splitting the concrete as shown in Fig. 3.35. The transverse spacing and longitudinal spacing of the bolts in Fig. 3.33 must be sufficiently large to allow the full dowel strength to be achieved. Design rules for all these failure mechanisms are available from the design of stud shear connectors.

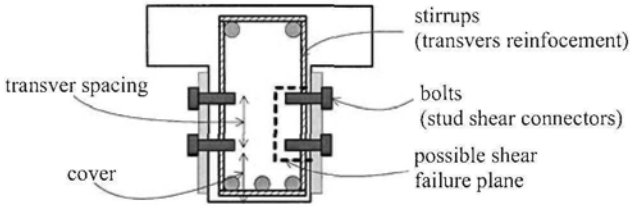

Figure 3.34 Design of bolt shear connectors

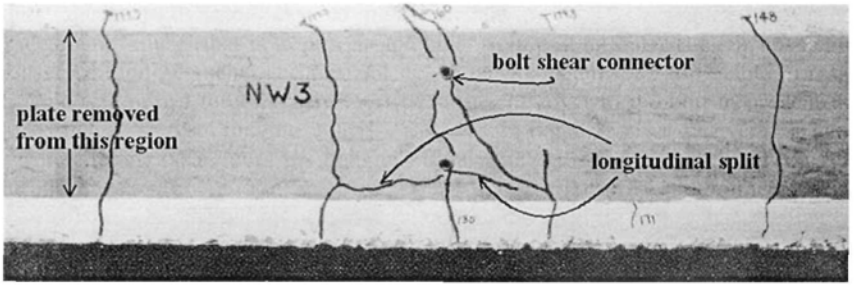

Figure 3.35 Failure of bolt shear connectors

It is often much easier to bolt the sides of beams as in Fig. 3.35 where only the stirrups have to be avoided, than to bolt the tension face of beams, where the congestion of the tension reinforcing bars may make it impossible to extend the bolt well past the concrete cover to ensure that embedment failure does not occur.

3.4.2 *Unpropped structure*

3.4.2.1 Adhesively bonded tension face plated beam

The problem with FRP plating in particular, is that the IC debonding strains as determined from tests, as shown in rows 1-2 and 5-6 in Table 2.2, are about the same magnitude as the yield strain of high yield tension reinforcing bars and, because the tension face plate is further from the neutral axis than the tension reinforcing bars, as shown in Fig. 3.36(b), there is a very good chance that the tension face plate will debond before the reinforcing bars yield which would produce a very brittle sectional and beam behaviour. One way of overcoming this problem is to plate the beam when it is unpropped, so the beam is preloaded with at least its own weight prior to plating. Hence, the plate will only help resist the additional live load whilst the tension reinforcing bars are resisting all of the dead and live load. If this is still not sufficient

to prevent IC debonding prior to the reinforcing bars yielding, then it is theoretically possible to pre-load the beam prior to plating to further increase the difference between the reinforcing bar strains and the plate strains.

The flexural analysis of a propped beam in Fig. 3.36(A) is compared with that of an unpropped beam in Fig. 3.36(B). The propped analysis in Fig. 3.36(A) follows the procedures already described in Section 3.4.1; at plate debonding, at a plate strain of ε_{db} in Fig. 3.36(b), the strain in the tension reinforcing bars is $(\varepsilon_{bar})_{propped}$ is less than the IC debonding plate strain of $\varepsilon_{IC} = \varepsilon_{db}$.

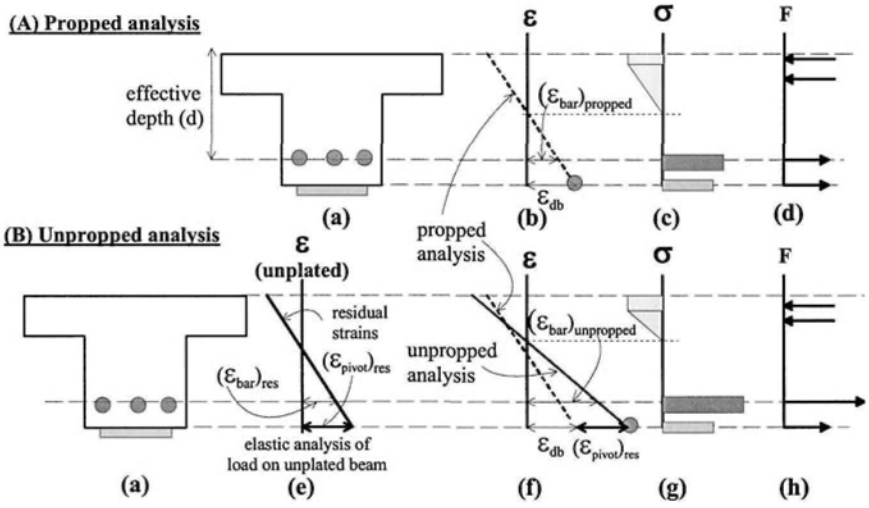

Figure 3.36 Flexural analysis of an unpropped plated beam

When the unplated beam is unpropped or preloaded, then there are already strains within the section which will be referred to as the *residual strains* and which are shown in Fig. 3.36(e). These strains can be determined from a straightforward linear elastic analysis of the section under the serviceability loads that are acting; depending on the state of the beam and the loads that are acting and have acted, will determine whether an uncracked or cracked sectional analysis is appropriate. The residual strain in the tension reinforcing bars is shown as $(\varepsilon_{bar})_{res}$ in Fig. 3.36(e). The residual strain at the tension face of the concrete is shown as $(\varepsilon_{pivot})_{res}$ and it is the residual strain at the level of the future pivotal point; the strain $(\varepsilon_{pivot})_{res}$ is really an effective strain as it defines the strain profile but it may not be the actual strain in the concrete due to flexural cracking. When the unpropped beam is plated, and prior to any further increase in load, the plate strain is zero and the concrete strain adjacent to it is $(\varepsilon_{pivot})_{res}$, so that this strain difference between the plate and the adjacent concrete will always exist upon loading. This is similar to the signature strain difference $\Delta\varepsilon_p$ between prestressing tendons and the concrete at the level of the tendons in prestressed concrete which is fixed at the time of stressing.

On loading the plated beam, the plate will eventually debond at a plate strain of $\varepsilon_{db} = \varepsilon_{IC}$. Therefore the strain in the adjacent concrete is $\varepsilon_{db} + (\varepsilon_{pivot})_{res}$ as shown in Fig. 3.36(f). This is the pivotal point for the strain profile in the RC beam as shown in Fig. 3.36(f). Having fixed the pivotal point, the analysis follows the standard

procedure already described in Section 3.4.1. By comparing Figs. 3.36(b) and (f), it can be seen that as the pivotal point strain has increased, the strain in the reinforcing bars has increased from $(\varepsilon_{bar})_{propped}$ to $(\varepsilon_{bar})_{unpropped}$ at failure. This increase may be sufficient to allow the reinforcing bars to yield.

3.4.2.2 Adhesively bonded side plated beam

The analysis of an unpropped side plated beam is shown in Fig. 3.37 and follows the same procedure as for the tension face plated beam in Fig. 3.36. The residual stresses in the unplated beam prior to plating have first to be determined as shown in Fig. 3.37(b). When the side plates are adhesively bonded to the beam and prior to any further loading, the plate will not have any stresses and, therefore, the difference between the plate strain and the RC beam strain will be given by the strain profile in Fig. 3.37(b). Any two points need to be known to fix this strain difference. For convenience these will be chosen at the level of the compression edge of the plate where the residual strain is $(\varepsilon_{comp.edge})_{res}$ and at the tension edge of the plate where the residual strain is $(\varepsilon_{pivot})_{res}$, where the tensile strain in the plate will eventually be its highest and, therefore, where debonding will eventually initiate.

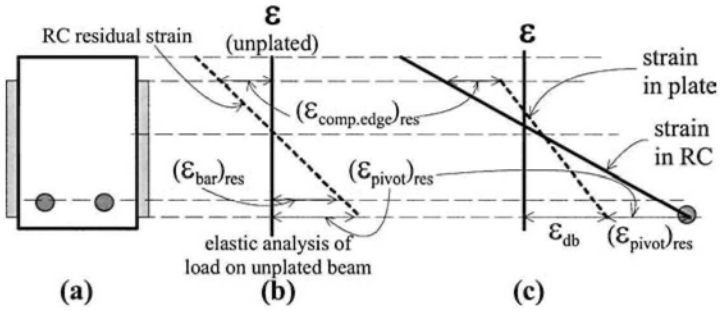

Figure 3.37 Flexural analysis of an unpropped side plated beam

As the beam is loaded, the strain profile in the RC beam will change but the plate strains will always lag behind the RC strains by a value of $(\varepsilon_{comp.edge})_{res}$ at the top of the plate and $(\varepsilon_{pivot})_{res}$ at the bottom of the plate, until just prior to plate debonding the pivotal strain is $\varepsilon_{db} + (\varepsilon_{pivot})_{res}$ as shown in Fig. 3.37(c). To find a solution, the strain profile in the RC beam is swung around the pivotal point in Fig. 3.37(c), bearing in mind that the plate strain profile lags behind by the values $(\varepsilon_{comp.edge})_{res}$ and $(\varepsilon_{pivot})_{res}$ as shown in Fig. 3.37(c), until longitudinal equilibrium is achieved. As with the tension face plate in Fig. 3.36, the strains in the reinforcing bars at plate debonding will increase. If this is not sufficient to allow the bars to yield, then either a pre-load can be applied to the beam prior to plating or the bottom level of the FRP plate in Fig. 3.37(a) could be raised, thereby, raising the pivotal point in Fig. 3.37(c), which will cause the strains in the reinforcing bars to increase prior to debonding.

3.5 Analyses and parametric studies

The design procedure for flexural strengthening based on IC debonding will be illustrated for adhesive bonding tension FRP face plates, adhesive bonding steel side

plates and bolting steel, aluminium or FRP plates to either slab structures or beam structures. These analyses supplement a comprehensive set of worked examples fully described in Chapter 7 that covers all forms of debonding. All safety factors and load factors have been removed from the analyses as it is assumed the designers will apply their own national values.

The design procedure for flexural strengthening based on IC debonding applies to both the hinge approach described in Section 2.5.2 and the anchorage approach in Section 2.5.1. However, the IC debonding resistances from pull tests are used in the following analyses, which means that the results are typical of the hinge approach. The anchorage approach allows the use of higher debonding strains and examples of analyses with these higher strains are given in Chapter 7.

3.5.1 Slab structure with adhesively bonded FRP plates in sagging region

A slab is strengthened along one span by adhesive bonding carbon FRP plates to the sagging region. Brief specifications are first given (the full specifications are given in Chapter 7), then moment redistribution is considered to determine the theoretical maximum increase in the strength of the sagging region to achieve the maximum increase in overall strength. The slab is then plated as propped and unpropped for comparison.

3.5.1.1 Slab specifications

An internal bay of a continuous slab has been chosen to illustrate the design procedure. Details of a 1 meter width of the slab are shown in Fig. 3.38. The slab spans 5m, as shown in Fig. 3.38(a) and the cross-sectional details for both the hogging (-ve) and sagging (+ve) regions are shown in Fig. 3.38(d). The unplated slab has a hogging strength of 41 kNm and a sagging strength of 31 kNm, as shown in Fig. 3.38(b), such that the static moment at failure is 72 kNm which converts to a uniformly distributed load at failure of 22.9 kN/m as shown in Fig. 3.38(a). The elastic distribution for the static moment is shown as the dashed line in Fig. 3.38(b) and it can be seen that the slab has been designed for a moment redistribution from the hogging region of 15%; that is the strength of the hogging region is 15% less than its elastic moment. The maximum vertical shear load is 57 kN as shown in Fig. 3.38(c).

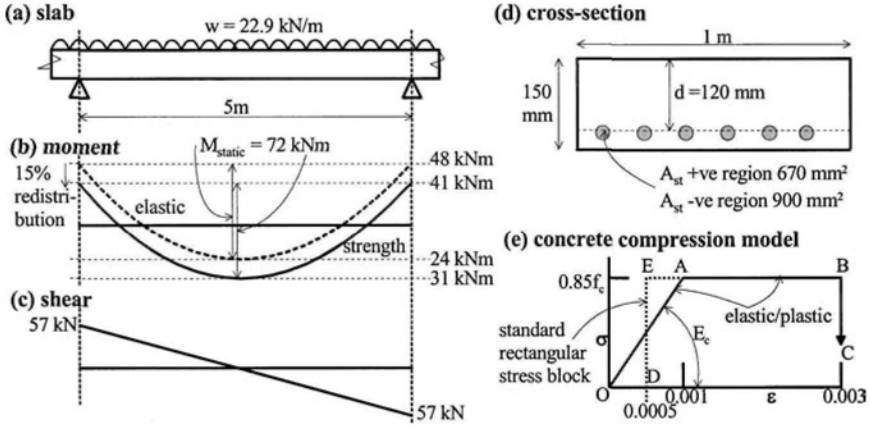

Figure 3.38 Slab structure

For convenience, the concrete compressive constitutive model has been assumed to have a pseudo linear-elastic/perfectly-plastic variation O-A-B-C, as shown in Fig. 3.38(e), with a strain capacity of $\varepsilon_c = 0.003$. Any variation can be used in the following calculations such as the well-known parabolic/rectangular shape. However, the pseudo elastic/plastic variation has been used here to help to illustrate to the reader, in the following calculations, how IC debonding can occur well before the concrete crushes at its ultimate strain ε_c and whilst the concrete is pseudo-elastic. For interest, the elastic/plastic relationship O-A-B-C has been compared in Fig. 3.38(e) with the standard rectangular stress block at ultimate (which is only applicable when the maximum concrete strain has reached ε_c) used in Australia and elsewhere of O-D-E-B-C. The depth of the standard rectangular stress block D-E-B-C is typically defined by a factor γ of the neutral axis depth $k_u d$ and is a function of f_c. It may also be worth noting that in design examples, where the concrete crushing strain ε_c is reached, the difference in the ultimate flexural strength between using the perfectly plastic rectangular distribution O-D-E-B-C and the pseudo elastic/plastic distribution O-A-B-C was very small, more often less than 1%. Hence, the elastic/plastic variation O-A-B-C can be used at all stages of loading, such as when all the concrete is in the pseudo-elastic region O-A. Whereas the rectangular variation O-D-E-B-C cannot cope with any stress distribution other than that at ultimate when ε_c has been reached.

In the following examples, the concrete cylinder compressive strength $f_c = 30$ MPa, the yield strength of the reinforcing bars $f_y = 400$ MPa and their yield strain $\varepsilon_y = 0.002$, the Young's modulus of the concrete $E_c = 25.5$ GPa, and the Brazilian tensile strength of the concrete $f_{cb} = 2.7$ MPa. Hence for the value of f_c and E_c used in the following examples, the strain at point A in Fig. 3.38(e), that is the transition from elastic to plastic behaviour, is 0.001. For the hogging region, the neutral axis depth factor $k_u = 0.14$ and the vertical shear capacity of the slab, from a national standard, is $V_c = 119$ kN. For the sagging region, $k_u = 0.10$ and $V_c = 108$ kN. It can be seen that the shear load on the slab of 57 kN in Fig. 3.38(c) is well within its shear capacity of 119 kN. The slab is to be plated with 1.2 mm thick carbon FRP plates of Young's modulus $E_p = 160$ GPa, which from Eq. 2.1 and Table 2.2 has a characteristic IC debonding strain of $\varepsilon_{IC} = 0.00267$, a characteristic debonding stress of $\sigma_{IC} = 427$ MPa (for convenience it has been assumed that $b_p/b_c = 0.5$ throughout) and from Eq. 2.3 an anchorage length of $L_e = 187$ mm.

3.5.1.2 Moment redistribution

In this example, we are only allowed to plate the sagging region with FRP plates as shown in Fig. 3.39(a). The first stage of the design is to determine if there are any limits to increasing the load on the continuous slab when strengthening the sagging region only with FRP plates. The moment distribution at failure of the unplated beam is shown as line A in Fig. 3.39(b); the static moment, being the sum of the hogging and sagging strengths of 41 kNm and 31 kNm, is 72 kNm. The sagging region is to be plated with carbon FRP plates and, therefore, it will be assumed that a plastic hinge cannot form in the sagging region for the reasons given in Section 3.3.1. The hogging regions are unplated and have a small neutral axis factor $k_u = 0.14$ which for some codes in Fig. 3.14 allows 30% redistribution which will be assumed.

The largest increase in the overall strength of the continuous beam, that is the largest increase in the load that can be applied to the continuous beam, occurs when the maximum moment is redistributed from the hogging region to the sagging region. As the hogging hinges in Fig. 3.39(a) can redistribute 30% of their elastic moment, the elastic moments at the hogging hinges are $(M_h)_u/0.7 = 59$ kNm which are shown

as points E in Fig. 3.39. As a check, 30% redistribution from 59 kNm gives the hogging strength of 41 kNm. As the hogging moments at points E are part of the elastic distribution, the elastic sagging moment must be half the hogging moment and is shown as point F of magnitude $(M_h)_u/0.7/2 = 29$ kNm. Hence, the maximum static moment that can be achieved by allowing for 30% redistribution from the hogging region to the sagging region is 59 + 29 = 88 kNm which is shown as $(M_{static})_{pl}$; the subscript *pl* has been used as this static moment can only be achieved after plating. The static moment has been increased from 72 kNm to 88 kNm, that is a 22% increase in strength. Moment redistribution will allow the elastic moment distribution E-F-E (line B in Fig. 3.39(b)) to drop to H-G-H (line C), such that the hogging moment has reduced by 18 kNm (30%) and is now that of the unplated structure $(M_h)_u$. Hence, the sagging elastic moment has increased by the same magnitude from 29 kNm to 47 kNm. Therefore, the maximum increase in the strength of the continuous beam occurs when the sagging strength has been increased from 31 kNm to 47 kNm. The next stage in the design is to see if this increase in strength can be achieved by plating.

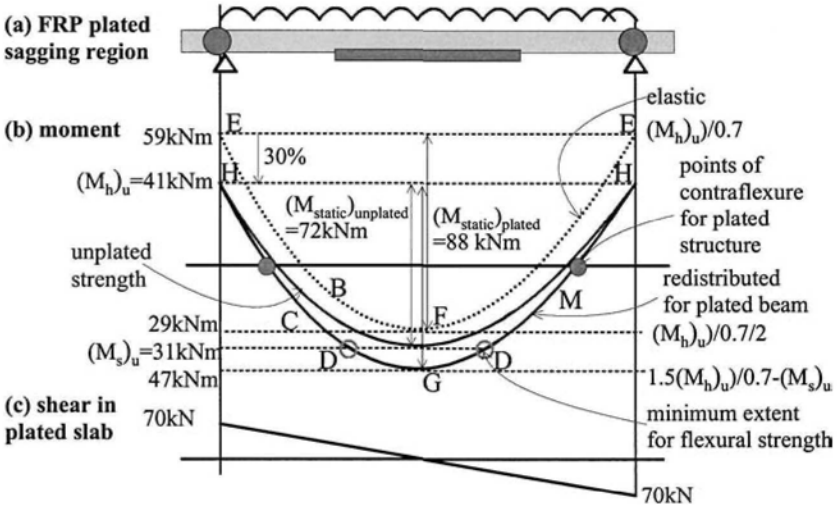

Figure 3.39 FRP plating sagging region of slab

It is worth considering what would happen if the sagging strength capacity is increased above this theoretical maximum value 47 kNm. If, for example, the sagging strength is increased to say 61 kNm, then the theoretical static moment at failure is 41 + 61 = 102 kNm. The elastic distribution of this static moment would require a hogging moment of two-thirds of 102 kN that is 68 kN. The capacity of the hogging region is 41 kNm. Hence the redistribution required is (68 - 41)/68 = 40% which is greater than the 30% the k_u value of the hogging region allows.

3.5.1.3 Propped flexural analysis

The flexural analysis is shown in Fig. 3.40. The pivotal point $(\varepsilon_{pivot})_{RC}$ in Fig. 3.40(b) always represents the strain in the concrete adjacent to the plate. Hence, the strain profile that extends from the pivotal point is the strain profile in the RC structure. As this is a propped analysis, the pivotal strain is the plate debonding strain $(\varepsilon_{pivot})_{RC} = \varepsilon_{db}$

= 0.00267. The strain $(\varepsilon_c)_{max}$ is the maximum strain in the concrete at debonding; χ is the curvature at debonding; ε_{bar} is the strain in the reinforcing bars at plate debonding; d_y is the depth of the pseudo plastic zone in the concrete and is negative in the following analyses when the concrete remains fully in the elastic zone; F_{c1} and F_{c2} are the resultant forces in the plastic zone and elastic zone of the concrete respectively; F_s is the force in the steel reinforcing bars which yield at a strain of 0.002; F_p is the axial tensile force in the plate required for longitudinal equilibrium; and b_p is the width of 1.2 mm CFRP plate required.

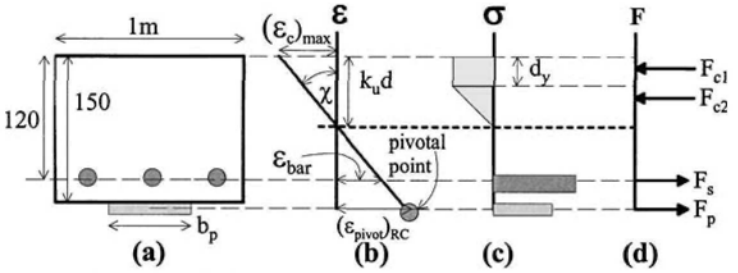

Figure 3.40 Flexural analysis: CFRP tension face plate in sagging region

The results of the spreadsheet analyses are summarised in Table 3.2. The spreadsheet procedure used here was to determine the plate size required for a specific neutral axis depth. As an example, let us consider the first row of results in Table 3.2. The pivotal strain $(\varepsilon_{pivot})_{RC}$ in the reinforced concrete slab is the plate IC debonding strain 0.00267; the neutral axis depth has been fixed at 48 mm, this gives a curvature of 2.6 x 10^{-5} mm^{-1}; a reinforcing bar strain of 0.00187; a maximum concrete strain of 0.00125; and a depth of the concrete plastic zone of 9.6 mm. From the forces in Fig. 3.40(d), the force in the plate required for longitudinal equilibrium is 483 kN; as the stress in the plate at debonding is 427 MPa and the plate thickness is 1.2mm, the width of plate required is 942 mm. By taking moments of the forces in Fig. 3.40(d) can be determined the moment capacity 91 kN; this capacity is greater than the required value of 47 kNm and hence the neutral axis depth is reduced until the required capacity is reached in row 4 which is shown highlighted.

Table 3.2 Summary of *propped* flexural analysis: CFRP tfp in sagging region

	$(\varepsilon_{pivot})_{RC}$	$k_u d$ [mm]	χ (10^{-5}) [mm^{-1}]	ε_{bar}	$(\varepsilon_c)_{max}$	d_y [mm]	F_p [kN]	b_p [mm]	k_u	M_{cap} [kNm]
1	0.00267	48	2.6	0.00187	0.00125	9.6	483	942	0.40	91
2	0.00267	45	2.5	0.00190	0.00114	5.4	389	759	0.38	79
3	0.00267	40	2.4	0.00193	0.00097	-1.4	234	458	0.33	60
4	**0.00267**	**36**	**2.3**	**0.00196**	**0.00085**	**-6.4**	**132**	**257**	**0.30**	**47**

It can be seen in row 4 of Table 3.2 that the reinforcing bars have not quite yielded prior to debonding and even if they had just managed to yield the section would still be very brittle. It can also be seen that the maximum concrete stress is still in the elastic zone and, hence, the negative value of d_y. The width of plate required is 257 mm per meter width of slab. The length of plate required has to cover the region D-D in Fig. 3.39 where the applied moment, for the strengthened structure, exceeds

the strength of the unplated section. The plates should at least be extended beyond this region by their anchorage length of L_e = 187 mm. It is also worth noting that the neutral axis depth factor is 0.30 but as the maximum strains in the concrete have not reached their crushing strain, then this factor cannot be used for moment redistribution even though it would appear from Fig. 3.14 that some redistribution could be allowed.

3.5.1.4 Unpropped flexural analysis

The unpropped analysis is also depicted in Fig. 3.40. From an elastic cracked sectional analysis of the unplated beam under serviceability loads, it was determined that the residual stress in the unplated beam just prior to plating was $(\varepsilon_{pivot})_{res}$ = 0.00139 so that the pivotal point $(\varepsilon_{pivot})_{RC}$ = 0.00267 + 0.00139 = 0.00406 as shown in column 2 in Table 3.3. As mentioned previously, $(\varepsilon_{pivot})_{RC}$ is the strain in the RC beam, the strain in the plate is ε_{db}, so that the plate strain lags behind the concrete strain by $(\varepsilon_{pivot})_{res}$. The steps in the analyses have already been described in Section 3.5.1.3.

The final result is summarised in row 5 in Table 3.3. It is worth comparing these results with those for the propped analysis in Table 3.2. Plating the unpropped beam as compared to the propped beam, has increased the curvatures by 48%, the strains in the reinforcing bars are now well above the yield strain and have increased by 55%, the concrete strains are still very low and barely within the plastic zone and have only increased by 19%, the force in the plate has reduced slightly by 8% so that slightly less FRP is required. Importantly from these analyses, plating the unpropped beam has increased the ductility.

Table 3.3 Summary of *unpropped* flexural analysis: CFRP tfp in sagging region

	$(\varepsilon_{pivot})_{RC}$	$k_u d$ [mm]	χ (10^{-5}) [mm^{-1}]	ε_{bar}	$(\varepsilon_c)_{max}$	d_y [mm]	F_p [kN]	b_p [mm]	k_u	M_{cap} [kNm]
1	0.00406	48	4.0	0.00285	0.00190	22.7	634	1104	0.40	111
2	0.00406	45	3.8	0.00288	0.00173	19.0	548	954	0.38	101
3	0.00406	40	3.7	0.00294	0.00147	12.8	405	704	0.33	83
4	0.00406	35	3.5	0.00299	0.00123	6.5	261	455	0.29	65
5	**0.00406**	**30**	**3.4**	**0.00303**	**0.00101**	**0.4**	**121**	**211**	**0.25**	**47**

3.5.2 Beam structure with adhesively bonded plates

In this example, we will only be concerned with strengthening the hogging sections of a continuous beam and not with the overall behaviour of the continuous beam as in Section 3.5.1, and propped construction will only be considered.

3.5.2.1 Beam specifications

The details of the continuous beam are given in Fig. 3.41. The hogging flexural capacity is 339 kNm. The variation of the moment distribution at failure, that is the strength, is very close to the elastic distribution so that the beam has been designed without moment redistribution. The concrete, reinforcing bar, and FRP plate material properties are the same as those described in Section 3.5.1. The hogging region of the beam has k_u = 0.29 and V_c = 134 kN and the sagging region k_u = 0.14 and V_c = 104 kN.

3.5.2.2 Tension face plates on underside of flange in hogging region

Plating the tension face of a beam can sometimes be a problem as the strains in the plate $(\varepsilon_{pivot})_{RC}$ in Fig. 3.40(a) will generally be greater than that in the reinforcing bars ε_{bar} as shown in Fig. 3.40(b) for a propped analysis. This may not be the case for an unpropped analysis where the residual stresses in the reinforcing bars increase their strains relative to that of the plate. In a propped analysis, this may lead to debonding of the plate prior to yielding of the reinforcing bars. One solution is to plate the underside of the flange as shown in Fig. 3.42(a), as this will drop the pivotal point below the tension reinforcing bars which will ensure that the reinforcing bar strains are higher than those in the plates.

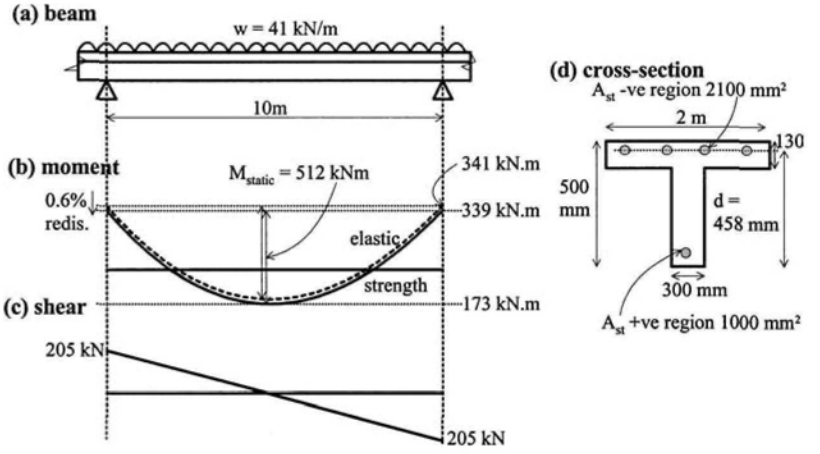

Figure 3.41 Beam structure

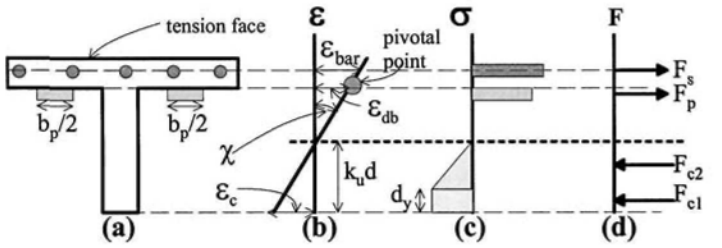

Figure 3.42 Propped balanced flexural analysis of plating underside of flange in hogging region

A practical upper limit to the strengthening technique is to use a balanced analysis as shown in Fig. 3.42(b) where the concrete reaches its ultimate strain capacity $\varepsilon_c = 0.003$ at the same time as the plate reaches its debonding strain ε_{db}. In which case, the strain profile and, hence, the stress profile in Fig. 3.42(c) are now fixed, so that it is just a question of finding a cross-sectional area of plate in which the resulting force F_p in Fig. 3.42(d) provides longitudinal equilibrium, that is the sum of the forces is zero. The results of the analyses are summarised in Table 3.4 for CFRP plates with thicknesses varying from 0.6 mm to 3.6 mm. The cross-section area of the

plate required for longitudinal equilibrium A_p is given in column 8 and in the last column %ΔM is the percentage increase in strength over that of the unplated section.

It can be seen in column 5 in Table 3.4 that plating the underside of the flange has ensured that the reinforcing bars yield prior to debonding even for the very thick plate of 3.6 mm in row 4. For the thinner plates, the reinforcing bar strains are much greater than their yield strain of 0.002 which suggests a nice ductile behaviour as the moment increases gradually along the plastic zone in Fig. 3.18. It can be seen in column 3, that as the plate thickness is increased the stress at debonding reduces quite substantially. However, the force in the plate does increase as shown in column (8) but only because the cross-sectional area of plates in column 7 increases significantly. For example, let us compare the results for the 0.6 mm plate in row 1 with the 3.6 mm plate in row 4. Increasing the plate thickness from 0.6 mm to 3.6 mm has increased the moment capacity by 31% but the cross-sectional area of plate required has increased by 770%. It would appear that using thick FRP plates is not economical.

Table 3.4 Summary of *propped* balanced flexural analysis: CFRP plating underside of flange in hogging region

	t_p [mm]	ε_{db}	σ_{db} [MPa]	χ (10^{-5}) [mm^{-1}]	ε_{bar}	F_p [kN]	A_p [mm^2]	M_{cap} [kNm]	ΔM [%]
	(1)	(2)	(3)	(4)	(5)	(6)	(7)	(8)	(9)
1	0.6	0.0038	605	1.83	0.0054	203	336	388	14
2	1.2	0.0027	427	1.53	0.0040	408	955	436	29
3	2.4	0.0019	302	1.32	0.0031	607	2007	471	39
4	3.6	0.0015	246	1.23	0.0026	719	2917	490	45

3.5.2.3 Side plates over full depth of web in hogging region

Let us consider plating the full depth of the web in the hogging region as shown in Fig. 3.43(a). From Eq. 2.1 and also shown in Table 2.3, it can be derived that for a steel plate of Young's modulus 200GPa and yield strength f_y = 300 MPa, the plate thickness at which yield and debonding occur simultaneously is 3.0 mm. This is a transition thickness between IC debonding and yield.

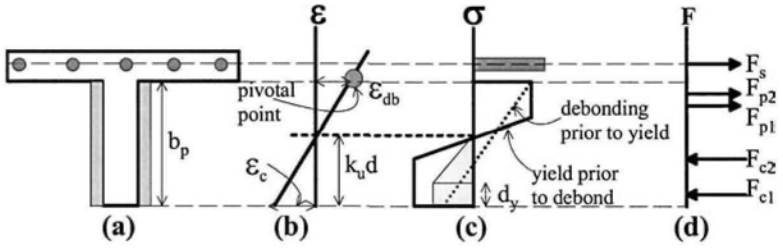

Figure 3.43 Propped flexural analysis of full depth web plate in hogging region

If the plate thickness is just above the transition thickness of 3 mm, then the plate will debond prior to yielding. The analysis is shown in Fig. 3.43(b) where the pivotal point is at ε_{db}, and in Fig. 3.43(c) for the plate stress distribution given by the broken line where yield in the plate can only occur at the pivotal point. In this case, the moment capacity is 374 kNm which is 10% more than that of the unplated structure of 339 kNm. However, if the plate thickness is just below 3mm so that debonding does not occur, then the beam can be reanalysed with the pivotal point at ε_c

= 0.003. This allows the steel to yield through the plate depth as shown by the solid line plate stress distribution in Fig. 3.43(c), in which case the moment capacity increases to 403 kNm, that is by 19%. The curvature also increases three fold from $7.8\text{x}10^{-6}$ to $20.0\text{x}10^{-6}$ mm^{-1}. In the latter analysis where yielding preceded debonding, it was assumed that debonding never occurred. However tests have shown, such as those in rows 8 and 9 in Table 2.2 and rows 1 to 3 in Table 3.1, that metal plates do eventually debond even if designed to yield prior to debonding. Therefore when the analysis is complete, it will be necessary to ensure that the debonding strain capacity after yield, as given in Tables 2.2 and 3.1, has not been exceeded and if so then this will be the new pivotal point.

The transition thickness between yield and debonding for aluminium of yield strength 215 MPa and Young's modulus 63 GPa is about 1.8 mm. At this thickness, the yield and debonding strains are 0.00341. When debonding controls, the moment capacity is 355 kNm which gives a 5% increase in strength. When the aluminium can yield prior to debonding, so that concrete crushing controls the pivotal point at ε_c = 0.003, then the moment capacity is 362 kNm which is only a 7% increase in strength. In this example, there is little benefit in using aluminium plates.

3.5.3Beam structure with bolted plates

3.5.3.1 Full interaction flexural analysis

A comparison is made of bolting different types of plates to the sides of the web as in Fig. 3.44(a). The plates considered are of steel of Young's modulus 200 GPa and yield strength 300 MPa, aluminium of Young's modulus 63 GPa and yield strength 125 MPa, and glass/carbon FRP plates of Young's modulus 51 GPa and a fracture strength of 600 MPa. The plate thicknesses have been adjusted so that the moment capacities are almost equal.

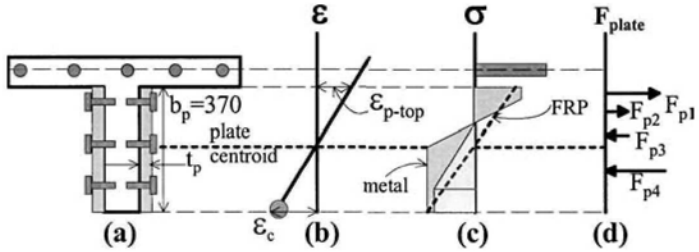

Figure 3.44 Full interaction flexural analysis of bolted plated section

A full interaction flexural analysis of a bolted plated beam is shown in Fig. 3.44. This analysis is referred to as full interaction as it assumes that there is no slip between the plate and the RC beam. Hence, the strain profile shown in Fig. 3.44(b) applies to both the plate and to the reinforced concrete beam. As this is a bolted structure and not an adhesively bonded structure, IC debonding does not occur. For the metal plates, only one pivotal point at the concrete crushing strain, as shown in Fig. 3.44(b), needs to be considered. For the FRP plate, this is also a good starting position for the pivotal point. However from this analysis, an additional check has to be made to ensure that the FRP fracture strain has not been exceeded. If it has been exceeded, then this fracture strain should be the new pivotal point. The analyses started with 10 mm thick steel plates over the full depth of the web, after which the

thicknesses of the aluminium and FRP plates were adjusted to achieve the same capacity. The results of the analyses are summarised in Table 3.5.

The 10 mm thick steel plates increased the capacity from 339 kNm to 542 kNm, in column 4 of Table 3.5, which is a 60% increase in strength. The maximum tensile strain in the plate at concrete crushing is 0.0037, in column 3, which suggests a ductile behaviour; this is the hallmark of bolted plated RC structures as there is not much, if anything at all, that can fail in a brittle fashion. To achieve the same capacity as the steel plated beams, 20 mm thick aluminium and 25 mm thick carbon/glass FRP plates are required. Because the real bolted structure will have slip between the plate and the beam, there will be a difference in curvature between the plate and the beam as shown in Fig. 3.33(b). It was recommended in Section 3.4.1.5 that the increase in the flexural capacity be reduced by 15%. Hence the increase in the flexural capacity, given by ΔM_{cap} in column 5 in Table 3.5, has been reduced by 15% in column 6 to give the design strength of the plated beam in column 7.

Table 3.5 Summary of full interaction flexural analysis: Side bolted plates

t_p [mm]	material	$\varepsilon_{p\text{-}top}$	M_{cap} [kNm]	ΔM_{cap} [kNm]	85% ΔM_{cap} [kNm]	Design M_{cap} [kNm]	P_{plate} [kN]	M_{plate} [kNm]
(1)	(2)	(3)	(4)	(5)	(6)	(7)	(8)	(9)
10	steel	0.0037	542	203	173	512	220	190
20	aluminium	0.0035	551	212	180	519	256	188
25	C/G FRP	0.0035	543	204	173	512	250	190

3.5.3.2 Bolt forces

In order to design the bolt shear connectors, we need to know the length of the hogging region L, as shown in Fig. 3.33, and in particular the length of the plate in each shear span in the hogging region $L_{sh\text{-}sp}$. Let us assume that the left shear span plate $(L_{sh\text{-}sp})_{left}$ = 1.5 m and the right shear span plate $(L_{sh\text{-}sp})_{right}$ = 2.0 m. We also need to know the axial force in the plate P_{plate} and the moment in the plate M_{plate}. These stress resultants can be derived from the stress distribution in the plate as shown in Figs 3.44(c) and (d). It is easiest to determine the resultant force in each rectangular and triangular portion of the stress distribution. For the metal plate in Fig. 3.44(c), these are shown as F_{p1} to F_{p4} in Fig. 3.44(d). The longitudinal sum of these forces is equal to P_{plate} and the moment of these forces about the centroid of the plate is equal to M_{plate}. These have been determined for all the plates in columns 8 and 9 in Table 3.5 where M_{plate} and P_{plate} are the stress resultants in both side plates in a shear span as in Fig. 3.44..

As an example, let us determine the bolts required for the carbon/glass FRP plate of 25 mm thickness in Table 3.5. For the left shear span in Fig. 3.33, the bolt shear connectors have to resist a longitudinal force of P_{plate} = 250 kN. The vertical shear force in both plates on the left shear span is $(V_{plate})_{left} = M_{plate}/0.7(L_{sh\text{-}sp})_{left}$ = 190/(0.7x1.5) = 181 kN. Therefore, the total vertical shear force in the left shear span is $2(V_{plate})_{left}$ = 2 x 181 = 362 kN; there being two vertical forces in each shear span. Therefore, the total shear force that the bolts have to resist in the left shear span is 250 + 362 = 612 kN. The shear capacity of bolt shear connectors can be determined from the manufacturer's recommendations or from simple push tests. If we assume that the strength of the bolt shear connectors for the carbon/glass plate is 20 kN, then the number of bolts required in the left shear span is 612/20 = 30.6. The number required on one side of the left shear span is 30.6/2 = 15.3. If we assume that there are two

rows of bolts, then the number per row is 15.3/2 = 8. Therefore, the longitudinal spacing in Fig.3.33 in the left shear span is 1500/8 = 188 mm.

The number of bolts in the right shear span will be slightly less than the left shear span as the right shear span is longer and, hence, there is a larger lever arm to resist M_{plate}. The right shear span has to resist the same longitudinal force of P_{plate} = 250 kN. $(V_{plate})_{right} = M_{plate}/0.7(L_{sh\text{-}sp})_{right}$ = 190/(0.7x2.0) = 136 kN. Therefore, the total vertical shear force is $2(V_{plate})_{right}$ = 2 x 136 = 272 kN. The total shear force is 250 + 272 = 522 kN. The number of bolts required in the right shear span is 522/20 = 26.1, the number on one side is 13.0, and assuming two rows gives 7 bolts per row. Therefore, the longitudinal spacing in the right shear span is 2000/7 = 286 mm.

3.5.4 Moment redistribution in metal plated hinges: flexural rigidity approach

The slab in Fig. 3.45(a) has the same amount of tension reinforcing bars in the hogging and sagging regions as shown in Fig. 3.45(d); the flexural capacity of the unplated section is 31 kNm. The slab is to be strengthened using the same mild steel plates in the hogging and sagging regions as shown in Fig. 3.45(d) where A_p is the cross-sectional area of the plate, so that the moment capacity increases to 55 kNm. These plates are to be designed so that they yield before they debond; but it is worth bearing in mind that the steel plates will definitely debond after yielding but at a much higher plate strain ε_{db} given in Tables 2.2 and 3.1. As the strength of the plated hogging region is the same as that of the plated sagging region as shown in Fig.3.45(b), the variation of the moment at failure, the *strength* line in Fig. 3.45(b), is different from the *elastic* distribution as shown. To reduce the hogging moment from 73 kNm to 55 kNm requires a moment redistribution of 25% of the hogging moment; this will allow both the hogging and sagging capacities to be reached in the continuous beam. It needs to be determined what is the minimum debonding strain that will allow sufficient ductility for full moment redistribution. Once this debonding strain is determined, then the plate thickness can be chosen from, for example, those in rows 1 to 3 in Table 3.1 and rows 8 and 9 in Table 2.2.

The flexural rigidity approach described in Section 3.3.2 will be used to determine the required debonding strain capacity. To apply this technique, we need the moment/curvature relationship for the plated sections, such as those shown in Fig. 3.17, as well as the variation in the plate strain with the curvature. These relationships can be determined directly from the iterative analyses described in Fig. 3.29 where the pivotal point is now the plate strain ε_p instead of ε_{db} in Fig. 3.29(c). Pivoting about a specific plate strain ε_p will give the moment M and curvature χ and, hence, the following secant flexural rigidity for that specific plate strain ε_p.

$$EI = \frac{M}{\chi} = \frac{M(1-k_u)d}{\varepsilon_p} \qquad 3.6$$

where for convenience the effective depth d is taken as the full depth of the beam as in Fig. 3.15. The complete M/χ relationship and χ/ε_p relationship can be determined by changing the magnitude of ε_p. Alternatively, the relationships can be approximated as follows.

The M/χ variation has been approximated to the bi-linear relationship shown in Fig. 3.46. The flexural capacity M_u = 55 kNm can be determined from standard analyses of RC beams with steel reinforcement that can yield if required and in which debonding is ignored. The flexural rigidity of the cracked plated section $EI_{hcr} = EI_{scr}$ =

$EI_{cr} = 2.84x10^{12}$ Nmm^2 was calculated from a linear elastic analysis that assumed that the tensile strength of the concrete was zero. Knowing M_u and EI_{cr}, the curvature at point A can be determined as $\chi_A = 1.9x10^{-5}$ mm^{-1}, and the plate strain as $(\varepsilon_p)_A = 0.0021$. As we are dealing with metal plates that yield, the plastic zone DF can be assumed to be horizontal and failure occurs when the concrete crushes at point C at $\varepsilon_c = 0.003$. The curvature at point C is $\chi_C = 14.4x10^{-5}$ mm^{-1} and $(\varepsilon_p)_C = 0.0185$. The problem is to define what is happening between points D and F, that is, to relate the flexural rigidity, such as at point E, of $EI_{\varepsilon p}$ with the strain in the plate ε_p.

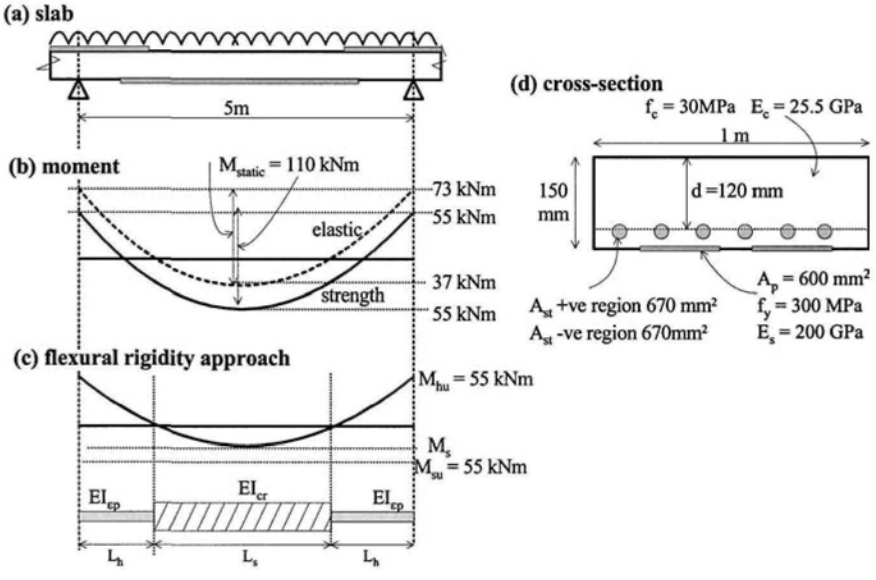

Figure 3.45 Moment redistribution in a steel plated slab

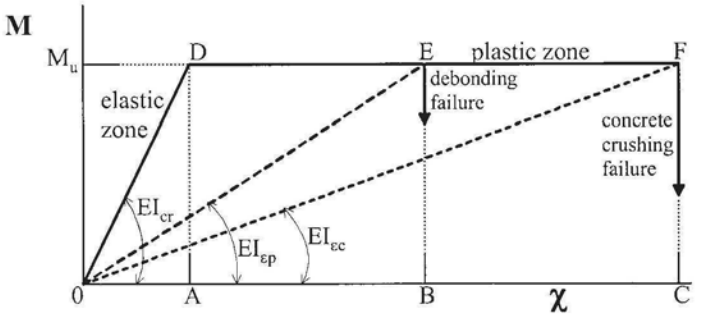

Figure 3.46 Idealised moment/curvature relationship

The method of approximating the flexural rigidity for a given plate strain is illustrated in Fig. 3.47. The depth of the slab is d in Fig. 3.47(a) and the distance from the reinforcing bars to the tension face is c. In the strain profile in Fig. 3.47(b), the plate strain is ε_p and this is used as the pivotal point as in the propped construction;

otherwise, the residual stress will have to be added to ε_p to get the pivotal point as explained in Section 3.4.2. The strain in the concrete at the transition from the elastic zone to the plastic zone is ε_e which, in this example, has a value of 0.001 as shown in Fig. 3.38(e). The vertical position of ε_e in Fig. 3.47(b) is given in terms of β as shown. The stress profile is given in Fig. 3.47(c). It is assumed that the reinforcing bars have yielded and as the strain in the plate is known as it is the pivotal point, the stress in the plate is also known. The resulting forces are given in Fig. 3.47(d) and their distance from the top compressive fibre in Fig. 3.47(e).

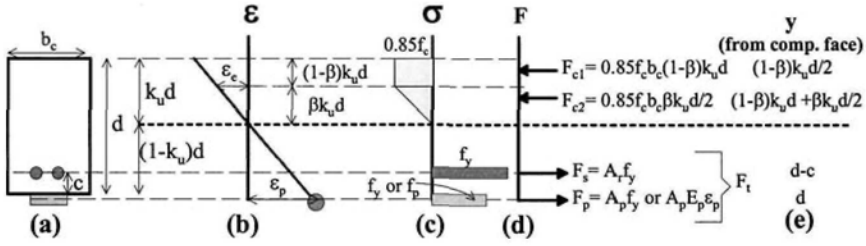

Figure 3.47 Flexural rigidity

From compatibility in Fig. 3.47(b), the position of the transition strain ε_e is given by the following α term

$$\beta = \frac{\varepsilon_e}{\varepsilon_p}\frac{1-k_u}{k_u} \tag{3.7}$$

Note that the following equations are derived for the case shown in Fig. 3.47(b), that is for $\beta \leq 1$. From equilibrium of the longitudinal forces in Fig. 3.47(d)

$$F_t = 0.85 f_c b_c k_u d(1-0.5\beta) \tag{3.8}$$

where F_t is the total tensile force and in which it is assumed that the reinforcing bars have yielded. If this cannot be assumed, then the standard iterative procedure as described in Section 3.4 has to be applied. Eliminating β from Eqs 3.7 and 3.8 gives the neutral axis depth factor as

$$k_u = \frac{(2F_t\varepsilon_p)+(0.85 f_c b_c d\varepsilon_e)}{0.85 f_c b_c d(2\varepsilon_p+\varepsilon_e)} \tag{3.9}$$

Hence the flexural rigidity at a plate strain of ε_p can now be derived from Eq. 3.6, where d is the depth of the beam and M is the moment in the beam when the plate strain is ε_p. For metal plates the moment M can be assumed to be the ultimate moment capacity M_u as the plastic zone is generally considered horizontal. However, if a more accurate value is preferred, then the moment can be determined by taking moments of the forces in Fig. 3.47(d) where their lever arm from the compression face is given in Fig. 3.47(e).

Having determined the M/χ relationship in Fig. 3.46 and in particular its dependence on the plate strain ε_p, the analysis procedure can follow the steps described in Section 3.3.2 and illustrated in Fig. 3.45(c). As the hogging moment is redistributing its moment to the sagging region, the flexural rigidity of the sagging region will remain at EI_{cr} in Fig. 3.46 whilst the hogging region moves along the plastic zone D-F in Fig. 3.46 with varying secant flexural rigidities $EI_{\varepsilon p}$, depending on the strain in the plate. For a given plate strain ε_p, we know the flexural rigidity $EI_{\varepsilon p}$ from Fig. 3.46 and as we already know the sagging flexural rigidity, these can be inserted into the beam in Fig. 3.45(c). Any magnitude of load can be applied and the analysis iterated until the step changes in the EI variations along the beam coincide with the points of contraflexure. When they do coincide, the analysis will give the ratio of the maximum hogging to maximum sagging moments M_h/M_s. As the hogging joint is redistributing moment $M_h = M_u$, this will give M_s. If $M_s < M_u$ then the debonding strain will have to be increased to reduce the flexural rigidity of the hogging region to try to achieve the moment redistribution required that is when $M_s = M_u$.

The analysis described in the previous paragraph was carried out for the slab structure shown in Fig. 3.45. The results are summarised in Table 3.6 for a range of plate debonding strains ε_p within the plastic zone D-F in Fig. 3.46. The values for the length of the hogging L_h, shown in Fig. 3.45(c), and M_h/M_s in Table 3.6 were determined using a basic plane frame analysis program. An iterative solution technique was required to solve for L_h such that L_h is located at the point of contraflexure, that is the moment is zero. To coincide with the example slab shown in Fig. 3.45 a uniformly distributed load of 35.2 kN/m was used in the plane frame analysis so that $M_{static} = 110$ kNm. The corresponding percent moment redistribution, %MR, for the given plate strain is given in the last column of Table 3.6 and is shown graphically in Fig. 3.48 where it can clearly be seen that the required debonding strain for increasing moment redistribution increases at an increasing rate.

Table 3.6 Summary of the moment redistribution analysis using the flexural rigidity approach

ε_p ($\times 10^{-3}$)	k_u (Eq. 3.9)	β (Eq. 3.7)	$EI_{\varepsilon p}$ ($\times 10^{12}$) [Nmm^2] (Eq. 3.6)	L_h [mm]	M_h/M_s	%MR
4	0.215	0.912	1.619	900	1.450	10.8
5	0.197	0.813	1.324	850	1.296	14.9
6	0.185	0.734	1.121	800	1.178	18.5
7	0.176	0.669	0.971	760	1.091	21.4
8	0.169	0.614	0.857	730	1.016	24.0
9	0.164	0.568	0.767	710	0.957	26.3
10	0.159	0.528	0.694	690	0.905	28.4
11	0.156	0.494	0.633	670	0.861	30.3
12	0.152	0.463	0.583	650	0.821	32.1
13	0.150	0.437	0.540	630	0.789	33.6
14	0.148	0.413	0.502	610	0.759	34.9
15	0.146	0.391	0.470	600	0.732	36.3
16	0.144	0.372	0.441	590	0.708	37.5
17	0.142	0.354	0.416	580	0.685	38.8
18	0.141	0.338	0.394	570	0.664	39.9

Figure 3.48 is used to determine that the minimum required debonding strain for the steel plates proposed to strengthen the slab in Fig. 3.45 and achieve the 25%

moment redistribution of the hogging moment is 0.0085. From row 9 in Table 2.2 and rows 1 to 3 in Table 3.1 the steel plate thickness required to achieve this debonding strain is less than 2 mm.

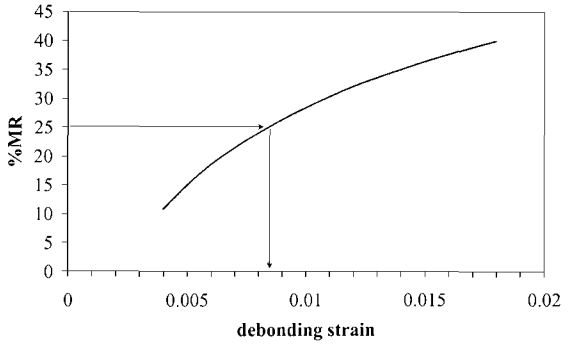

Figure 3.48 Minimum required debonding strain for steel plates

3.6 Conclusions

IC debonding affects both the sectional flexural strength and ductility, as well as the ability of a beam to redistribute moment. Generic analysis techniques have been described for determining the flexural strength and ductility for any type of plated structures as well as determining the amount of moment redistribution that IC debonding allows. We have now covered IC debonding at positions of maximum moment such as those shown in Fig. 2.1. The next stage of the analysis is to ensure that critical diagonal crack (CDC) debonding does not weaken the structure and this is covered in Chapters 4 and 5.

3.7 References

Oehlers, D. J. and Bradford, M. A. (1995). *Composite Steel and Concrete Structural Members: Fundamental Behaviour*. Pergamon Press, Oxford.

Oehlers, D.J. and Bradford, M.A. (1999). *Elementary behaviour of Composite Steel and Concrete Structural Members*. Butterworth Heinemann, Oxford.

Oehlers, D.J., Ahmed, M., Bradford, M.A and Nguyen, N.T. (2000) "Retrofitting reinforced concrete beams by bolting steel plates to their sides. Part 2: Transverse interaction and rigid plastic design." *Journal of Structural Engineering and Mechanics,* An International Journal, September, Vol.10, No.3.

Oehlers, D.J., Ju, G., Liu, I., and Seracino, R., (2003a) "Moment redistribution in continuous plated RC beams. Part 1 Tests". Submitted for publication.

Oehlers, D.J., Liu, I., Ju, G., and Seracino, R., (2003b) "Moment redistribution in continuous plated RC beams. Part 1 Design". Submitted for publication.

Smith, S.T., Bradford, M.A. and Oehlers, D.J. (1999) "Local buckling of side-plated reinforced concrete beams. Part 1: Theoretical study. *ASCE Structural division, Journal of Structural Engineering,* June, 622-634.

Smith, S.T., Bradford M.A. and Oehlers, D.J. (2000) "Unilateral buckling of elastically restrained rectangular mild steel plates". *Journal of Computational Mechanics,* Vol.26, No.4, 317-324.

Smith, S.T., Bradford, M.A., and Oehlers, D.J. (2001) "Buckling tests on steel plates restrained at discrete points in the retrofit of reinforced concrete beams", *Proc. ICE, Structs. & Bldgs,* 146(2), 115-127, May.

Chapter 4: CDC Debonding of Tension Face Plates

4.1 Introduction

Chapter 3 is concerned with the effect of IC debonding on the flexural strength, flexural stiffness and flexural ductility of adhesively bonded plated beams and slabs. It was shown that the IC debonding resistance controls the initial stages of the design as it determines: the size, type and position of the adhesively bonded plate; the region where adhesive bonding can be applied; the amount of moment redistribution that can occur; and the maximum increase in the overall strength of the beam that can be attained. Hence at this stage, the beam or slab has been designed at the positions of maximum moment, as in Fig. 2.1, and this is based on the IC debonding resistance. The longitudinal extent of the plate, that is the length of plate beyond the position of maximum moment in Fig. 2.1, depends on the region of the beam where the flexural strength has to be increased over that of the unplated beam such as the region D-D in Fig. 3.39. Furthermore, the extent of plating depends on the IC debonding design philosophy that has been applied, as described in Section 2.5. For the anchorage philosophy described in Section 2.5.1, the plate has to be extended to at least the points of contraflexure. Whereas for the hinge philosophy in Section 2.5.2, the plates can be terminated short of the points of contraflexure.

Having designed for IC debonding, the next step in the design procedure is to ensure that the plate does not debond due to the rigid body displacement induced by the formation of a critical diagonal crack (CDC) as shown in Figs. 1.17 to 1.19, which is the subject of this chapter. An example of CDC debonding in a tension face plated beam in which the plate ends are trapped by the supports is shown in Fig. 4.1. As the plate ends were trapped by the supports, plate end debonding as explained in Section 1.3.3 could not have occurred. Furthermore, IC debonding needs flexural or flexural-shear cracks which are not present. This leaves CDC debonding which requires a rigid body shear displacement on either side of the critical diagonal crack which is clearly visible.

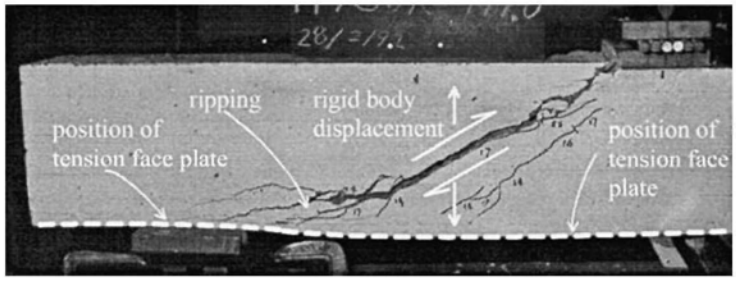

Figure 4.1 CDC debonding of tension face plate trapped by supports

It must be emphasised that a CDC is not the inclined crack associated with flexural-shear cracks such as those in Fig. 1.15. A CDC is the diagonal crack that extends virtually through the depth of the beam or slab as shown diagrammatically in Fig. 2.1 and can clearly be seen in Figs. 1.18, 119, 1.38, 1.39 and 4.1. It is the rigid body displacement across this CDC, in the form of sliding and/or rotation, that

governs the shear capacity of the beam or slab without stirrups V_c. The position of the CDC also controls the extent of plating. As CDC debonding depends on the formation of the critical diagonal crack, CDC debonding is rarely a problem in plated slabs as the vast majority of slabs are designed without stirrups and, hence, are designed for V_c so that a CDC does not occur. However, most beams have stirrups and, therefore, rely on both the concrete shear capacity V_c and the shear resisted by the stirrups V_s. Hence beams are prone to CDC debonding when the shear load exceeds V_c which may be well before the shear capacity of the beam V_c+V_s has been attained. Beams are particularly prone to CDC debonding in the hogging regions where the vertical shear force is at its largest, as shown in Fig. 2.1(a). Hence in some beams, it may not be possible to adhesively bond plates in the hogging region due to CDC debonding, in which case the plates can be bolted. However, it may be possible to adhesively bond plates to the sagging regions where the vertical shear is less and because plates inhibit the formation of the CDC, that is increase V_c.

As the design guidelines listed in Table 1.1 only cover tension face plates as in Fig. 2.1(b), this chapter has been restricted to CDC debonding of tension face plates so that a comparison between the different design guidelines can be made. The CDC debonding of all the other types of plates and positions, as in Figs. 2.1(c) and (d), is covered in Chapter 5. It will be shown that CDC debonding depends on the IC debonding resistance of the plate spanning the CDC, that the CDC debonding resistance is the same mechanism as that which controls the vertical shear capacity of beams without stirrups, and that stirrups do not inhibit CDC debonding.

4.2 CDC debonding mechanism

4.2.1 CDC debonding mechanism

The rigid body displacement across a critical diagonal crack that induces CDC debonding has already been described in Section 1.3.2 and illustrated in Fig. 1.17. The sliding action across the CDC A-B in Fig. 1.17, accompanied by some rotation as shown, causes the plate to peel away, starting from the root of the crack at B, and propagating towards the plate end at C. Numerous tests with metal plates and pultruded FRP plates have shown that the presence of stirrups has virtually no affect on CDC debonding; probably because the plates debond at the very early stage of the rigid body displacement which is not sufficient to stretch the stirrups to resist shear. Therefore, CDC debonding is not a function of the shear resisted by stirrups V_s, but it is a function of the shear capacity of the beam without stirrups V_c.

The ability of a reinforced concrete element without stirrups to transfer shear across a crack, V_c, is illustrated in Fig. 4.2 for a cracked concrete element with longitudinal reinforcing bars that span the crack. Shear is directly transferred across the crack by the dowel action of the reinforcing bars P_{dowel}; this dowel action is induced by the shear displacement across the crack which causes these bars to transfer the shear by bearing against the concrete, in much the same way as stud shear connectors transfer shear in composite steel and concrete beams. Shear is also transferred by the mechanism of aggregate interlock. The aggregate interlock mechanism requires that the crack surface is very uneven with numerous protrusions and indentations formed by the individual aggregates, so that any shear displacement across the crack causes the crack surfaces to separate by riding over each other which induces tensile forces in the reinforcing bars P_{bar} as shown. These tensile forces require compressive forces P_{inter} across the interface to maintain equilibrium, as

shown. They are referred to in Fig. 4.2 as passive normal forces as they disappear when the shear force is removed. These passive normal forces induce the passive shear resistance which transfers the shear and which is much larger than a frictional force because of aggregate interlock. Hence the reinforcing bars resist the interface shear by dowel action directly and provide the normal interface force for the shear transferred by aggregate interlock.

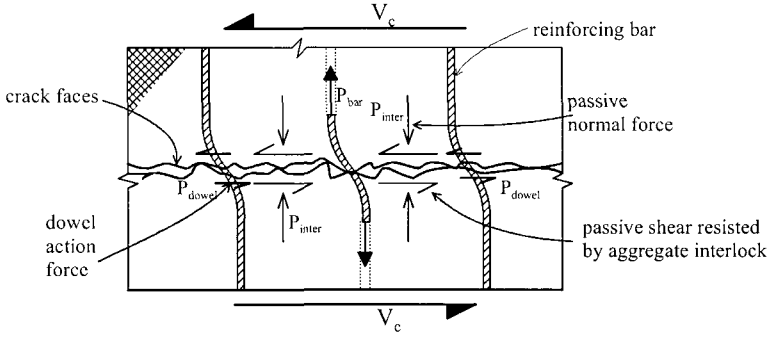

Figure 4.2 Passive aggregate interlock forces

The mechanism of transferring shear across a pre-existing crack, described in Fig. 4.2, also transfers some of the shear across a critical diagonal crack. Consider the critical diagonal crack at B in Fig. 4.3 which has been shown as a smooth straight interface but in reality is very rough with protrusions and indentations and also curved which further enhances the shear transferred by aggregate interlock. The sliding action across this crack, due to the shear rigid body displacement, is resisted directly by the dowel force P_{dowel}; although this dowel contribution may be quite small as the reinforcement is close to the concrete surface at a distance c and, hence, the dowel strength will probably be reduced considerably due to ripping along the level of the longitudinal reinforcing bars as shown in Fig. 4.1. However, the bars can still resist the opening of the diagonal crack induced by the aggregate interlock mechanism. The bars resist the aggregate interlock crack opening mechanism by going into tension with a force shown as P_{bar} which has an upper limit of the axial capacity of the bar $A_s f_y$. The tensile force in the bar P_{bar} must induce a compressive force across the interface P_{inter} for equilibrium, which then transfers the shear through aggregate interlock. The same can be said for the plate spanning the diagonal crack, where the dowel force contribution is probably even less than that contributed by the longitudinal bars particularly for FRP plates which are generally very thin. However, the tensile force in the plate, which depends on the IC debonding resistance P_{IC} can be quite substantial, and also contributes to the interface force P_{inter} and, hence, to the shear transferred by aggregate interlock.

It can be seen in Fig. 4.3 that the plate can be considered to act as additional longitudinal reinforcing bars by providing an additional passive compressive interface force P_{inter} across the crack. Alternatively, the plate can be considered to directly provide a passive prestress P_{inter} across the crack that is induced by the aggregate interlock mechanism. It can also be seen in Fig. 4.3 that the IC debonding resistance provided by the plate P_{IC} depends on the bonded anchorage length L_p between the root of the CDC and the plate end; the anchorage length required to achieve full anchorage L_e is quantified in Eq. 2.3 and, hence, P_{IC} also depends on the position of the diagonal

crack. For example, the anchorage length available for the diagonal crack at A is $(L_p)_A$, if this is greater than L_e then the full IC debonding resistance can be achieved. When the anchorage length L_p is less than L_e, then the IC debonding resistance reduces until, at the critical diagonal crack at C where $L_p = 0$, the IC debonding resistance is zero.

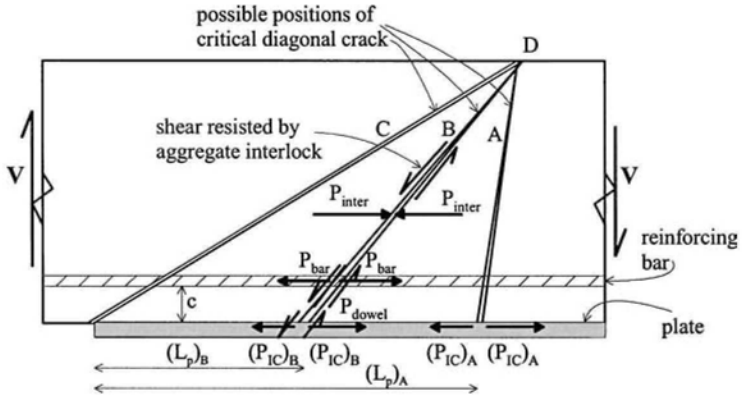

Figure 4.3 Affect of IC resistance on CDC debonding

4.2.2 Examples of CDC debonding of tension face plates

Examples of CDC debonding of tension face plated beams without stirrups are shown in Figs 1.18 and 1.38; in these tests, the tension face plate was terminated just short of the support. It was explained and shown that a critical diagonal crack can suddenly appear in a previously uncracked zone of a beam and, simultaneously, cause plate debonding. For example, the cracks marked 120 in Fig. 1.18, 188 in Fig. 1.19 and 20 in Fig. 1.38 were not the extension of flexural-shear cracks, such as those shown in Fig. 2.2, but suddenly formed and caused CDC debonding.

An example of CDC debonding in a tension face plated beam with stirrups is shown in Fig. 4.4. The presence of stirrups tends to cloud the debonding mechanism because, unlike plated beams without stirrups where the formation of the critical diagonal crack causes the beam to fail at V_c, the presence of stirrups allows the beam to resist the shear load after the critical diagonal crack has formed. The failure mechanism may appear at first sight to be different. However numerous direct comparisons of the same plated beam with and without stirrups have shown that the shear load at debonding $V_{c\text{-plate}}$ is the same; in fact in one series of tests, sufficient stirrups were provided to increase the shear capacity of the unplated beam to $4V_c$ but on plating these beams, the plated beams were found to debond at the same shear load $V_{c\text{-plate}}$ as the beams without stirrups.

The beam in Fig. 4.4 was loaded under displacement control. The diagonal shear crack marked *A* first formed, but as it did not intercept the plate, it did not initiate debonding. Critical diagonal crack debonding first occurred at the formation of the CDC marked *B* which caused CDC debonding from the root of the CDC to the plate end shown by the arrow marked 1. As with IC debonding, the debonding crack propagates towards the plate end. Because of the formation of these new cracks, the stiffness of the beam reduced, thereby, reducing the applied load as the hydraulic jack was under displacement control. The applied load was then increased and when it reached near to the previous level, the CDC marked *C* formed, followed immediately

by crack propagation marked 2 and the load reduced again. The same sequence of loading produced the remaining critical diagonal cracks and debonding cracks. Of importance, the critical diagonal cracks formed at about the same shear load $V_{c\text{-plate}}$, the debonding cracks always propagated from the root of the CDC to the plate end. However, the CDC debonding cracks spread away from the supports. Hence in reality, although the distribution of the cracks in the beam with stirrups in Fig. 4.4 would at first glance appear to be different from those beams without stirrups in Figs 1.19, 1.38 and 4.1, the mechanism of debonding is exactly the same.

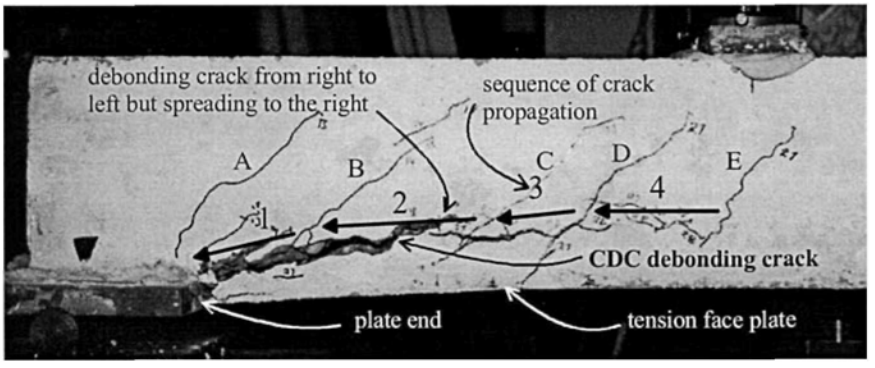

Figure 4.4 CDC debonding of a tension face plated beam with stirrups

It is also worth comparing, the distribution of cracks in Fig. 4.4, that were induced by CDC debonding in a beam with stirrups with those in Fig. 2.19 that were induced by IC debonding. They would appear to be similar with *concrete teeth* forming between the cracks, but the mechanisms that formed them, as has been explained, are totally different. IC debonding in Fig. 2.19 is induced by axial forces in the plate, starts at several positions in the region of maximum moment, and propagate and spread towards the plate end. In contrast, CDC debonding in Fig. 4.4 is induced by the rigid body shear displacement across a diagonal crack, starts at the root of a diagonal crack, propagates towards the plate end and spreads away from the plate end.

4.3 Concrete shear capacity of unplated beams or slabs

It has been shown that CDC debonding of a plated beam at $V_{c\text{-plate}}$ is controlled by the same mechanism that controls the concrete shear capacity V_c. Hence a good starting point, to develop a mathematical model for CDC debonding, is to start with the mathematical model for the shear capacity of a beam or slab without stirrups, that is V_c. In this section, we will first look at examples of the formation of critical diagonal cracks in RC beams and then qualitatively describe a procedure by Zhang (1997) for determining the concrete shear capacity V_c. Zhang's procedure has been chosen as it not only quantifies the capacity of V_c but also the position of the critical diagonal crack, which is an important criterion in determining P_{IC} and, hence, the extent of plating. It may be worth noting that Zhang's approach is a semi-empirical approach and consequently has a few dimensionally incorrect equations, but it has been calibrated with well over a hundred tests and, hence can be used with confidence.

4.3.1 Critical diagonal cracks in RC beams

Figure 4.5 shows shear failure of an RC beam without stirrups. The numbers on the beam are the applied loads. It can be seen that a series of vertical flexural and slightly inclined flexural-shear cracks first formed in the lower half of the beam and in the vicinity of the applied load. Then in a completely uncracked region, a critical diagonal crack formed through the depth of the beam and, as the beam did not have stirrups, this one critical diagonal crack caused failure. The shear failure is the concrete shear capacity of the beam V_c.

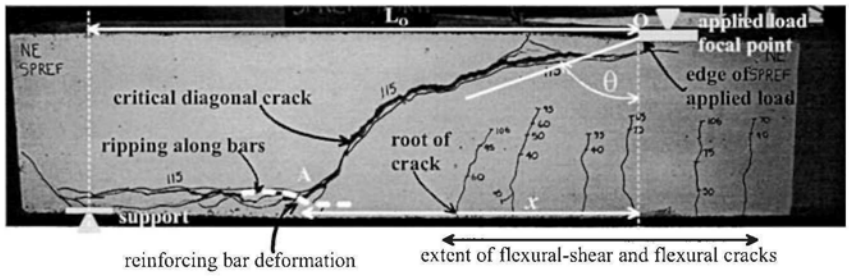

Figure 4.5 Critical diagonal crack in beam without stirrups

The critical diagonal crack in Fig. 4.5 spans between the edge of the applied load at point O, which will be referred to as the focal point, to the root of the crack at point A, that is over a length x of the shear span of length L_o. The horizontal cracking, along the level of the reinforcing bars from point A to the support, is due to the ripping action, as the reinforcing bars on the left side of A are pushed down due to the rigid body shear displacement across the two sides of the critical diagonal crack. The deformation of the reinforcing bar across the CDC is shown as the broken white line next to point A. It is this deformation, due to the rigid body displacement across the CDC, that causes the bars to the left of the CDC to break away from the beam as their cover is relatively small. As a matter of interest, it is this same action that causes plates that cross the CDC to debond as can be seen in Figs 1.19, 1.38 and 4.4.

For beams with concentrated loads, the focal point O usually occurs at the edge of the concentrated load as shown in Fig. 4.5 and it is a question of finding the inclination of the critical diagonal crack θ that gives the weakest strength. For convenience, the critical diagonal crack is represented by a straight line. For beams with uniformly distributed loads, the position of the focal point O of the critical diagonal crack is not so easy to define as it depends on the rate of change of the applied shear, so it may be necessary to try several positions to determine the weakest position, relative to the applied shear, that of the critical diagonal crack.

The formation of the critical diagonal cracks in beams with stirrups in Fig. 4.6 would appear to be much more confusing when compared to the single critical diagonal crack in Fig. 4.5 in a beam without stirrups. However, the first critical diagonal crack in Fig. 4.6 will form at the same position as in a beam without stirrups, as the presence of stirrups has virtually no effect on the formation of cracks, as stirrups only start to resist significant force when they span a crack. It is the formation and then rigid body displacement of this first critical diagonal crack that causes a plate to debond and not the ensuing diagonal cracks. After the formation of the first critical diagonal crack, and because the beam does not fail due to the presence of stirrups, other diagonal cracks can form as can be seen in Fig. 4.6.

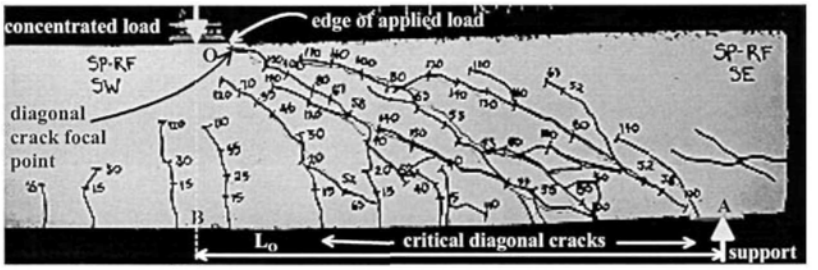

Figure 4.6 Critical diagonal cracks in beam with stirrups

4.3.2 Qualitative description of CDC analysis

An RC beam or slab without stirrups fails in vertical shear by first forming a diagonal crack after which failure occurs when the vertical shear resistance of that diagonal crack is exceeded. Hence, the shear capacity at a given section of a beam depends on two parameters: the vertical shear load that is required to form a diagonal crack $(V_{dat})_{cr}$ and the shear capacity that that diagonal crack can resist $(V_{dat})_u$. The CDC analysis for the hogging region of a beam follows the same procedure as that for the sagging region.

As an example of the analysis for vertical shear failure, let us consider one shear span of a hogging region of a plated beam as shown in Fig. 4.7(a). In the analysis, it is convenient to determine the shear load at any convenient datum point V_{dat} at which shear cracking or failure occurs within the shear span. In this example, we will assume that the datum point is at the point of contraflexure as shown and also that there is no applied load between the point of contraflexure and the support, so that in this example the vertical shear force is constant along the shear span at V_{dat}.

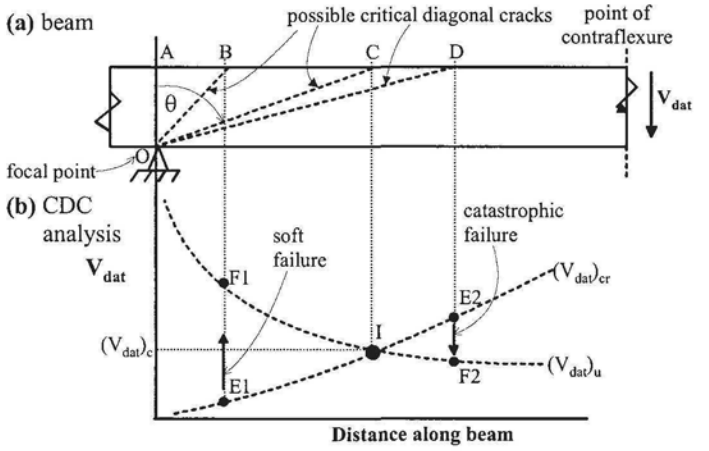

Figure 4.7 CDC analysis of unplated RC beam

Consider the diagonal crack O-B in the unplated beam in Fig. 4.7(a). The shear load V_{dat}, at the point of contraflexure, required to induce the diagonal crack is shown as point E1 in Fig. 4.7(b). The shear load V_{dat} to overcome the shear resistance of the crack is at point F1. Hence when the beam is gradually loaded, the diagonal

crack will first form at $(V_{dat})_{cr}$ = E1, but the diagonal crack will not fail until the shear has increased to $(V_{dat})_u$ = F1. It can be seen that there is prior warning of failure, so that this is called a soft failure. For the diagonal crack O-D in Fig. 4.7(a), the shear load to cause cracking is E2 and the shear load V_{dat} required to overcome the shear resistance of that diagonal crack is F2. Hence, for the diagonal crack O-D, nothing would happen until the shear crack formed at $(V_{dat})_{cr}$ = E2 and, immediately, there would be a catastrophic failure as the shear load to achieve the shear capacity $(V_{dat})_u$ = F2 is less than that to cause cracking.

It can be seen in Fig. 4.7(b) that for every position of the diagonal crack (that is as the diagonal crack rotates θ in Fig. 4.7(a) about the focal point O) the shear load at the datum point V_{dat} to cause cracking can be plotted as a line which is shown as $(V_{dat})_{cr}$. Similarly V_{dat} to cause the diagonal crack to fail can be plotted as $(V_{dat})_u$ (these iterative analyses are ideally suited for spreadsheets, however, direct but less accurate approaches are also presented in Section 4.5). Where the lines $(V_{dat})_{cr}$ and $(V_{dat})_u$ intercept at point I in Fig. 4.7(b) gives the weakest strength and, hence, the shear load at the datum point to cause shear failure in a beam without stirrups $(V_{dat})_c$, as well as the position of the critical diagonal crack A-C in Fig. 4.7(a). In this example, because we have assumed that V is constant along the hogging region, it will be shown in the next section that the shear force $(V_{dat})_c$ is also the shear capacity of the beam without stirrups V_c. It is also worth noting that cracking is a fairly random occurrence depending on the vagaries of the concrete properties. Hence, it is unlikely that the critical diagonal crack will occur exactly at point I in Fig. 4.7(b). If it occurs to the left there will be a soft failure and if it occurs to the right there will be rapid failure; this analysis explains what has been found to occur in practice and in tests.

4.3.3 Zhang's iterative approach

Zhang (1997) derived a lower bound to the shear capacity which is equivalent to a characteristic strength that can be used in design. The CDC analysis procedure has been described in qualitative terms in Section 4.3.2 and illustrated in Fig. 4.7. Consider the shear span B-C in Fig. 4.8. In theory, it would be necessary to determine the shear capacity at any position of the focal point, such as O_1, O_2 and O_3, and for each position it would be necessary to consider all possible inclinations θ of the crack. The weakest or critical diagonal crack will give V_c. The generic procedure for doing this will be described in this section. However, it is worth bearing in mind, that the position of the focal point is often known, such as at the position of the concentrated load in Fig. 4.5.

Let us consider the CDC analysis of the shear span A-B in Fig. 4.8 with the focal point at O, as shown, so that we need to determine the angle θ of the critical diagonal crack that gives the weakest shear capacity. The datum point is at a distance L_o from the focal point, where the shear load is V_{dat} as shown in Fig. 4.8(a) and the moment is M_{dat}. It is required to determine the shear load V_{dat} at the datum point to cause cracking for every possible rotation θ of the critical diagonal crack, which is shown as $(V_{dat})_{cr}$ in Fig. 4.7 as described in Section 4.3.2. We also need to determine the shear at the datum point V_{dat} to cause shear failure or crack sliding through an existing diagonal crack in any part of the shear span which is shown as $(V_{dat})_u$ in Fig. 4.7. We will be analysing the sagging region in Fig. 4.8, but the same analysis applies to the hogging region.

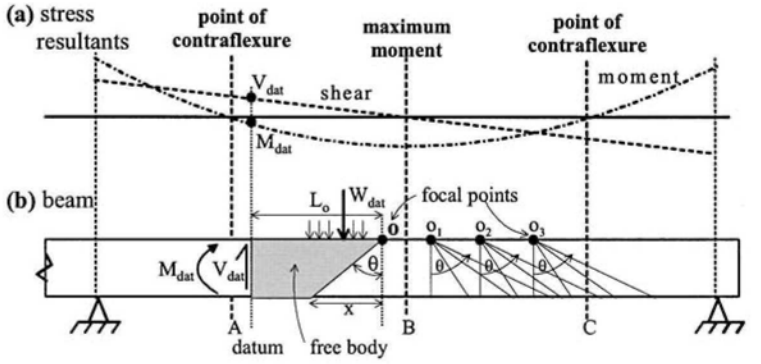

Figure 4.8 CDC analysis of free body

4.3.3.1 Vertical shear to cause cracking

The free body diagram in Fig. 4.8(b) has been shown enlarged in Fig. 4.9. It is necessary to determine the shear load at the datum point $(V_{dat})_{cr}$, that will cause the diagonal crack at an angle θ to form, that is the vertical shear to cause cracking. The beam is assumed to be prestressed with the prestressing tendon at a vertical distance d_{ps} from the focal point and a prestressing force of F_{ps}. The axial force in the longitudinal reinforcement is ignored as prior to cracking the stresses in the reinforcing bars are negligible. The shear load at the datum point to cause cracking $(V_{dat})_{cr}$ is our reference stress resultant. Hence $(M_{dat})_{cr}$ is the moment at the datum point when $(V_{dat})_{cr}$ is acting. Therefore, $(M_{dat})_{cr}$ is a function of $(V_{dat})_{cr}$, that is $(M_{dat})_{cr} = K_M(V_{dat})_{cr}$. Furthermore, $(W_{dat})_{cr}$ is the resultant of the applied loads acting on the free body of length L_o when $(V_{dat})_{cr}$ is acting and, hence, it is also proportional to $(V_{dat})_{cr}$ such that $(W_{dat})_{cr} = K_W(V_{dat})_{cr}$. The resultant applied load $(W_{dat})_{cr}$ acts at a distance e from the focal point. The depth of the beam is h, the inclination θ of the diagonal crack is defined by the distance *x* and the effective tensile strength of the concrete is f_{tef}.

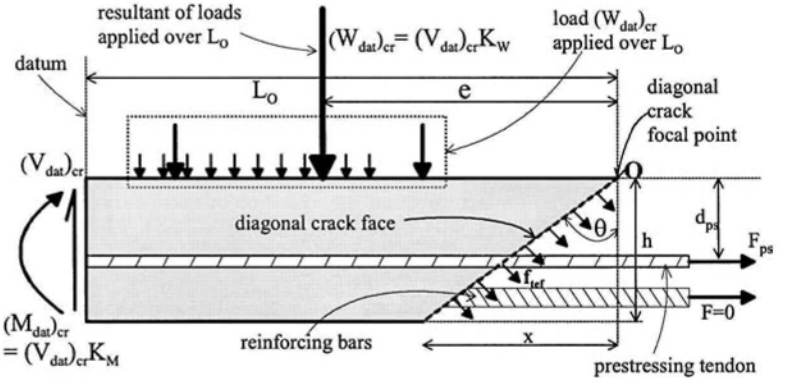

Figure 4.9 Shear load to cause cracking

From rotational equilibrium of the stress resultants in Fig. 4.9, the shear load at the datum point required to cause cracking is given by

$$(V_{dat})_{cr} = \frac{\left(\left(x^2 + h^2\right)\left(\frac{b_c f_{tef}}{2}\right)\right) + \left(F_{ps} d_{ps}\right)}{L_O + K_M - K_W e} \qquad 4.1$$

where b_c is the width of the slab, or 1 m width of slab for convenience, or the width of the web of a beam, and the effective tensile strength of the concrete is given by

$$f_{tef} = 0.156 f_c^{2/3}\left(\frac{h}{100}\right)^{-0.3} \qquad \text{[N and mm]} \qquad 4.2$$

which is not the actual tensile strength of the concrete but an effective tensile strength that has been derived empirically to allow for the non-uniform stress distribution of tensile stress within the depth of the beam. Hence the shear load at the datum point to cause cracking for various positions of the root of the diagonal crack x in Fig. 4.9 can be plotted as in Fig. 4.7(b) for $(V_{dat})_{cr}$.

Equation 4.1 may appear to be unduly complicated but it has been deliberately written to encompass all forms of loading and positions of the datum point. In general, the datum point will be taken at a point of contraflexure so that $(M_{dat})_{cr}$ is zero, that is $K_M = 0$. Furthermore, $(W_{dat})_{cr}$ is either a uniformly distributed load so that its relationship to $(V_{dat})_{cr}$, that is K_W, is known or it can be assumed to be negligible.

4.3.3.2 Vertical shear to cause crack sliding

After the diagonal crack has formed in Fig. 4.9, the vertical shear capacity of the diagonal crack V_u in Fig. 4.10 needs to be determined. As described in Section 4.2.1 and Figs 4.2 and 4.3, the shear capacity depends on the reinforcing bars crossing the crack and the prestress force F_{ps} across the crack, as they induce passive interface forces.

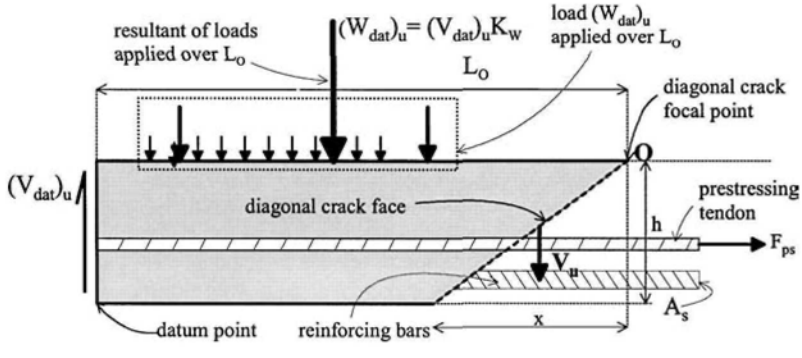

Figure 4.10 Vertical loads to cause crack sliding at failure

The shear load at the datum point to cause failure $(V_{dat})_u$, better referred to as crack sliding, can be determined from vertical equilibrium of the free body in Fig. 4.10. The applied load $(W_{dat})_u$ acts over the length L_o of the free body when $(V_{dat})_u$ is acting. Hence, $(W_{dat})_u$ is a function of $(V_{dat})_u$, that is $(W_{dat})_u = (V_{dat})_u K_W$. The vertical shear resistance across the diagonal crack is V_u. From vertical equilibrium

$$(V_{dat})_u = \frac{V_u}{1 - K_w} \tag{4.3}$$

where the shear capacity across the diagonal crack is given by

$$V_u = \frac{1}{4}\gamma_O f_c b_c h\left(\sqrt{1+\left(\frac{x}{h}\right)^2} - \frac{x}{h}\right) \tag{4.4}$$

and where the cohesive effectiveness factor γ_O is given by

$$\gamma_O = \lambda f_1(f_c) f_2(h) f_3(\rho) f_4\left(\frac{\sigma_{ps}}{f_c}\right) \tag{4.5}$$

The functions in Eq. 4.5 are given below with their units, as well as the ranges in which they have been calibrated and within which their use should be restricted. The concrete contribution to the strength is given by

$$f_1(f_c) = \frac{3.5}{\sqrt{f_c}} \qquad \text{[N and mm]} \quad 5 < f_c < 60\,MPa \tag{4.6}$$

the size effect by

$$f_2(h) = 0.27\left(1 + \frac{1}{\sqrt{h}}\right) \qquad \text{[m]} \quad 0.08 < h < 0.7 \tag{4.7}$$

the contribution of the longitudinal reinforcement by

$$f_3(\rho) = 0.15\rho + 0.58 \qquad \rho = \frac{A_s}{b_c h} \times 100 \;\; and \;\; \rho < 4.5 \tag{4.8}$$

where A_s is the cross-section area of all of the longitudinal reinforcement crossing the critical diagonal crack, that is at all levels of the beam and it is suggested those within b_c. The contribution through prestressing is given by

$$f_4\left(\frac{\sigma_{ps}}{f_c}\right) = 1 + 2\frac{\sigma_{ps}}{f_c} \qquad where\ \sigma_{ps} = \frac{F_{ps}}{b_c h} \tag{4.9}$$

Zhang proposed that the coefficient λ in Eq. 4.5 should be taken as 1.6 for concentrated applied loads and 1.2 for uniformly distributed applied loads. There does not appear to be any theoretical justification for this difference and it can only be assumed that these coefficients were derived empirically through calibration of the mathematical model with test results. It is suggested that λ = 1.6 should be used throughout for all types of loads and load combinations as: most shear failures are associated with concentrated loads such as at supports of continuous beams where the vertical shear is at its highest; a brief comparison with code values shows reasonable

correlation when using $\lambda = 1.6$; and more importantly, it will be suggested later in Section 4.4 that the CDC analysis should, preferably, be used to determine only the increase in V_c due to plating $\Delta V_{c\text{-plate}}$, to be used in conjunction with $(V_c)_{code}$ from the national code so that any differences in the overall strength will be minimised.

The shear load at the datum point to cause failure after a diagonal crack has formed can be derived as follows from Eqs 4.3 and 4.4 with $\lambda = 1.6$

$$(V_{dat})_u = \frac{0.4\left(f_1(f_c)f_2(h)f_3(\rho)f_4\left(\frac{\sigma_{ps}}{f_c}\right)\right)f_c b_c h\left(\sqrt{1+\left(\frac{x}{h}\right)^2}-\frac{x}{h}\right)}{1-K_W} \qquad 4.10$$

and can be plotted as $(V_{dat})_u$ in Fig. 4.7(b).

4.3.3.3 Concrete shear capacity of RC beams and slabs

Let us consider a beam or slab without stirrups so that the formation of the critical diagonal crack will cause failure as the concrete shear component V_c has been exceeded. Equations 4.1 and 4.10 can be used to plot both the shear load at the datum point to cause cracking at any position along the beam which is $(V_{dat})_{cr}$ in Fig. 4.7(b), and the shear load at the datum point to cause crack sliding or failure at any position along the beam which is $(V_{dat})_u$ in Fig. 4.7(b). The intercept of these two lines is the shear load at the datum point to cause the region of the beam being analysed to form a critical diagonal crack and fail which is shown as $(V_{dat})_c$.

If the applied shear load at the datum point $(V_{dat})_{applied}$ is less than $(V_{dat})_c$, then the region will not fail, that is a critical diagonal crack will not form in this region, and vice versa. Furthermore specifically for the critical diagonal crack, in Eq. 4.3 $(V_{dat})_u$ is $(V_{dat})_c$ and V_u is V_c. Hence the concrete shear capacity is given by

$$V_c = (1-K_W)(V_{dat})_c \qquad 4.11$$

It may be worth noting that when the applied load along the shear span L_O in Fig. 4.10 is zero then $K_W = 0$ in Eq. 4.11 so that $V_c = (V_{dat})_c$ in Eq. 4.11 and Fig. 4.7(b). It may also be worth noting that for a beam with stirrups that V_c may not be the failure load, but it is the shear load at which the first diagonal crack or critical diagonal crack slides which is also the shear load at which CDC debonding of plates occurs as described in Section 4.4.

4.4 CDC debonding of tension face plates

Zhang's analysis, in Section 4.3.3, for determining the vertical shear capacity of a beam or slab without stirrups is adapted in Section 4.4.1 to allow for the contributions of adhesively bonded tension face plates. The CDC analysis is then incorporated into a general CDC design procedure in Section 4.4.2 based on either the hinge approach in Section 2.5.2 or the anchorage approach in Section 2.5.1. As this approach for plated beams is based directly on Zhang's lower bound analysis, it can be considered to give a characteristic or lower bound value suitable for design.

4.4.1 Iterative CDC analysis

It has been shown that critical diagonal crack debonding of an externally bonded plate is exactly the same mechanism as that which governs the concrete shear capacity of a beam without stirrups V_c. Hence, it is a question of determining the enhanced concrete shear capacity due to plating $V_{c\text{-}plate}$. Furthermore, $V_{c\text{-}plate}$ also governs the CDC debonding of plates bonded to beams with stirrups, as the rigid body deformation across the critical diagonal crack or crack sliding, associated with CDC debonding, is required to stretch the stirrups so that they can resist shear as quantified by the stirrup shear component V_s. However, tests have shown that, before any significant portion of V_s can be achieved, the rigid body deformation or crack sliding causes CDC debonding.

The generic CDC analysis for an unplated RC beam or slab has been described in Sections 4.3.2 and 4.3.3. In theory, the critical diagonal crack can emanate from any position along the beam, such as the focal points O_1 to O_3 in the shear span B-C in Fig. 4.8. To reduce the amount of analyses, guidelines are given in Section 4.4.1.1 to the probable positions of the focal points. Externally bonded plates inhibit or delay the formation of the critical diagonal crack and this is covered in Section 4.4.1.2. After the critical diagonal crack has formed, the plate can be considered to act as additional longitudinal reinforcement in Section 4.4.1.3, where the shear is resisted by dowel action and through aggregate interlock as described in Section 4.2.1 and Figs 4.2 and 4.3. Alternatively after diagonal cracking, the plate resistance is considered to act as a passive prestressing force in Section 4.4.1.4, where the axial force in the plate induces the passive normal force P_{inter} in Fig. 4.2 that is required to resist the shear by aggregate interlock.

4.4.1.1 Position of diagonal crack focal and datum points

The first requirement of the CDC analysis is to identify the *focal point* of the diagonal crack that has the weakest shear capacity. The *focal point* is always on the compression face of the beam. For beams with concentrated or point loads on the compression face, the focal point is assumed to occur adjacent to the edge of the concentrated load on the compression face, such as in Figs 1.19, 4.1 and 4.6. Illustrations of focal points that emanate from concentrated loads that are applied to the compression faces of continuous beams are shown in Fig. 4.11. For example, the support reaction at E is a concentrated or point load that is being applied to the compression face of the hogging region of the beam. Hence, point E at the edge of the support is a focal point for determining the shear capacity of a beam without stirrups V_c or crack sliding in a plated beam that induces CDC debonding $V_{c\text{-}plate}$. Large concentrated loads applied to the beam, as may occur in vehicular bridge beams, can also be the focal point for critical diagonal cracks. An example is shown in shear span B-C where the concentrated load or point load is being applied to the compression face in the sagging region.

For sagging regions subjected to predominantly uniformly distributed loads (udl), as shown in shear span C-D in Fig. 4.11, the position of the focal point is not as clearly defined as that for concentrated loads so it may be necessary to vary the position of the focal point to find the CDC. It needs to be stressed that if it is not clear where the critical focal point is, that is the focal point where the weakest diagonal crack emanates, then the CDC analyses can be applied to several points along the beam, such as O_1 to O_3 in Fig. 4.8, to find the critical focal point. This may occur when there are combinations of loads to be dealt with. It is also worth remembering

that the weakest diagonal crack is the weakest diagonal crack relative to the applied shear at that position.

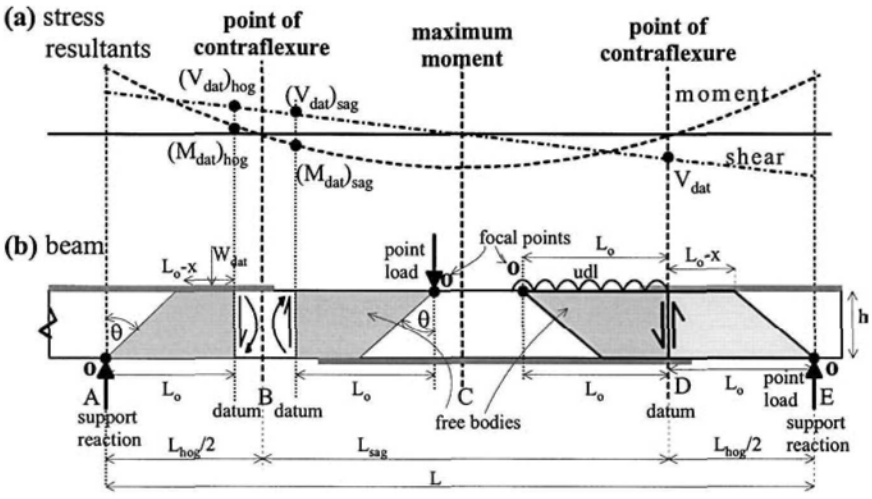

Figure 4.11 Diagonal crack focal points and datum points in continuous beams

The focal point establishes one side of the free body required in the CDC analysis as shown in Fig. 4.11. The other side, which is the datum point, can be anywhere. The shear load at the datum point to cause cracking, as in Eq. 4.1 for $(V_{dat})_{cr}$ in the unplated beam and later in Eq. 4.18 for $(V_{dat})_{cr\text{-}plate}$ in the plated beam depends on the following coefficient

$$K_M = \frac{M_{dat}}{V_{dat}} \qquad 4.12$$

where K_M can be derived directly from the ratio of the stress resultants at the datum point as shown in Fig. 4.11(a) and which is not difficult to determine. However, as $K_M = 0$ at a point of contraflexure, it is convenient to choose a point of contraflexure as a datum point as shown for the free bodies in the shear spans C-D and D-E in Fig. 4.11.

The shear load at the datum point to cause cracking in Eqs 4.1 and 4.18 as well as the shear load to cause crack sliding or failure that is $(V_{dat})_u$ in the unplated beam in Eq. 4.10 and later $(V_{dat})_{u\text{-}metal}$ for the plated beam in Eq. 4.21 depends on load shear ratio

$$K_W = \frac{W_{dat}}{V_{dat}} \qquad 4.13$$

where W_{dat} is the portion of the applied load, that induces V_{dat}, that is acting on the free body as shown in the shear span A-B in Fig. 4.11.

For example, if there is no applied load acting along the free body, such as on the free body in shear span B-C and D-E in Fig. 4.11, where the concentrated load is not acting along the body but on the edge at the focal point, then

$$K_W = \frac{W_{dat}}{V_{dat}} = 0 \qquad 4.14$$

Furthermore, if the continuous beam in Fig. 4.11 is only subjected to a uniformly distributed load of w per unit length, then for the CDC analysis of the free body in the shear span C-D, the shear load at the datum point D is

$$\left(\left(V_{dat}\right)_{poc}\right)_{udl} = \frac{wL}{2} - \frac{wL_{hog}}{2} \qquad 4.15$$

so that the factor K_W for the free body in the sagging shear span C-D is given by

$$\left(\left(K_W\right)_{sag}\right)_{udl} = \frac{wL_O}{\frac{wL}{2} - \frac{wL_{hog}}{2}} = \frac{2L_O}{L_{sag}} \qquad 4.16$$

and similarly for the free body in the hogging shear span D-E

$$\left(\left(K_W\right)_{hog}\right)_{udl} = \frac{w\left(L_O - x\right)}{\frac{wL}{2} - \frac{wL_{hog}}{2}} = \frac{2\left(L_O - x\right)}{L_{sag}} \qquad 4.17$$

4.4.1.2 Shear to cause cracking of tension face plated sections

The stress resultants involved in determining the vertical shear to cause a diagonal crack to form in an unplated beam in a sagging region is shown in Fig. 4.9. This can be compared with those required in a tension face plated beam in the sagging region B-C in Fig. 4.11 which is shown fully in Fig. 4.12. The only difference between the unplated beam in Fig. 4.9 and the plated beam in Fig. 4.12 is the additional force in the tension face plate $(F_{plate})_{cr}$ that has to be overcome to allow the concrete to crack. This force was determined by simply transforming the plate into an equivalent area of concrete.

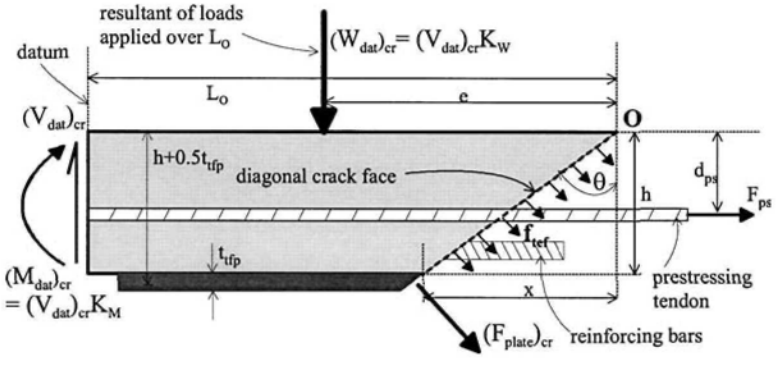

Figure 4.12 Shear load to cause cracking in a tfp beam in the sagging region

The shear load at the datum point to cause cracking in a tension face plated beam or slab in the sagging region is given by

$$\left(\left(V_{dat}\right)_{cr-plate}\right)_{sag} = \frac{\left(\left(x^2+h^2\right)\left(\frac{b_c f_{tef}}{2} + \frac{m_p f_t b_{tfp} t_{tfp}\left(h+0.5t_{tfp}\right)}{h^2}\right)\right) + \left(F_{ps} d_{ps}\right)}{L_O + K_M - K_W e} \qquad 4.18$$

where m_p is the modular ratio of the plate material stiffness to that of the concrete E_p/E_c. f_t is the tensile strength of the concrete in the beam which if not measured directly can be taken as $0.4\sqrt{f_c}$ [N/mm^2], b_{tfp} and t_{tfp} are the width and thickness of the tension face plate such that their product is the cross-sectional area of plate, and $(h + 0.5t_{tfp})$ is the vertical distance from the plate centroid to the focal point which for tension face plates can be taken as h, but it will be left in this form to show later how Eqs 4.1 and 4.18 are special cases of a generic equation which will be developed in Chapter 5.

The stress resultants in the free body in shear span A-B in the hogging region in Fig. 4.11(b) are shown in Fig. 4.13. The only real difference between Fig. 4.12 (sagging region) and Fig. 4.13 (hogging region) is that in Fig. 4.13 the moment of the applied load $W_{dat}e$ about the focal point acts in the opposite direction to the remaining moments on the free body as compared with that in Fig. 4.12. Furthermore, W_{dat} in Fig. 4.13 is applied over a smaller length L_O-x as compared with L_O in Fig. 4.12.

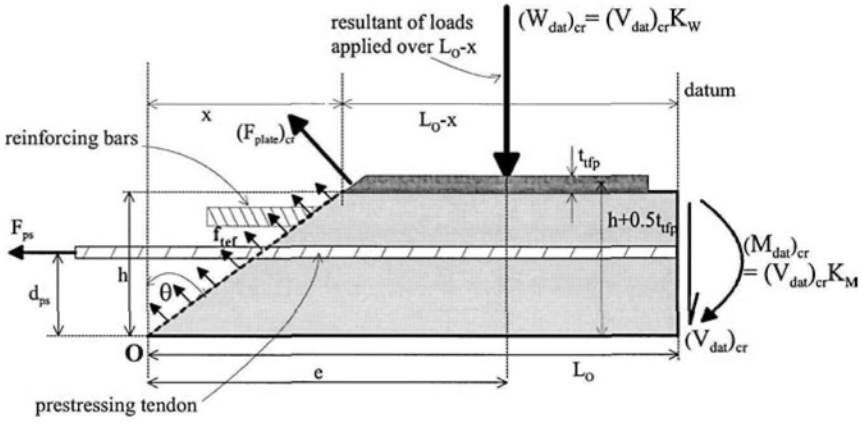

Figure 4.13 Shear load to cause cracking in a tfp beam in the hogging region

From rotational equilibrium of the stress resultants in Fig. 4.13, the shear load at the datum point to cause cracking for a tension face plated beam in the hogging region is given by

$$\left(\left(V_{dat}\right)_{cr-plate}\right)_{hog} = \frac{\left(\left(x^2+h^2\right)\left(\frac{b_c f_{tef}}{2} + \frac{m_p f_t b_{tfp} t_{tfp}\left(h+0.5t_{tfp}\right)}{h^2}\right)\right) + \left(F_{ps} d_{ps}\right)}{L_O + K_M + K_W e} \qquad 4.19$$

The difference between the sagging result in Eq. 4.18 and the hogging result in Eq. 4.19 is the change in sign of the $K_w e$ term in the denominator, which is due to the reversal in the moment $W_{dat}e$ relative to the other moments as explained previously.

It can be seen that both Eqs 4.18 and 4.19 can be used to determine the shear load at the datum point to cause cracking for unplated beams $(V_{dat})_{cr}$ by simply substituting $t_{tfp} = 0$ into the equations. There is now no need to revert back to Eq. 4.1 or its equivalent for the hogging region for a CDC analysis of an unplated beam.

4.4.1.3 Shear to cause crack sliding in tension face plated sections – longitudinal reinforcement approach

The shear to cause crack sliding in an unplated beam in a sagging region is described in Section 4.3.3.2 and the stress resultants involved are shown in Fig. 4.10. Those required to cause crack sliding in a tension face plated beam or slab in a sagging region are shown in Fig. 4.14. The only additional force is the maximum possible force in the plate P_{plate}. The maximum force in the plate P_{plate} is the lesser of: the yield capacity, if it is a metal plate, of $A_p f_{yp}$; the IC debonding force P_{IC} whose magnitude depends on the available anchorage length L_p in Fig. 4.14 which depends on the effective length L_e in Eq. 2.3 and the IC debonding resistance of the plate in Eq. 2.1; and the fracture strength $A_p f_{FRP}$ if it is an FRP plate. It may be worth noting that the plate force $(F_{plate})_{cr}$ in Figs 4.12 and 4.13 does not depend on the anchorage length L_p as it is the force in the plate just prior to cracking, whereas P_{plate} in Fig. 4.14 is the force the plate can resist after cracking which depends on, for example, the resistance to IC debonding and hence L_p.

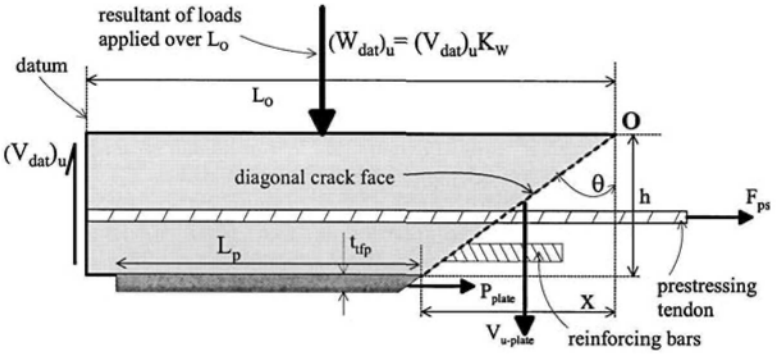

Figure 4.14 Shear load to cause crack sliding in a tfp beam in the sagging region

The plate force P_{plate} in Fig. 4.14 can be assumed to act as additional longitudinal reinforcing bars as described in Section 4.2.1. The function which governs this contribution in an unplated beam is given by Eq. 4.8 which depends on the cross-sectional area of all of the longitudinal reinforcing bars A_s. Hence P_{plate} has to be converted to an equivalent area of longitudinal reinforcement. This conversion can be made for metal plates as they have a yield capacity as do reinforcing bars, but it is difficult to make this conversion for FRP plates as they do not yield and, hence, this *longitudinal reinforcement approach* is restricted to metal plates. To be on the conservative side, so as not to over-estimate the equivalent area of reinforcing bar, we can assume that P_{plate} is equivalent to an area of metal plate that has yielded at its yield capacity f_{yp}, so that the longitudinal reinforcement function for unplated beams in Eq. 4.8 becomes

$$f_3(\rho_{plate}) = \frac{15}{b_c h}\left(A_s + \frac{P_{plate}}{f_{yp}}\right) + 0.58 \le 1.26 \qquad 4.20$$

The shear load to cause crack sliding in unplated beams in Eq. 4.10 now becomes for metal tension face plated beams

$$\left((V_{dat})_{u-metal}\right)_{sag} = \frac{0.4\left(f_1(f_c)f_2(h)f_3(\rho_{plate})f_4\left(\frac{\sigma_{ps}}{f_c}\right)\right)f_c b_c h\left(\sqrt{1+\left(\frac{x}{h}\right)^2} - \frac{x}{h}\right)}{1 - K_W} \qquad 4.21$$

To complete the picture, the stress resultants in the hogging region are shown in Fig. 4.15, and the shear load at the datum point to cause crack sliding is given by Eq. 4.22 which differs from Eq. 4.21 by the sign of the K_W coefficient.

$$\left((V_{dat})_{u-metal}\right)_{hog} = \frac{0.4\left(f_1(f_c)f_2(h)f_3(\rho_{plate})f_4\left(\frac{\sigma_{ps}}{f_c}\right)\right)f_c b_c h\left(\sqrt{1+\left(\frac{x}{h}\right)^2} - \frac{x}{h}\right)}{1 + K_W} \qquad 4.22$$

Equations 4.21 and 4.22 can only be used for metal plates. Furthermore, they can also be used for determining the shear load at the datum point to cause crack sliding in an unplated beam $(V_{dat})_u$ by simply substituting $P_{plate} = 0$ in Eq. 4.20. Hence there is no need to use Eq. 4.10 or its equivalent for the hogging region for an unplated beam.

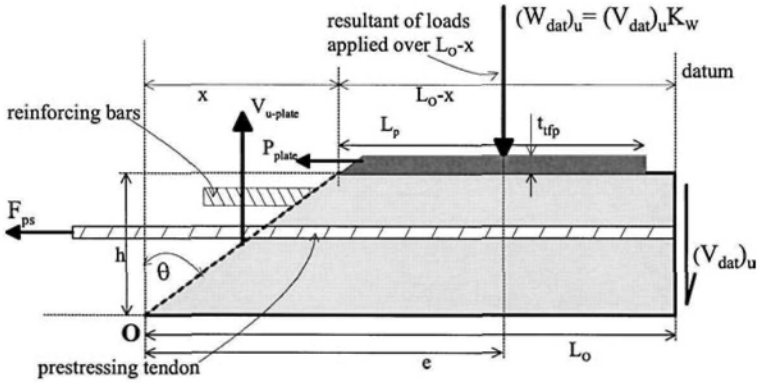

Figure 4.15 Shear load to cause crack sliding in a tfp beam in the hogging region

4.4.1.4 Shear to cause crack sliding in tension face plated sections – passive prestress approach

An alternative to converting the maximum plate force P_{plate} into an equivalent area of longitudinal reinforcement, as in Section 4.4.1.3, is to assume that the maximum plate force P_{plate} directly applies a passive prestress across the diagonal crack as explained in Section 4.2.1 and in Figs 4.2 and 4.3. In which case, the prestress force term F_{ps} in

the prestress function of Eq. 4.9 for unplated beams is increased to $F_{ps}+P_{plate}$. A comparison of this increase in the shear capacity with tests in which critical diagonal cracks were known to occur (Oehlers et al 2004a) showed that the coefficient 2 in Eq. 4.9 gives a conservative estimate of the increase in the shear to cause CDC debonding. A coefficient of 4 was found to correlate well with test data and also with prestressed code approaches described in Section 4.5.2. Hence, the prestress function of Eq. 4.9 has been adapted as follows to include a passive prestress term.

$$f_4\left(\frac{\sigma_{ps}}{f_c}\right)_{plate} = 1 + 2\frac{F_{ps}}{f_c b_c h} + 4\frac{P_{plate}}{f_c b_c h} \qquad 4.23$$

where the passive prestress $\sigma_{pp} = P_{plate}/b_c h$. This approach has the benefit that it can be used for both metal and FRP plates and that the plate force P_{plate} can be used directly instead of having to be converted into an equivalent area of longitudinal reinforcing.

The shear force at the datum point to cause crack sliding in a sagging region in Fig. 4.14 using the passive prestress approach is given by

$$\left((V_{dat})_{u-pres}\right)_{sag} = \frac{0.4\left(f_1(f_c)f_2(h)f_3(\rho)f_4\left(\frac{\sigma_{ps}}{f_c}\right)_{plate}\right)f_c b_c h\left(\sqrt{1+\left(\frac{x}{h}\right)^2}-\frac{x}{h}\right)}{1-K_W} \qquad 4.24$$

and for the hogging region in Fig. 4.15

$$\left((V_{dat})_{u-pres}\right)_{hog} = \frac{0.4\left(f_1(f_c)f_2(h)f_3(\rho)f_4\left(\frac{\sigma_{ps}}{f_c}\right)_{plate}\right)f_c b_c h\left(\sqrt{1+\left(\frac{x}{h}\right)^2}-\frac{x}{h}\right)}{1+K_W} \qquad 4.25$$

It needs to be emphasised that the passive prestress induced by the plate P_{plate} does not act before an intermediate diagonal crack has formed as it is induced by the aggregate interlock sliding action across the crack. Hence, the passive prestress P_{plate} does not affect the shear load to cause cracking $(V_{dat})_{cr\text{-}plate}$ as it simply does not exist prior to cracking. In contrast, the active prestressing force F_{ps} in Fig. 4.12 acts prior to cracking and that is why it is included in the shear load to cause cracking in Eqs 4.18 and 4.19.

Equations 4.24 and 4.25 can be used for metal and FRP plates, in fact plates of any material. Furthermore and to stress and reiterate a point, they can also be used for determining the shear load at the datum point to cause crack sliding in an unplated beam or slab $(V_{dat})_u$ by simply substituting $P_{plate} = 0$ in Eq. 4.23. Hence there is no need to use Eq. 4.10 or its equivalent for the hogging region for an unplated beam.

4.4.1.5 Shear capacity analysis

An application of the CDC analysis for a tension face plated beam is shown in Fig. 4.16. The equations used in the analysis of the hogging region are given in Fig. 4.16(b), as well as those that would be required for the analysis of a sagging region for reference.

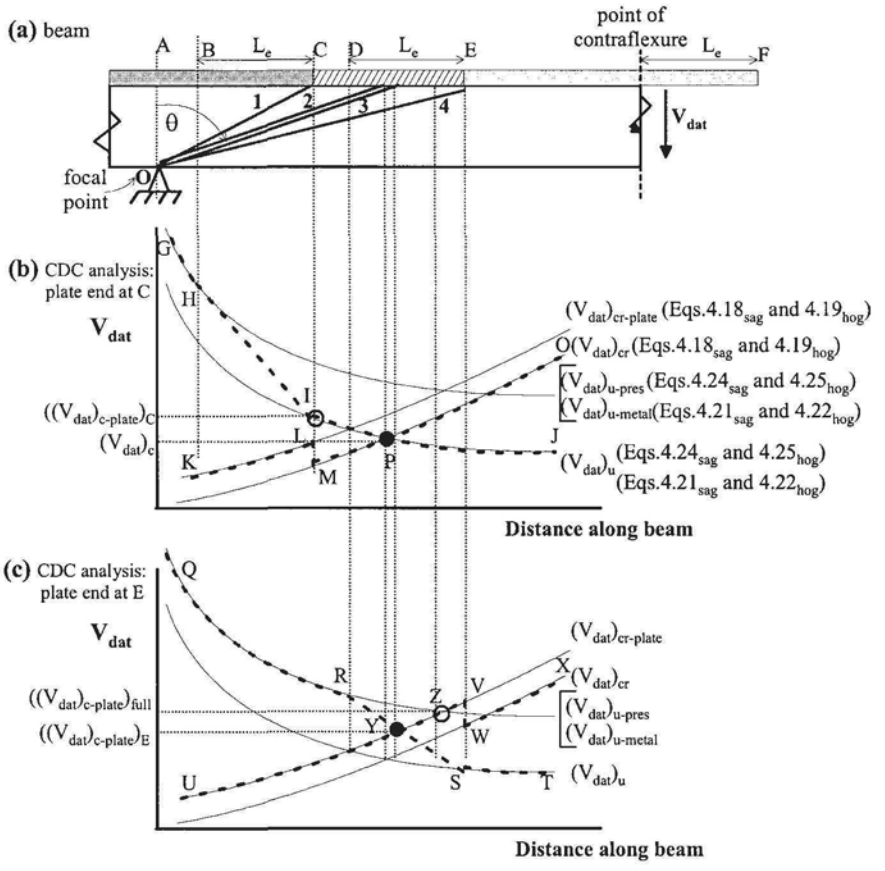

Figure 4.16 Shear capacity of partially plated beams

The beam has been analysed first as unplated so that Eq. 4.19, with the plate thickness equal to zero, has been used to determine the variation of the shear load at the datum point to cause a diagonal crack $(V_{dat})_{cr}$ in Figs 4.16(b) and (c). Equations 4.22 or 4.25, with P_{plate} equal to zero, can be used to determine the variation of the shear load at the datum point to cause crack sliding or failure $(V_{dat})_u$. The beam has then been assumed to be fully plated and also that the plate is fully anchored in the hogging region so that the plate has been extended past the point of contraflexure in Fig. 4.16(a) by an effective length L_e. Hence at every possible position of the CDC along the hogging region, the full plate strength P_{plate} can be achieved. The shear load at the datum point to cause cracking is given by Eq. 4.19 and that to cause crack sliding by Eqs 4.22 or 4.25 with P_{plate} constant and at its maximum value. Just to illustrate the procedure, we will assume that the maximum plate strength P_{plate} is the IC debonding resistance P_{IC} that requires a minimum anchorage length of L_e. Hence, it could be said that the two unplated curves and the two fully plated curves form the bounds of the 'failure envelopes'.

Let us first consider a short tension face plate of length A-C in Fig. 4.16(a); so that A-B is fully anchored and the force in the plate reduces over the effective length L_e from its maximum at B, being fully anchored, to zero at C, where there is no

anchorage. Hence in Fig. 4.16(b), the load to cause cracking follows the path K-L, along the plated section, and then at the plate end at L drops to M and follows the path M-O along the unplated section. The load to cause crack sliding follows the path G-H and then from H on the fully anchored curve to I on the unplated curve, over the effective length L_e, after which it follows the path I-J on the unplated beam. The paths cross at point P, $(V_{dat})_c$, which lies beyond the plate. This means that a critical diagonal crack will first form in the unplated region as shown by the diagonal crack marked 2 in Fig. 4.16(a) which would cause failure in beams without stirrups. If the beam had stirrups so that the shear load could be increased, then the diagonal crack marked 1 would occur at the plate end at the shear load marked I, $((V_{dat})_{c\text{-}plate})_C$ in Fig. 17(a) and this would be the shear load to cause debonding in the plated region.

Let us now extend the plate to E in Fig. 4.16(a). The load to cause cracking follows the plated path U-V in Fig. 4.16(c) to the plate end, then drops to W in the unplated beam and then W-X along the unplated beam. The load to cause crack sliding follows the plated path Q-R, then from R to S, over the effective length L_e, and then S-T along the unplated beam. The paths cross at Y, $((V_{dat})_{c\text{-}plate})_E$. Hence the critical diagonal crack is the diagonal crack marked 3 in Fig. 4.16(a) which occurs within the anchorage zone of the plate.

It is also worth considering the fully anchored analyses in Fig. 4.16(c) which is given by the lines $(V_{dat})_{cr\text{-}plate}$ and $(V_{dat})_{u\text{-}pres/metal}$. These lines cross at point Z which is, therefore, the position of the critical diagonal crack for the fully plated member with a shear capacity of $((V_{dat})_{c\text{-}plate})_{full}$, in Fig. 4.16(c). This gives the maximum possible strength. Hence, extending the plate a further distance L_e to the right of Z is all that is required to achieve the greatest benefit from this plate; this is the minimum extent of plating required to achieve the greatest increase in $V_{c\text{-}plate}$. It may be worth noting that there is a tendency for plating to move the position of the root of the critical diagonal crack towards the datum, that is to increase the inclination of the critical diagonal crack θ. This does not always occur but does tend to occur as illustrated in the example in Fig. 4.16 where the critical diagonal crack moves from *P* in the unplated beam to *Y* in the partially plated beam and then to Z in the fully anchored plated beam.

If the concrete shear capacity of the plated beam $V_{u\text{-}plate}$ in Figs 4.14 and 4.15 is required, then from Eq. 4.11 and also from Eqs 4.24 and 4.25

$$V_{c-plate} = (1 \pm K_W)(V_{dat})_{c-plate} \qquad 4.26$$

where $(V_{dat})_{c\text{-}plate}$ is shown on the ordinates of Figs 4.16(b) and (c) which includes $(V_{dat})_c$ for the unplated beam as a special case of the plated beam. The factor K_W is negative in the sagging regions and positive in hogging regions. This is because in the sagging region, as in Fig. 4.11, the shear load at the datum point, which is always nearer to the point of contraflexure than the focal point, is always larger than at the focal point. Hence, V_{dat} at the datum point has to be reduced to determine the shear force at the focal point. Conversely, in the hogging region in Fig. 4.11, the shear load at the datum point is lower than at the focal point so that K_W is positive to allow for the increased shear at the diagonal crack. It is also worth noting that $V_{c\text{-}plate}$ in Eq. 4.26 is the shear load to cause crack sliding and hence debonding in a plated beam.

4.4.2 Design approach for CDC debonding

At this stage of the analysis, the plates required at the positions of maximum moment in Figs 4.17(b) and (c) have been designed to resist the maximum moments in Fig.

4.17(a) and this has been based in Chapter 3 on IC debonding. The next step is to design against CDC debonding along a region of the beam, that is within the hogging or sagging region, which depends on the magnitude and distribution of the vertical shear force in Fig. 4.17(a) and which also controls the extent of plating. Having already described the CDC analysis, we will now describe a CDC design procedure. The design procedure depends on the design philosophy that is being adopted as explained in Section 2.5: the anchorage approach is shown in Fig. 4.17(b); and the hinge approach in Fig. 4.17(c).

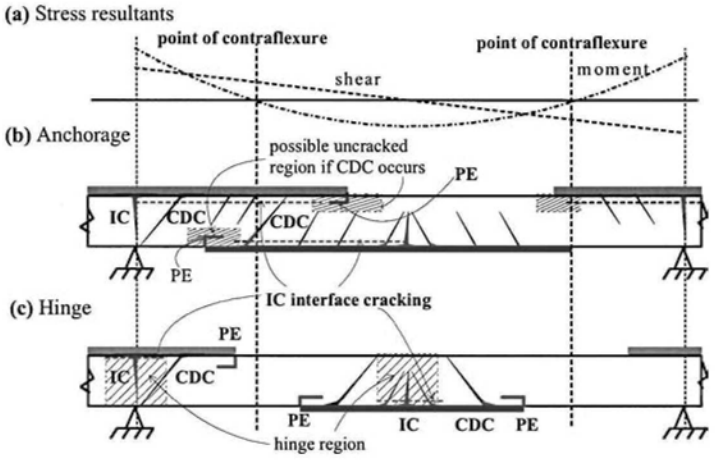

Figure 4.17 Design philosophies

4.4.2.1 CDC design procedure in hinge approach

Let us start with the *hinge approach* in Fig. 4.17(c). The hinge approach restricts the IC interface crack to within a relatively small region or hinge. This allows the plates to be terminated short of the points of contraflexure, so that it will be necessary to determine the extent of plating as well as the resistance to CDC debonding. The extent of plating is also controlled by plate end debonding and this is covered in Chapter 6. The CDC design procedure is the same in the hogging region and the sagging region, so let us consider the hogging region over the left support in Fig. 4.17(c) which is shown in Fig. 4.18.

The design procedure for the hinge approach is illustrated in Fig. 4.18(a) and consist of the following steps.

1. First assume that the beam is fully plated along the region and for every possible position θ of the diagonal crack, such as O-C in Fig. 4.18(a), assume that the plate is fully anchored beyond the diagonal crack, that is it extends at least the effective length L_e beyond the root of the diagonal crack. Hence the maximum plate force P_{plate} can be assumed to be constant along the region which simplifies the analysis.
2. From a CDC analysis as described in Section 4.4.1 determine the position A-C of the weakest diagonal crack that is the critical diagonal crack, and the shear force $(V_{dat})_{c\text{-}plate}$ at the datum point to cause shear failure or crack sliding.
3. If the shear force at the datum point required to cause crack sliding $(V_{dat})_{c\text{-}plate}$ exceeds the applied shear force at the datum point $(V_{dat})_{applied}$, then the plate will

not debond. Otherwise, the design load cannot be achieved and some other plating arrangement or system of plating such as bolting may need to be considered.

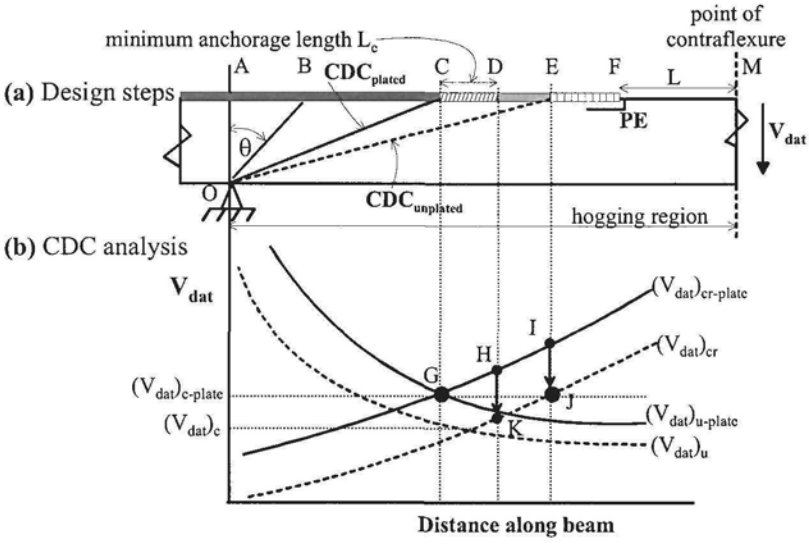

Figure 4.18 CDC design procedure using hinge approach

4. If the plated structure is strong enough, extend the plate at least one effective length L_e (Eq. 2.3) to Point D, to ensure that the plate is fully anchored as per the assumption in the CDC analysis in step (1).
5. A critical diagonal crack could also occur in the unplated region D-M in Fig. 4.18(a). However, this is not a debonding problem as a critical diagonal crack in the unplated region will not induce plate debonding. For beams with stirrups, it may be necessary to ensure that the shear in the unplated region is less than $V_c + V_s$. For a slab without stirrups, a critical diagonal crack in the unplated region may be undesirable particularly if the increase in the shear capacity due to plating is required to resist the increased applied load that this plating rehabilitation allows. In which case, the plate should be extended as in the following steps, to ensure that the critical diagonal crack occurs within the plated region.
6. To ensure that a critical diagonal crack does not occur within the unplated region, a CDC analysis of the unplated beam, as described in Section 4.4.1 and using the same equations as for the plated beam, needs to be performed to give the lines $(V_{dat})_{cr}$ and $(V_{dat})_u$ in Fig. 4.18(b).
7. As the root of the critical diagonal crack moves from C to D in Fig. 4.18(a), the path of the shear load to cause failure moves from G to H along $(V_{dat})_{cr\text{-}plate}$ in Fig. 4.18(b), and then to K on $(V_{dat})_{cr}$ at the plate end. Hence at position D, the shear to cause failure in the unplated region may be less than that to cause failure of the fully anchored plate at point C. Hence, it will be necessary to extend the plate to point E where the shear to cause failure J in the unplated beam is the same as that in the fully anchored plated beam at C.
8. It may be necessary to extend the plate beyond E to say point F to ensure plate end debonding does not occur as described in Section 1.3.3 and quantified in Chapter 6. However, it may be worth noting that PE debonding will rarely if ever prevent

adhesive bonding plates as it can be easily prevented by simply terminating the plate at the point of contraflexure.

These analyses have determined the extent of plating A-E in Fig. 4.18(a). They have also determined the shear load at the datum point to cause failure which is $(V_{dat})_{c\text{-}plate}$ in Fig. 4.18(b), from which can be deduced the vertical shear capacity within the plated region $V_{c\text{-}plate}$ in Eq. 4.26. The same can be said for the unplated beam. From $(V_{dat})_c$ in Fig. 4.18(b), can be deduced the vertical shear capacity of the unplated beam V_c from Eq. 4.11, which is really the same as Eq. 4.26. Hence the increase in the shear capacity $\Delta V_{c\text{-}plate} = V_{c\text{-}plate} - V_c$ due to plating is given by

$$\Delta V_{c-plate} = (1 \pm K_W)\left((V_{dat})_{c-plate} - (V_{dat})_c\right) \qquad 4.27$$

where K_W is defined in Eq. 4.13 and is negative in sagging regions and positive in hogging regions. For a continuous beam such as in Fig. 4.11 subjected to a uniformly distributed load, K_W has the values in Eqs 4.16 or 4.17. Furthermore, for a portion of the beam where no concentrated loads are acting within the free body of the CDC analysis then $K_W = 0$ as in Eq. 4.14.

It is suggested for design, that the value of the concrete shear capacity of the unplated beam from the national code should be used $(V_c)_{code}$ with the increase in the shear capacity due to plating $\Delta V_{c\text{-}plate}$ in Eq. 4.27. Hence the concrete shear capacity of the plated section is given by

$$V_{c-plate} = (V_c)_{code} + \Delta V_{c-plate} \qquad 4.28$$

which is also the shear load to cause crack sliding and, hence, CDC debonding in a plated beam. This will help overcome the probability that there may be slight differences between the national code values for $(V_c)_{code}$ and those calculated using the CDC analysis V_c.

4.4.2.2 CDC design procedure in anchorage approach

The anchorage approach is in many ways more straightforward than the hinge approach, as described in Section 4.4.2.1, because the anchorage approach requires the plate end to be fully anchored in an uncracked region as shown in the left hogging region in Fig. 4.17(b) and in Fig. 4.19(a). This requirement, of anchoring the plate in an uncracked region, would suggest that the plate is terminated at least up to the point of contraflexure if not beyond.

For the anchorage approach, the design steps for the hinge approach simplifies to the following.

1. The beam is fully plated and the plate fully anchored along the region A-E in Fig. 4.19(a) so that the plate extends an anchorage length L_e to point F.
2. From a CDC analysis, Section 4.4.1, determine the shear force $(V_{dat})_{c\text{-}plate}$ at the datum point to cause crack sliding.
3. If the shear force at the datum point $(V_{dat})_{c\text{-}plate}$ required for crack sliding exceeds the applied shear force at the datum point $(V_{dat})_{applied}$, then the plated structure is strong enough. Otherwise, the design load cannot be achieved and some other plating arrangement or system may need to be considered.

4. Determine the increase in the shear capacity due to plating from a CDC analysis of the unplated beam to give the lines $(V_{dat})_{cr}$ and $(V_{dat})_u$ in Fig. 4.19(b) and $(V_{dat})_c$ at point L in Fig. 4.19(b). Hence $\Delta V_{c\text{-}plate}$, the increase in the concrete shear capacity due to plating, can be obtained from Eq. 4.27 and the overall shear strength from Eq. 4.28.
5. It may be necessary to check for plate end debonding at F in Fig. 4.19(a) as described in Section 1.3.3 and quantified in Chapter 6.
6. It may be necessary to check that CDC debonding does not occur in the sagging region such as the diagonal crack J-G in Fig. 4.19(a) and this can be determined from a CDC analysis of the sagging region. This is unlikely to be a problem for the hogging plate in Fig. 4.17(b), as the shear at the plate end diminishes as the plate is extended into the sagging region. However it may be a problem in extending the tension face plate in the sagging region in Fig. 4.17(b) into the hogging region, as the vertical shear force at the plate end increases as the plate is extended; so that it may not be possible to find a region that is uncracked in both shear and flexure, that is it may not be possible to prevent the cracking shown in Figs 1.38 and 1.39.

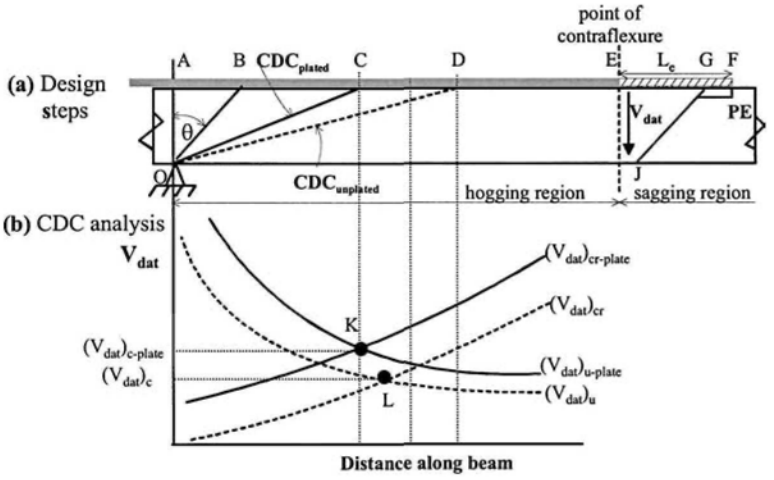

Figure 4.19 CDC design procedure using anchorage approach

4.5 Direct CDC debonding analysis

The critical diagonal crack analysis technique described in Section 4.4 is a highly adaptable iterative procedure suitable for spreadsheet analyses; it can cope with a wide variety of structures, applied loads, beam restraints, plating configurations and extent of plating. However, although easy to apply using spread sheets, it is iterative.

The direct approaches described in this section tend to be less accurate. Furthermore because they do not predict the position of the CDC, the whole region, that is the hogging region or the sagging region has to be fully plated as well as being fully anchored by an effective length L_e as in Fig. 4.20. However as they are direct approaches, they may be more suitable for design, particularly for the early stages. A comparison is also made of the CDC approaches in the guidelines in Table 1.1.

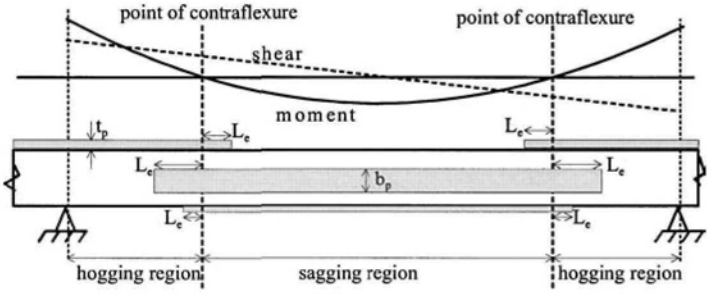

Figure 4.20 Extent of plating for direct approaches

4.5.1 Mean approach

4.5.1.1 Development of mean approach procedure

A relatively simple and conservative approach (Farrant et al 2002) for directly determining the shear capacity can be deduced from the typical shapes of the curves derived in the CDC analyses such as those in Figs 4.16(b) and (c) and 4.21(b). The shear load at the datum point required to cause cracking $(V_{dat})_{cr\text{-}plate}$ is at its lowest when the crack is vertical, that is $\theta = 0$ in Fig. 4.21(a); simply because this represents a flexural crack which commonly occurs at low applied loads. As the inclination θ of the crack increases, the crack gets longer and is less influenced by flexure so that the shear required to induce the crack increases, giving the typical increasing path with x for $(V_{dat})_{cr\text{-}plate}$ in Fig. 4.21(a). In contrast, the shear load to cause failure or crack sliding after cracking $(V_{dat})_{u\text{-}pres/metal}$ in Fig. 4.21(b) has its maximum value when the crack is vertical because the passive interface forces acting across the crack as shown in Figs 4.2 and 4.3, induced by the plate and the longitudinal reinforcing bars, act perpendicular to the crack face and so have their greatest effect. As the angle θ of the crack face increases as in Fig. 4.21(a), the passive interface forces become inclined to the face and become less effective as well as the dowel force shown in Figs 4.2 and 4.3 which will have less resistance from the surrounding concrete due to the inclination of the surface. Hence as the angle of the diagonal crack θ increases, we get the typical reducing path with x for $(V_{dat})_{u\text{-}pres/metal}$ in Fig. 4.21(a). Where these paths cross at point C in Fig. 4.21 is the capacity of the critical diagonal crack.

On either side of point C in Fig. 4.21(b), where the critical diagonal crack occurs, one of the shear capacity components, $(V_{dat})_{cr\text{-}plate}$ or $(V_{dat})_{u\text{-}pres/metal}$, will always overestimate and the other shear capacity will always underestimate the capacity of the CDC at point C. Hence it may be expected that the mean of $(V_{dat})_{cr\text{-}plate}$ and $(V_{dat})_{u\text{-}pres/metal}$ shown as $(V_{dat})_{mean}$ in Fig. 4.21 will approximate the CDC capacity. An extensive parametric study (Farrant et al 2002) of the shape of the mean curve $(V_{dat})_{mean}$ in Fig. 4.21(b) showed that it had the consistent and typical shape shown. There was always a region B-C where the mean value slightly underestimated the strength and the position of this region was always between the focal point and the position of the critical diagonal crack at C and always adjacent to the position of the critical diagonal crack as needs be as $(V_{dat})_{mean}$ will always pass through the position of the critical diagonal crack by definition of this crack.

If an inclination θ of a critical diagonal crack can be found that always lies within the conservative zone B-C in Fig. 4.21(b), that is within the range θ_{min} and θ_{max} in Fig. 4.21(a), then this could be used to provide a direct solution to the iterative procedure described in Section 4.4. An example of a part of an extensive parametric

study (Farrant et al 2002) to determine the range θ_{min} and θ_{max} is shown in Fig. 4.22; the position of a concentrated load L_O was varied in a shear span, such as in the free body depicted in the shear span B-C in Fig. 4.11 but with the datum point at the point of contraflexure, and the beam was analysed as fully plated and fully anchored.

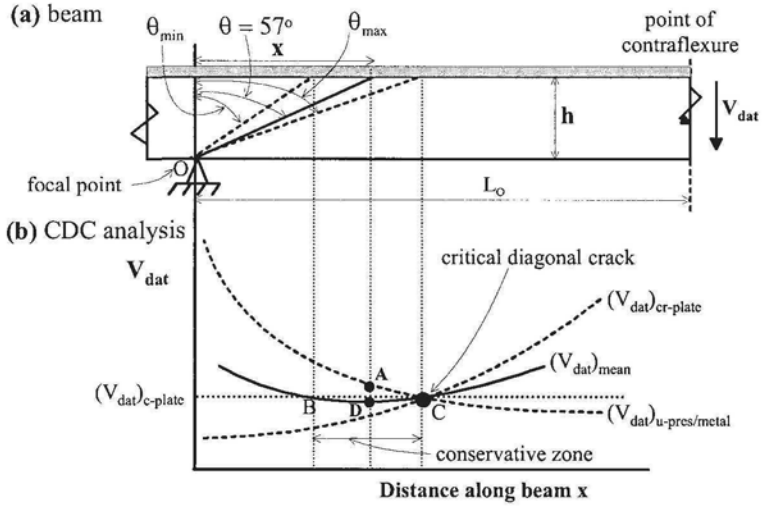

Figure 4.21 CDC debonding analysis – mean approach

In Fig. 4.22, the vertical distance between the lines marked *maximum angle* (θ_{max} in Fig. 4.21(a)) and *minimum angle* (θ_{min}) represents the conservative or safe zone B-C in Fig. 4.21. It can be seen in Fig. 4.22 that as L_O/h increases both θ_{max} and θ_{min} increase. However, the crack inclination from 56° to 57° always falls within θ_{max} and θ_{min}. From further parametric studies, the angle $\theta = 57°$ was chosen as an angle of a critical diagonal crack that would always give a conservative estimate of the strength of the critical diagonal crack. This is shown in Fig. 4.21(a) as the diagonal crack at $\theta = 57°$. This position of crack will have a capacity shown as point *A* in Fig. 4.21(b) which is greater than the strength of the critical diagonal crack at *C* but the *mean strength* is given by point *D* which is smaller than the strength of the CDC. This relationship between the strengths at points A, D and C needs to be emphasised. The critical diagonal crack at $\theta_{mean} = 57°$ given in the following equation, is chosen because the *mean strength* is conservative. Hence for the *mean approach*, a conservative estimate of the shear capacity is given by

$$\tan\theta_{mean} = \frac{x}{h} = 1.54 \qquad 4.29$$

It is also worth noting in Fig. 4.22, that the line marked *maximum angle* (θ_{max}) gives the position of the critical diagonal crack that is point C in Fig. 4.21 which also governs the extent of plating. This position is much more difficult to define and, hence, this *mean approach* procedure should be restricted to regions of the beam that are fully plated and fully anchored; that is the hogging region or sagging region must have a plate covering its full length and extended beyond the points of contraflexure

by at least the effective length L_e which is similar to the requirement of the anchorage approach in Section 4.4.2.2.

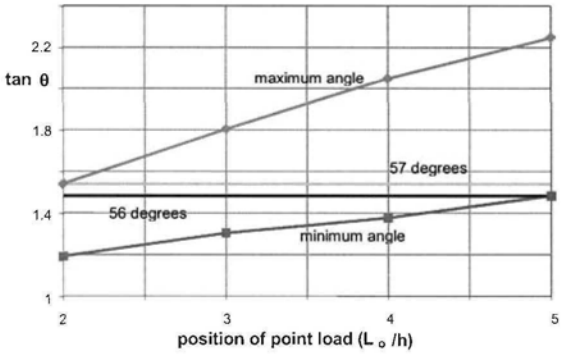

Figure 4.22 Determining conservative design region

4.5.1.2 Mean approach analysis

As the angle of inclination of the critical diagonal crack has now been defined by Eq. 4.29, the equations in the iterative approach in Section 4.4 can be used directly.

The shear load at the datum point to cause cracking $(V_{dat})_{cr\text{-}plate}$ are given in Eqs 4.18 and 4.19 for the sagging and hogging regions. In these equations, the following parameter, which controls the inclination of the crack, can be simplified as shown using Eq. 4.29.

$$\left(x^2 + h^2\right) = 3.37h^2 \quad \text{(for use in Eqs 4.18 and 4.19)} \tag{4.30}$$

The shear load at the datum point to cause crack sliding or failure is given in Eqs 4.21 and 4.22 for the *longitudinal reinforcement* approach $(V_{dat})_{u\text{-}metal}$, and in Eqs 4.24 and 4.25 for the *passive prestress* approach $(V_{dat})_{u\text{-}pres}$. The following parameter that controls the crack inclination can be simplified as shown by substituting Eq. 4.29.

$$\sqrt{1+\left(\frac{x}{h}\right)^2} - \frac{x}{h} = 0.296 \quad \text{(for use in Eqs 4.21, 4.22, 4.24 and 4.25)} \tag{4.31}$$

The *mean strength* at $\theta_{mean} = 57^\circ$ is given by

$$\left(V_{dat}\right)_{c-plate-mean} = \frac{\left(V_{dat}\right)_{cr-plate} + \left(V_{dat}\right)_{u-pres/metal}}{2} \tag{4.32}$$

where $(V_{dat})_{cr\text{-}plate}$ can be determined from Eq. 4.30 and $(V_{dat})_{u\text{-}pres/metal}$ can be determined from Eq. 4.31. The subscript *pres/metal* in Eq. 4.32 simply refers to the fact that the designer can choose either Eqs 4.21 and 4.22 where the *longitudinal reinforcement approach* is used, or Eqs 4.24 and 4.25 where the *passive prestress approach* is used.

To achieve consistency in the notation, Eq. 4.27 becomes

$$\Delta V_{c-plate} = \left(1 \pm K_w\right)\left(\left(V_{dat}\right)_{c-plate-mean} - \left(V_{dat}\right)_{c-mean}\right) \tag{4.33}$$

where $\Delta V_{c\text{-}plate}$ is the increase in the shear capacity or resistance to sliding due to plating; $(V_{dat})_{c\text{-}plate\text{-}mean}$ is the shear load at the datum point to cause failure or crack sliding in the plated beam given by Eq. 4.32; $(V_{dat})_{c\text{-}mean}$ is the shear load at the datum point to cause failure or crack sliding of the unplated beams that can be derived using the same equations as those used to derive $(V_{dat})_{c\text{-}plate\text{-}mean}$ but with the plate thickness equal to zero; and the coefficient K_W has been defined in Eqs 4.13 to 4.17 and which is negative in sagging regions and positive in hogging regions. It may also be worth noting that K_W, and hence e, should also be derived using Eq. 4.29.

4.5.2 Prestressed code approach

National concrete codes prescribe methods of determining the shear capacity of prestressed concrete beams by incorporating the stress due to prestressing into the shear strength equation which lends itself well to the passive prestress approach. Unlike the crack sliding model, code approaches generally do not require iteration to solve for the shear capacity but, unfortunately, are unable to predict the position of the CDC requiring the entire hogging or sagging region to be fully plated and anchored as in Fig. 4.20 and which is similar to the anchorage design approach in Section 2.5.1.

Not all national prestress code models are suitable for predicting CDC debonding. As an example, let us compare the ACI (2002) and Eurocode (1992) models for predicting the concrete component of the shear capacity of prestressed beams. These are given in Eqs. 4.34 and 4.35 for the case of a beam or slab with a rectangular cross-section of width b_c and effective depth d.

$$\left(V_{pp}\right)_{ACI} = \left(0.29\sqrt{f_c} + 0.3\sigma_{ps}\right)b_c d \qquad 4.34$$

$$\left(V_{pp}\right)_{Euro} = \left(\tau_{Rd}\left(1.6-d\right)\left(1.2+\frac{40A_{st}}{b_c d}\right)+0.15\sigma_{ps}\right)b_c d \qquad 4.35$$

where the compressive prestress in the concrete due to the prestressing force F_{ps} is $\sigma_{ps} \approx F_{ps}/b_c d$, A_{st} = cross-sectional area of tension reinforcing bars and τ_{Rd} is a basic design shear strength.

The ACI approach of Eq. 4.34 predicts an increase in the shear capacity due to prestress of $0.3\sigma_{ps}b_c d$ which is twice that predicted by the Eurocode approach of Eq. 4.35 of $0.15\sigma_{ps}b_c d$. Hence there would appear to be a very large difference between these two approaches. However, it should be remembered that the ACI approach of Eq. 4.34, as with the ACI rigorous approach based on principal stresses (ACI 2002), is based on predicting the formation of a critical diagonal crack in a prestressed beam and is not suitable, or cannot be used, for predicting the shear capacity of unprestressed beams. In contrast, the Eurocode approach of Eq. 4.35 is applicable to both prestressed and unprestressed beams and is based on the shear capacity of the critical diagonal crack. As the increase in the shear capacity due to the passive prestress approach is mainly based on the increase in the shear resistance to crack sliding, that is on the shear capacity after the CDC has formed, the Eurocode approach can only be adapted for the passive prestress approach, that is, only nation standard models that predict the concrete component of the shear capacity of both prestressed and unprestressed beams can be adapted for the passive prestress approach.

It needs to be stressed that there is nothing wrong with the conceptual approaches of the ACI. It would appear that the ACI is recognising the fact that for

prestressed beams the shear load to cause cracking V_{cr}, as represented by Eqs 4.18 and 4.19, is generally greater than the shear load to cause crack sliding after the crack has formed V_u, as represented by Eqs 4.21 and 4.22, and, hence, the importance of determining when diagonal cracks occur in prestressed beams. In contrast, the *Eurocode approach* (1992) is primarily based on the capacity after the critical diagonal crack has formed V_u, as represented by Eqs 4.21 and 4.22.

From Eq. 4.35, the increase in the shear capacity due to prestress is $0.15\sigma_{ps}b_cd \approx 0.15F_{ps}$. Hence, it can be assumed that the increase in the shear capacity due to the passive prestress P_{plate} is $0.15P_{plate}$, that is 15% of P_{plate}. A comparison of this 15% theoretical increase with tests on tension face and side plated beams (Oehlers et al 2004b) gave very good correlation. It is also worth noting that a parametric comparison of the increase in the shear capacity based on the Eurocode approach of Eq. 4.35 with $0.15P_{plate}$ with that of Zhang's adapted approach in Eq. 4.23 can show that the coefficient shown as 4 in Eq. 4.23 can vary from about 4.2 to 5.6. Hence there is also good correlation between the indirect crack sliding approach of Eq. 4.23 and the direct code approach of Eq. 4.35. A lower bound of 4 was used for the coefficient in Eq. 4.23, as this was 10% less than that determined from tests. It is suggested that a lower bound of 0.13 should be used for the coefficient in Eq. 4.35. Hence the increase in the shear capacity due to passive prestress is given by

$$(V_{incr})_{pp} = 0.13\sum P_{plate} \qquad 4.36$$

that is the increase in the concrete shear capacity is directly proportional to the total maximum axial force in all the plates ΣP_{plate} which for each individual plate is the lesser of the yield capacity of metal plates A_pf_{yp}, the fracture capacity of FRP plates A_pf_{FRP}, and the IC debonding resistance $(P_{IC})_{max}$ when fully anchored. The latter should be based on the IC debonding resistance in pull tests, as given by Eq. 2.1 and the α coefficients in Table 2.1. This is because a pull-test represents a plate with one intermediate crack which is equivalent to a single diagonal crack intercepting a plate. It is felt that for T and L-beams, P_{plate} should be only derived from those plates adhesively bonded close to the web of the beam.

4.5.3 Comparison with guidelines

In the European guidelines in Table 1.1, Blaschko (1997) in a seminar paper suggested that peeling off at shear cracks may be prevented by limiting the shear force to the shear resistance of RC members without shear reinforcement V_c, with the following modification of the shear capacity by treating the FRP as additional reinforcing bars.

$$\rho_{eq} = \frac{A_{sl} + A_p\dfrac{E_p}{E_s}}{b_c d} \qquad 4.37$$

where ρ_{eq} is an equivalent area of longitudinal reinforcing bars.

It can be seen in Eq. 4.37 that the cross-sectional area of plate has been transformed into an equivalent steel area of longitudinal reinforcement of the same axial stiffness but not axial strength. Hence unlike Eqs 4.20 and 4.23 which depend on the bond strength of the plate, Eq. 4.37 does not consider the maximum axial force

that the plate can resist. It should be used with care as by not recognising the IC debonding resistance of the plate, Eq. 4.37 does encourage the use of thick plates which it is felt might debond prematurely. As has been pointed out in Section 2.3.1.3 and Fig. 2.16, the bond or anchorage behaviour of externally bonded plates is totally different from that of the internal reinforcing bars encased in concrete. Hence, converting externally bonded FRP plates, that have a brittle bond characteristic and a brittle material characteristic, to embedded steel reinforcing bars, that have a ductile bond and ductile material characteristic, should be used with care.

Also in the European guidelines in Table 1.1, Jansze (1997) in his PhD thesis also computes an effective shear resistance of the beam V_c which does not appear to depend on the cross-section of the FRP plate but on the extent of plating and which suggests that if the plate is terminated at a support then the shear capacity is infinite. However, terminating a plate at a support as shown in Figs 1.19, 1.38 and 1.39 does not prevent shear failure nor debonding. As can be deduced from Section 4.4, plating does inhibit but does not prevent the formation of critical diagonal cracks within the plated region which depends on the properties of the plates such as their axial strengths.

In the Hong Kong approach in Table 1.1, Smith and Teng (2001) restrict the vertical shear to $1.4V_c$ which is reasonable as the addition of longitudinal plates can easily increase the concrete component of the shear capacity by 40%, as will be illustrated in Section 5.5.1, but it is felt that this is more of a rule of thumb guidance.

4.6 Results of CDC analyses

The following results were from an iterative CDC analysis as described in Section 4.4.1 and which used the hinge approach described in Section 4.4.2.1. Full and comprehensive worked examples are given in Chapter 7.

4.6.1 Hinge approach with FRP plates in hogging region of beam

The reinforced concrete beam in Section 3.5.2.1 and Fig. 3.41 has already been strengthened in the hogging region with a 1.2 mm thick carbon FRP tension face plate that is 600 mm wide. The plate increased the flexural capacity from 339 kNm to 450 kNm. The plate has been designed using the hinge approach, Section 2.5.2 and 4.4.2.1, so that it can be terminated short of the point of contraflexure. To maintain an elastic moment distribution, the sagging region of the beam must also be strengthened to increase the moment capacity from 173 kNm to 225 kNm. Hence, the new total static moment that is to be resisted is 675 kNm which equates to a 30% increase in the total applied load from 41 kN/m to 54 kN/m. The corresponding maximum shear force at the supports is 270 kN. The shear and moment distributions for the beam are shown in Fig. 4.23. As $V = 270$ kN is greater than $V_c = 134$ kN in the hogging region, calculated using the Australian concrete code AS3600, a CDC will occur in the unplated beam and hence, the plate is also required to increase the concrete component of the shear capacity V_c. The questions are: where to terminate the plate so that the critical diagonal crack falls within the plated region; and whether the increase in the concrete component of the shear capacity is sufficient to prevent CDC debonding within the hogging region.

For the elastic moment distribution shown in Fig. 4.23 the point of contraflexure is located 2113 mm from the support. Normally, the point of contraflexure is a convenient position to use as the datum point as the moment is zero.

However, to illustrate the use of the K_M factor in Eq. 4.12 the datum point will be taken at L_O = 1500 mm from the support as shown in Fig. 4.23 where it can be seen that V_{dat} = 270 – 54(1.5) = 189 kN and M_{dat} = 450 – 0.5(270+189)(1.5) = 106 kNm. Furthermore, there may not always be a point of contraflexure where the moment is zero as in vehicular bridges where there is an envelope of stress resultants. From Eq. 4.12, $K_M = 106x10^6/189x10^3$ = 561 mm and for a shear span in the hogging region subjected to a udl, $K_W = 2(1500 - x)/5774 = (0.52 - 0.346x10^{-3}x)$ from Eq. 4.17. The next step in the CDC design follows the procedure in Section 4.4.2.1 for the hinge approach where the load to cause cracking is given by Eq. 4.19 and the load to cause crack sliding by Eq. 4.25 using the *passive prestress approach* as we are using an FRP plate in this example.

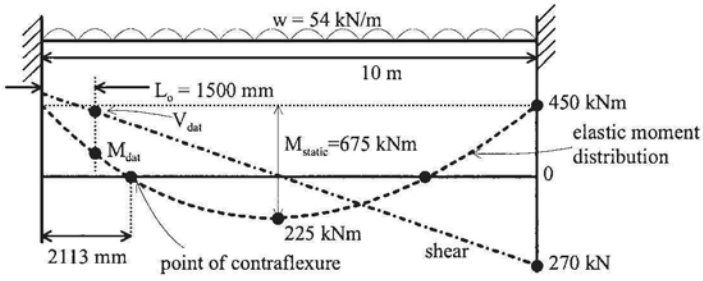

Figure 4.23 Shear and moment distributions for hogging analysis

The procedure begins by assuming that the beam is fully plated along the hogging region, that is the plate extends at least the effective length L_e (Eq. 2.3) beyond the root of any diagonal crack so that the maximum plate force P_{plate} can be assumed to be constant along the region and given by the IC debonding resistance. From Eq. 2.1 P_{plate} = 294 kN using α = 0.427 from Table 2.1 which is the mean debonding coefficient from pull tests, the same material properties as given in Section 3.5.2.1, and b_p/b_c = 0.3 but based on the suggested limit described in Section 2.4.3 was taken as 0.33. Using a spreadsheet analysis, the solid curves in Fig. 4.24 are produced for the fully plated beam where it can be seen that the critical diagonal crack in the plated region of beam intersects the tension face 1235 mm from the focal point (that is the support in this example) at a shear force $(V_{dat})_{c\text{-}plate}$ = 133 kN at the datum point. Hence, the *minimum* extent of plate required is 1235 mm plus L_e = 187 mm (Eq. 2.3) to achieve the maximum IC debonding resistance and an additional h/2 = 250 mm is recommended considering shear cracks are not linear as idealized in the analysis giving a total length of plate of 1672 mm measured from the internal support. Unfortunately in this example, $(V_{dat})_{c\text{-}plate}$ = 133 kN is less than V_{dat} = 189 kN due to the applied loads and hence CDC debonding would occur prior to achieving the increased applied load of 54 kN/m. To increase the CDC debonding resistance, an alternative plating arrangement could be investigated or the plates could be bolted.

Even though this plating arrangement did not work, the increase in the concrete component of the shear capacity after plating can be determined using Eq. 4.27 where K_W is taken as positive in the hogging region to give $\Delta V_{c\text{-}plate}$ = 28.4 kN. In Eq. 4.27, the shear force at the datum point to cause the CDC in the unplated beam $(V_{dat})_c$ = 107 kN and is given by the intersection point of the dashed lines shown in Fig. 4.24, which were calculated using Eqs 4.19 and 4.25 with t_{tfp} = 0. As $(V_c)_{code}$ = 134 kN for the hogging region as given previously, the concrete component of the

shear capacity of the plated beam is determined using Eq. 4.28 to give $V_{c\text{-plate}}$ = 162.4 kN, a 21% increase from the unplated beam strength.

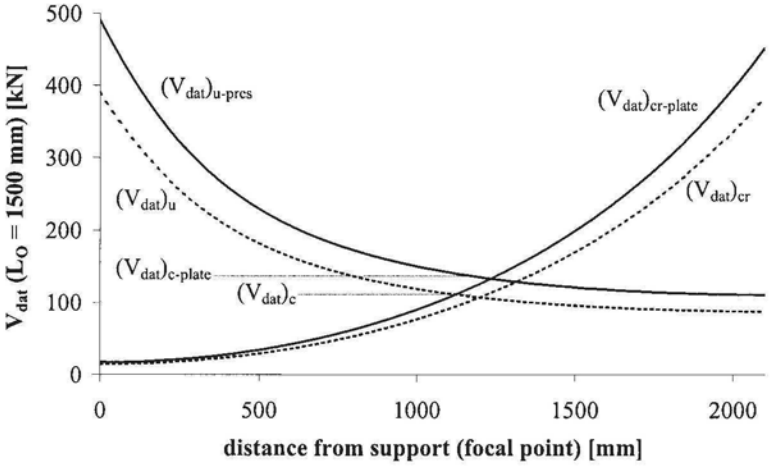

Figure 4.24 CDC analysis of FRP tension face plated beam in the hogging region

For comparison, the *simplified mean approach* described in Section 4.5.1 is also used to predict the increase in the concrete component of the shear capacity after plating. Using the simplifications given by Eqs 4.29-4.31 for an assumed crack inclination of 57°, Eq. 4.19 was used to calculate $(V_{dat})_{cr\text{-}plate}$ = 58.8 kN and Eq. 4.25 to calculate $(V_{dat})_{u\text{-}pres}$ = 176.2 kN so that from Eq. 4.32 $(V_{dat})_{c\text{-}plate\text{-}mean}$ = 117.5 kN. Using the same procedure but taking t_{fp} = 0, $(V_{dat})_{c\text{-}mean}$ = 95 kN for the unplated beam so that from Eq. 4.33 the increase in the concrete component of the shear capacity using the mean approach is $\Delta V_{c\text{-}plate}$ = 28.2 kN. In this example, the increase is only slightly less than that obtained using the rigorous iterative CDC analysis described above.

The increase in the concrete component of the shear capacity can also be determined using the *prestress code approach* described in Section 4.5.2 where the increase in shear capacity due to passive prestress is simply given by Eq. 4.36 so that $(V_{incr})_{pp}$ = 38.2 kN.

4.6.2 Anchorage approach with steel plates in sagging region of slab

The reinforced concrete slab shown in Fig. 3.38, with the specifications in Section 3.5.1.1, has been strengthened in the sagging region with 3 mm thick steel tension face plates of width 140 mm per meter width of slab. The plate increased the flexural capacity from 31 kNm/m to 47 kNm/m width of slab as shown in Fig. 4.25. The steps in the flexural analyses are given in Section 3.5.1.4 (for *unpropped* construction) and the complete analysis for the slab in Chapter 7. To summarise briefly, the 22% increase in the sagging flexural capacity is required to accommodate the maximum 30% moment redistribution from the hogging region. Consequently, the increase in applied load from 23 kN/m/m to 28 kN/m/m in Fig. 4.25 has increased the maximum shear force at the supports from 57.5 kN/m to 70 kN/m. The final shear and moment diagrams shown in Fig. 3.39 are repeated in Fig. 4.25. The plates are fully anchored beyond the points of contraflexure using the anchorage approach, Section 2.5.1 and

4.4.2.2, and it is now a question of determining whether the increase in the shear capacity is sufficient to prevent CDC debonding within the sagging region.

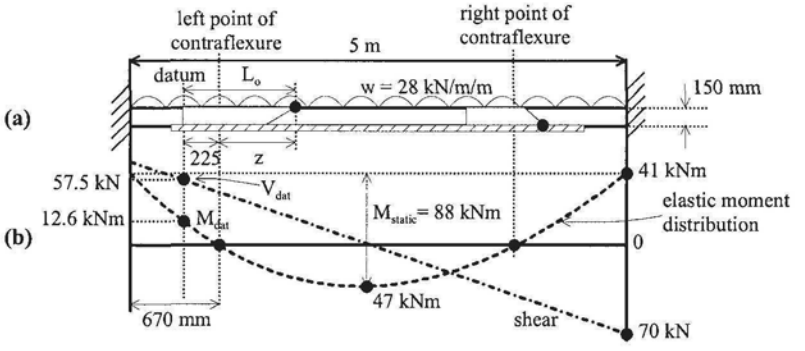

Figure 4.25 Shear and moment distributions for sagging analysis

As the absolute maximum shear force V = 70 kN/m is much less than the code concrete shear capacity 108 kN/m in the sagging region, a critical diagonal crack will *not* occur in the plated section. Hence, a CDC debonding analysis is obviously not necessary. However to illustrate the CDC debonding analysis, the example is continued to quantify the increase in V_c due to the addition of the plate. For the redistributed moment distribution in Fig. 4.25, the point of contraflexure is located 670 mm from the support as shown. In the following analyses, we will determine the shear capacity in the sagging region adjacent to the point of contraflexure. We will only consider focal points on the compression face of the sagging region as shown adjacent to the left point of contraflexure in Fig. 4.25(a). To complete the analyses, focal points in the hogging region as shown on the right point of contraflexure may have to be considered as these critical diagonal cracks may extend into the sagging region.

As discussed in Section 4.4.1.1, the position of the focal point, on the left hand side of Fig. 4.25(a), is not as clearly defined for sagging regions of beams with uniformly distributed loads as for concentrated loads. It would be expected to lie in the vicinity of the point of contraflexure where the applied shear is near its maximum but its exact position will have to be determined by trial and error. As it is theoretically possible for the CDC to pass through the point of contraflexure, it may be more convenient to choose a free body with a datum in the hogging region as shown adjacent to the left point of contraflexure in Fig. 4.25(a).

Examples of free bodies for use in the CDC analyses are shown Fig. 4.26. In Fig. 4.26(a), the focal point is at the point of contraflexure and the diagonal crack which is in the hogging region crosses both the top and bottom longitudinal reinforcing bars. It may be worth noting that Zhang's crack sliding approach in Section 4.3.3 and the indirect crack sliding CDC analyses described in Section 4.4 do not require the designer to distinguish between tension reinforcing bars and compression reinforcing bars as the cross-sectional area of the reinforcing bars A_s in Eq. 4.8 consists of all the fully anchored bars. Hence, there is not a sudden step change in the strength when moving from the sagging region to the hogging region. It will also be shown in Chapter 5, that compression, side and tension face plates can also be treated in the same way and all add to the shear capacity; this further

emphasises the versatility of this crack sliding approach. Figure 4.26(b) shows an example of a critical diagonal crack crossing the point of contraflexure and, hence, the reason for the datum being away from the point of contraflexure, and Fig. 4.26(c), shows an example of a CDC within the sagging region.

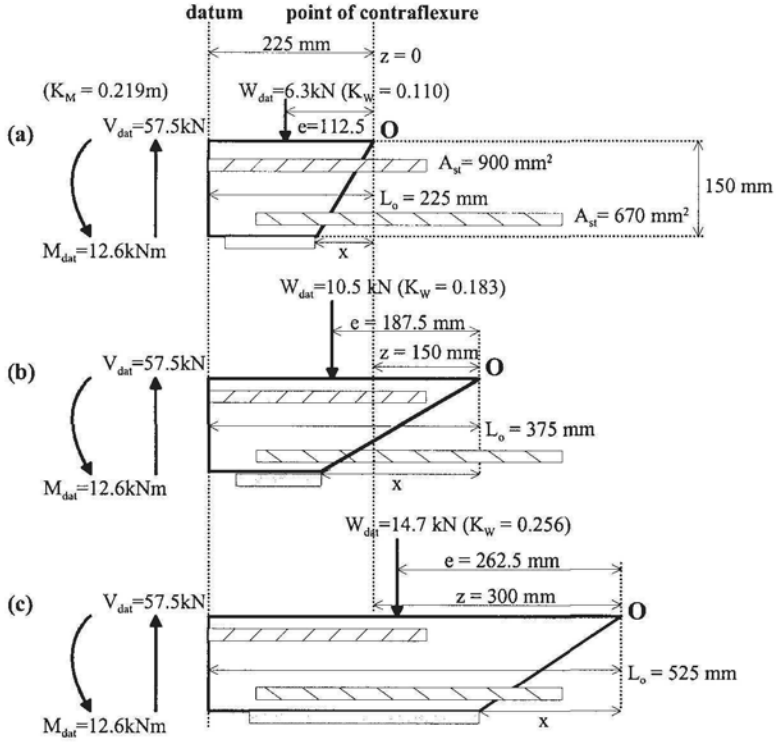

Figure 4.26 Free body diagrams for CDCs near point of contraflexure

The stress resultants at the datum in Fig. 4.26 are constant and hence K_M from Eq. 4.12 is fixed at 0.219 m as shown. However, the resultant force on the free body due to the uniformly distributed load varies as shown giving the variation in K_W from Eq. 4.13 as shown. From a comparison of the stress resultants in Fig. 4.26 with those in Fig. 4.12, it can be seen that the only difference is the direction of M_{dat} so that K_M in Eq. 4.18 changes from $+K_M$ to $-K_M$ as follows

$$\left(\left(V_{dat}\right)_{cr-plate}\right)_{sag} = \frac{\left(\left(x^2+h^2\right)\left(\frac{b_c f_{tef}}{2} + \frac{m_p f_t b_{ifp} t_{ifp}\left(h+0.5t_{ifp}\right)}{h^2}\right)\right) + \left(F_{ps} d_{ps}\right)}{L_O - K_M - K_W e} \qquad 4.38$$

The figure for the shear load to cause crack sliding in Fig. 4.14 remains unchanged so that the crack sliding resistance of Eq. 4.24 with Eq. 4.23 remains unchanged.

The next step in the CDC design follows the procedure in Section 4.4.2.2 for the anchorage approach where the load to cause cracking is given by Eq. 4.38 and the

load to cause crack sliding by Eq. 4.21 using the *longitudinal reinforcement approach*, which can be used in this example only because we are using a metal plate.

As we are using the anchorage approach in this example the slab must be fully plated in the sagging region and fully anchored so that the plate must extent at least the effective length L_e = 330 mm (Eq. 2.3) beyond the point of contraflexure. It is also suggested that the plate be extended an additional h/2 to allow for possible variations in the position of the point of contraflexure due to variations in the applied load so that the *minimum* length of plate required in this example is $L_{sag} + 2L_e + h$ = 4470 mm. If the CDC extends beyond the point of contraflexure into the hogging region as illustrated in Figs 4.26(a) and (b), then the plate must be extended $L_e + h/2$ beyond the end of the CDC. As discussed in Section 2.4.4, the 3 mm thick 300 MPa steel tension face plate will yield prior to IC debonding hence the maximum force in the plate is governed by the yielding giving P_{plate} = 126 kN/m width of slab. Using a spreadsheet analysis, the solid curve representing $(V_{dat})_{c\text{-}plate}$ in Fig. 4.27 is produced for the fully plated beam by equating Eqs 4.38 and 4.21 for increasing z from the point of contraflexure. From Eq. 4.26, the concrete shear capacity of the fully plated beam $V_{c-plate}$ is found where it can be seen that the capacity is greater than maximum applied shear force at the focal point given by $(V_{max})_{Lo}$. Hence, CDC debonding will not occur confirming the original observation.

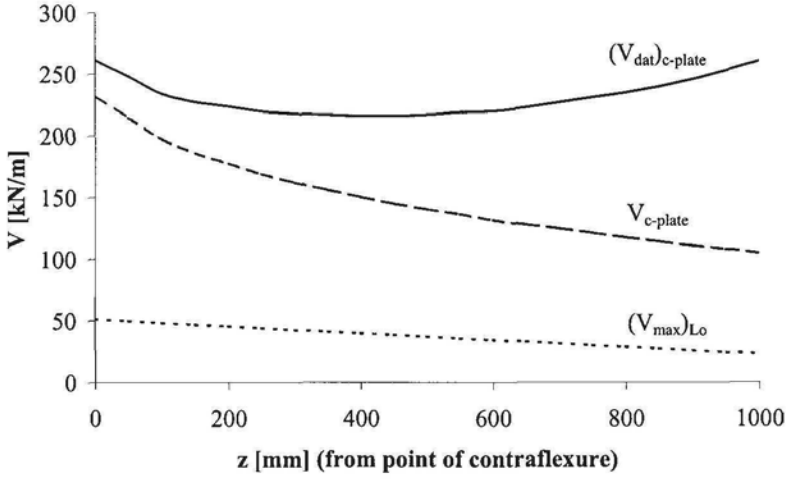

Figure 4.27 CDC analysis of steel tension face plated slab in the sagging region

It is interesting to note that $V_{c\text{-}plate}$ in Fig. 4.27 decreases as the focal point moves from the point of contraflexure to the midspan in the sagging region, that is as *z* increases in Fig. 4.26. This can be explained using the CDC analysis as the shear load to cause cracking, for example $(V_{dat})_{cr}$ in Fig. 4.24, reduces as the moment increases towards the midspan in the sagging region, hence, $(V_{dat})_c$ also reduces.

4.7 References

ACI 440.2R-02 (2002). Emerging Technology Series. "Guide for the Design and Construction of Externally Bonded FRP Systems for Strengthening Concrete Structures". Reported

by ACI Committee 440. American Concrete Institute, Farmington Hills, Michigan, USA.

Bay, B., Nguyen, T., Webster, A., and Wilkins, S. (2003). "Vertical shear strength of FRP plated reinforced concrete beams." 4th year research report, Dept. of Civil and Env., Engng, Adelaide University.

Blaschko, M. (1997), "Strengthening with CFRP". Munchner Massivbau Seminar, TU Munchen.

Eurocode 2: "Design of concrete structures Part 1: General rules and rules for buildings (1992)". BSI Standards.

Farrant, K., Kollevris, V., Modistach, A., and Young, T. (2002) "Study and application of retrofitting techniques." 4th year research project, Dept. of Civil and Environmental engineering, University of Adelaide.

Jansze, W. (1997), "Strengthening of reinforced concrete members in bending by externally bonded steel plates". PhD dissertation, TU Delft, The Netherlands

Oehlers, D.J., Liu, I., and Seracino, R., (2004a) "Passive prestress approach for CDC debonding of adhesively bonded steel and FRP plates." Submitted November 2003.

Oehlers, D.J., Liu, I., and Seracino, R., (2004b) "Prestress code approach for shear deformation debonding of adhesively bonded plates." Provisional acceptance Proceedings Structures and Buildings Journal, November 2003.

Smith, S.T. and Teng, J.G. (2002) "FRP strengthened RC beams – II: assessment of debonding strength models", *Engineering Structures.* 24(4): 397-417, April.

Zhang J.P. (1997) "Diagonal Cracking And Shear Strength Of Reinforced Concrete Beams." *Magazine of Concrete Research.* Vol.49, No.178, Mar., pp 55-65

Chapter 5: Generic Rules for CDC Debonding

5.1 Introduction

The generic design approach for CDC debonding developed in this chapter applies to all plating arrangements and plating combinations, some of which are shown in Fig. 5.1. The plates can be applied to the tension faces as shown at *A* which is probably the most common form of plating. The tension face plate at *B* can be extended into the compression face at *C*, which also inhibits the formation of the critical diagonal crack in this region. Tension face plates can also be positioned at the underside of the flange as at *D*, which encourages the tension reinforcing bars to yield before the plates debond. Plates can be adhesively bonded to the sides of the beam at *E*, which often allows a greater area of plate to be used, particularly on the sagging region of beams where the width of the web may severely restrict the amount of plate that can be bonded. The side plates can be placed at any level along the web, in the tension zone at *F* or in the compression zone at *G* and, wherever they are placed, tests have shown that they can substantially increase the concrete component of the shear capacity. Furthermore, angle or channel sections can be used such as at *H*. Any combination of these plates can be used and any type of material or combinations of materials can be used. All of these plates must be checked for IC debonding as described in Chapters 2 and 3 and for plate end debonding, as will be described in Chapter 6; although plate end debonding is never a problem as PE debonding can always be prevented by terminating the plate at the point of contraflexure.

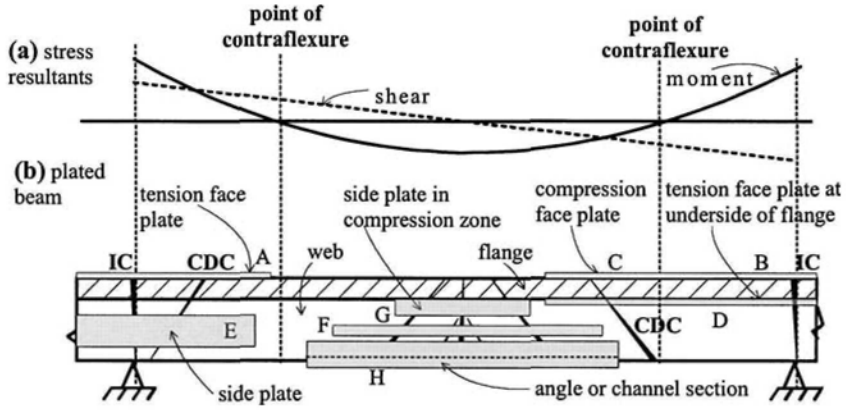

Figure 5.1 Plating arrangements

The design procedure, that has so far been dealt with in preceding chapters in this book, has consisted of first deciding what plates are required for a specific increase in the flexural strength at a section, and this has been based on the IC debonding resistance as described in Chapters 2 and 3. Having chosen the adhesively bonded plating system, the next step was to decide on how far to extend the plate along the beam and to ensure that the plate does not debond prematurely due to CDC debonding; this was covered in Chapter 4, specifically for tension face plates as these are covered in the guidelines in Table 1.1. Hence, the emphasis, so far, has been on

flexural strengthening, although it was shown in Chapter 4 that longitudinal tension face plates can enhance the shear capacity of slabs without stirrups.

In this chapter, we will place more emphasis on the increase in the shear capacity due to plating and, in particular, for all types of longitudinal plating such as the range shown in Fig. 5.1. Generic rules are developed for CDC debonding for all types of longitudinal plates and combinations of longitudinal plates. It will be shown how substantial increases in the shear capacity can be attained through longitudinal plating. Furthermore, the interaction between the shear enhancement due to longitudinal plating and that due to transverse plating, that is externally bonded stirrups, will be described. The generic CDC analysis is first explained in this chapter, this is then incorporated into a generic design procedure that covers both the hinge and anchorage design philosophies, unusual cases are then considered such as compression face plates or short side plates in the vicinity of the ends of tension face plates, followed by examples of the ability to enhance the shear capacity and then some typical analyses. As this generic approach is based on Zhang's work, it can be considered to give a characteristic or lower bound value suitable for design.

5.2 Generic CDC debonding analysis

The fundamental principles behind critical diagonal crack analyses have been explained in Chapter 4 in terms of unplated and tension face plated beams. The governing equations are now given in a generic form that can be applied to all plate materials, plate positions and combinations of plates. To allow this chapter to be self contained some of the equations in Chapter 4 have been repeated. Furthermore, some of the notation used in Chapter 4 will be changed to become more consistent and the terminology will be clarified.

The subscript *dat* will refer to the datum point. The subscript *crack* will refer to the formation of a diagonal crack at a specific position of the beam such as O-A in Fig. 5.2. The term *diagonal crack* will refer to cracks that can spread through the depth of the beam, such as those in Figs. 4.5 and 4.6, across which a rigid body sliding action can take place if their shear capacity is reached; the term diagonal crack does not refer to the flexural-shear cracks in Fig. 4.5. The subscript *slide* will refer to the rigid body displacement or crack sliding across a specific diagonal crack that already exists such as O-A in Fig. 5.2. Hence for beams or slabs without stirrups, the subscript *slide* infers both plate debonding and shear failure at a specific diagonal crack. Whereas for beams or slabs with stirrups, the subscript *slide* will refer to plate debonding only at a specific diagonal crack.

The subscript *crit* will refer to the weakest critical diagonal crack in a region, that is the weakest relative to the distribution of the applied shear. Hence for beams or slabs without stirrups, the subscript *crit* will refer to shear failure and to critical diagonal crack (CDC) plate debonding. However, for beams or slabs with stirrups, the subscript *crit* will refer to CDC debonding. The subscript *conc* will refer to the shear capacity at the weakest or critical diagonal crack, which is equivalent to the concrete shear capacity in unplated beams in national standards which will be referred to as $(V_c)_{code}$. However, the subscript *conc* will be used for both the shear capacity of plated and unplated structures. Where it is necessary to differentiate between plated and unplated structures, then the subscript *pl* will refer to plated and *un* to unplated.

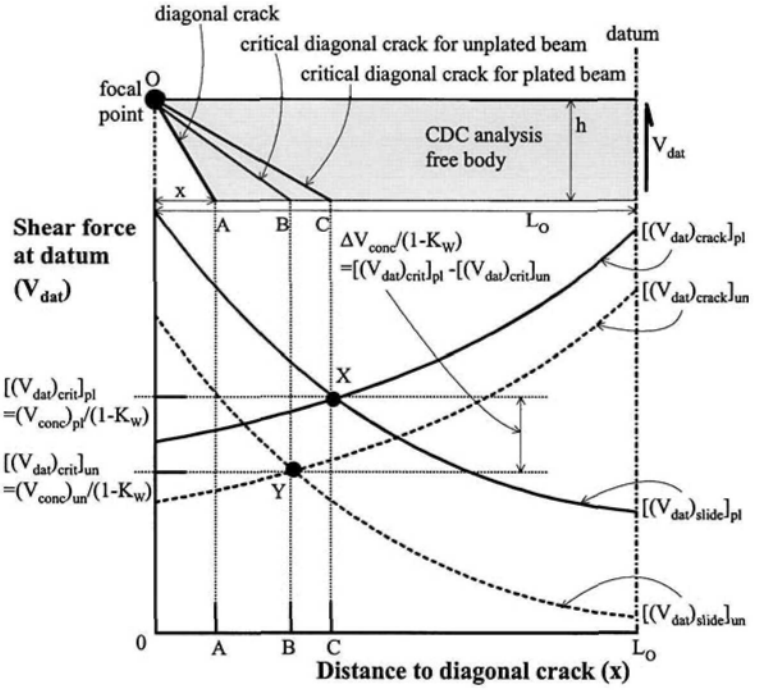

Figure 5.2 CDC analysis, notation and terminology

5.2.1 Iterative approach

Examples of free bodies that can be used in a CDC analysis are shown in Fig. 5.3 for the hogging and sagging regions of part of a span of a continuous beam from a support to the position of maximum moment. In Fig. 5.3(c) are examples of free bodies that are fully encompassed within a hogging region or sagging region, and in Figs 5.3(d) and (e) are examples of free bodies that lie within both regions, that is the free body straddles the point of contraflexure. The *focal points* O in Fig. 5.3 fixes one side of the free body and the *datum* the other side. The focal point must be on a compression face but it can be anywhere on the compression face. It is a question of finding the angle θ of the diagonal crack that emanates from the focal point that has the weakest resistance to the vertical shear forces for that particular position of the focal point. It is then a question of finding the position of the focal point that has the weakest of the weakest resistances to find the critical diagonal crack.

The datum, at a distance L_O from the focal point in Fig. 5.3(c), can be at any position. The beam is subjected to the applied loads shown in Fig. 5.3(b). These applied loads induce the moment M_{dat} and shear force V_{dat} distributions in Fig. 5.3(a). Furthermore, part of the applied load in Fig. 5.3(b), that is shown shaded and referred to as W_{dat}, is acting directly on the free bodies used in the CDC analyses in Fig. 5.3(c). Hence, it can be seen that M_{dat}, W_{dat} and V_{dat} are all related to the distribution of applied loads in Fig. 5.3(b). For analytical convenience, M_{dat} and W_{dat} are written in terms of V_{dat}, that is $M_{dat} = K_M V_{dat}$ in Fig. 5.3(a) and $W_{dat} = K_W V_{dat}$ in Fig. 5.3(b). It is worth bearing in mind that the factors K_M and K_W are not affected by the magnitude of the applied loads but by their distribution, so that if the distribution can be assumed to be constant then K_M and K_W remain constant in the analysis. A free

body in Fig. 5.3(c) is subjected to a shear force V_{dat}, moment $M_{dat} = K_M V_{dat}$ at the datum and the applied loads acting on the free body $W_{dat} = K_W V_{dat}$ as shown in Fig. 5.3(b). The applied load W_{dat} is the load acting on the free body due to dead and live load. For the hogging region it is shown as that part of the total applied load resisted by the length of the beam L_O-x and for the sagging region that part resisted by L_O.

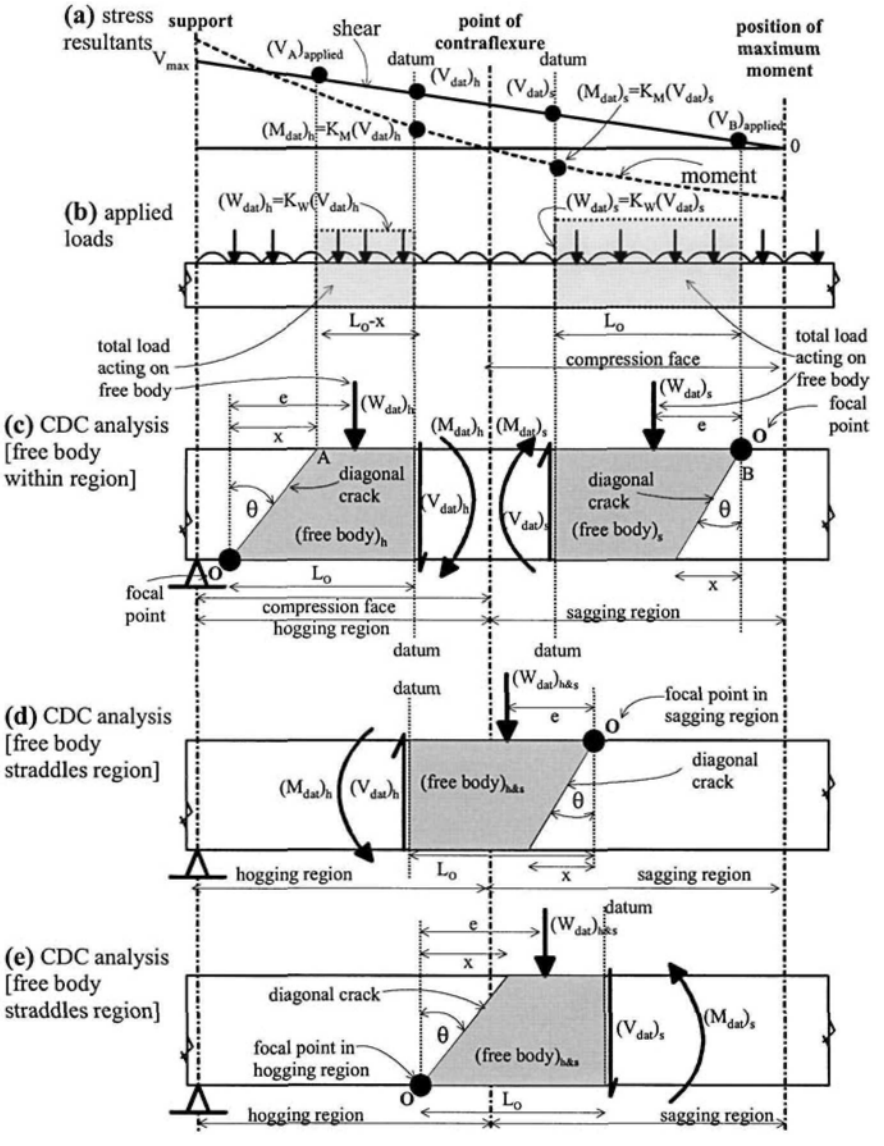

Figure 5.3 CDC analysis free bodies

5.2.1.1 Shear to cause cracking

The free body in the hogging region of Fig. 5.3(c) is shown in Fig. 5.4, and that for the sagging region in Fig. 5.5. For ease of analysis, each rectangular element of plate is considered independently. From rotational equilibrium, the shear load at the datum point V_{dat} to cause a diagonal crack at a position x from the focal point is given by

$$(V_{dat})_{crack} = \frac{\left(\left(x^2 + h^2\right)\left(\frac{b_c f_{tef}}{2} + \frac{f_t \sum\left(m_p A_{rect} L_{rect}\right)}{h^2}\right)\right) + \left(F_{ps} d_{ps}\right)}{L_O \pm K_M \pm K_W e} \qquad 5.1$$

where h is the total depth of the beam or slab; b_c is the width of the slab or the width of the web of a beam; f_{tef} is an effective tensile strength of the concrete; f_t is the actual tensile strength of the concrete which can be taken as $0.4\sqrt{f_c}$ (N and mm) when not measured directly; m_p is the modular ratio of the plate Young's modulus to that of the concrete E_p/E_c; A_{rect} is the area of a rectangular section of the plate; L_{rect} is the lever arm from the centroid of the rectangular section to the compression face, for example, for the tension face plate $A_{rect} = b_{tfp}t_{tfp}$ and $L_{rect} = h+0.5t_{tfp}$; the summation applies to each individual rectangle of plate; F_{ps} is the prestressing force; d_{ps} the lever arm of the prestressing force from the compression face; L_O is the length of the free body; the moment factor K_M is given by the stress resultants at the datum as follows

$$K_M = \frac{M_{dat}}{V_{dat}} \qquad 5.2$$

where K_M is positive when the free body is fully contained within a region as shown in Fig. 5.3(c) and where K_M is negative when the free body straddles a point of contraflexure as shown in Figs 5.3(d) and (e); the load factor K_W is given by

$$K_W = \frac{W_{dat}}{V_{dat}} \qquad 5.3$$

where $K_W e$ in Eq. 5.1 is negative when the focal point is in the sagging region and positive when the focal point is in the hogging region; the effective tensile strength of the concrete is given by the following equation in which the units are N and mm.

$$f_{tef} = 0.156 f_c^{2/3}\left(\frac{h}{100}\right)^{-0.3} \qquad 5.4$$

It can be seen in Figs 5.4 and 5.5 that, for analytical convenience, each rectangular portion of plate is treated individually and this would also apply to channel and angle sections that were adhesively bonded where the webs and flanges would be treated as individual rectangular sections. Because the longitudinal reinforcing bars are assumed not to affect the load to cause cracking, they have been omitted from the figures.

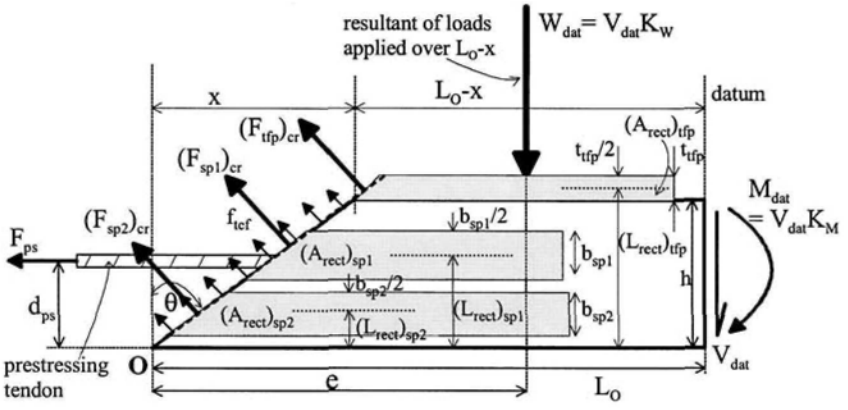

Figure 5.4 Hogging region – shear to cause cracking

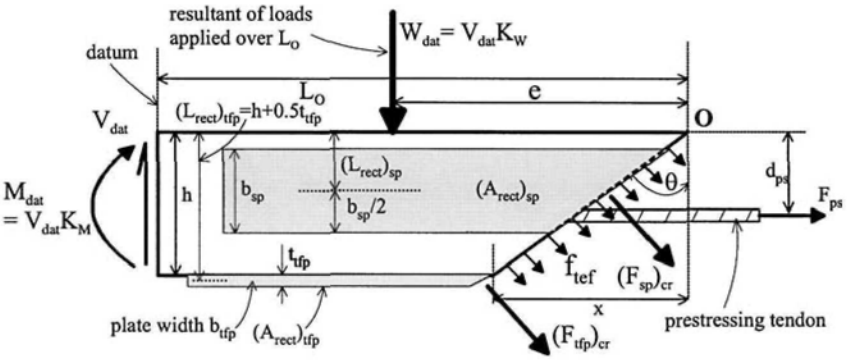

Figure 5.5 Sagging region – shear to cause cracking

5.2.1.2 Shear to cause crack sliding

The hogging region free body in Fig. 5.3(c) is shown in Fig. 5.6 and that for the sagging region in Fig. 5.7. The resistance to shear across the diagonal crack V_{conc} depends on the cross-sectional area of all the longitudinal reinforcing bars crossing the diagonal crack A_s; all the fully anchored longitudinal reinforcing bars at all levels of the beam or slab, are included in A_s. The shear resistance also depends on the sum of all the individual maximum axial forces in the plates P_{plate}. For a metal plate of yield capacity f_{yp}, P_{plate} is limited by $P_y = A_p f_{yp}$ where A_p is the cross-sectional area of the plate $b_p t_p$. For an FRP plate, P_{plate} is limited by its fracture capacity $P_u = A_p f_{FRP}$ where f_{FRP} is the fracture stress of the FRP plate. For both metal and FRP plates, P_{plate} is also limited by the intermediate crack debonding resistance $P_{IC} = A_p \sigma_{IC}$. The IC debonding resistance stress σ_{IC} is given by Eq. 2.1 which depends on the minimum of the anchor lengths on either side of the diagonal crack $(L_p)_{left}$ and $(L_p)_{right}$ in Fig. 5.6 and the effective length L_e as given by Eq. 2.3. For deep plates as in Fig. 5.7, it may be necessary to allow for the variation in the anchorage length from $(L_p)_{min}$ to $(L_p)_{max}$ by simply subdividing the plate width b_{sp} into narrow strips and treating each

individually and with a mean anchorage length as in Fig. 5.6 or just use $(L_p)_{min}$ as a lower bound. The shear capacity also depends on the prestressing force F_{ps}.

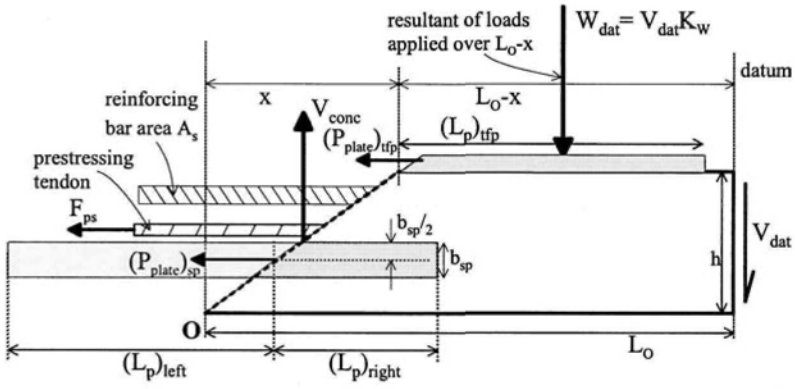

Figure 5.6 Hogging region – shear to cause crack sliding

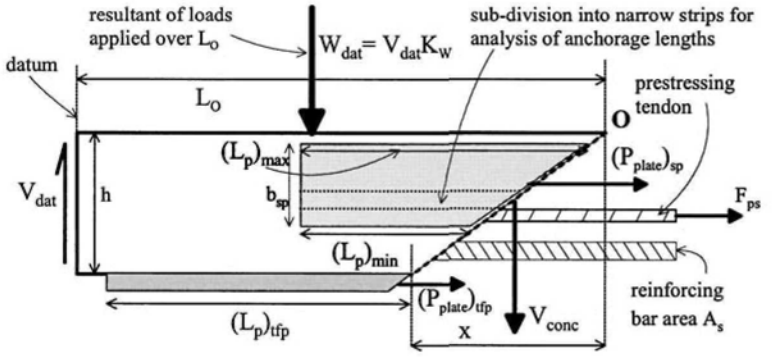

Figure 5.7 Sagging region – shear to cause crack sliding

The shear force at the datum point V_{dat}, in Figs 5.6 and 5.7, to cause crack sliding at a diagonal crack at a distance x from the focal point is given by the following equation which is based on the passive prestress approach described in Section 4.4.1.4; the passive *prestress approach* is used as it is a generic approach that can be applied to both metal and FRP plates as compared to the *longitudinal reinforcement approach* in Section 4.4.1.3 that can only be applied to metal plates.

$$(V_{dat})_{slide} = \frac{0.4 f_c b_c h \left(1 + \dfrac{2F_{ps} + 4\sum P_{plate}}{f_c b_c h}\right)\left(\sqrt{1+\left(\dfrac{x}{h}\right)^2} - \dfrac{x}{h}\right) f_1(f_c) f_2(h) f_3(\rho)}{1 \pm K_W} \qquad 5.5$$

where the summation is for all the axial forces in the plates crossing the diagonal crack and for each plate it is the lesser of P_y, P_u and P_{IC}; the load factor K_W is negative when the focal point is in a sagging region and positive when the focal point is in a

hogging region; and the remaining functions are defined below with the units required when the equation is dimensionally incorrect and also with the range of test data from which they were developed.

$$f_1(f_c) = \frac{3.5}{\sqrt{f_c}} \qquad \text{[N and mm]} \quad 5 < f_c < 60\,MPa \tag{5.6}$$

$$f_2(h) = 0.27\left(1 + \frac{31.6}{\sqrt{h}}\right) \qquad \text{[mm]} \quad 80 < h < 700 \tag{5.7}$$

$$f_3(\rho) = \frac{15A_s}{b_c h} + 0.58 \qquad \frac{A_s}{b_c h} \le 0.045 \tag{5.8}$$

5.2.1.3 Critical diagonal crack

Equation 5.1 can be used to plot the shear load at the datum point V_{dat} to cause the formation of a diagonal crack in the plated beam, which is shown as the line $[(V_{dat})_{crack}]_{pl}$ in Fig. 5.2, for every position x of the diagonal crack. Equation 5.5 can be used to plot the shear load at the datum point to cause crack sliding in the plated beam, $[(V_{dat})_{slide}]_{pl}$ in Fig. 5.2, for every position of the diagonal crack x. The intercept of these two lines at point X gives the shear load at the datum point to cause crack sliding in the critical or weakest diagonal crack $(V_{dat})_{crit}$ which is the shear load at the datum point to cause debonding.

The shear $(V_{dat})_{crit}$ is an indirect measure of the capacity of the plated beam as it is the shear load at the datum point to cause debonding and not the shear load at the critical diagonal crack. If the applied load or design load, such as in Fig. 5.3(b), induces a shear load at the datum point $(V_{dat})_{applied}$ which is greater than the capacity $(V_{dat})_{crit}$ then the plate will debond prior to the design load being reached and vice versa.

An alternative way of interpreting the CDC analysis is to consider the shear at the critical diagonal crack at which crack sliding occurs which is given by the following shear capacity

$$(V_{conc})_{pl} = [(V_{dat})_{crit}]_{pl}(1 \pm K_w) \tag{5.9}$$

where K_W is negative when the focal point is in a sagging region and positive when the focal point is in a hogging region. $(V_{conc})_{pl}$ is the shear capacity at a section through the focal point O in the sagging region in Fig. 5.3(c) shown as point B, or at point A in the hogging region which is through the root of the diagonal crack at the distance x from the focal point. It may be worth noting that the K_W factor in Eq. 5.9 simply allows for the difference in the vertical shear between the datum point, V_{dat} in Fig. 5.3(a) and the critical diagonal crack, $(V_A)_{applied}$ or $(V_B)_{applied}$. The shear capacity at the critical diagonal crack can then be compared with the applied shear at the critical diagonal crack, that is $(V_B)_{applied}$ or $(V_A)_{applied}$ in Fig. 5.3(a) to determine whether premature debonding occurs. A safe design would be to ensure that the applied shear did not exceed this shear capacity throughout the plated region.

It is suggested that a preferred approach is to determine the increase in the sliding resistance due to plating and to add this to the national code value for the concrete shear capacity $(V_c)_{code}$, to determine the shear to cause crack sliding and

hence debonding. This will help tie the design approach directly to the designers national code. If this approach is preferred, then a CDC analysis will have to be performed on the unplated section to give the shear load at the datum point to cause cracking, $[(V_{dat})_{crack}]_{un}$ in Fig. 5.2 and the shear load to cause crack sliding $[(V_{dat})_{slide}]_{un}$. The intercept of these two lines at Y will give shear load at the datum point to form the critical diagonal crack $[(V_{dat})_{crit}]_{un}$. Hence, the shear capacity at the critical diagonal crack is

$$(V_{conc})_{un} = [(V_{dat})_{crit}]_{un}(1 \pm K_w) \qquad 5.10$$

$(V_{conc})_{un}$ in Eq. 5.10 is the concrete shear capacity of the unplated beam which is also given in national codes $(V_c)_{code}$. $(V_{conc})_{un}$ and $(V_c)_{code}$ are bound to differ slightly, as does $(V_c)_{code}$ between codes, which would place the designer in a dilemma in deciding which to use. To overcome this dilemma, it is suggested that the following approach is used. The difference between Eqs 5.9 and 5.10 is the increase in the shear capacity due to plating given by

$$(\Delta V_{conc})_{pl} = \{[(V_{dat})_{crit}]_{pl} - [(V_{dat})_{crit}]_{un}\}(1 \pm K_w) \qquad 5.11$$

which can then be added to the national concrete code strength $(V_c)_{code}$ as follows.

$$(V_{conc})_{code} = (V_c)_{code} + (\Delta V_{conc})_{pl} \qquad 5.12$$

Hence it is suggested that the national code value $(V_c)_{code}$ be used and the CDC analysis procedure is only used to determine the increase in shear due to plating.

5.2.1.4 Simplifications

Examples of free bodies that can be used in CDC analyses are shown in Fig. 5.8 for both a hogging and sagging region. The applied stress resultants are shown in Fig. 5.8(a), the applied loads are in the diagrams with the subscript 1 such as (b_1) and the CDC analyses are in the diagrams with the subscript 2 such as (b_2).

The focal points O always occur on the compression face of the beam or slab. The focal point with the weakest, or critical diagonal crack, often occurs at a concentrated load P that is on the compression face, such as in Figs 5.8(b_2) and (d_2) where the concentrated load is the support reaction and in Fig. 5.8(c_2) where the concentrated load is applied to the beam. As the concentrated loads P in Figs 5.8(b_2), (c_2) and (d_2) are acting at the focal points, they do not contribute to the CDC analysis of Eq. 5.1. Furthermore, they are not included in W_{dat} in Fig. 5.8 in the vertical equilibrium in Eq. 5.5 as they reduce the shear force acting on the free body. By not including these concentrated forces on the free body, we are in effect comparing the shear capacity with the maximum applied shear just to the side of the concentrated load. The reader may wish to both include and not include the concentrated force P on the free body to confirm what has been said. When the region of the beam is subjected to predominantly uniformly distributed loads *w* as in Fig. 5.8(e_1), then the position of the focal point of the CDC in Fig. 5.8(e_1) has to be determined by trial. It is likely that the CDC is close to the point of contraflexure where the shear in the sagging region is at its maximum so that it may be convenient to choose a datum point away from the point of contraflexure as shown in Fig. 5.8(f_2) so that the CDC can pass through the

point of contraflexure. It may also be necessary to check for possible critical diagonal cracks with focal points in the hogging region as shown in Fig. 5.8(f_2)*.

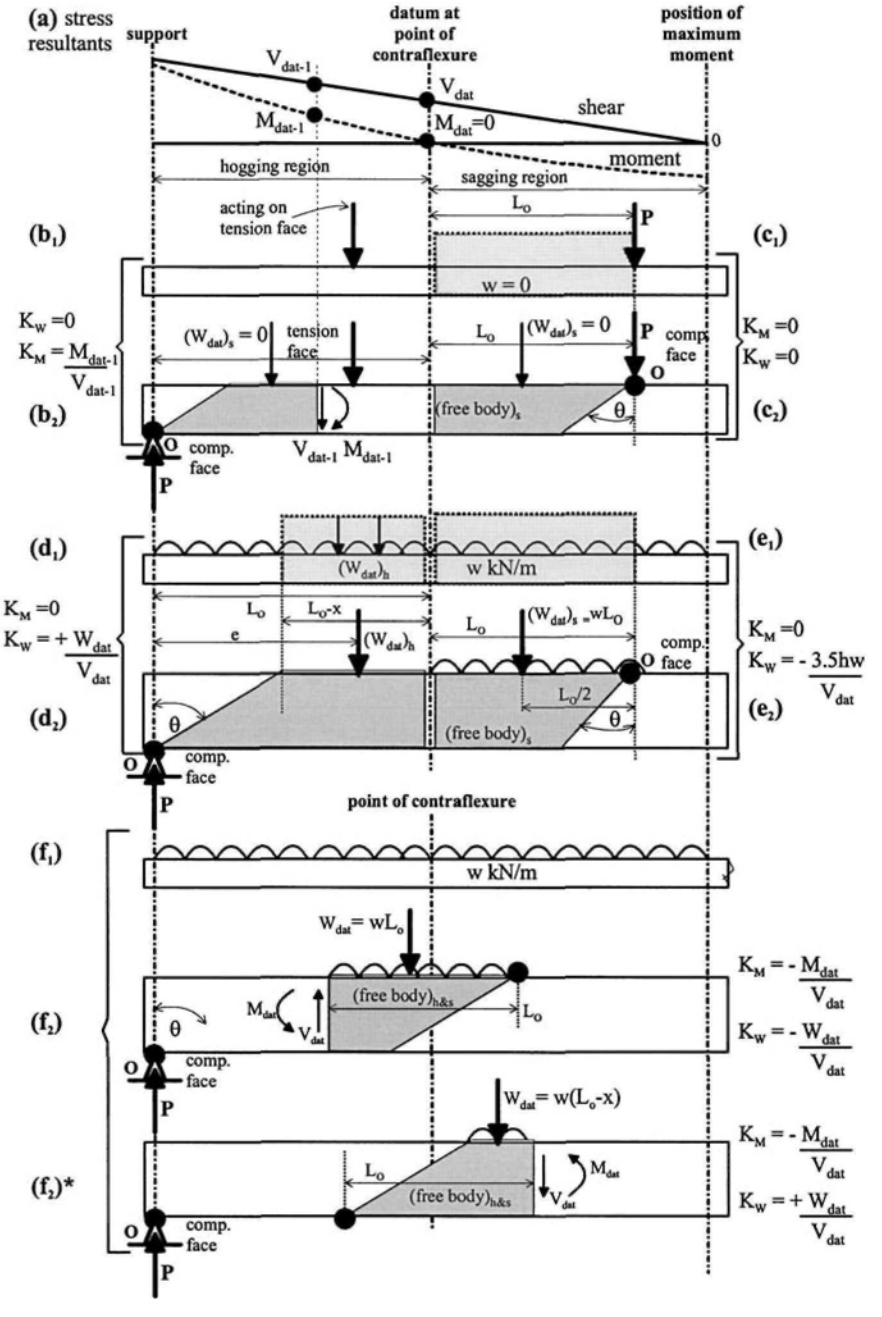

Figure 5.8 Simplification in CDC analysis

The most convenient position for the datum point is at the point of contraflexure as in Figs 5.8(c), (d) and (e) as this ensures that the moment factor K_M of Eq. 5.2 is zero in the CDC analysis of Eq. 5.1. When the applied load *w* is insignificant compared with the concentrated load P in Fig. 5.8(c_1), then the load factor K_W, from Eq. 5.3, can be considered to be zero in Eqs 5.1 and 5.5. When a concentrated load is acting on the tension face as in Fig. 5.8(b_1), then it may be more convenient to move the free body away from this concentrated load.

A further discussion and simplification of the K_M and K_W factors is given in Section 4.4.1.1. If it is unclear where the best position for the focal point is, then a few positions should be tried to find the critical diagonal crack.

5.2.1.5 Interpretation of CDC analysis results

Figure 5.2 can be used for the CDC analysis of fully plated and fully anchored beams as well as the CDC analysis of partially plated beams, and its interpretation is considered in Fig. 5.9. To help in the discussion of Fig. 5.9, it will be assumed that there are no applied loads, $W_{dat} = 0$, acting on the free body of the CDC analysis, such as in Fig. 5.8(c), in which case $K_W = 0$ in Eq. 5.9 so that the shear load at the datum point is also the shear load at the diagonal crack.

(a) Short plates

Let us first consider terminating the plate close to the supports at point A_2 in Fig. 5.9(a). As the effective length of the plate is L_e, point A_1 represents the position of the plate where the plate is fully anchored, that is plate O-A_2 is fully anchored over the length O-A_1. As position A_1 is fully anchored, the shear load at the datum point to cause a critical diagonal crack through A_1 is shown as point 1 in Fig. 5.9(b), that is $(V_{dat})_1$ which lies on the shear load to cause crack sliding in the plated beam $[(V_{dat})_{slide}]_{pl}$. Furthermore, just beyond the plate end at A_2, the beam is unplated so that the shear load at the datum point to induce a critical diagonal crack through this position is shown as point 2, that is $(V_{dat})_2$ which lies on the shear load to cause crack sliding in the unplated beam $[(V_{dat})_{slide}]_{un}$. It is also worth noting that $(V_{dat})_2$ is the shear load to cause the plate near to the plate end to debond. This is because adjacent to the plate end, the shear load to causing cracking is given by points P on the plated line and Q on the unplated line in Fig. 5.9(b) both of which are below $(V_{dat})_2$. Hence a crack will first form, and then it will fail at the end of the plated region at $(V_{dat})_2$ on $[(V_{dat})_{slide}]_{un}$ which is really $[(V_{dat})_{slide}]_{pl}$ with the anchorage length of the plate tending to zero.

If a critical diagonal crack is not to occur in plate O-A_2 in Fig. 5.9(a), then the shear load must not be greater than $(V_{dat})_2$. If it is greater than $(V_{dat})_2$, then part of the plate will debond, in effect moving A_2 to the left and consequently A_1 to the left, thereby, reducing the length of the fully anchored region O-A_1. As $(V_{dat})_2$ is greater than the shear to cause a *critical* diagonal crack in a fully plated beam $[(V_{dat})_{crit}]_{pl}$, it can be seen that it is possible for the shear load required to cause CDC debonding to be greater, in a very short partially plated beam, than that required to cause the fully plated beam to debond at $[(V_{dat})_{crit}]_{pl}$. However, the shear load to cause debonding can also be less as shown for the plate terminating at B_2; in which case the shear load to cause the plate end to debond is given by point 4 on $[(V_{dat})_{slide}]_{un}$ which is just weaker than $[(V_{dat})_{crit}]_{pl}$. It is also worth considering terminating the plate at C_2, in which case the plate debonds at point 6 which is on the $[(V_{dat})_{crack}]_{pl}$ line, as the crack within the plate forms and fails at this shear load as the shear capacity after cracking $[(V_{dat})_{slide}]_{un}$

is less. It can be seen that the shear load to cause plate debonding is given by the broken line U-V-X where V is at the intercept between $[(V_{dat})_{crack}]_{pl}$ and $[(V_{dat})_{slide}]_{un}$.

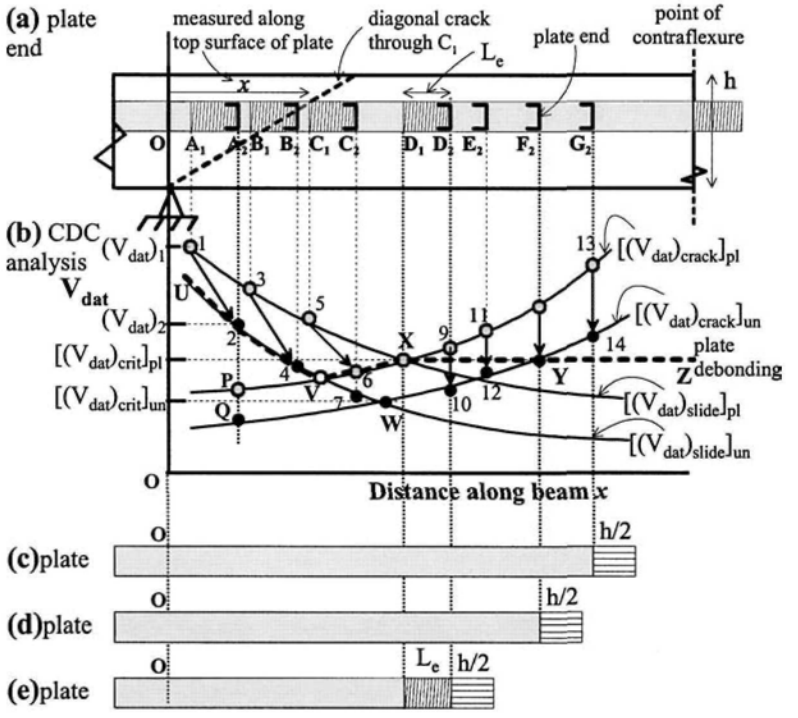

Figure 5.9 Shear capacity of partially plated members

When the plate is terminated at A_2, then the shear can be increased to $(V_{dat})_2$ which is greater than the shear capacity of the unplated beam $[(V_{dat})_{crit}]_{un}$ at point W. This is fine just as long as the total shear capacity of the unplated region V_c+V_s is greater than $(V_{dat})_2$. If not, then shear failure of the unplated beam will precede plate debonding. It is suggested that short plates by themselves should not be used in design as their strength is greatly influenced by the assumed position and shape of the diagonal crack. Instead medium or long plates should be used.

(b) Long plates

Let us now consider terminating the plate closer to the point of contraflexure such as plate O-G_2 in Fig. 5.9(a). The debonding resistance at G_2 is governed by the shear load to cause cracking $[(V_{dat})_{crack}]_{pl}$ at point 13 and not the shear load to cause crack sliding $[(V_{dat})_{slide}]_{pl}$ as the latter has a lower strength at position G_2. This means that the plate in this region does not need to be anchored as shown in Fig. 5.9(c) although it is suggested that the plate is extended a further distance h/2 to allow for the fact that the diagonal crack is usually curved and for variations in the distribution of the applied loads. As the plate is extended from D_1 to G_2 in Fig. 5.9(a), the shear load to cause cracking in this region and within the plated beam $[(V_{dat})_{crack}]_{pl}$ increases and is always greater than the shear to cause the critical diagonal crack $[(V_{dat})_{crit}]_{pl}$ at X, so that the shear load to cause debonding remains on the broken line X-Y-Z, that is

at $[(V_{dat})_{crit}]_{pl}$. Hence the failure envelope to cause plate debonding is given by the broken line U-V-X-Y-Z.

(c) Medium plates

When the plate is terminated at position G_2 in Fig. 5.9(a), a diagonal crack could form adjacent to the plate end in the unplated beam at the shear load 14. As this is greater than the shear load to cause the plate to debond $[(V_{dat})_{crit}]_{pl}$ at point X, the plate will debond at position D_1 prior to crack sliding at the plate end. Hence the shear capacity of the unplated region is of no consequence. Therefore, it can be concluded that it is only necessary to terminate the plate at F_2 where the shear load to cause cracking and subsequently crack sliding in the unplated region at Y is equal to the shear required to cause plate debonding at X. This maximum extent of plating is shown in Fig. 5.9(d) where it is recommended that the plate is extended a further distance h/2 to allow for vagaries in the distribution of the applied loads. Extending the plate any further is of no benefit.

To achieve $[(V_{dat})_{crit}]_{pl}$ at point X, the plate has to be fully anchored at D_1 so that the plate has to be extended by an effective length to position D_2 in Fig. 5.9(a). The shear to cause debonding in the anchorage length D_1-D_2 is greater than at X in Fig. 5.9(b) as it follows the path X-9 on $[(V_{dat})_{crack}]_{pl}$. So that plate debonding in this anchorage length will not precede plate debonding at X. This is in contrast to plate debonding for short plates such as that terminated at B_2 where the cracking shear is smaller than the sliding shear so the plate requires to be anchored.

The shear to cause failure in the unplated beam at D_2 is given by point 10 which is greater than that of the unplated beam at point W. However, in this case point 10 is smaller than that at point X to cause plate debonding. If the beam or slab has stirrups and just as long as the total shear capacity V_c+V_s in the unplated beam is greater than $[(V_{dat})_{crit}]_{pl}$, then crack sliding in the unplated region is of no consequence so that the plate can be terminated as shown in Fig. 5.9(e). However, if the beam or slab does not have stirrups, then shear failure within the unplated region will first occur which will probably be undesirable so that so the plate should be extended to that in Fig. 5.9(d).

To conclude, the failure envelope for the shear to cause CDC debonding in a partially plated beam is given by the broken line U-V-X-Y-Z in Fig. 5.9(b). If the shear to cause CDC debonding in the plated region is sufficient to cause a critical diagonal crack in an unplated region, then stirrups are required in the unplated region.

5.2.2 *Direct approaches*

The iterative approach outlined in Section 5.2.1 may be tedious for design purposes but it does quantify the position of the critical diagonal crack and, hence, does allow for partial plating. It is also worth noting, that the iterative approach automatically allows for the variation in the applied vertical shear and the variation in the vertical shear capacity along the length of the beam. Hence shear failure may occur at a section where the applied shear is not at its maximum. For example in the hogging region in Fig. 5.3(c), the minimum shear capacity $(V_{conc})_{pl}$ of the critical diagonal crack O-A should be compared with the applied shear $(V_A)_{applied}$ and not with the maximum applied shear of V_{max}; this can be done as the position of the critical diagonal crack is known. However, comparing the capacity $(V_{conc})_{pl}$ with V_{max} would give a safe conservative design.

The following approaches were developed to give directly safe estimates of the minimum shear capacity $(V_{conc})_{pl}$ but they do not give the position of the critical

diagonal crack. Hence these direct approaches require the whole region, either the hogging region or the sagging region, to be fully plated and fully anchored as shown in Fig. 4.20. These direct approaches also require the minimum shear capacity within a region $(V_{conc})_{pl}$ to be compared directly with the maximum applied shear V_{max} and hence will give a safe design.

5.2.2.1 Mean approach

The mean approach is described in Section 4.5.1.2. The shear load at the datum to cause crack sliding, Eq. 4.32, can be written with the following notation.

$$\left[\left(V_{dat}\right)_{crit}\right]_{mean} = \frac{\left[\left(V_{dat}\right)_{crack}\right]_{mean} + \left[\left(V_{dat}\right)_{slide}\right]_{mean}}{2} \tag{5.13}$$

where substituting the parameter in Eq. 4.30 into Eq. 5.1 gives

$$\left[\left(V_{dat}\right)_{crack}\right]_{mean} = \frac{\left(3.37h^2\left(\frac{b_c f_{tef}}{2} + \frac{f_t \sum\left(m_p A_{rect} L_{rect}\right)}{h^2}\right)\right) + \left(F_{ps} d_{ps}\right)}{L_O \pm K_M \pm K_W e} \tag{5.14}$$

where K_M is positive when the free body is contained within a region (that is a sagging region or a hogging region) and negative when the free body straddles a point of contraflexure, and where K_W is negative when the focal point is in the sagging region and positive when in the hogging region. Substituting the coefficient in Eq. 4.31 into Eq. 5.5 gives

$$\left[\left(V_{dat}\right)_{slide}\right]_{mean} = \frac{0.118 f_c b_c h\left(1 + \frac{2F_{ps} + 4\sum P_{plate}}{f_c b_c h}\right) f_1(f_c) f_2(h) f_3(\rho)}{1 \pm K_W} \tag{5.15}$$

Equation 5.13 can be used to determine the shear load at the datum to cause crack sliding in both the fully plated fully anchored beam $[[(V_{dat})_{crit}]_{mean}]_{pl}$ and the shear load at the datum to cause crack sliding in the unplated beam $[[(V_{dat})_{crit}]_{mean}]_{un}$. Hence, changing the notation in Eq. 5.11 gives the increase in the shear capacity due to plating as

$$\left(\Delta V_{conc}\right)_{pl} = \left\{\left(\left[\left(V_{dat}\right)_{crit}\right]_{mean}\right)_{pl} - \left(\left[\left(V_{dat}\right)_{crit}\right]_{mean}\right)_{un}\right\}\left(1 \pm K_w\right) \tag{5.16}$$

where K_W is positive when the focal point is in the hogging region and negative when in the sagging region. The shear capacity of the plated section $(V_{conc})_{code}$ is the sum of the code shear capacity of the unplated section $(V_c)_{code}$ plus the increase due to plating in Eq. 5.16 as in Eq. 5.12.

The whole region, hogging or sagging, needs to be plated and fully anchored by extending the plate beyond this region by at least an effective length L_e (Eq. 2.3). Furthermore, the applied shear force within the whole plate length must not exceed $(V_{conc})_{code}$.

5.2.2.2 Prestressed code approach

The passive prestress code approach is described in Section 4.5.2. It was shown that the increase in the concrete component of the shear capacity due to plating is given by

$$(V_{incr})_{pp} = 0.13\sum P_{plate} \qquad 5.17$$

where the summation applies to all the longitudinal plates, and the maximum axial force in a plate P_{plate} is the lesser of the yield capacity $A_p f_{yp}$ for metal plates, the fracture capacity $A_p f_{FRP}$ for FRP plates, and IC debonding resistance $A_p \sigma_{IC}$ for a fully anchored plate in a pull test which is given by Eq.2.1 with $\beta_L = 1$ and with α from the pull test results in Table 2.1. This increase can only be applied to fully plated and fully anchored regions as shown in Fig. 4.20.

The vertical shear load to cause CDC debonding is, therefore, given by

$$V_{c-plate} = (V_c)_{code} + 0.13\sum P_{plate} \qquad 5.18$$

where $(V_c)_{code}$ is the concrete shear capacity of the unplated RC section given by the national code. Equation 5.18 applies to both prestressed and unprestressed beams. For unprestressed beams, the national code value for $(V_c)_{code}$ can be used directly. However, care must be taken in deciding what value to use for prestressed beams as only code equations that are applicable to both prestressed and unprestressed beams, such as the Eurocode approach (1992) in Eq. 4.35, should be used.

5.3 Generic design approach for CDC debonding

The generic design procedure for CDC debonding is illustrated in Fig. 5.10, which uses the hogging region in Fig. 5.3 to illustrate the approach; although the same procedure applies to the other regions of the beam. The full sequence of design is given which includes IC, CDC and PE debonding and it covers the hinge approach in Section 2.5.2 and the anchorage approach in Section 2.5.1.

5.3.1 Basic analyses

The initial steps in the generic design procedure consist of the following.

- Determine the distribution of the design stress resultants in Fig. 5.10(a).
- Check for IC debonding at the position of maximum moment, M_{max} in Fig. 5.10(a) as described in Chapters 2 and 3. This may already have been done in determining the plates required for flexure. However, additional plates may have been added to increase the shear capacity.
- Perform a CDC analysis of the unplated beam to obtain $[(V_{dat})_{crack}]_{un}$ and $[(V_{dat})_{slide}]_{un}$ in Fig. 5.10(d) and the shear load at the datum point to cause the critical diagonal crack $[(V_{dat})_{crit}]_{un}$ at point N.
- Assume the plates extend over the whole region A-F in Fig.5.10(c) and beyond by at least the effective length L_e, so that the region is fully plated and the plates fully anchored throughout the region. Hence, the maximum force in each of the plates P_{plate} is constant along the region and depends on the minimum of: the maximum IC debonding resistance $P_{IC} = A_p \sigma_{IC}$; their fracture capacity, if an FRP plate, of $P_u = A_p f_{FRP}$; or their yield capacity, if a metal plate, of $P_y = A_p f_{yp}$.

- Analyse the fully plated and fully anchored plated beam for CDC debonding to obtain $[(V_{dat})_{crack}]_{pl}$ and $[(V_{dat})_{slide}]_{pl}$ in Fig.5.10(d) and the shear load at point L for critical diagonal crack debonding in the plated section $[(V_{dat})_{crit}]_{pl}$.

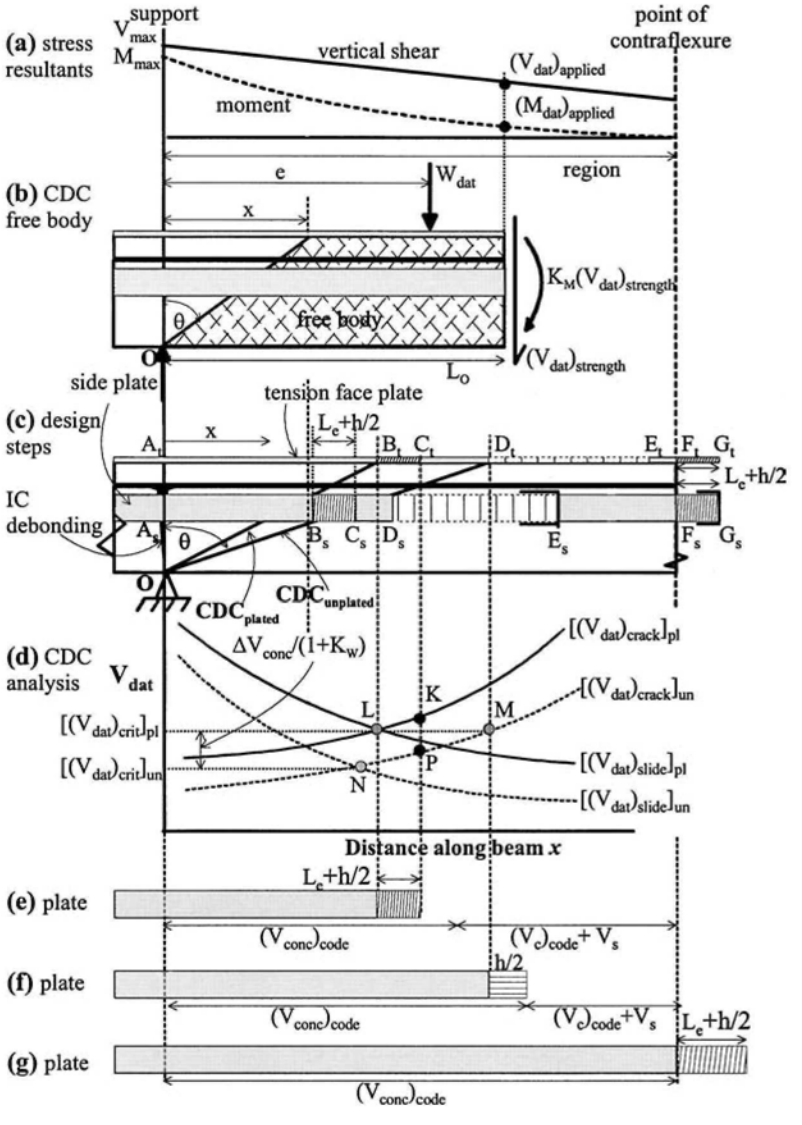

Figure 5.10 Generic CDC design approach

5.3.2 Shear load at datum point V_{dat} to cause CDC debonding

The CDC analysis procedure, depicted in Fig. 5.10(d), gives the shear load at some convenient datum point $V_{dat,}$ as shown in Fig. 5.10(b), to cause a diagonal crack to form at position x and also to cause that diagonal crack to fail. It may be worth noting

that position x in the CDC analysis is measured along the tension face of the beam as shown in Fig. 5.10(c). Therefore, this distance denotes the length of the tension face plate but the diagonal, such as O-B, denotes the extent of the upper edge of the side plate. The shear load V_{dat} is not necessarily the shear at the critical diagonal crack because of the applied loads acting on the CDC analysis free body W_{dat}. The design procedure can be based on the shear load at the datum point V_{dat} as will be described in this section. However, if it is necessary to relate the design to the national code value for the concrete shear capacity $(V_c)_{code}$, then this approach is described in Section 5.3.3.

The shear at the datum point V_{dat} in Fig. 5.10(d) is the shear required to cause cracking or crack sliding which depends on the capacity of the section. Hence V_{dat} in the CDC analyses represents the strength of the structure $(V_{dat})_{strength}$ as shown in Fig. 5.10(b). In contrast, from the loads applied to the structure in Fig. 5.10(a), the applied shear load at the datum point will be referred to as $(V_{dat})_{applied}$. When the capacity $(V_{dat})_{strength}$ is less than the applied $(V_{dat})_{applied}$, then CDC debonding occurs. Continuing with the design steps in Section 5.3.1.

- Consider the analysis, in Fig. 5.10(d), of the fully anchored fully plated beam, that is the lines $[(V_{dat})_{crack}]_{pl}$ and $[(V_{dat})_{slide}]_{pl}$ and the shear load at the datum point to cause debonding $[(V_{dat})_{crit}]_{pl}$. If the capacity $[(V_{dat})_{crit}]_{pl} = (V_{dat})_{strength}$ is smaller than the design shear load at the datum point $(V_{dat})_{applied}$ in Fig. 5.10(a), then the plate will debond before the design load is reached. In which case, another arrangement of adhesively bonded plates needs to be tried or another technique such as bolting.
- If the capacity $[(V_{dat})_{crit}]_{pl}$ is sufficient to resist the applied $(V_{dat})_{applied}$, then CDC debonding can be prevented. The plates will have to be extended beyond the point where they intercept the diagonal crack at positions B in Fig. 5.10(c) in order to fully anchor the plate to comply with the initial assumption in the analysis. The plates will have to be extended by at least an effective length L_e as in Fig. 5.10(e) and it is suggested that it is extended by a length $L_e + h/2$ to points C, to allow for the fact that the diagonal crack is not a straight line but tends to curve.
- The strength along the partially anchored region B-C in Fig. 5.10(c), follows the path of the shear load to cause cracking $[(V_{dat})_{crack}]_{pl}$ in Fig. 5.10(d), from point L to point K which is just before the plate end. The strength along the plate L-K is always greater than at L so the anchorage length will not debond prematurely.
- Just beyond the plate end, the strength reduces to that of the unplated beam at point P which will be less than the capacity of the plated beam at L. This means that a critical diagonal crack will first form in the unplated region.
- For beams and slabs with stirrups, the formation of a critical diagonal crack at P, prior to a critical diagonal crack forming within the plated region at the shear load $[(V_{dat})_{crit}]_{pl}$ at L, will not cause failure if the shear capacity of the unplated beam or slab, V_c+V_s, is not exceeded by $[(V_{dat})_{crit}]_{pl}$. Furthermore, a critical diagonal crack in the unplated region will not cause CDC debonding in the plated region.
- For slabs and beams without stirrups, the critical diagonal crack just beyond the plate end will cause failure at a shear $(V_{dat})_{strength\text{-}P}$ at P in Fig. 5.10(d). If the shear capacity $(V_{dat})_{strength\text{-}P}$ is not sufficient to resist the design shear load at the datum point $(V_{dat})_{applied}$, then it may be worth considering extending the plate to D in Fig. 5.10(f) such that the shear load at the datum point to cause cracking just beyond the plate end at M in Fig. 5.10(d) is the same as that required to cause crack sliding within the plated region at L. The extent of plating is given by Fig. 5.10(f)

where it is shown that there is no need for an anchorage length L_e as debonding from B to D is governed by the load to cause cracking $[(V_{dat})_{crack}]_{pl}$ although it is suggested to extend the plate by h/2.

5.3.3 Shear capacity V_{conc} to cause CDC debonding

The analyses in Sections 5.3.1 and 5.3.2 have dealt with the shear load at the datum point V_{dat} to cause failure at a position that is not at the datum point, and compared this with the design shear load at the datum point to see if failure would occur. It has not been necessary to determine directly the shear capacity of the structure nor relate this to the shear capacity from code requirements $(V_c)_{code}$. If this is the preferred approach, then the following design procedure continues from Section 5.3.1.

- The CDC analyses in Fig. 5.10(d) gives the shear load at the datum point to cause CDC debonding in the fully anchored plated section at point L, that is $[(V_{dat})_{crit}]_{pl}$, as well as the shear load at the datum point to cause crack sliding in the unplated beam at point N, that is $[(V_{dat})_{crit}]_{un}$.
- The increase in the concrete shear capacity due to plating is shown in Fig. 5.10(d) as $(\Delta V_{conc})_{pl}$ /$(1\pm K_W)$. Hence the increase in the concrete shear capacity due to plating $(\Delta V_{conc})_{pl}$ can be determined directly from the CDC analyses. The increase in the shear capacity $(\Delta V_{conc})_{pl}$ can than then be added to the national code value of the concrete shear capacity $(V_c)_{code}$ to get the concrete shear capacity of the plated region $(V_{conc})_{code}$. The concrete shear capacity $(V_{conc})_{code}$ is the shear load to cause CDC debonding in a plated beam.
- Let us consider terminating the plates at positions C in Fig. 5.10(c) so that it is fully anchored at the point B where the critical diagonal crack in the plated region will occur. This is shown in Fig. 5.10(e) where an additional length of plate h/2 has been added to allow for the fact that the diagonal cracks are not straight. In the plated region, the applied shear must be restricted to $(V_{conc})_{code}$. This even applies to the partially anchored region L_e+h/2 as the shear required to form a diagonal crack in this region lies on $[(V_{dat})_{crack}]_{pl}$ which has a higher capacity than at L and which does not require to be anchored as it is the shear load to cause cracking. The unplated region has a strength $V_s+(V_c)_{code}$.
- Let us now consider extending the plate to point M in Fig. 5.10(d), so that the shear load to cause crack sliding in the plated and unplated regions is the same. This is shown as the plate in Fig. 5.10(f). In this case there is no need for an anchorage length as the shear to cause cracking, $[(V_{dat})_{crack}]_{pl}$ in Fig.5.10(d), controls debonding at the plate end. The shear should be restricted $(V_{conc})_{code}$ in the plated region and $V_s+V_{c\text{-}code}$ in the unplated region.

5.3.4 Further extension of plate

So far the plate ends have been extended to positions D in Fig. 5.10(d) in Sections 5.3.2 and 5.3.3. This covers the hinge approach requirements for partially plated beams in Section 2.5.2. Continuing with the analysis in Sections 5.3.2 and 5.3.3.

- It may still be necessary to extend the plates further to position E in Fig. 5.10(c) in order to prevent plate end debonding and this is covered in Chapter 6.
- If the anchorage approach at Section 2.5.1 is being applied, the plate is automatically extended to a flexurally uncracked region, which can be assumed to be a point of contraflexure and then anchored by a length L_e+h/2 beyond the point of contraflexure as shown in Fig. 5.10(g).

- In which case, the shear force in the plated region which is the whole of the sagging region or hogging region must be restricted to $(V_{conc})_{code}$ from Section 5.3.3 or the shear load at the datum point $[(V_{dat})_{crit}]_{pl}$ from Section 5.3.2, depending on which analysis technique is being applied.
- In the hogging region shown in Fig. 5.1(b), the plate would be being extended into a reducing shear region and moment region as shown in Fig. 5.1(a). So that the plate end is being subject to less shear and curvature and therefore less likely to debond due to CDC or PE debonding. Hence the plate extension $L_e+h/2$ into the sagging region in Fig. 5.10(g) is unlikely to debond.
- However a plate in a sagging region in Fig. 5.1(a) would be being extended into a region of increasing shear so that it may not be possible to find an uncracked region to anchor the plates, that is the plate ends would be susceptible to CDC debonding. In which case a CDC analysis of the hogging region with the sagging plates extended into this region will have to be done to ensure that the plate ends do not debond. This is discussed further in Section 5.4.3.

5.4 Further plate combinations and positions

Plates can be attached to any surface of a beam or combinations of surfaces to enhance both the flexural and shear capacity of the beam. It will be shown that the generic CDC analyses described in Section 5.2 can cope with all combinations.

5.4.1 Angle and U-sections

Fibre reinforced polymer U-shaped plates, as in section A-A in Fig. 1.12, are often formed in the wet lay up process using bi-directional fibres in order to enhance both the flexural and shear capacities, as it is felt that the portion of the U-plate bonded to the tension face of the beam will be good at improving the flexural capacity whilst the portion of the U-plate bonded to the sides will be good at increasing the shear capacity as well as inhibiting the debonding of the tension face component.

As a further example of this form of construction, the beam in Fig. 5.11 was strengthened by adhesively bonding metal angle sections to both of the bottom corners. The angle plates were terminated close to the supports and eventually detached due to CDC debonding.

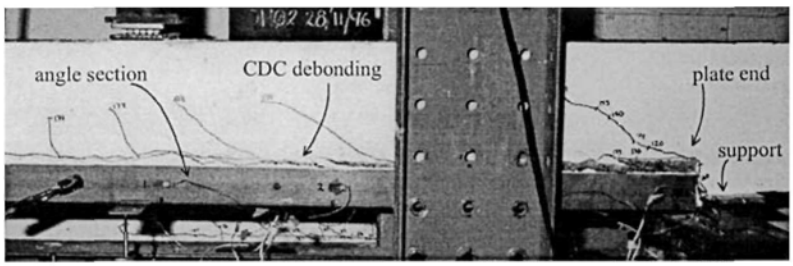

Figure 5.11 CDC debonding of angle section

The CDC analyses described in Section 5.2 can be applied directly to this form of construction by simply treating the portion of the plate bonded to the sides separately from those bonded to the tension face as illustrated in Figs 5.4 to 5.7.

5.4.2 Short side plates

Short longitudinal side plates can be adhesively bonded to the sides of beams above the plate end of a tension face plate as shown in Fig. 5.12. This combination of plates has been found to inhibit the debonding of the tension face plate due to plate end debonding, as the side plate reduces the curvature in the vicinity of the plate end of the tension face plate as will be explained in Chapter 6.

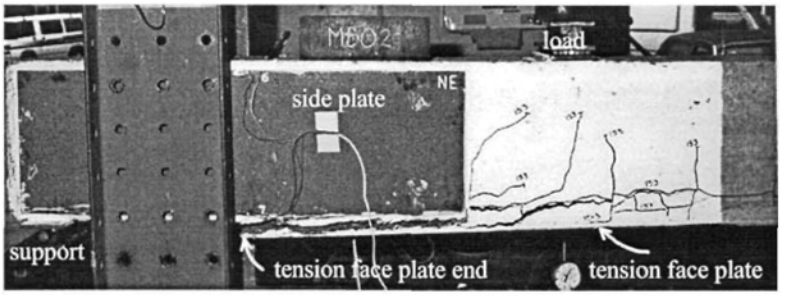

Figure 5.12 Short side plates with tension face plates

However, this combination of side plates and tension face plate also inhibits the CDC debonding in the vicinity of the tension face plate end as shown in Fig. 5.12. This may be useful in the anchorage approach for the design of longitudinal tension face plates, as the anchorage approach requires the tension face plate to be anchored in an uncracked region. As explained in Section 5.3.4, it may be difficult to find uncracked regions for sagging region plates, as extending the plates toward the points of contraflexure increases the vertical shear that the plate ends are subject to. Hence, it simply may not be possible to find an uncracked region as can be seen in Figs. 1.38 and 1.39. Plating the sides in the vicinity of the plate end may be sufficient to prevent diagonal cracks in this region and allow the tension face plate to be anchored in an uncracked region.

The CDC analyses described in Section 5.2 can also be applied directly to this form of construction. However care needs to be taken, particular in deriving the maximum axial force that the plate can resist P_{plate} in the crack sliding analysis in Section 5.2.1.2. Take for example the side and tension face plated CDC free body in Fig. 5.13 for a sagging region. The resultant axial force in the plate will be the smaller of the maximum axial force on the left of the diagonal crack $(P_{plate})_{left}$, which depends on the anchorage length to the right of the diagonal crack, and that to the right of the diagonal crack. A simple solution would be to slice the plate into narrow horizontal strips and sum the individual strengths which depend on their individual anchorage lengths based on the crack inclination. It may also be worth noting that the position of the plate relative to the diagonal crack is important; for example in Fig.5.13, the upper part of the plate does not intercept the diagonal crack and, therefore, this part of the plate is ineffective.

5.4.3 Compression face plates

Extending the tension face plate in the hogging region, such as in Fig. 4.17(b), into the compression face of the sagging region can increase the resistance to the formation of the critical diagonal crack. The free body for the CDC analysis is shown in Fig. 5.14. The shear load at the datum point to cause cracking $[(V_{dat})_{crack}]_{pl}$ is unaffected by the compression face plate as the plate intercepts the diagonal crack at the focal point.

However, the compression face plate does contribute to the shear load to cause crack sliding as the plate provides an additional force $(P_{plate})_{cfp}$ across the diagonal crack. Hence extending the tension face plate, in the hogging region in Fig. 4.17(b), into the compression face of the sagging region will help prevent CDC debonding of the tension face in the sagging region, which may be useful in applying the anchorage approach to the sagging region where the plate has to be terminated in an uncracked region.

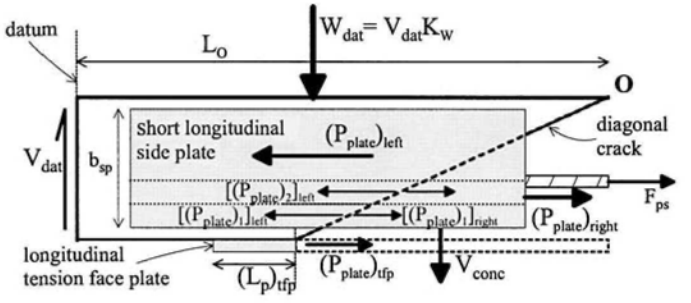

Figure 5.13 Short side plates with tension face plates in sagging region

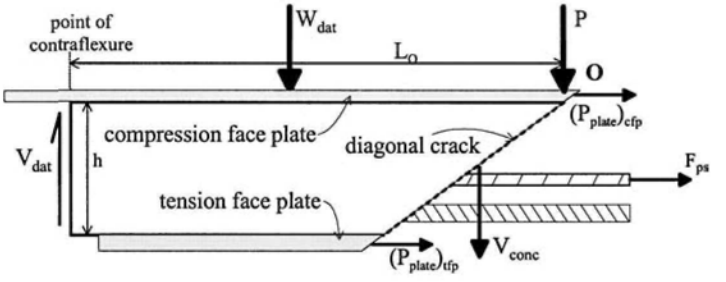

Figure 5.14 CDC analysis of compression face plate in sagging region

An example of a compression face plated beam test is shown in Fig. 5.15 where it can be seen that the compression face plate has debonded in the vicinity of the applied load but still remains intact over the support.

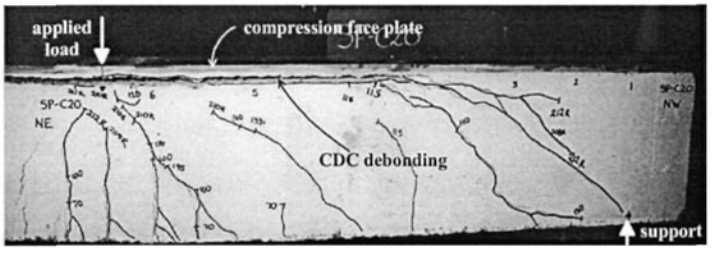

Figure 5.15 CDC of compression face plate

Extending the tension face plate in the sagging region in Fig. 4.17(b) into the compression face of the hogging region will have little effect on the CDC debonding of the tension face plate in the hogging region. This is because a compression face plate in the hogging region will not intercept a diagonal crack emanating from a support, unless of course the plate is placed over the support which is probably not possible in most cases.

5.5 Enhancement of shear capacity

This book is mainly concerned with the use of longitudinal plates to increase the flexural and shear capacities of reinforced concrete beams and slabs. The ability of longitudinal plates to increase the shear capacity as measured in tests is first illustrated in the following section, after which the interaction between the vertical shear enhancement of longitudinal plates and transverse plates is discussed.

5.5.1 Increase in shear capacity attained by longitudinal plating

Longitudinal plates can increase the concrete component of the shear capacity substantially. To illustrate the magnitude of the increase that can be obtained, a series of beams were cast with identical size, longitudinal reinforcement and concrete, and tested under identical loading conditions, so that any variations in strength were due to the externally bonded plates.

An unplated beam without stirrups was tested to determine the concrete shear capacity of the unplated beam, $(V_{conc})_{un}$, directly; this is the shear capacity given in codes $(V_c)_{code}$. The tested beam is shown in Fig. 5.16 and failed at a shear load of 81 kN due to crack sliding along the critical diagonal crack. This test will be used as our reference strength for comparison with the plated beams.

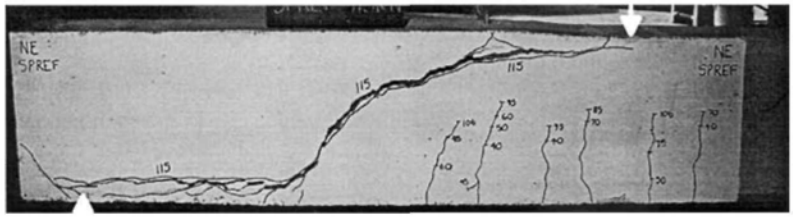

Figure 5.16 Reference beam unplated without stirrups: $(V_{conc})_{un}$ = 81 kN

The same beam as in Fig. 5.16 was fully plated along the tension face as in Fig. 5.17. The tension face plate was stopped just short of the supports and the beam failed in shear and debonded due to crack sliding at 140 kN, which is a 73% increase over that of the unplated beam. This is a very important finding as the increase in the shear capacity due to plating is normally associated with transverse or vertical plates which are often assumed to act like stirrups to increase the shear capacity. It can be seen that longitudinal adhesively bonded tension face plates can significantly increase the concrete component of the shear capacity.

Let us consider the implications of this increase in the concrete shear capacity. Most reinforced concrete slabs are designed without stirrups so that their shear capacity is limited by the concrete component of the shear capacity $(V_c)_{code}$. When the flexural capacity of an RC slab is increased using longitudinal tension face plates,

then the concrete shear capacity is also increased so that there is a good chance that the vertical shear capacity will not limit the flexural strengthening.

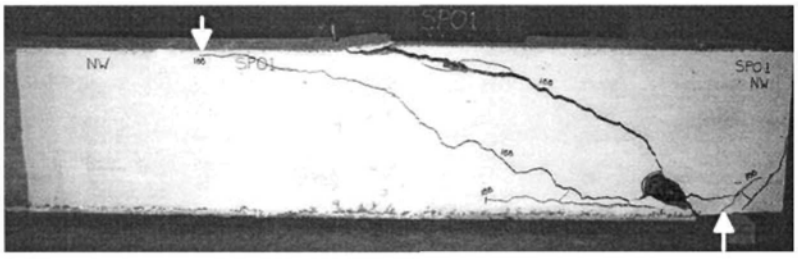

Figure 5.17 Tension face plate without stirrups: $(V_{conc})_{tfp}$ = 140 kN (73% increase)

The reinforced concrete beam in Fig. 5.18 is plated on both sides of the beam with side plates that extended from one support to the other, that is the beam is fully plated but not fully anchored. The beam did not have internal stirrups and failed by shear failure and CDC debonding due to crack sliding when a critical diagonal crack occurred at 156 kN which is a 93% increase in the shear capacity over that of the unplated beam. Hence longitudinal side plates can also substantially increase the concrete shear capacity.

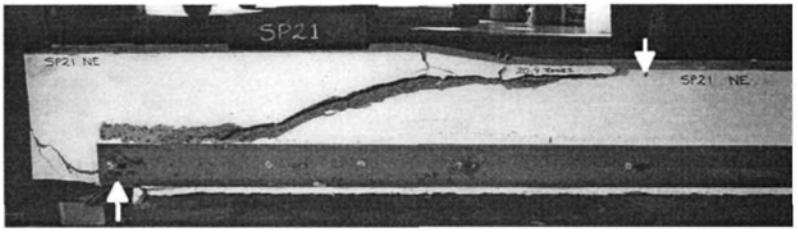

Figure 5.18 Side plates without stirrups: $(V_{conc})_{sp}$ = 156 kN (93% increase)

The plated beam in Fig. 5.19 is exactly the same as in Fig. 5.18, except that the beam has stirrups. In this test, CDC debonding occurred due to crack sliding at 162 kN but the beam did not fail in shear due to the stirrups. The shear load at crack sliding has increased by 100% over that of the unplated beam. But of much greater significance is the fact the shear load at crack sliding in the beam without stirrups in Fig. 5.18 is almost the same as that in the beam with stirrups in Fig. 5.19. This is just one of numerous tests that have shown that the presence of stirrups does not affect CDC debonding, as the plate debonds before the stirrups can be stretched to resist shear.

The findings from the tests in Figs. 5.18 and 5.19 have two important implications in the plating of continuous beams. Consider the continuous beam in Fig. 4.17. Prior to plating, let us assume that the maximum applied shear at the supports in Fig. 4.17(a) is significantly greater than the concrete shear capacity $(V_c)_{code}$ of the unplated beam, hence, stirrups are required to resist the vertical shear, that is the maximum applied shear in Fig. 4.17(a) requires a shear resistance of $(V_c)_{code}+V_s$. Even if the addition of longitudinal plates in the hogging region doubles the shear to cause crack sliding to $(V_{conc})_{pl}$, there is a good chance that $(V_{conc})_{pl} < (V_c)_{code}+V_s$ so that a critical diagonal crack will occur in the hogging region causing debonding

before the design shear is reached. Hence there is a good chance that CDC debonding will prevent the hogging regions of a beam from being plated using adhesively bonded plates, in which case bolting may have to be considered. In contrast, the sagging region in Fig. 4.17(a) is subjected to substantially less shear than in the hogging region, so that there is a good chance that $(V_{conc})_{pl}$ will be greater than the applied shear in this region so that adhesively bonded plates could be used in the sagging region. It can be seen that CDC debonding may restrict the use of adhesively bonded plates in some regions of a beam.

Figure 5.19 Side plates with stirrups: $(V_{conc})_{sp}$ = 162 kN (100% increase)

In the plated beam in Fig. 5.18, the side plate is placed as close to the tension face as possible and this increased the shear capacity by 93%. The same beam was tested with the plate at mid-depth as shown in Fig. 5.20, and shear failure and CDC debonding occurred at an increase of 97%, that is at virtually the same load.

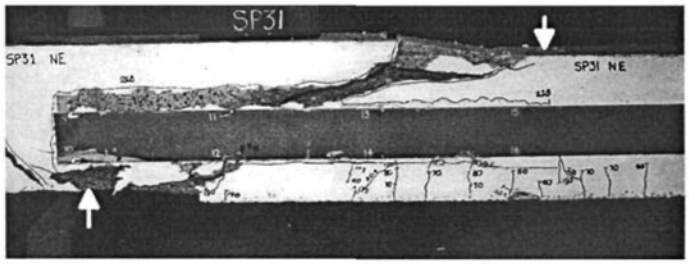

Figure 5.20 Side plates without stirrups: $(V_{conc})_{sp}$ = 160 kN (97% increase)

Placing the side plate next to the compression face in Fig. 5.21 increased the shear capacity and the resistance to crack sliding by 55% when the beam had nominal stirrups but by only 13% when there were no stirrups present. So it is recommended that side plates in the compression region of a beam be used only for beams with nominal stirrups which will rarely be a restriction as most beams have nominal stirrups. It can be seen that side plates at any level of the beam can substantially inhibit the formation of the critical diagonal crack and, hence, inhibit debonding.

5.5.2 Shear enhancement design philosophy

As described in Section 2.2.3, wherever a plate traverses an intermediate crack, as in Fig. 5.22, axial forces P_{plate} are induced in the plate which have an upper limit of the IC debonding resistance; this plate force may be reduced if the plate yields or fractures. These axial forces exist in longitudinal plates, shown in Fig. 5.22(a), whether the intermediate crack is induced by flexure or shear. These axial forces also exist in transverse plates, shown in Fig. 5.22(b), when the plates traverse a diagonal

crack. Hence the axial forces in both the longitudinal plates and transverse plates are induced by the IC debonding resistance as described in Chapter 2.

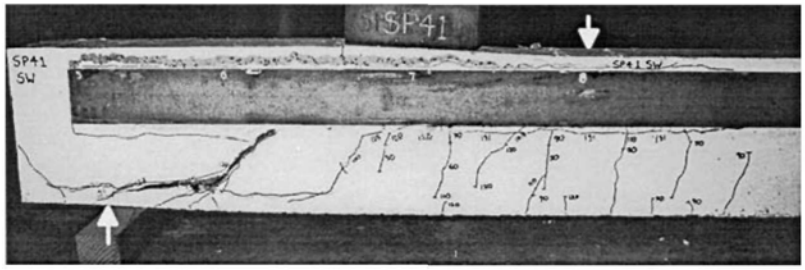

Figure 5.21 Side plates with nominal stirrups: $(V_{conc})_{sp}$ = 126 kN (55% increase)

The axial forces in the longitudinal and transverse plates in Fig. 5.22 help to increase the shear capacity of the beam, but they are considered to do so in different ways.

(a) Longitudinal plates – concrete component

As has been described in Sections 4.4.1.3 and 4.4.1.4, the longitudinal plates, as in Fig. 5.22(a), can be considered to solely increase the concrete shear capacity $(V_c)_{code}$ by acting as additional longitudinal reinforcing bars or as an additional prestressing force. Hence the longitudinal plates can be considered to enhance the concrete shear capacity as in the following equation.

$$(V_{conc})_{pl} = (V_c)_{code} + (\Delta V_{conc})_{pl} \qquad 5.19$$

Furthermore, tests have clearly shown that the concrete component $(V_{conc})_{pl}$ is not affected by internal steel stirrups as the plates debond as soon as $(V_{conc})_{pl}$ is achieved.

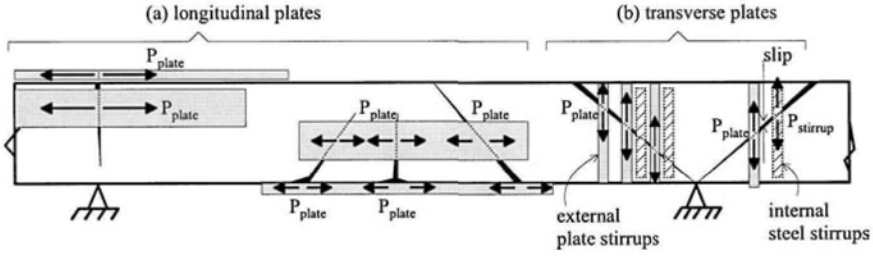

Figure 5.22 Axial forces in longitudinal and transverse plates

(b) Transverse plates – stirrup component

Transverse plates which can be referred to as externally bonded stirrups, in Fig. 5.22(b), are often treated in the same way as internal steel stirrups. Their contribution to the vertical shear resistance $(V_{stirrup})_{transverse}$ is assumed to be simply the sum of the plate forces P_{plate} traversing the diagonal crack. Hence the maximum shear force that can be resisted by the internal stirrups V_s and the external bonded stirrups $(V_{stirrup})_{transverse}$ is given by

$$\left(V_{stirrups}\right)_{pl} = V_s + \left(V_{stirrup}\right)_{transverse} \qquad 5.20$$

However it is extremely important to realise that Eq. 5.20 is an upper bound to the strength. As shown in Fig. 2.16, the slip required for a reinforcing bar to achieve its maximum bond stress, and hence the maximum force in the bar, is an order of magnitude greater than the slip required for the externally bonded plates to reach their maximum bond stress, and hence the maximum force in the plate. Therefore, as the diagonal crack in Fig. 5.22(b) starts to open up, the crack width being half the slip, the plates will reach their maximum force P_{IC} well before the internal stirrups yield. This applies in particular to transverse plates that are not anchored. Whereas, anchored and thin wet lay up plates may fail by rupture having allowed the steel stirrups to yield. As can be seen in Fig. 2.16, beyond the slip at which the plates achieve their maximum strength, the bond capacity of the plate reduces very rapidly. Hence, it is very unlikely that the maximum force in the external plate will be achieved at the same time or displacement as the maximum force in the steel stirrups. Consequently, it is not recommended to use Eq. 5.20 which should be viewed with extreme caution. A safe design would be to rely solely on $(V_{stirrup})_{transverse}$.

5.6 Analysis

The following results were from an iterative CDC analysis as described in Section 5.2 and which used the hinge approach described in Section 5.3. Full and comprehensive worked examples are given in Chapter 7.

5.6.1 Hinge approach with full depth steel plates in sagging region of beam

The reinforced concrete beam in Section 3.5.2.1 and Fig. 3.41 has already been strengthened in the sagging region with 3 mm thick steel plates over the full depth of the web. The plate increased the flexural capacity from 173 kNm to 277 kNm. The plate has been designed using the hinge approach, Section 5.2, so that it can be terminated short of the point of contraflexure. To maintain an elastic moment distribution, the hogging region was also strengthened as described in Section 4.6.1 and the total applied load can increase by 30% to 54 kN/m. The shear and moment distributions for the beam are the same as those shown in Fig. 4.23 where it can be determined that the applied shear force $V_{applied}$ = 156 kN at the point of contraflexure. From the Australian concrete code AS3600 (1994), $(V_c)_{code}$ = 104 kN in the sagging region, which is less than $V_{applied}$ hence, a CDC will occur in the unplated beam and therefore the plates are also required to increase the concrete component of the shear capacity V_c. The questions are: where to terminate the plate so that the critical diagonal crack falls within the plated region; and whether the increase in the concrete component of the shear capacity is sufficient to prevent CDC debonding within the sagging region.

The free body shown in Fig. 5.8(f_2) will be used in the CDC analysis to allow for the possibility that the CDC may straddle the point of contraflexure because we are dealing with a uniformly distributed load (udl) in the sagging region and hence, the position of the focal point O to give the *minimum* CDC is not known. The datum point was chosen 1000 mm from the point of contraflexure so that it is within the hogging region of the beam. Therefore M_{dat} = 183 kNm and V_{dat} = 210 kN so that the

factor K_M = 871 mm and, as in the example in Section 4.6.2 and Fig. 4.26, K_W varies with L_O.

The CDC analysis using the hinge approach begins by assuming that the beam is fully plated and fully anchored along the sagging region, that is the plate extends at least the effective length L_e (Eq. 2.3) beyond the root of any diagonal crack so that the maximum plate force P_{plate} can be assumed to be constant along the region. As discussed in Section 2.4.4, a 3 mm thick 300 MPa steel plate will yield prior to IC debonding hence the maximum force in the plate is governed by yielding so that P_{plate} = 666 kN. Using a spreadsheet analysis, the curve $(V_{dat})_{c\text{-}plate}$ in Fig. 5.23 is produced for the fully plated beam by equating the load to cause cracking (Eq. 5.1) and the load to cause crack sliding (Eq. 5.5) for increasing z from the point of contraflexure, using the procedure illustrated in Fig. 4.26 and where z is also defined. $(V_{dat})_{c\text{-}plate}$ in Fig. 5.23 is compared with V_{dat} = 210 kN, where it can be seen that the shear force at the datum point required to cause CDC debonding anywhere within the sagging region is greater than the applied shear force at the datum point. Hence, CDC debonding will not occur. This is further illustrated in Fig. 5.23 by comparing the concrete shear capacity of the plated beam $(V_{conc})_{pl}$, determined from Eq. 5.9, which always exceeds the maximum applied shear force at the focal point given by $(V_{max})_{Lo}$.

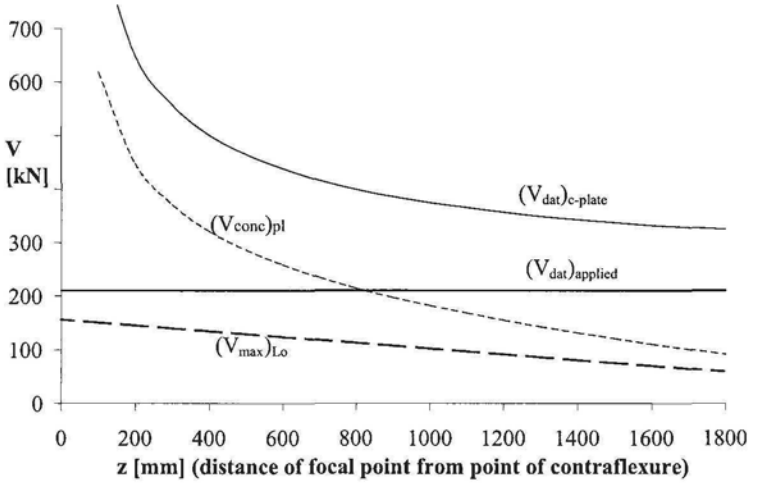

Figure 5.23 CDC analysis of steel side plated beam

Figure 5.24 shows $(V_{conc})_{pl}$ from Fig. 5.23 and the concrete shear capacity of the original unplated beam $(V_{conc})_{un}$, which was determined using the same iterative CDC analysis procedure. It is interesting to note that $(V_{conc})_{un}$ exceeds $(V_{max})_{Lo}$ everywhere along the sagging region suggesting that a CDC will not occur in the unplated beam and therefore the plates are not required to increase the concrete component of the shear capacity V_c as originally indicated when compared with $(V_c)_{code}$. The difference between $(V_{conc})_{pl}$ and $(V_{conc})_{un}$ is shown as $(\Delta V_{conc})_{pl}$ in Fig. 5.24 and represents the increase in shear capacity due to plating using the CDC analysis as defined in Eq. 5.11. From Eq. 5.12, adding the AS3600 concrete code strength $(V_c)_{code}$ to $(\Delta V_{conc})_{pl}$ gives the concrete component of the shear capacity of the plated beam $(V_{conc})_{code}$ in Fig. 5.24, which as already concluded, demonstrates that CDC debonding will not occur in the plated section as it exceeds $(V_{max})_{Lo}$ everywhere.

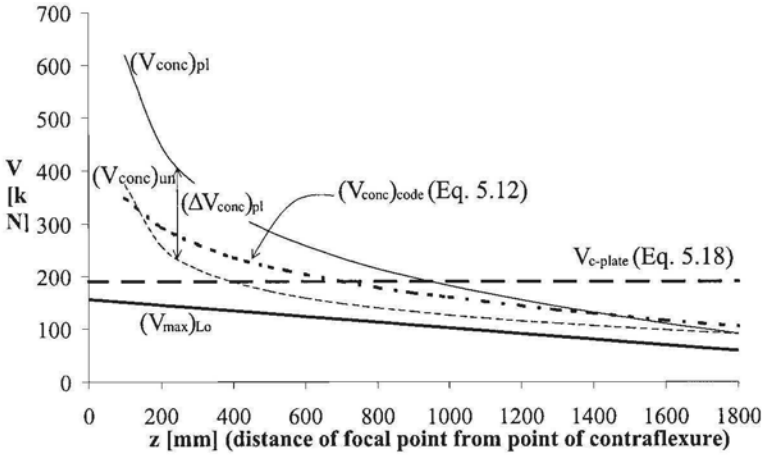

Figure 5.24 Comparison with prestress code approach

The analysis using the direct *passive prestress approach* is also shown in Fig. 5.24. Using P_{plate} = 666 kN, the increase in the concrete component of the shear capacity due to plating is 86 kN from Eq. 5.17, which is an 82% increase and from Eq. 5.18, the shear load to cause CDC debonding $V_{c\text{-}plate}$ = 190 kN. As $V_{c\text{-}plate}$ is greater than the applied shear force at the point of contraflexure, that is $(V_{max})_{Lo}$ = 156 kN at z = 0, this analysis confirms once again that CDC debonding will not occur.

5.7 References

Please note that as the generic design equations developed in this chapter are based on the fundamental principles described in Chapter 4; the references in Chapter 4 are also directly applicable to this chapter.

Eurocode 2: "Design of concrete structures Part 1: General rules and rules for buildings (1992)". BSI Standards.

AS 3600 – 1994. "Australian Standard Concrete Structures.". Standards Australia.

Chapter 6: Plate End (PE) Debonding

6.1 Introduction

The plate was first designed, in Chapters 2 and 3, for IC debonding due to the axial strains induced in the plate by flexure at the position of maximum moment. The plate was then extended, in Chapters 4 and 5, beyond the position of maximum moment to encompass the rigid body shear deformation that induces CDC debonding. It is now necessary to ensure that the end of the plate does not debond prematurely due to the curvature in the vicinity of the plate end, which is referred to as plate end (PE) debonding. This is the final stage of the design procedure for plating. Unlike IC debonding and CDC debonding, PE debonding will rarely, if ever, prevent plating, as this form of debonding can be easily prevented by terminating the plate at a point of contraflexure. After completion of the check for PE debonding, the three major debonding mechanisms due to axial strains in the plate, due to shear deformations in the beam and due to curvature in the beam have been designed for. Theoretically, it should now be necessary to check for interface shear stress ((VAy)Ib) debonding as described in Section 1.3.4, which tests have shown rarely occurs.

The plate end debonding mechanism is first described in this chapter, followed by generic analysis procedures that cover all forms of plating and combinations of plates. The PE debonding analysis is then placed in context with the CDC and IC debonding analyses in a design procedure where the interaction between these debonding mechanisms is also discussed. The chapter is completed with design examples to illustrate the circumstances in which PE debonding may affect the extent of plating.

6.2 PE debonding mechanism

6.2.1 PE debonding mechanism

The plate end (PE) debonding mechanism was explained in Section 1.3.3. As can be seen in Fig. 1.20, when curvature is applied to the beam, the plate tries to stay straight which can cause debonding from the plate end inwards. The PE debonding crack propagation is in the opposite direction to IC debonding where the debonding cracks propagate outwards towards the plate ends, as can be seen in Figs. 1.14 and 2.20, and it is also in the opposite direction to CDC debonding where the debonding cracks propagate outwards to the plate ends but spread inwards as in Fig. 4.4. It is also worth noting that the IC and CDC debonding resistances are associated with regions of the beam that are subjected to ultimate failure of the beam, that is flexural and shear failure, which require the sections to behave in a non-linear fashion. In contrast, PE debonding is associated with those regions of the beam where the flexural forces are small and where a critical diagonal crack has not occurred, so that the section at which PE debonding occurs can be assumed to behave in a linear fashion, that is linear elastic sectional analyses can be used albeit that the concrete has cracked in tension.

Whether the plate is on the side of the beam, as in Fig. 6.1(a), or on the tension face of the beam, the mechanism of debonding is the same. The beam in Fig. 6.1(a) is subject to a constant moment, M_{beam}, and the plate is terminated within the constant moment region.

6.2.1.1 Tension face plates

Let us first consider the tension face plate of the beam in Fig. 6.1(a). The curvature in the composite plated beam χ induces the same curvature in the plate χ and an axial strain in the plate $\varepsilon_{tfp} = \chi d_{tfp}$, where d_{tfp} is the distance between the neutral axis of the composite plated section and the centroid of the plate, as shown in Fig. 6.1(a). Hence, the tension face plate is subject to an axial force P_{tfp} due ε_{tfp} and a moment M_{tfp} due to χ. Another way of visualising the problem is that the stress resultants P_{tfp} and M_{tfp} have to be applied to the ends of the initially straight tension face plate, in Fig. 6.1(b), to achieve the same deformation as in the tension face plate in Fig. 6.1(a). These stress resultants, P_{tfp} and M_{tfp}, have to be transferred across the plate-beam interface, and this is done through the interface shear stresses τ and normal stresses σ_n, that is perpendicular to the plate/concrete interface, which are shown at position *C* in Fig. 6.1(a) and also shown enlarged in Fig. 6.1(d).

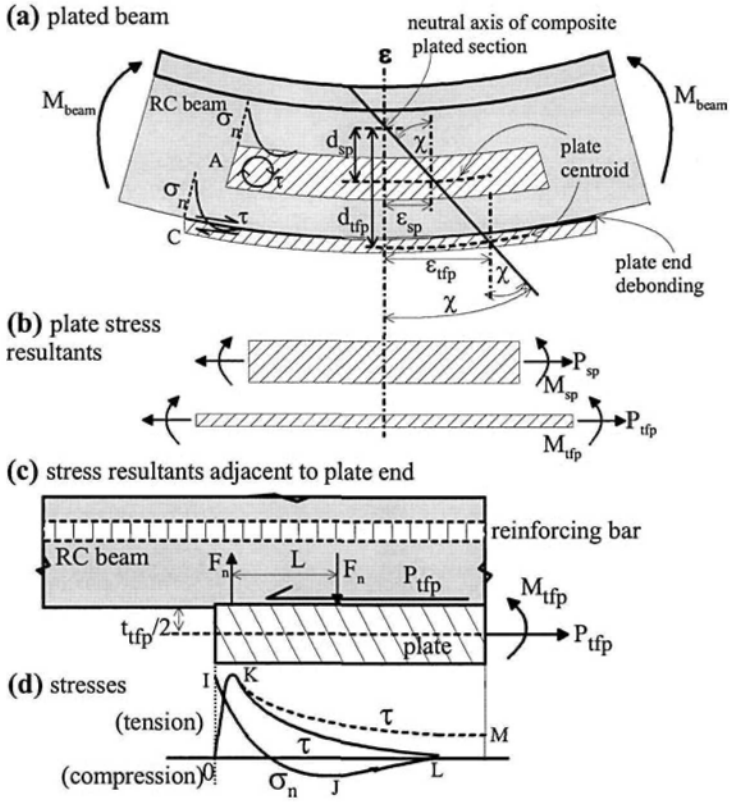

Figure 6.1 Plate end debonding mechanism

The forces acting on a free body of the plate that is near the plate end are shown in Fig. 6.1(c). The axial force in the plate P_{tfp} requires an interface shear force of the same magnitude to maintain equilibrium, as shown. Furthermore, the moment acting on the plate $M_{tfp} + P_{tfp}t_{tfp}/2$ requires a counter moment due to the normal

interface forces F_n of F_nL, as shown. The shear force P_{tfp} on the interface induces the shear stress τ distribution O-K-L in Fig. 6.1(d) which must be zero at the plate end, due to the free surface, and zero at L, because the plate is in a constant moment region. If the plated beam was in a region of varying moment, then the shear stress distribution would be O-K-M, where M is given by the interface shear stress VAy/Ib discussed in Section 1.3.4. The moment $F_nL = M_{tfp} + P_{tfp}t_{tfp}/2$, in Fig. 6.1(c), induces the normal stress distribution σ_n of I-J-L in Fig. 6.1(d), where the peak normal stress occurs at the plate end at I and which has a greater magnitude than the compressive normal stress at J. Finite element analyses of the constant moment region in Fig. 6.1(a) show that the interface stresses σ_n and τ in Fig. 6.1(d) are concentrated towards the plate ends and that the spread of the interface stresses O-L is a function of the plate thickness, for plated beams in which the plate thickness is much less than the beam depth, which is the usual case for tension face plates. It is the stresses at the plate end in Fig. 6.1(d) that induce PE debonding.

6.2.1.2 Compression face plates

For compression face plates, the stress distribution of the interface stresses for tension face plates in Fig. 6.1(d) applies, except that the signs of the stresses are reversed. In which case for compression face plates, the maximum normal tensile stress now occurs away from the plate end at J which is much smaller than the maximum normal compressive stress now at the plate end at I. Hence compression face plates are less likely to debond than tension face plates, but they can and do debond because tensile stresses do exist at J. It is also worth noting that analysing a compression face plate as if it were a tension face plate would give a safe design, although design rules are available for compression face plates.

6.2.1.3 Side plate with centroid in tensile zone

The same logic, as for tension face plates, can be applied to the side plate in Fig. 6.1(a). The curvature χ induces an axial force in the plate P_{sp} and a moment M_{sp}. The moment component M_{sp} is now resisted by interface shear stresses τ, as shown at position *A* in Fig. 6.1(a); this is in contrast to the moment component in the tension face plate which is resisted by normal stresses as shown at position *C*. The axial force in the side plate P_{sp} is resisted by interface normal stresses σ_n (that is in a direction perpendicular to the side-plate/concrete interface), at position *A* in Fig. 6.1(a), in the same way as the axial force in the tension face plate at position *C*, which is shown enlarged as I-J-L in Fig. 6.1(d). The interaction between the shear stress τ and the peak of the tensile normal stress σ_n near the plate end at position A determines when debonding occurs.

6.2.1.4 Side plate with centroid in compression zone

Let us consider what happens when the position of the side plate centroid, d_{sp} in Fig. 6.1(a), lies above the neutral axis of the composite plated member, that is in the compression zone. As the curvature is the same at all levels of the beam, the moment component is unchanged so the interface shear τ at position *A* in Fig. 6.1(a) remains unchanged. However, moving the plate centroid above the neutral axis of the composite plated beam causes the resultant axial force in the plate P_{sp} to change from being tensile to compressive, so that the peak stress at the plate end at I in Fig. 6.1(d) is now compressive but the relatively smaller stress at J is now tensile. This reduction

in the magnitude of the peak tensile stress is beneficial and will delay, that is inhibit, debonding but it may not prevent debonding.

It can be seen that a safe design would be to treat side plates with centroids in the compression zone as if they were in the tension zone. This is the recommendation in the following analyses for sections that are bonded to the sides of the beam, because the beneficial effect of having a plate with the centroid in the compression zone has as yet not been quantified. Under no circumstance can the sign of d_{sp} be made negative as this ignores the fact that there are tensile stresses at J which will reduce the resistance to plate end debonding.

6.2.2 Examples of PE debonding

In order to illustrate plate end (PE) debonding, the reinforced concrete beams in the following tests were plated within a constant moment region; the plate ends were terminated well within this constant moment region as shown in Fig. 6.2 for a tension face plated beam. This set up ensured that CDC debonding, Section 1.3.2, and interface shear stress (VAy/Ib) debonding, Section 1.3.4, did not occur, as the vertical shear was zero. Furthermore, IC debonding as in Section 1.3.1, did not occur as all the specimens debonded from the plate end inwards which is characteristic of PE debonding and in the opposite direction to that associated with IC debonding.

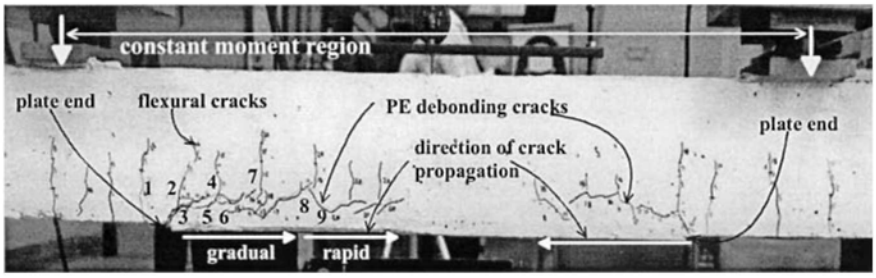

Figure 6.2 PE debonding of a tension face plate

6.2.2.1 Plates bonded to horizontal surfaces

In the tension face plated beam in Fig. 6.2, flexural cracks first formed adjacent to the plate ends such as that marked 1. These flexural cracks increased the local curvature near the plate ends and simultaneously induced the flexural crack marked 2 and a short horizontal crack marked 3. The horizontal debonding crack 3 is at the level of the tension reinforcing bars, and slowly propagated inwards as the applied load was increased. The horizontal debonding crack, or peeling crack, was preceded by flexural cracks. For example, when the debonding crack reached position 3, the flexural crack at 4 formed which increased the curvature locally and allowed the horizontal crack to propagate to 5 and 6, after which the flexural crack at 7 formed. The crack gradually propagated to position marked 8. After which from position 9 onwards, there was a very rapid crack propagation at the same load which caused the strains in the plate at mid-span to reduce even under increasing applied load. Plate end debonding is characteristically a gradual failure; the moment to cause the first horizontal crack at 3 to form being about half of that to cause the rapid crack propagation at 9, so that there is plenty of prior warning.

For tension face plated beams, the PE debonding crack invariably occurs at the level of the longitudinal tension reinforcing bars which is at the same level as in CDC

debonding in Fig. 4.4. This is in contrast to IC debonding which occurs in the concrete adjacent to the plate as in Fig. 2.3. Research on PE debonding has found that the scatter of results for tension face plates is much greater than that associated with side plates, and it is felt that it is the influence of the tension reinforcing bars which is causing this increase in scatter.

Extending the tension face plate, as in the left hogging region in Fig. 4.17(b), into the compression face does not necessarily prevent PE debonding, as can be seen in Fig. 6.3 where the compression face plate has debonded. In contrast to the tension face plate in Fig. 6.2 where the debonding crack starts at the plate end, the debonding crack in the compression face plate started away from the plate end as shown in Fig. 6.3. This was to be expected, as discussed in Section 6.2.1.2 for compression face plates, as the peak tensile normal stress, that is the stress perpendicular to the plate/concrete interface, now occurs at J in Fig. 6.1(d). The debonding crack also occurred at a level adjacent to the plate as can be seen in Fig. 6.3 which can be compared to that of the tension face plate in Fig. 6.2 which shows that it is not influenced by any longitudinal compression reinforcement.

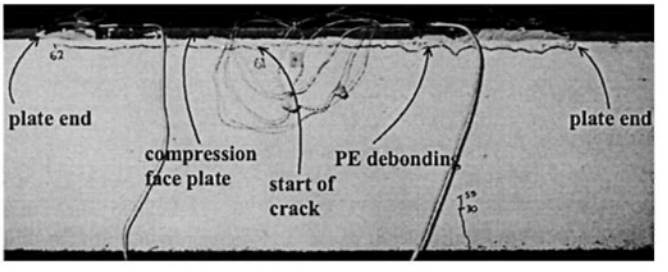

Figure 6.3 PE debonding of a compression face plate

The compression face plate in Fig. 6.3 has been removed in Fig. 6.4 to show the debonding failure surface in the concrete which is adjacent to the plate. This is typical of PE debonding failure surfaces in compression face plates as well as in side plates and in angle plates adhesively bonded to the sides, where it has been found that the scatter of results is much less than those associated with tension face plated specimens.

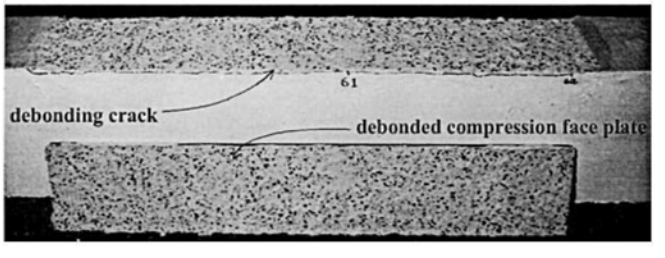

Figure 6.4 PE debonding adjacent to plate

6.2.2.2 Plates bonded to vertical surfaces

An example of plate end debonding in a side plated beam is shown in Fig. 1.21. In this beam, the depth of the plate was quite small compared to the depth of the beam, so that the plated beam can be considered to be a shallow plated beam with the side

plate in the tension zone. Even though the plates are on the sides, the sequence of crack propagation is the same as that described for the tension face plated beam in Fig. 6.2: the flexural crack marked 1 first formed which increased the local curvature; inducing the debonding crack at the plate end which gradually propagated along both the top and bottom edges of the plate; being preceded by the flexural cracks; until there was rapid crack propagation at which the plate strains at mid-span, on the left strain gauge, reduced even with increasing applied load. It can be seen that some of the flexural cracks traverse the plate confirming that the side plate was bonded to the tension zone of the beam.

In contrast to the shallow side plated beam in Fig. 1.21, Fig. 6.5 shows a deep side plated beam. It can be seen in Fig. 6.5, that the flexural cracks do not extend above the plate, in fact the flexural cracks to the side of the plate stop short of the top level of the plate, so that the top of the plate is in the compression zone of the plated beam. However, the same PE debonding sequence of crack propagation has occurred, with the flexural cracks first forming adjacent to the plate end, followed by the debonding cracks around the edges of the plate. The debonding failure plane in both the shallow side plated beam in Fig. 1.21 and the deep plated beam in Fig. 6.5 was the same as that in the compression face plate in Fig. 6.4, that is in the concrete adjacent to the plate.

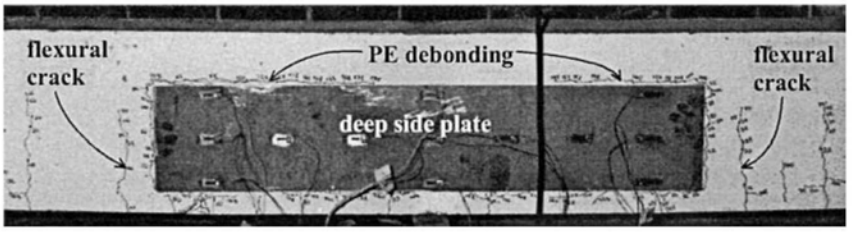

Figure 6.5 PE debonding in deep side plated beam

Finally in Fig. 6.6 is an example of an angle section in which the web has been adhesively bonded to the side of the beam and the flange has been adhesively bonded to the tension face of the beam. Once again, the sequence of PE debonding crack propagation was the same as previously described. However, the analysis of the test results showed that the flange first debonded from the tension face at an early stage of loading after which the web remained bonded to the side and hence the angle section acted as a side plate.

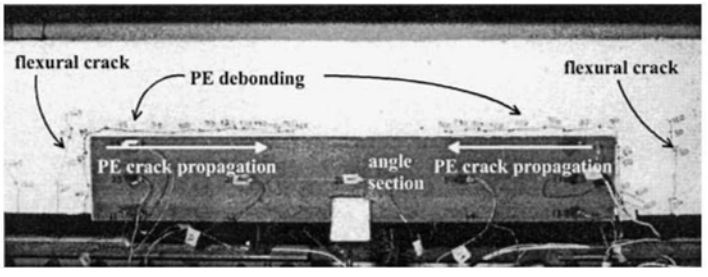

Figure 6.6 PE debonding in angle plated beam

6.3 Generic PE debonding analysis

6.3.1 PE debonding curvature capacity

It was explained in Section 6.2.1 and illustrated in Fig. 6.1 that plate end debonding is a function of the curvature χ in the composite plated section. It is this curvature, which induces a moment in an individual plate M_p and an axial force in the plate P_p that have to be resisted by the interface plate stresses, which can lead to PE debonding. The mathematical model for the curvature in a composite plated beam to cause plate end debonding in an individual plate χ_{PE} (Nguyen et al 1998) is given in the following generic form

$$\chi_{PE} = \frac{f_{cb}}{f(M_p) + f(P_p)} = \chi_{cap} \qquad 6.1$$

where: f_{cb} is the concrete splitting tensile strength, sometimes referred to as the Brazilian or indirect tensile strength, which can be assumed to be $0.53\sqrt{f_c}$ (N and mm) if not measured directly; the function $f(M_p)$ allows for the moment in the plate; and the function $f(P_p)$ for the axial force in the plate. It must be stressed that Eq. 6.1 applies to an individual plate at a cross-section, so that if there are multiple plates, as in Fig. 5.1, then each plate must be checked individually for PE debonding. Equation 6.1 is the curvature capacity χ_{cap} and it is derived from the geometric and material properties of the plated cross-section. For example, $f(M_p)$ depends on the flexural rigidity of the plate $(EI)_p$, and $f(P_p)$ depends on the axial rigidity $(EA)_p$ as well as the distance of the plate centroid from the neutral axis of the composite plated member d_p, such as d_{sp} and d_{tfp} in Fig. 6.1(a).

6.3.2 Plate end applied curvature

It is the applied curvature at the plate end and, hence, the moment at the plate end that determines whether plate end debonding occurs. Furthermore, it is the additional curvature applied after plating at the plate end, χ_{add}, that induces PE debonding. The curvature that is applied after a beam has been plated can be considered to consist of the following components.

$$\chi_{short} + \chi_{creep} + \chi_{shrink} = \chi_{add} \qquad 6.2$$

where χ_{short}, χ_{creep} and χ_{shrink} are the curvatures applied at the plate end after plating due to short term loads, concrete creep due to long term loads and concrete shrinkage. It must be emphasised that tests have shown that it is the additional curvature at the plate end after plating that induces PE debonding, and any existing curvature prior to plating does not affect PE debonding. This is because plates tend to stay straight when adhesively bonded to a curved surface with the glue thickness allowing for the difference in shape, so that M_{sp} and M_{tfp} in Fig 6.1(b) tend to zero. Furthermore, the axial component P_{sp} and P_{tfp} in Fig. 6.1(b) will certainly be zero on adhesive bonding the plate to a beam already loaded, as the plate is not stretched longitudinally prior to adhesive bonding so that P_{sp} and P_{tfp} are zero on adhesive bonding. Hence it is the additional curvature after plating that induces PE debonding.

The procedures in national standards for determining the shrinkage curvature for deriving the shrinkage deflection can be used to determine χ_{shrink} in Eq. 6.2. The

following equation is typical of equations available in national standards for determining the shrinkage curvature.

$$(\chi_{shrink})_{code} = \frac{1.15\varepsilon_{sh}}{d}\left(1 - \frac{A_{sc}}{A_{st}}\right) \qquad 6.3$$

where: ε_{sh} is the shrinkage strain in the concrete which for the PE debonding analysis would be the increase in the concrete shrinkage strain after plating; d is the effective depth of the RC member; A_{sc} is the cross-sectional area of the compression reinforcing bars which for the PE analysis would include the area of any plates in the compression zone of equivalent stiffness, that is A_pE_p/E_s, as the A_{sc} term in Eq. 6.3 provides a stiffness restraint against the shrinkage deformations; and where A_{st} is the cross-sectional area of the tension reinforcing bars plus an equivalent area for plates in the tension zone for the PE debonding analysis. Often, structures are retrofitted by plating well after the concrete has stopped shrinking in which case this term tends to zero.

The short term curvature χ_{short} is simply given by $\chi_{short} = M_{short}/(EI)_{short}$, where M_{short} is the moment at the plate end due to short term loadings such as live loads. The flexural rigidity $(EI)_{short}$ is the short term flexural rigidity of the cracked plated section which is derived using the short term modulus of elasticity of the concrete for $(E_c)_{short}$ and assuming in the derivation that the tensile strength of the concrete is zero. Similarly, the curvature due to creep is given by $\chi_{creep} = M_{crcep}/(EI)_{creep}$, where M_{creep} is usually the moment due to long term loads such as dead loads and sustained live loads, and $(EI)_{creep}$ is the long term flexural rigidity of the cracked plated section where the long term Young's modulus of the concrete $(E_c)_{long}$ should be used. It needs to be noted that only the creep expected after the beam is plated needs to be considered. Furthermore, as plating is required to strengthen/stiffen the structure, most likely the dead load or sustained live load would have increased which will result in additional creep.

The standard elementary analysis to determine the flexural rigidity of a cracked plated section is illustrated in Fig. 6.7, just to emphasise to the reader the importance of using the cracked sectional flexural rigidity in determining the curvatures. The plated cross-section in Fig. 6.7(a) has been transformed into a cracked concrete section in Fig. 6.7(b) in which the tensile strength of the concrete in flexure is assumed to be zero, where $m_{p1} = E_{p1}/E_c$, $m_{p2} = E_{p2}/E_c$, and $m_s = E_s/E_c$, and where the Young's modulus of the concrete E_c is either the short term material stiffness or the long term material stiffness that allows for creep. The depth of the neutral axis d_{na} in Fig. 6.7(b) can be found by equating the first moment of area about the neutral axis for elements on either side of the neutral axis, and then the second moment of area about the neutral axis I can be obtained from the parallel axis theorem.

6.3.3 Plate end debonding design

6.3.3.1 PE curvature capacity and applied curvature

The aim of the design is to ensure that the additional curvature, χ_{add} in Eq. 6.2, is always less than curvature capacity, χ_{cap} in Eq. 6.1, that is

$$\chi_{short} + \chi_{creep} + \chi_{shrink} \le \frac{f_{cb}}{f(M_p) + f(P_p)} \qquad 6.4$$

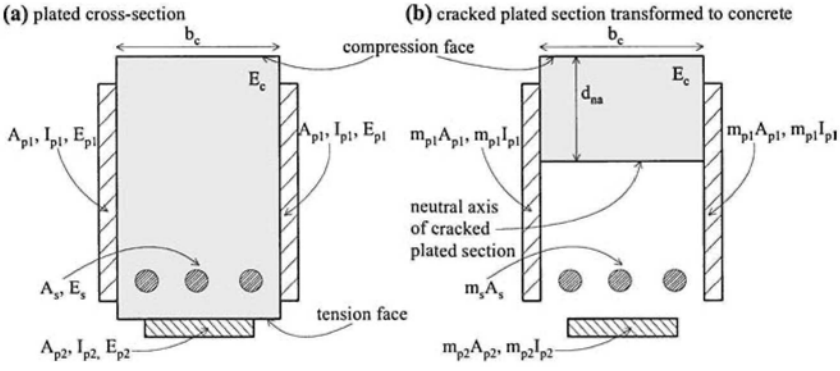

Figure 6.7 Cracked plated section

If an RC structure is plated soon after it has been built so that creep and shrinkage will be significant after plating, then it will be necessary to ensure that at the plate end

$$\frac{M_{short}}{(EI)_{short}} + \frac{M_{creep}}{(EI)_{creep}} \leq \frac{f_{cb}}{f(M_p) + f(P_p)} - \chi_{shrink} \qquad 6.5$$

It is then a question of terminating the plate at a position along the beam where the increase in the moment due to the live load M_{short} plus that due to dead load and sustained live load if applicable M_{creep} is less than the curvature capacity reduced by shrinkage.

6.3.3.2 PE debonding design for short term loads

Let us consider an RC structure that is plated many years after it has been built so that any additional creep and shrinkage after plating can be assumed to be negligible. Let us also consider the case when the beam or slab is not propped prior to plating so that the unplated beam is resisting its dead load prior to plating, in which case the plated structure will only be resisting the live load. Under these circumstances, which are probably common, Eq. 6.5 becomes

$$\frac{M_{short}}{(EI)_{short}} \leq \frac{f_{cb}}{f(M_p) + f(P_p)} \qquad 6.6$$

It may be worth emphasising that the left had side of Eq. 6.6 deals with the cross-sectional properties of the whole plated beam whilst the right hand side deals with those of an individual plate. If the beam is propped prior to plating, which may be required if the structure is plated to reduce deflections or crack widths, then M_{short} in Eq. 6.6 will have to include the dead load as well as the live load or $M_{creep}/(EI)_{creep}$ included on the left hand side for the dead load if creep can still occur as in the following section. Either way this would mean extending the plate further. It is interesting to note that it was shown in Sections 3.4.1 and 3.4.2 that with regard to IC debonding it is better to plate an unpropped beam. The same conclusion has been

drawn for PE debonding. Hence wherever possible, unpropped beams or slabs should be plated.

For design purposes, Eq. 6.6 can be written in the following form which is applicable to structures in which creep and shrinkage do not occur after plating

$$M_{short} \le \frac{(EI)_{short} f_{cb}}{f(M_p) + f(P_p)} \qquad 6.7$$

so that the plate end is terminated in a region where the moment is less than that on the right hand side of Eq. 6.7. As an example, the design consists simply of extending the plate in Fig. 5.10(c) to a position where the applied moment in Fig. 5.10(a) is less than M_{short}, assuming that the moment in Fig. 5.10 is due to the live loads.

6.3.3.3 PE debonding design for long term effects

For structures in which creep and shrinkage occur after plating, Eq. 6.5 can be written in the following form for design

$$M_{short} \le (EI)_{short} \left(\frac{f_{cb}}{f(M_p) + f(P_p)} - \chi_{shrink} - \frac{M_{creep}}{(EI)_{creep}} \right) \qquad 6.8$$

Equations 6.7 and 6.8 should be applied to each individual plate to check for their individual resistance to debonding. It may be worth noting that the flexural rigidities $(EI)_{short}$ and $(EI)_{creep}$ are the flexural rigidities of the whole section as shown in Fig. 6.7(b) and, hence, in its calculation they should include all the plates at that section. However the remaining variables in Eqs. 6.7 and 6.8 relate to a single plate; even the tensile strength of the concrete f_{cb} is the tensile strength of the concrete adjacent to the plate being analysed and, hence, could be varied to allow for deterioration of the concrete in parts of the structure if so required. We are determining the moment at a section that will cause a specific plate to debond. Eventually, all plates will have to be checked for PE debonding.

6.4 PE analysis for bonded interface perpendicular to bending axis

Let us first consider plates that are adhesively bonded to a surface that is perpendicular to the axis of bending, such as the side plate at position A in Fig. 6.8. Tests on adhesively bonded angle sections, described in Section 6.2.2.2, have shown that the flange of the angle section that is bonded to the tension face debonds first leaving the angle attached to the beam through the web adhesively bonded to the side. Hence the angle section at position B in Fig. 6.8 is also an example of a plate bonded to an interface perpendicular to the bending axis.

The following PE debonding design rules are given in the form of Eq. 6.7. However if shrinkage and creep occur after plating, the following design rules will have to be adapted to the form shown in Eq. 6.8, where the curvature capacity is reduced by the shrinkage and creep curvature.

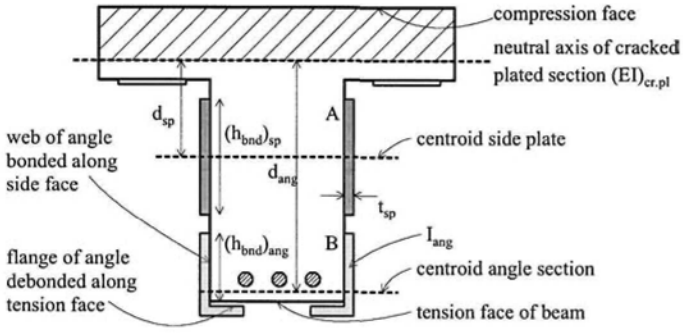

Figure 6.8 Plates bonded to the sides of beam in sagging region

6.4.1 Angle plates

The plate must be terminated at a section where the moment at the plate end is less than the PE debonding moment capacity $(M_{PE})_{ang.sp}$ (Nguyen et al 1998)given by the right hand side of Eq. 6.9

$$(M_{PE})_{ang.sp} = \frac{K(EI)_{cr.pl} f_{cb} (h_{bnd})_{ang}^3}{E_p \left(2.22 I_{ang} + 0.0185 |d_{ang}| (h_{bnd})_{ang}^3\right)} \qquad 6.9$$

where: K = 0.88 for the mean capacity and 0.40 for the 5% characteristic capacity which can be used for design; $(h_{bnd})_{ang}$ is the depth of the portion of the web of the angle adhesively bonded to the side of the beam as shown in Fig. 6.8; E_p is the Young's modulus of the plate and if it is an FRP plate, it is the Young's modulus in the longitudinal direction of the beam; I_{ang} is the second moment of area of the angle about the centroid of the angle and about an axis parallel to the axis of bending, as shown in Fig. 6.8; and d_{ang} is the distance between the angle centroid and the neutral axis of the cracked plated section. The coefficients 2.22 and 0.0185 in Eq. 6.9 were calibrated from test results in which the flexural rigidity of the cracked plated section $(EI)_{cr.pl}$ was used in this calibration and, hence, this form of the flexural rigidity has to be used in the design. It should be noted that $(EI)_{cr.pl}$ in Eq. 6.9 is the flexural rigidity of the whole cross-section as in Fig. 6.8 which includes all the plates at that section, whereas, the remaining parameters on the right hand side of Eq. 6.9 relate to a single plate.

6.4.2 Side plates

Equation 6.9 is a generic equation as it applies to all plates that are attached to the sides of the beam. Inserting the properties of a flat side plate into Eq. 6.9 gives the following resistance to PE debonding of a side plate (Oehlers et al 2000).

$$(M_{PE})_{sp} = \frac{K(EI)_{cr.pl} f_{cb}}{E_p \left(0.185 t_{sp} + 0.0185 |d_{sp}|\right)} \qquad 6.10$$

where K = 1 for the mean capacity and 0.81 for the 5% characteristic capacity for design. The distance d_{sp} is the distance between the centroid of the side plate and the neutral axis of the cracked plated section, as in Fig. 6.8. This distance remains

positive even when the plate centroid is in the compression zone as in Fig. 6.9 as explained in Section 6.2.1.4. It is interesting to note how Eq. 6.9 has simplified to Eq. 6.10 because the bonded length $(h_{bnd})_{sp}$ is also equal to the width of the plate.

6.5 PE analysis for bonded interface parallel to bending axis

As with plates bonded to surfaces perpendicular to the bending axis, generic design rules have also been developed for plates bonded to surfaces parallel to the axis of bending. These rules apply to angle sections as in Fig. 6.10, channel sections, tension face plates and compression face plates. The following debonding capacities have been given in the form of Eq. 6.7, but if the beam is affected after plating by long term material variations then Eq. 6.8 should be used.

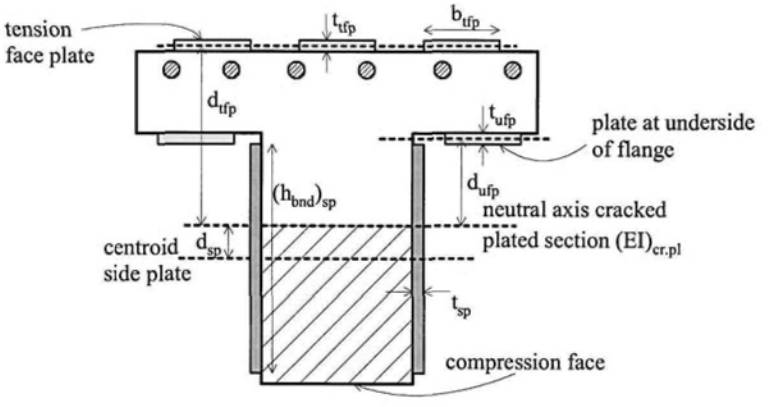

Figure 6.9 Plates bonded to a beam in the hogging region

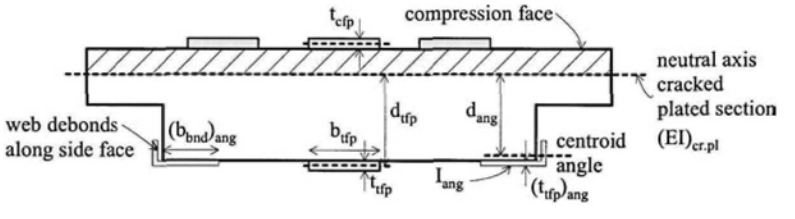

Figure 6.10 Plates bonded to horizontal surfaces in the sagging region

6.5.1 Angle plates

Tests have shown that angle sections tend to first debond at the tension face, as in Fig. 6.8, after which they behave as side plated beams. The following equation (Nguyen et al 1998) was derived for the case where the angle section first debonds from the side, as in Fig. 6.10, so that the plate remains attached to the tension face. None of the tests failed in this way so the scatter has not been determined directly, instead it will be assumed that the scatter is the same as for tension face plates which are just one form of this generic model. The moment at the plate end at which PE debonding occurs is given by

$$(M_{PE})_{ang.tfp} = \frac{K(EI)_{cr.pl} f_{cb} (t_{tfp})^2_{ang} (b_{bnd})_{ang}}{5.69 E_p I_{ang}} \qquad 6.11$$

where: K = 1 for the mean capacity and 0.53 for the 5% characteristic capacity; $(t_{tfp})_{ang}$ is the thickness of the plate in the angle attached to the tension face of the beam as shown in Fig. 6.10; $(b_{bnd})_{ang}$ is the width of the bonded region in Fig. 6.10; I_{ang} is the second moment of area of the angle about the angle centroid about an axis parallel to the axis of bending; and d_{ang} is the distance between the centroid of the angle and that of the cracked plated section. In summary, an angle section or channel section should be checked for initial debonding on the tension face and eventual debonding on the side face using Eq. 6.10 and also for initial debonding on the side face and eventual debonding on the tension face using Eq. 6.11 so that the debonding resistance is the lesser of these two possible modes.

6.5.2 Tension face plates

6.5.2.1 Basic analysis

Equation 6.11 can be used to develop the following mathematical model for tension face plates, although the coefficients in Eq. 6.12 vary slightly from those which would be derived from Eq. 6.11 as they were calibrated using different populations of test results (Oehlers and Moran 1990).

$$(M_{PE})_{tfp} = \frac{K(EI)_{cr.pl} f_{cb}}{0.474 E_p t_{tfp}} \qquad 6.12$$

where: K = 1 for the mean capacity and 0.53 for the 5% characteristic capacity; t_{tfp} is the thickness of the tension face plate as in Fig. 6.10; and d_{tfp} is the distance between the centroid of the tension face plate and that of the cracked plated section.

Equation 6.12 can also be applied to the plate at the underside of the flange in the hogging region in Fig. 6.9 of plate thickness t_{ufp} and at a distance from the neutral axis of d_{ufp}. The stress resultants in a tension face plate are shown in Fig. 6.1(c) where the couple $P_{tfp}t_{tfp}/2$ acts in the same direction as M_{tfp}. The difference between the tension face plate and underside of flange plate in Fig. 6.9 is that the couple $P_{tfp}t_{tfp}/2$ now acts in the opposite direction to M_{tfp} for the underside plate; this reduces the overall moment and, hence, reduces the interface normal debonding stresses in Fig. 6.1(d), leading to a safe design. Hence for underside of flange plates, the plate end moment capacity is given by

$$(M_{PE})_{ufp} = \frac{K(EI)_{cr.pl} f_{cb}}{0.474 E_p t_{ufp}} \qquad 6.13$$

where it can be assumed that the mean and scatter are the same as for the tension face plates, that is K = 1 for the mean capacity and 0.53 for the 5% characteristic capacity. Although it is felt that the scatter may be less as the underside of the flange is probably not influenced as much by the tension reinforcement.

6.5.2.2 Comparison of PE debonding rules for tension face plates

The plate end debonding rules in the design guidelines in Table 1.1 have been briefly discussed and compared in Section 1.6.3 and Fig. 1.36.

The European approach refers to plate end debonding as *concrete rip-off* but does not give any rules to prevent this form of failure. As the European approach requires the plate end to be anchored in an uncracked section, there will be a good chance the plate ends will be terminated near points of contraflexure where the applied curvature is low. Furthermore, the European approach only deals with thin FRP plates so that the curvature capacity from Eq. 6.12 will be high, as the plate thickness is in the denominator. As the European approach requires plated sections of high curvature capacity to be terminated in regions of low applied curvature, it is unlikely that PE debonding will occur using the European design approach. Should it be necessary to terminate the plate beyond the points of contraflexure in the compression face regions as in the left hand hogging region in Fig. 4.17(b), then the PE debonding capacity increases as will be shown in Eq. 6.15. Hence, it is understandable that plate end debonding is not considered in the European approach as quite simply it is not necessary for the anchorage design approach.

The British approach refers to PE debonding as *peeling failure* and uses the interface shear stress $\tau = VAY/Ib$, as described in Section 1.3.4, to prevent plate end debonding. This approach should be used with great caution as plate end debonding occurs in plates in constant moment regions ($V = 0$) as described in Section 6.2.2 and as can be seen in Figs. 1.21, 6.2 to 6.6. Furthermore because of the dependence on the vertical shear force V, this approach may encourage terminating the plate in a high moment, low shear region. For example, in a simply supported beam or in the sagging region of a continuous beam with uniformly distributed loads, this approach encourages the termination of the plate away from the supports or the points of contraflexure, that is closer to the mid-span where the curvatures are greater. The European, Australian and Hong Kong approaches discourage this and it is felt quite rightly.

The Hong Kong approach uses the term *concrete cover separation* for plate end debonding and restricts the moment at the plate end to two-thirds the ultimate moment capacity. Hence, they do restrict the curvature at the plate end. The combination of restricting the curvature at the plate end and the use of only thin FRP plates may be sufficient to prevent PE debonding, but it is felt that this is a rule of thumb approach which may be useful as an initial guideline.

6.5.3 Compression face plates

Tests that directly compared plate end debonding of compression face plates, such as those in Fig. 6.3, with tension face plates found that compression face plates were much less likely to debond, and this was attributed to the reversal of sign of the interface normal stresses I-J-L in Fig. 6.1 as explained in Section 6.2.1.2. To allow for this increase in capacity, Eq. 6.12 was adapted as follows

$$\left(M_{PE}\right)_{cfp} = \frac{K\left(EI\right)_{cr.pl} f_{cb}}{0.208 E_p t_{cfp}} \qquad 6.14$$

where t_{cfp} is the thickness of the compression face plate as in Fig. 6.10. As there were a limited number of tests, the scatter was assumed to be the same as in tension face plates so that $K = 1$ for mean capacity and 0.53 for the 5% characteristic capacity, although it is felt that the scatter for compression face plates will be less as they will not be affected by stress concentrations from the tension reinforcing bars.

6.6 Design for PE debonding

6.6.1 Generic design approach

The full sequence of design that encompasses all forms of debonding is outlined in Section 5.3 and illustrated in Fig. 5.10. In summary, the plate is first designed for its flexural strength for IC debonding at the position of maximum moment, as shown in Fig. 5.10(c). The length of the plate is governed by the region where the flexural strength has to be increased. The plate is then extended, if necessary, to encompass the position of the critical diagonal crack such as position C in Fig. 5.10(c). Extended if necessary to D to ensure a critical diagonal crack does not occur in the unplated region. The plate is then extended further if required, such as to position E, to ensure that the curvature at the plate end does not allow PE debonding. Then if the design is based on the anchorage approach, the plate is extended into a region that is uncracked in flexure and shear.

The design procedure is further illustrated in Fig. 6.11 for a continuous beam with a uniformly distributed dead and live load as well as uniformly distributed concrete shrinkage. The distribution of curvature along the beam is shown in Fig. 6.11(b). This consists of the shrinkage curvature $(\chi_{shrink})_{plate}$ that occurs after plating and which can be obtain from national standards using equations similar to Eq. 6.3. The curvature due to the live load $(\chi_{short})_{plate}$ which depends on the live load distribution as well as the short term Young's modulus of the concrete. And the curvature due to the dead load $(\chi_{creep})_{plate}$ which depends on the dead load distribution as well as the long term Young's modulus for the concrete. The subscript *plate* used in the notation for the curvatures is to remind the reader that it is the curvature after plating that can cause debonding. Also shown is the *anchorage* approach to design in Fig. 6.11(c) and the *hinge* approach in Fig. 6.11(d). The sequence of design from IC, to CDC and then to PE can be seen in Figs. 6.11(c) and (d). The three curvatures at each plate end in Figs. 6.11(c) and (d) are shown as groups of three dots in Fig. 6.11(b) and it is these curvatures that induce PE debonding.

Let us consider the hinge approach in Fig. 6.11(d) and its application to the hogging region over the left support. After the IC and CDC analyses, the plate end is then checked for PE debonding such as at section B-B. It is necessary to ensure that the sum of the three possibly induced curvatures at the plate end, shown as the three dots on the line B-B in Fig. 6.11(b), is less than the curvature capacity which is given by Eqs. 6.9 to 6.15 less the flexural rigidity term $(EI)_{cr,pl}$. It is simply a question of extending the plate towards the point of contraflexure until the applied curvature is low enough. There will always be a solution at the point of contraflexure. The same approach can be applied to the sagging region in Fig. 6.11(d), such as at Section D-D, where once again there will always be a solution at the point of contraflexure.

Let us now consider the left hand hogging region in the anchorage approach in Fig. 6.11(c). The anchorage approach requires that the plate is terminated in an uncracked region which is not cracked through either flexure or shear. Extending the plate to the point of contraflexure will ensure that flexural cracking will not occur at the plate end. It is also unlikely that a critical diagonal crack will occur at the plate end before a critical diagonal crack occurs in the vicinity of the support where the shear is greater, so that cracking due to shear at the plate end is unlikely. The plate end will have to be taken past the point of contraflexure, such as at C-C, in order to fully anchor the plate. In which case, the plate end may be subjected to curvature and subsequently PE debonding, but as it is on the compression face PE debonding is less likely to occur. The same procedure can be applied to the sagging plate in Fig.

6.11(c). However in this case, the plate is being extended into a region where the shear is increasing so that it may be difficult to find an uncracked region in which to anchor the plate.

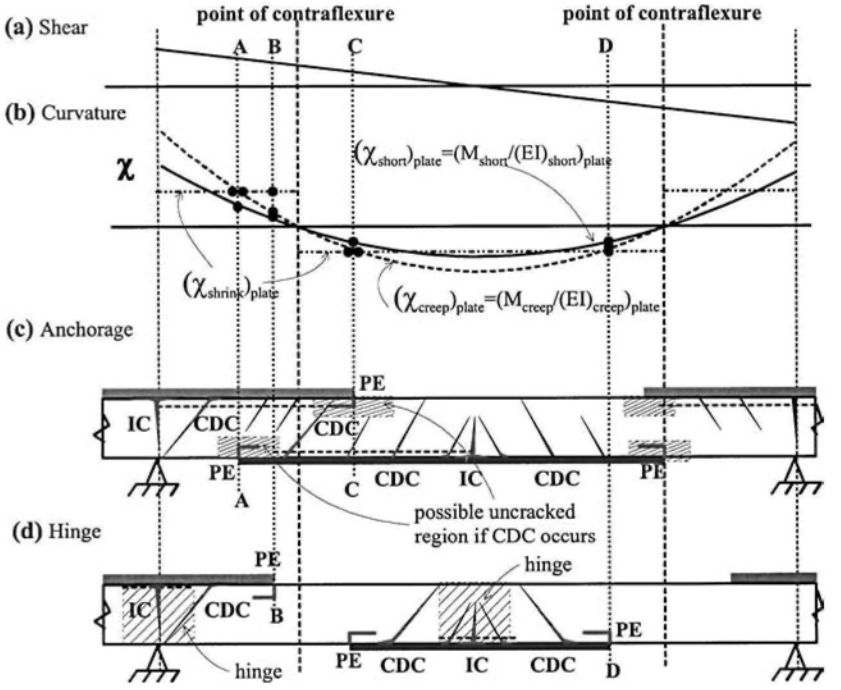

Figure 6.11 Summary of generic design procedure

6.6.2 Interaction between PE, IC and CDC debonding

It is essential, in whichever design approach is being used, to ensure that IC debonding and PE debonding do not coincide as existing design rules do not cover this scenario. In the hinge approach in Fig. 6.11(d), this is achieved by restricting the IC interface cracks to a small region around the position of maximum moment so that the IC interface cracks do not extend to the plate end where PE debonding may occur. In the anchorage approach in Fig. 6.11(c), this is achieved by terminating the plate in an uncracked region where the curvature is low so that PE debonding will not occur in the anchorage length which is required to resist IC debonding.

It can be seen in Fig. 6.11(d) for the hinge approach for partially plated beams that CDC and PE debonding can occur in the same region in the vicinity of the plate end. Research in the early nineties did appear to suggest that there was an interaction between PE and CDC for tension face plates. However, recent advances in the analysis and understanding of CDC debonding that was applied to these original partially tension face plated tests suggested that most of the beams failed by shear failure beyond the plated region, so that CDC debonding was not being measured. Recent tests on partially plated beams with compression face plates and sides plates showed that there was no direct interaction or at least no detrimental interaction between PE and CDC debonding. It is interesting to note that what interaction there was was found to be beneficial. Take for example the situation of extending the

hogging region plate in Fig. 6.11(c) past the point of contraflexure into the compressive face of the sagging region. This is simulated in the test in Fig. 6.12 where the compression face plate is placed over the supports. In this test, the formation of the diagonal crack under the plate end relieved the curvature in the compression face plate and significantly increased the moment to cause PE debonding. It is, therefore, recommended that CDC debonding, IC debonding and PE debonding can be treated independently in the design, and that the design procedure must ensure that IC and PE debonding do not occur in the same region as do both the hinge and anchorage approaches.

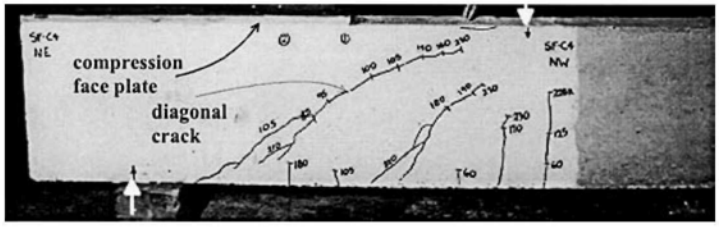

Figure 6.12 Relief of curvature in compression face plate

6.7 Examples

The plated structures first analysed in Chapters 3, 4 and 5 for IC and CDC debonding are now analysed for PE debonding. In this chapter, we will only compare the PE moment capacity with the ultimate flexural capacity of the plated beam $(M_u)_{pl}$ to illustrate the circumstances when PE debonding does and does not affect plating. The full analyses, including the extent of plating are given in Chapter 7. Some of the material and geometric properties of the beam, slab and plates used in the subsequent calculations are constant and are given by the following: E_c = 25.5 GPa; f_{cb} = 2.9 MPa; t_p = 1.2 mm for CFRP plates and 3 mm for steel plates so that they yield prior to IC debonding; and E_p = 160 GPa for CFRP plates and 200 GPa for steel plates.

Table 6.1 summarises the results of the PE debonding analysis for the slabs in Sections 3.5.1.4 and 4.6.2, which were strengthened with CFRP and steel tension face plates respectively in the sagging region. The mean and characteristic PE debonding moment $(M_{PE})_{tfp}$ was calculated using Eq. 6.12 and it can be seen that the characteristic PE debonding moment is less than the flexural moment capacity of the plated section $(M_u)_{pl}$ in both cases. This means that the plate end must be terminated where the applied moment is less than the characteristic PE debonding moment. The axial stiffness E_pA_p of the steel plate is substantially larger than that of the CFRP plate, so that the flexural rigidity $EI_{cr,pl}$ of the steel plated beam is larger than that of the CFRP plated beam. Hence the steel plated beam is stiffer than the CFRP plated beam and more resistant to PE debonding as can be seen in Eq.6.12. However because the steel plate is thicker than the CFRP, this makes it more prone to PE debonding.

Table 6.2 gives the results of the PE debonding analysis for the beams in Sections 4.6.1 and 3.5.2.2, which were strengthened with CFRP tension face plates and underside of flange plates respectively in the hogging moment region. Also included in Table 6.2 are the beams with full depth steel side plated beams in the hogging and sagging moment regions analysed in Sections 3.5.2.3 and 5.6 respectively. Recall that a plate is attached to each side of the web for the full depth

steel side plated beams. Equation 6.12 was used to calculate M_{PE} for the first tension face plated beam, Eq. 6.13 for the underside of flange plated beam, and Eq. 6.10 for the two side plated beams.

Table 6.1 PE debonding analysis of tension face plated slabs

Section	Plate material	$b_p x t_p$ [mm]	$I_{cr,pl}$ x10^6 [mm^4]	$(M_{PE})_{tfp}$ [kNm/m]		$(M_u)_{pl}$ [kNm/m]
				mean	5% char	
3.5.1.4	CFRP	211x1.2	73.5	59.6	31.6	47
4.6.2	Steel	140x3	95.9	24.9	13.2	47

Table 6.2 PE debonding analysis of strengthened beams

Section	Plate mat.'l	Plate location	$b_p x t_p$ [mm]	$I_{cr,pl}$ x10^9 [mm^4]	(M_{PE}) [kNm]		$(M_u)_{pl}$ [kNm]
					mean	5% char	
4.6.1	CFRP	tfp – hog	600x1.2	2.30	1868	990	450
3.5.2.2	CFRP	ufp – hog	795x1.2	2.06	1674	887	436
3.5.2.3	Steel	sp – hog	370x3	2.05	1107	897	403
5.6	Steel	sp – sag	370x3	2.62	200	162	277

The results for the two CFRP plated beams are similar with the tension face plated beam having a higher second moment of area and flexural moment capacity for a smaller cross-sectional area of plate because the plates are farther from the neutral axis maximising the efficiency. However, the underside of flange plated beam will have an improved ductility as the strain in the tension reinforcement will be higher. The mean PE debonding strength for both of these beams is very high and even though the characteristic strength is substantially lower due to the scatter of experimental results, both are much greater than $(M_u)_{pl}$. Hence, for these two beams PE debonding will never govern the location of the plate end.

The situation is different for the two steel full depth side plated beams. The PE debonding resistance in the hogging region will never govern the location of the plate end. However, both the mean and characteristic PE debonding strength in the sagging region are less than $(M_u)_{pl}$ hence, the plate end must be located where the applied moment is less than the characteristic PE debonding moment so that this form of debonding is prevented. The primary factor resulting in the difference in PE debonding resistance in side plated beams is d_{sp}. In the hogging region, where the neutral axis of the fully cracked plated section is in the web, d_{sp} was only 7 mm. However, in the sagging moment region the neutral axis was in the flange and because the centroid of the plates is still in the web, d_{sp} increased to 232 mm.

6.8 References

Oehlers, D. J. and Moran, J. P. (1990). "Premature failure of externally plated reinforced concrete beams." Journal of the Structural Division of the ASCE, Vol. 116, No. 4, 978-995, April.

Oehlers, D.J., Nguyen, N.T., and Bradford, M.A. (2000) "Retrofitting by adhesive bonding steel plates to the sides of R.C. beams. Part 1: Debonding of plates due to flexure." Journal of Structural Engineering and Mechanics, An International Journal, Vol.9, No.5, May, 491-504.

Nguyen, N.T., Oehlers, D.J., and Bradford, M.A. (1998) "Models for the flexural peeling of angle plates glued to R.C. beams." J. of Advances in Structural Engineering. Vol. 1 No.4, pp 285-298.

Chapter 7: Design Examples

7.1 Introduction

This book on the *Design of FRP and Steel Plated RC Structures* deals with a unique and new form of structure, as it has numerous failure mechanisms that other existing codes, such as RC and composite steel and concrete codes, do not address. It is not the aim of this book to promote specific plating techniques nor to promote specific plating materials, as we believe that this can severely restrict the use of plating. The aims of this book are to: explain the fundamental behaviour of plated structures so that the designer develops a feel for plating and, hence, the confidence to apply the plating technique; illustrate the huge variety of plating options that are available and should be considered in addressing a retrofitting problem; provide a generic approach for debonding design that is independent of the design equations available; and to provide comprehensive analysis tools, for those plating options, that not only illustrate what can be done but also what cannot be done, so that they can be applied with confidence. It is hoped that these aims will allow designers to develop their own individual forms of plating, and allow them the freedom to combine different techniques and materials in order to find an efficient solution to their specific plating problem.

It is felt that the debonding failure mechanisms are now well understood and generally agreed upon and these have to be designed for. Design equations, and specifically characteristic or lower bound values, have been provided that can be used in design. No doubt, and hopefully, these design equations will be improved with time, and as more accurate equations become available these can be substituted into the general design procedure. It is felt that a major improvement in quantifying the IC debonding strain will help considerably. For example, if we could reduce the scatter and start designing for IC debonding at strains that are closer to their mean resistances in pull tests then this would allow us to use much thicker plates and higher stresses. There is really little need to improve the PE debonding equations as any refinement will only lead to nominal savings in material, particularly as this form of debonding can be easily prevented by simply terminating the plate in a region of low curvature. The CDC debonding equations are fairly accurate and allow a range of approaches from complex iterative techniques that can be applied to any combination of plates to simpler and direct approaches which may require a larger volume of plates. The fact that the CDC debonding equations have been tied to prestressed code rules suggest that they are more than adequate.

The examples used in this chapter are not meant to reflect the most efficient choice but to simply illustrate and provide some feel for the design procedure. Furthermore, they have not been restricted to within the range of test results from which the design equations were derived. This chapter starts with a summary of the debonding design approaches and design steps, and an illustration of the occurrence of the different forms of debonding. The first structure to be plated is a continuous slab in an internal bay. As slabs are usually designed without stirrups and, therefore, for the concrete shear capacity, CDC debonding is rarely a problem. Hence this design has been used to concentrate on IC debonding of tension face plates and, importantly, the moment redistribution that the IC debonding resistance allows. PE debonding is checked, just to illustrate how it affects the extent of plating. The second structure to

be plated is a continuous beam with stirrups which allows us to go beyond the restriction of just using tension face plates and instead adhesively bond plates to any surface of the beam. This beam is designed without moment redistribution, so that the analysis can concentrate on all the forms of debonding and in particular CDC debonding, where it is shown that CDC debonding may prevent the use of adhesively bonded plates in some regions of a beam. To overcome this problem of premature CDC debonding in beams, plates are bolted to the sides of a continuous beam in the final structure considered.

7.2 Summary of design procedure

The choice of the design philosophy to be used is first discussed, these are then followed by the items that need to be considered in the design steps, and this section is then completed by considering the prevalence of the different debonding modes.

7.2.1 *Design philosophies available*

7.2.1.1 Anchorage approach

The anchorage approach (Section 2.5.1) is illustrated in Fig. 7.1. To induce the maximum strain in the plate, the plate ends are anchored in regions, shown shaded in Fig. 7.1, that need to be uncracked through flexural cracks, flexural/shear cracks, and critical diagonal cracks. This anchorage allows the IC force in the plate to accumulate throughout the plate length. The behaviour is similar to stud shear connectors in composite steel and concrete beams where each individual shear connector contributes to the overall axial force in an element of the composite beam (Section 2.3.2). In tension face plated beams, the *concrete teeth* between flexural and flexural/shear cracks, Fig. 7.1, act as shear connectors, and there is also an additional force at the *end anchorage* that is similar to that obtained from pull tests (Section 2.3.1). The sum of all these shear forces is the maximum force in the plate at mid-span.

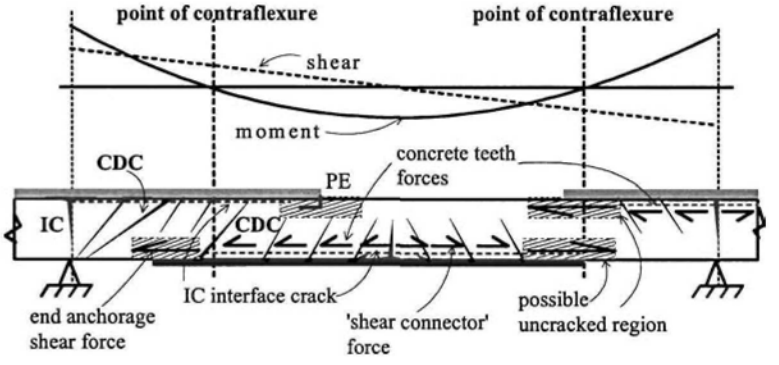

Figure 7.1 Anchorage approach

The anchorage approach requires the IC interface crack, shown as a broken line in Fig. 7.1, to spread over most of the plate. In order to prevent the interaction between IC and PE debonding, the plate end is anchored in an uncracked region where the curvature is small. Hence PE debonding should be checked, or at least

detailed against, by carefully choosing the position of the plate end, to ensure that the plate end is in a position where PE debonding is well designed against. The anchorage approach was developed for tension face plates and it is felt that this design approach should be restricted to tension face plates, as it is unclear whether the shear connector behaviour, through the *concrete teeth*, has the same effect with side plates, particularly when part of the side plate is in the compression zone of the beam. A problem may occur in trying to find a suitably uncracked zone, particularly for beams subjected to longitudinally moving loads where there is no stationary point of contraflexure, or for regions of the beam subjected to high vertical shear forces where critical diagonal cracks may occur near the points of contraflexure.

The anchorage approach is important because it achieves the maximum strains in the plate and, hence, minimises the cross-section area of plate required. Furthermore and just as importantly, by maximising the plate strains, the anchorage procedure also maximises the ductility of the structure and the capacity for moment redistribution.

7.2.1.2 Hinge approach

The hinge approach (Section 2.5.2) is illustrated in Fig. 7.2 and differs from the anchorage approach in Fig. 7.1 by allowing the plate to be terminated short of the point of contraflexure. As the plate in the hinge approach is terminated short of the point of contraflexure, that is in a region where there is curvature, PE debonding can occur at the plate end. Therefore, and in order to prevent the interaction between PE and IC debonding, the IC interface cracks must be restricted to a small region, or *hinge,* in the vicinity of the position of maximum moment, as shown hatched in Fig. 7.2. This is achieved by limiting the strain in the plate to that determined directly from pull tests (Section 2.4.3). Hence, the hinge approach restricts the force in the plate to the *end anchorage shear force* in the anchorage approach in Fig. 7.1 without the additional *shear connector forces* from the *concrete teeth*.

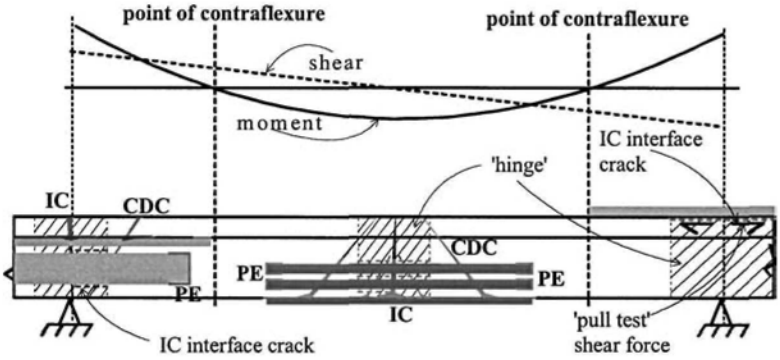

Figure 7.2 Hinge approach

In the hinge approach, the plate end can be terminated short of the point of contraflexure so that the hinge approach tends to concentrate the plate to where it is required for flexure. CDC and PE debonding have still to be checked. Because of the reduced strains allowed in the hinge approach, the hinge approach requires a greater cross-section of plate than the anchorage approach but over a shorter length. The anchorage approach is restricted to tension face plates, whereas the hinge approach

can be applied to plates on any surface such as those shown in Fig. 7.2. In the anchorage approach, the plate strains depend on the *shear connector force* in Fig. 7.1 and, making the analogy with shear connectors in composite steel and concrete beam, this would infer that the plate strains depend on the distribution of the applied loads and beam properties. In contrast, the plate strains in the hinge approach can be determined directly from pull tests. As the IC design strains in the hinge approach are smaller than those in the anchorage approach, the hinge approach will lead to less ductile beams with less ability to redistribute moment.

7.2.2 *Design steps*

The issues and items that may be worth considering in the design procedure are listed in the following design steps.

1) Stress resultants

- Require envelopes of the applied design moments and design vertical shear forces as in Fig. 7.3(a). In developing these envelopes, it may be necessary to consider moment redistribution.
- For flexural strengthening, there may be a need to further consider moment redistribution (Section 3.3.4.2) and its changes to the envelopes, as moment redistribution may allow greater increases in the overall capacity.

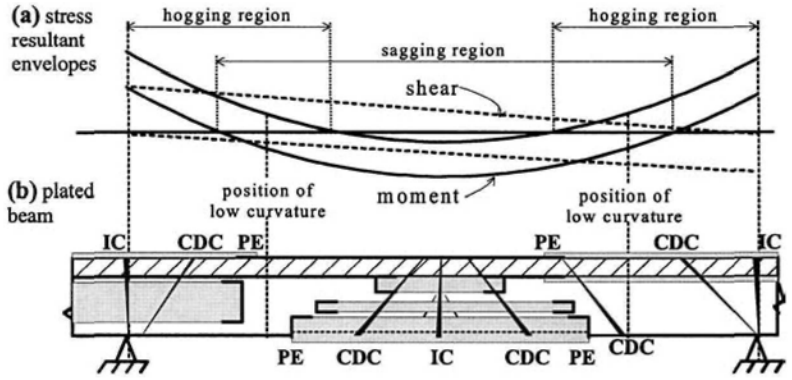

Figure 7.3 Design options

2) Plate material

- Choose type of plate material (Section 1.5) in the hogging and sagging regions in Fig. 7.3.
- For durability and ease of application, FRP may be the preferred option.
- Metal plates may be preferred for ductility and moment redistribution at a joint (Section 3.3.2) and for reducing deflections at serviceability.
- Combinations of plate materials can be considered. For example metal plates at potential plastic hinges where rotation is required (Section 3.3.2) and FRP plates where rotation is not required.

3) Plate position
- Consider plating any face and level of the beam (Section 1.2.2) in Fig. 7.3(b).
- Plate position may be chosen for convenience of adhesive bonding or bolting plate (Section 1.2.1).
- Position may be chosen for mechanical considerations such as flexural strengthening, shear strengthening (Section 1.2.2), increase in flexural rigidity for deflection; maximising ductility and moment redistribution (Section 3.3.4.2); and ensuring reinforcing bars yield prior to plate debonding.

4) Plate cross-sectional area
- Determine for flexural strength (Section 3.4) and sometimes the cross-sectional area for shear strength (Chapter 5).
- For serviceability such as deflections, metal plates may be the preferred option as thick plates may be used which can significantly increase the flexural rigidity.

5) Design philosophy
- Anchorage approach for tension face plates only (Section 2.5.1).
- Hinge approach for all positions of plates (Section 2.5.2).

6) Plate thickness
- Plate thickness governed by IC debonding at positions of maximum moment (Chapter 2).
- IC debonding strain depends on design philosophy (Section 2.5).

7) Plate extent
- Chapter 2: for each individual plate, check for IC debonding at position of maximum moment.
- Chapter 3: extend plate to cover region where flexural increase in strength required.
- Chapters 4 and 5: check for CDC debonding and extend plate to encompass critical diagonal crack.
- Chapter 6: check for PE debonding and extend plate if required.
- For the anchorage approach, extend plate into uncracked region and check for PE debonding if curvature exists at the plate end.

7.2.3 *Occurrence of IC, CDC and PE debonding*

Let us consider the possible debonding modes that can occur in a partially plated beam, as the plate end is extended along the length of the beam as shown in Fig. 7.4(a). The shear load at the point of contraflexure V_{dat} at which debonding occurs is the ordinate in Fig. 7.4(b) and the abscissa is the position of the plate end x.

The typical failure envelope for CDC debonding which was developed in Section 5.2.1.5 and illustrated in Fig. 5.9 has been reproduced in Fig. 7.4(b). Also included in Fig. 7.4(b) are families of individual failure envelopes for IC and PE debonding. The individual IC debonding failure envelopes have been shown as parabolas with a debonding strength of zero when the plate end is adjacent to the position of maximum moment, as the anchorage length is zero, and which increases to a maximum value when the plate end is anchored at a point of contraflexure. This shape was chosen because beam tests and analyses in Section 2.3.2.2 have shown that flexural cracks increase the strain at which IC debonding occurs so that extending the

plate way beyond the effective length of Eq. 2.3 will increase the strains in the plate at debonding. The PE debonding moment capacity is finite and independent of the position of the plate end, so that the shape of the failure envelope is governed by the shear at the datum point to induce that finite moment at the plate end. Hence, the individual PE failure envelopes tend to infinity as the plate end tends to the point of contraflexure.

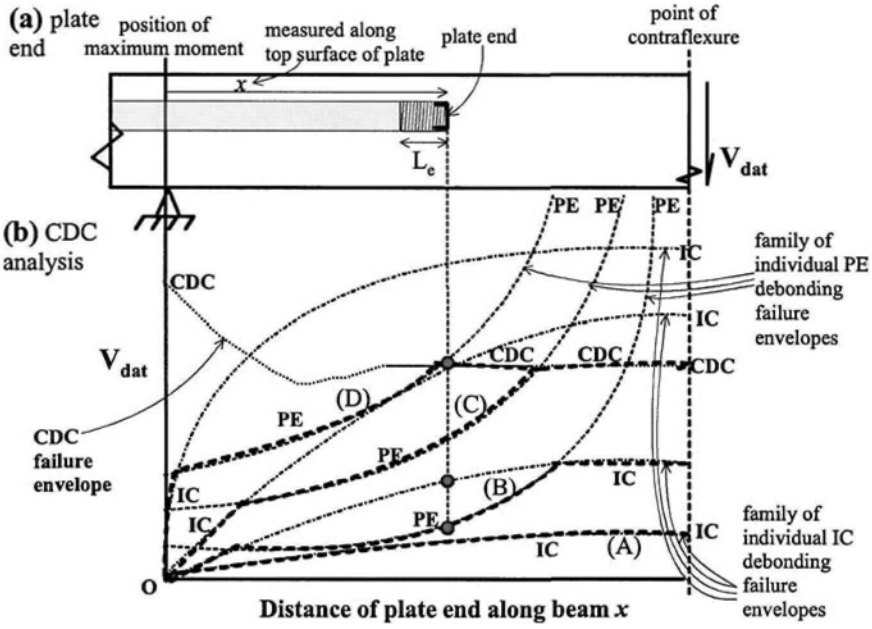

Figure 7.4 Interaction between IC, CDC and PE debonding

For a specific plate cross-section, one individual CDC failure envelope, one individual IC failure envelope, and one individual PE failure envelope control design. For a specific plate end position such as that shown in Fig. 7.4(a), there are three debonding resistances shown as dots in Fig. 7.4(b) which lie on the three individual failure envelopes. The lower bound to these three individual failure envelopes gives the typical shapes of the overall failure envelopes which are shown as thick broken lines in Fig. 7.4(b). The overall failure envelopes marked (A) and (B) fall below the individual CDC envelope and, hence, can be considered to apply to plated slabs where CDC failure rarely occurs. IC debonding will always govern when the plates are ludicrously short, which will never happen in practice. IC debonding can occur at any position of the plate end but PE debonding is more likely to occur when the plates are terminated in the middle regions. It is felt that failure envelopes (C) and (D) are more typical of plated beams where CDC debonding tends to govern fully plated beams and PE and IC debonding govern partially plated beams.

7.3 Continuous slab structure with adhesively bonded plates

This section deals with the strengthening of a slab across one of its spans. The same approach can be applied to the other span as, in practice, slabs have been plated in both directions. As we are dealing with a slab, CDC debonding is of minor importance. As the neutral axis depth factor k_u in a slab is usually quite small this usually allows substantial moment redistribution which will be covered in detail. To help in the analysis, a detailed slab specification is first given. This is then followed by examples of plating just one of the regions, so that moment redistribution is required from the unplated region based on the neutral axis depth approach in Section 3.3.1. After which both regions are plated. The ability to redistribute moment is first based on the neutral axis depth factor approach but then it is checked using the flexural rigidity approach in Section 3.3.2 to ensure that the IC debonding strain capacity can allow the required moment redistribution from the neutral axis depth factor approach.

7.3.1 *Detailed slab specifications*

The slab structure and some of its specifications have already been described in Section 3.5.1.1 and these details are repeated here and considerably expanded to include information useful in the analysis procedure.

7.3.1.1 Slab structure

(a) Slab strength

The internal continuous slab shown in Figs. 7.5(a) and (d) has been chosen to be retrofitted. For ease of calculation, we will assume that it is encastre, subjected to uniformly distributed loads, and we will deal with a 1 m width of slab. The slab has a hogging moment capacity of 41 kNm and a sagging capacity of 31 kNm, so that the distribution of moment at ultimate flexural failure is given by the *strength* curve in Fig. 7.5(b) where the static moment is 72 kNm. If the beam remained elastic, then for the static moment of 72 kNm, the *elastic* distribution in Fig. 7.5(b) would occur, where the hogging moment is twice the sagging moment (for this case of an encastre beam with uniformly distributed loads). The *strength* line differs from the *elastic* distribution, requiring a moment redistribution of 15% from the hogging region.

(b) Applied loads

The static moment capacity is 41+31=72 kNm which implies a uniformly distributed load of 22.9 kN/m to cause failure, and which induces the vertical shear distribution shown in Fig. 7.5(c) with a maximum shear of 57 kN. Of the 22.9 kN/m applied uniformly distributed ultimate load, we will assume that 10.4 kN/m is due to dead load and the remainder of 12.5 kN/m is due to live load. For serviceability, we will assume the unfactored dead load is 6.7 kN/m and this load will be used to determine the residual stresses prior to plating.

(c) Distribution of moment

To assist in the ensuing plating calculations, for a continuous beam with uniformly distributed load, the distance of the point of contraflexure from the nearest support L_{poc} in Fig. 7.5(b) is given by

$$wL_{poc}^2 - wL_{poc}L - 2M_h = 0 \qquad 7.1$$

where w is the applied uniformly distributed load, L is the span of the beam and M_h is the hogging moment at the support which is input as a negative value. Furthermore, the variation of the applied moment along the length of the beam M_x is given by

$$M_x = M_h - \frac{wx^2}{2} + \frac{wLx}{2} \qquad 7.2$$

where x is the distance from the nearest support, hogging moments are negative and sagging moments are positive.

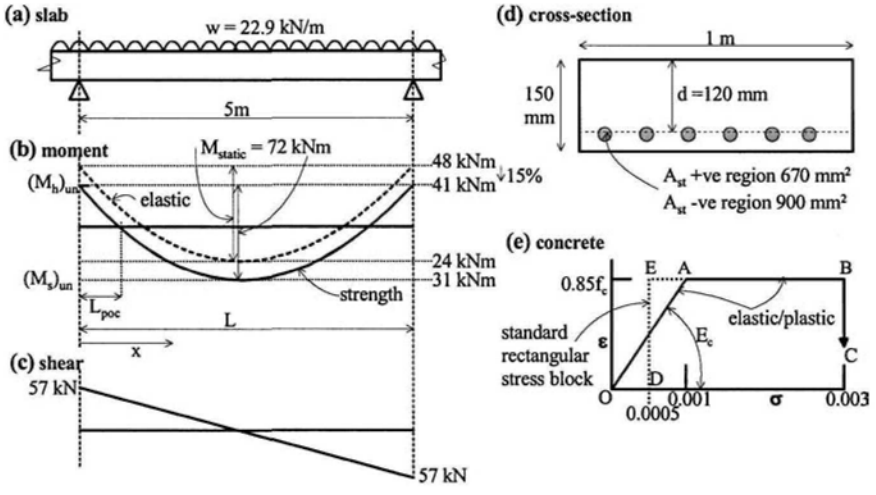

Figure 7.5 Slab structure

7.3.1.2 Reinforced concrete material properties

Concrete cylinder compressive strength f_c = 30 MPa; short term Young's modulus of concrete E_c = 25.5 GPa; long term Young's modulus of concrete = 13 GPa; tensile strength of concrete f_t = 2.2 MPa; indirect or Brazilian tensile strength of concrete f_{cb} = 2.7 MPa; depth of concrete rectangular stress block at concrete crushing = 84% of the effective depth of the slab; elastic/plastic concrete stress/strain distribution shown in Fig. 7.5(e); short term modular ratio (E_s/E_c) m_{short} = 7.8; long term modular ratio m_{long} =15.4; yield strength of reinforcing bars f_y = 400 MPa; Young's modulus of reinforcing bars E_s = 200 GPa. The shrinkage strain after plating is negligible, that is $\varepsilon_{sh} \rightarrow 0$.

7.3.1.3 Unplated slab mechanical properties

(a) Hogging section

Hogging moment capacity $(M_h)_{un}$ = 41 kNm; rigid plastic neutral axis depth as a proportion of the effective depth k_u = 0.14; concrete shear capacity from national standard $(V_c)_{code}$ = 119 kN; short term second moment of area of cracked section transformed to concrete $(I_{cracked})_{short}$ = 65.0x10^6 mm^4; elastic neutral axis depth of cracked section short term $(n_{crack})_{short}$ = 34.6 mm; $(EI_{cracked})_{short}$ = 1.66x10^{12} Nmm^2; long term second moment of area of cracked section transformed to concrete

$(I_{cracked})_{long}$ = 108x10^6 mm^4; elastic neutral axis depth from compression face of cracked section long term $(n_{crack})_{long}$ = 45.5 mm; $(EI_{cracked})_{long}$ = 1.41x10^{12} Nmm^2; static moment to cause residual strains $(M_{static})_{res}$ = 20.9 kNm based on dead load only; support moment to cause residual strains $(M_{hog})_{res}$ = 14.0 kNm; residual strain at tension face using unpropped construction and based on dead load moment of 14.0 kNm and long term properties ε_{res} = 0.00103.

(b) Sagging section

Sagging moment capacity $(M_s)_{un}$ = 31 kNm; rigid plastic neutral axis depth as a proportion of the effective depth k_u = 0.10; concrete shear capacity from national standard $(V_c)_{code}$ = 108 kN; $(I_{cracked})_{short}$ = 51.3x10^6 mm^4; elastic neutral axis depth from compression face of cracked section short term $(n_{crack})_{short}$ = 30.6 mm; $(EI_{cracked})_{short}$ = 1.31x10^{12} Nmm^2; $(I_{cracked})_{long}$ = 87.4x10^6 mm^4; elastic neutral axis depth of cracked section long term $(n_{crack})_{long}$ = 40.5 mm; $(EI_{cracked})_{long}$ = 1.14x10^{12} Nmm^2; static moment to cause residual strains $(M_{static})_{res}$ = 20.9 kNm based on dead load only; support moment to cause residual strains $(M_{hog})_{res}$ = 14.0 kNm; residual strain at tension face using unpropped construction and based on dead load moment of 7.0 kNm and long term properties ε_{res} = 0.00067.

7.3.1.4 Plate material properties

(a) Typical IC debonding strains

Examples and ranges of IC debonding strains are given in Table 7.1. Chen and Teng's results are based on the α values in columns 4 and 7 in Table 2.1 and use a value of b_p/b_c = 0.5 in Eq. 2.2. Chen and Teng's results tend to be on the low side. Hence in order not to be too restrictive in the following calculations, a value of α = 0.5 has been chosen for the pull test strengths, furthermore and in order to remove the iterations from the analysis, it has been assumed that b_p/b_c = 0.5; for example, for the CFRP plate this gives a debonding strain of 0.00267 which is close to Neubauer and Rostasy's (2001) recommendations in Table 7.1. Table 7.1 is also used in the ensuing flexural rigidity moment redistribution analyses to determine whether the plate has the required strain capacity.

Table 7.1 Typical IC debonding strains

Source	IC debonding strains
(1) Chen and Teng pull: 1.2 mm CFRP characteristic	0.0012-0.0019
(2) Chen and Teng pull: 1.2 mm CFRP mean	0.0016-0.0026
(3) Neubauer and Rostasy pull: 1.2 mm CFRP characteristic	0.0026
(4) Chen and Teng beam: 1.2 mm CFRP characteristic	0.0014-0.0023
(5) Chen and Teng beam: 1.2 mm CFRP mean	0.0036-0.0053
(6) Adelaide beam tests: 1.2 mm CFRP plates	0.0025-0.0052
(7) Adelaide beam tests: 3 mm steel plates	0.0044-0.0213
(8) Adelaide beam tests: 2 mm steel plates	0.0059
(9) Adelaide beam tests: 1 mm steel plates	0.0149

(b) Pultruded CFRP plate

Plate thickness t_p = 1.2 mm; Young's modulus of plate E_p = 160 GPa; effective length (Eq. 2.3) L_e = 187 mm; pull test stress at debonding $\sigma_{IC} = \sigma_{db}$ = 427 MPa; pull test strain at debonding $\varepsilon_{IC} = \varepsilon_{db}$= 0.00267; assume ultimate debonding strain in beams for *anchorage approach* is 75% greater i.e. $(\varepsilon_{db})_{anch} = 1.75\varepsilon_{db}$ = 0.00467, which is similar to the strains achieved in the beam tests at Adelaide in Table 7.1.

(c) Steel plate
Yield strength of plate f_{yp} = 300 MPa; Young's modulus of plate E_s = 200 GPa; stress at debonding for a 3 mm plate σ_{db} = 302 MPa from pull tests, that is it yields prior to debonding; effective length for 3 mm thick plate L_e = 331 mm.

(d) Aluminium plates
Yield strength of plate f_{yp} = 125 MPa; Young's modulus of plate E_{al} = 63 GPa; transition thickness between debonding and yield, i.e. when $\sigma_{db} = f_{yp}$, t_p = 5.52 mm; for t_p = 5.52 mm the effective length is L_e = 252 mm.

(e) Prefabricated FRP plates for bolting
Glass/carbon FRP plates have a fracture strength 600 MPa and a Young's modulus of 51 GPa. Glass FRP plates have a fracture strength of 390 MPa and a Young's modulus 25 GPa.

7.3.2 *Plating +ve region only (redistribution from unplated –ve region)*

Let us assume, that for practical reasons such as accessibility, we are only allowed to plate the tension face of the sagging region of the slab as in Fig. 7.6(a). The question is how much can we increase the overall capacity, that is how much can we increase the applied load on the structure. For comparison, we will look at plating the sagging region with FRP plates using the hinge approach, then with FRP plates using the anchorage approach, and finally with steel plates using the hinge approach.

7.3.2.1 Strengthening option based on moment redistribution

(a) Moment redistribution
The distribution at failure of the unplated beam, the *strength* curve in Fig. 7.5(b), is shown in Fig. 7.6(b) as the *unplated strength* curve A. As the maximum hogging moment in the *unplated strength* curve is less than twice the maximum sagging moment (which is the ratio required for an elastic distribution for this encastre beam with a uniformly distributed load), on loading the hogging capacity will be reached first. Therefore, hinges will first occur in the hogging regions which will then redistribute moments to the sagging region. From Section 7.3.1.3(b) for the sagging region, k_u = 0.1. From Fig. 3.14, it can be seen that for k_u =0.1 most national standards will allow 30% redistribution which is what we will use. We will also use the benefit of unpropped construction.

For the hogging region to achieve 30% redistribution from the *elastic* distribution, curve B in Fig. 7.6(b), and end up at $(M_h)_{un}$ = 41 kNm, the elastic moments at the hogging regions must be 41/0.7 = 58.6 ≈ 59 kNm as shown. Those are just two points (both hogging regions) on the elastic distribution, but it is enough to fix the elastic distribution as the sagging moment is half the elastic hogging moment; this gives a static moment of 1.5(58.6) ≈ 88 kNm. Hence, we can in theory increase the static moment from the original unplated static capacity of 72 kNm to 88 kNm, that is by 22%. Reducing the hogging elastic moment by 30%, that is reducing it by 18 kNm from 59 kNm to 41 kNm, drops the *elastic* moment distribution by 18 kNm to the *redistributed for plated beam* curve C in Fig. 7.6(b), so that the sagging moment has increased from 31 kNm to 88-41 = 47 kNm.

There is no point in making the sagging region any stronger. For example, if we attempt to increase the sagging capacity to say 57 kNm instead of the 47 kNm, then the static moment at failure would increase to 57+41 = 98 kNm. So that the elastic hogging moment for this static moment of 98 kNm would be two-thirds of 98

kNm, that is 65 kNm. The percentage redistribution required at the hogging region would be (65-41)/41 = 59% which is greater than the 30% redistribution capacity of the hogging region, that is the hogging region does not have the rotational capacity or ductility required for this 59% moment redistribution. There is no problem in making the sagging region weaker than 47 kNm, as this simply implies that the hogging regions have to redistribute less than their maximum capacity of 30%.

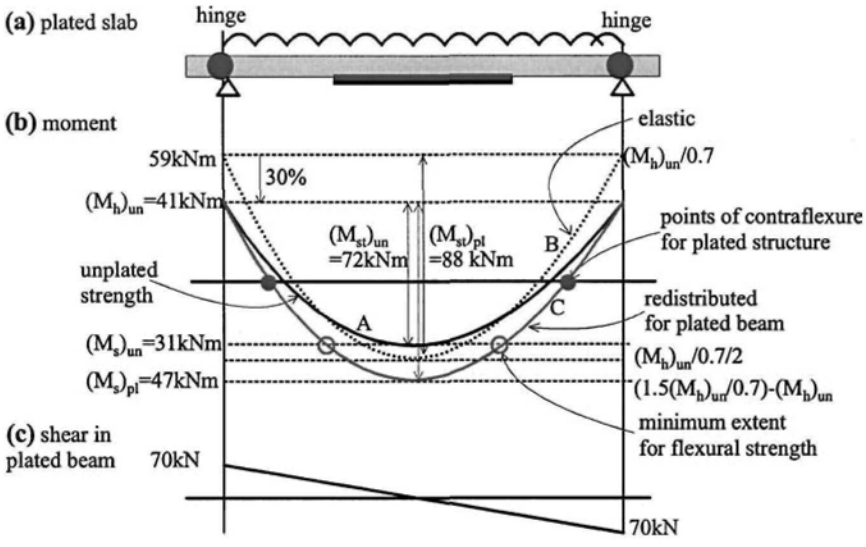

Figure 7.6 Plating sagging region only

To conclude, the analysis in this section has shown how the moment redistribution capacity has restricted the maximum increase in strengthening for the beam where plating is limited to the sagging region. The next step in the analysis is to determine whether plating can increase the sagging capacity by 47-31=16 kNm, that is by 52%. Any plate material can be used for the sagging region, as the sagging region is not required to redistribute moment and, hence, does not have to behave in a ductile fashion. However, FRP plates are often the preferred option due to their durability and ease of application.

(b) Applied loads

The plating proposal discussed in Section 7.3.2.1(a) increases the static moment from the original unplated static capacity of 72 kNm to 88 kNm, that is by 22%, which means that the applied loads can be increased by 22% from 22.9 kNm (Section 7.3.1.1(b)) to 27.9 kN/m. We will assume that this 22% increase in the overall capacity is due to an additional live load. Hence at failure of the plated beam, the dead load remains at 10.4 kN/m (Section 7.3.1.1(b)), whereas, the live load increases to 27.9-10.4=17.5 kN/m, that is the live load is 62% of the total load at ultimate. It is also worth noting that the increase in live load is 40%.

7.3.2.2 Option 1: Hinge approach, FRP plates in sagging region

(a) Flexural capacity (IC debonding)

We need to increase the sagging capacity from 31 kNm to 47 kNm (Section 7.3.2.1(a)). We are using the hinge approach so that the IC debonding strains are restricted to those from pull tests which are ε_{db} = 0.00267 (Section 7.3.1.4(b)). The beam is to be plated as unpropped, in which case the residual stresses due to the dead load are ε_{res} = 0.00067 (Section 7.3.1.3(b)). The concrete material properties are given in Fig. 7.5(e) where the crushing strain of the concrete ε_c = 0.003.

The flexural analysis (Section 3.4.2.1 and Fig. 3.36) is illustrated in Fig. 7.7 where the pivotal point in Fig. 7.7(b) is taken to be the strain in the RC beam at plate debonding $(\varepsilon_{pivot})_{RC}$ = 0.00267+0.00067 = 0.00334. The depth of the neutral axis d_n is varied in the analysis. For each position of d_n, the strain profile Fig. 7.7(b) and consequently the stress profile Fig. 7.7(c) is fixed. Hence, the force in the concrete F_c and reinforcing bars F_s are now known. Therefore as the sum of the forces equals zero, from longitudinal equilibrium, the required force in the plate F_p can be determined. Taking moments of the forces in Fig. 7.7(d) about any convenient axis gives the moment capacity. The neutral axis depth d_{na} is varied until the required capacity of 47 kNm is achieved. From the analysis in which the moment capacity is achieved F_p is known and as ε_{db} and, hence, σ_{db} is fixed, the cross-sectional area of the plate required can be determined.

The results of the flexural analysis are given in row 1 of Table 7.2. The bars have yielded, as the strain in the reinforcing bars ε_{bar} = 0.00249 is greater than the yield strain of 0.002. The maximum strain in the concrete $(\varepsilon_c)_{max}$ = 0.00091 is much less than the crushing strain of 0.003. In fact, the depth of the rectangular stress block, d_y in Fig. 7.7(c), is negative in Table 7.2, which shows that the concrete remains in the pseudo elastic range. It can be seen that plate debonding can occur well before the concrete crushes.

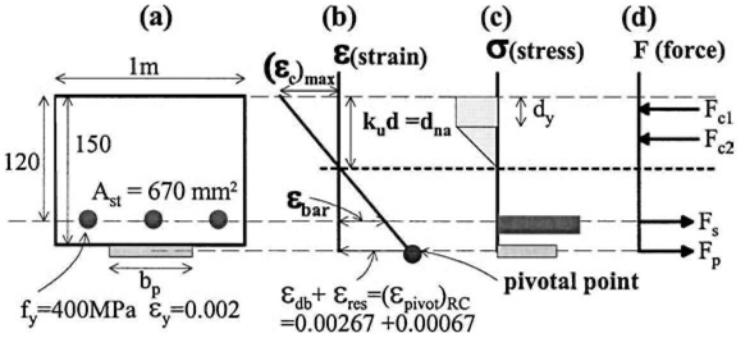

Figure 7.7 Flexural analysis of FRP plated slab in sagging region

From Table 7.2, the width of CFRP plate required is b_p = 198 mm, say 200 mm, for every meter width of slab. This plate has to extend between the points marked O in Fig. 7.6(b) which is the zone where the moment capacity has to be greater than that of the unplated section. The length of the plate required for flexure can be determined from Eq. 7.2, with M_x = +31 kNm, M_h = -41 kNm and w = 27.9 kN/m, and the plate extended at least a further effective length L_e = 187 mm (Section 7.3.1.4(b)) to ensure the plate is fully anchored as shown in Fig. 7.8(c).

Table 7.2 Plating sagging region only - unpropped

Details	$(\varepsilon_{pivot})_{RC}$	$k_u d$ [mm]	ε_{bar}	$(\varepsilon_c)_{max}$	d_y [mm]	F_p [kN]	b_p [mm]	M_{cap} [kNm]
1) FRP hinge	0.00334	32	0.00249	0.00091	-3.33	102	198	47.9
2) FRP anch.	0.00534	27	0.00404	0.00117	3.97	127	141	47.6
3) Steel hinge	0.02067	19	0.0159	0.00291	12.1	123	136	47.6

Figure 7.8 shows the sagging region of the plated beam. The length of the sagging region can be derived from Eq. 7.1 with w = 27.9 kN/m and M_h = -41 kNm. The stress resultants in Fig. 7.8(a) are from the *redistributed for plated beam* curve C in Fig. 7.6. The plate has to extend to where the applied moment is equal to the unplated strength of 31 kNm and then extended an effective length for anchorage as shown in Fig. 7.8(c). It can be seen that 69% of the sagging region has to be plated for flexure, this percentage includes the effective length required for full anchorage.

(b) Shear capacity (CDC debonding)

As the uniformly distributed load at failure of the plated beam is 27.9 kN/m (Section 7.3.2.1(b)), the maximum shear load in the sagging region of the plated beam at flexural failure is 51 kN as shown in Fig. 7.8(a). The concrete shear capacity of the unplated sagging region from a national standard is $(V_c)_{code}$ = 108 kN (Section 7.3.1.3(b)). As the concrete shear capacity of 108 kN is much greater than the maximum applied shear of 51 kN in Fig. 7.8(a), a critical diagonal crack will not form in the plated structure, that is CDC debonding will not occur. Hence, the extent of plating for CDC debonding required in the sagging region is shown as zero in Fig. 7.8(d). It is worth bearing in mind that plating will increase the concrete shear capacity above that of the unplated section of $(V_c)_{code}$ = 108 kN, which further increases the safety factor against CDC debonding. It may also be worth noting that if CDC debonding did control the extent of plating, then the plate may have to be extended by h/2 + L_e as shown in Fig. 5.10(e) or by just h/2 as in Fig. 5.10(f); the latter is the preferred option. However in this example, CDC debonding does not control the extent of plating but the additional lengths are represented in Fig. 7.8(d) just to remind the reader.

(c) Plate extent (PE debonding)

Unlike CDC and IC debonding which depend on the total load being applied at a section, PE debonding only depends on the load or shrinkage applied after plating. In this example, the beam is being plated as unpropped, so it will be assumed that the additional load after plating is only due to the live load of 17.5 kN/m which is 62% of the total applied load (Section 7.3.2.1(b)); this live load induces a moment which is shown as the curve *ultimate live load moment in plated beam* in Fig. 7.8(a). It will also be assumed that there is negligible concrete shrinkage after plating; if shrinkage had occurred after plating then it could have been allowed for using Eq. 6.5.

From Eq. 6.12, the moment at the plate end to cause debonding is M_{PE} = 29.0 kNm. Hence, it is a simple procedure to extend the plate in Fig. 7.8(e) until the applied moment at the plate end due to the live load only is less than or equal to M_{PE}. The position of M_{PE} can be derived from Eq. 7.2 where w is the live load w = 17.5 kNm, and the hogging moment M_h is due to the live load only, hence, M_h=(-0.62x41) The sagging moment is 0.62x47 = 29.1kNm, which is basically M_{PE}; theoretically, PE debonding will not occur so that the plate can be terminated anywhere along the sagging region. It may be worth noting that if the plate extent for PE debonding, $L_{PE}/2$, had been greater than zero there is no need to extend the plate an additional effective length of L_e as the plate end does not have to be anchored for PE debonding.

Furthermore, it is felt that it is not necessary to extend the plate a further distance h/2 as we are not dealing with the vagaries of the position or shape of critical diagonal cracks. From a comparison of the extent of plating required in Figs 7.8(c), (d) and (e), it can be seen that the length of plate required is controlled by the flexural strength requirements in Fig. 7.8(c).

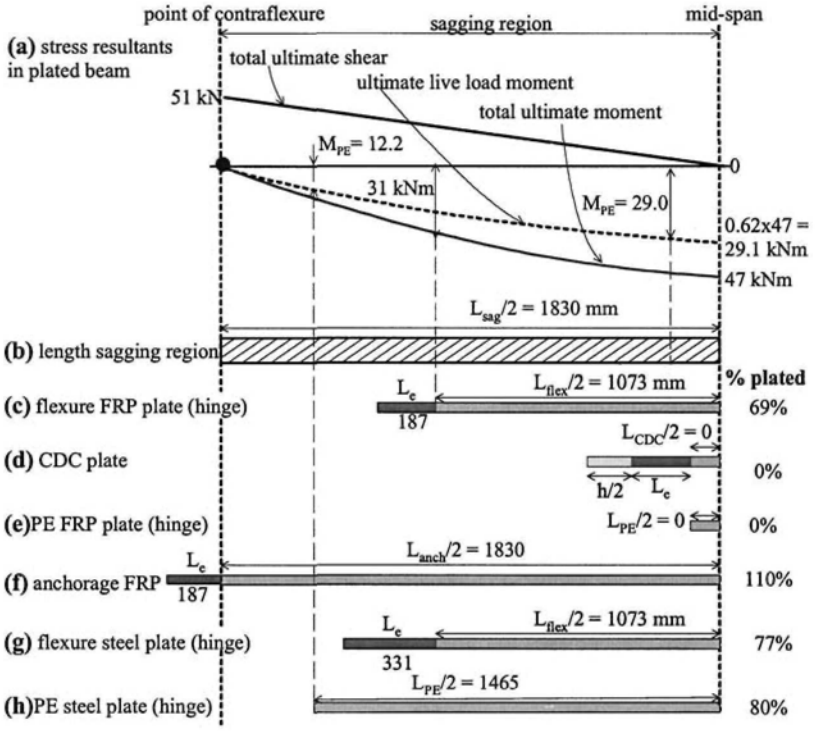

Figure 7.8 Extent of plating in sagging region – plated slab

It may be worth noting that in deriving M_{PE} from Eq. 6.12, the short term flexural rigidity for the cracked plated section was calculated as 1.85×10^{12} Nmm^2. This can be compared with that of the unplated section of 1.31×10^{12} Nmm^2 (Section 7.3.1.3(b)). Hence, the plating has increased the flexural stiffness by 41% which is an indication of the effect of plating on the deflections.

7.3.2.3 Option 2: Anchorage approach, FRP plates in sagging region

(a) Flexural capacity (IC debonding)

It is required to increase the sagging capacity from 31 kNm to 47 kNm (Section 7.3.2.1). As we are using the anchorage approach, the IC debonding strain can be increased to ε_{db} = 0.00467 (Section 7.3.1.4(b)). The beam is also to be plated as unpropped, in which case the residual stresses due to the dead load are ε_{res} = 0.00067 (Section 7.3.1.3(b)).

The flexural analysis is the same as in Fig. 7.7 except that the pivotal point now occurs at $(\varepsilon_{pivot})_{RC}$ = 0.00467+0.00067 = 0.00534. The results for this anchorage approach are given in row 2 of Table 7.2 and are worth comparing with those in row 1

which are the results for the hinge approach. It can be seen that using a larger plate debonding strain in the anchorage approach has substantially increased the strain in the reinforcing bars ε_{bar} so that there is little chance of IC debonding prior to the reinforcing bars yielding. There is a marginal increase in the concrete strains $(\varepsilon_c)_{max}$ but they are still well below the crushing strain of 0.003. The width of plate required has reduced from 198 to 141 mm per meter width of slab. The extent of plating required for flexure would be the same as that in the previous example shown in Fig. 7.8(c), as both the distribution of applied moment and the increase in the flexural strength are the same. However, this is irrelevant for the anchorage approach as, to achieve the increased plate strains, the plate has to be anchored beyond the point of contraflexure as shown in Fig. 7.8(f).

(b) Shear capacity (CDC debonding)

Even though the plate has been extended beyond the point of contraflexure in Fig. 7.8(f) and into the hogging region, the shear at the plate end of 56 kN is still considerably less than the concrete shear capacity $(V_c)_{code}$ of the hogging region of 119 kN (Section 7.3.1.3(a)). Hence CDC debonding will not occur.

(c) Plate extent (PE debonding)

The plate end has been terminated slightly beyond the point of contraflexure on the compression face of the hogging region to allow the plate to be fully anchored. Hence the plate end is now subject to some curvature, so Eq. 6.14, for compression face plates, could be used to determine the moment at the plate end to induce PE debonding. However, the combination of thin FRP plates, termination in a region of low curvature and in a compression face would suggest that PE debonding is very unlikely to occur.

As confirmation of the assumption above. From Eq. 7.2, the moment at the plate end is –6.3 kNm. A lower bound to the resistance to PE debonding can be derived by using the flexural rigidity of the cracked unplated section of 1.66×10^{12} Nmm^2 (Section 7.3.1.3(a)) into Eq. 6.14; this is a lower bound as plating will increase the flexural rigidity. This gives a PE capacity of –59 kNm which is much greater than the applied moment of –6.3 kNm. Hence PE debonding will not occur and, more importantly, there should be no interaction between PE and IC debonding in the anchorage zone.

7.3.2.4 Option 3: Hinge approach, steel plates in sagging region

(a) Flexural capacity (IC debonding)

It is required to increase the sagging moment capacity from 31 kNm to 47 kNm (Section 7.3.2.1).

Based on pull test results (as this is a hinge approach), a steel plate thickness of 3 mm was chosen so that the plate yields prior to IC debonding (Section 7.3.1.4 (c)). This means that if this steel plate was bonded to a concrete block and tested in a pull test as in Fig. 2.11, the plate above the block would yield and eventually fracture at very high strains without IC debonding, so that the strain at failure could be considered to be very large. However, this does not always occur in beams, as it has been found in beam tests that the plates do detach after yielding has occurred due to IC debonding. The beam test results in row 7 of Table 7.1 show that, in beams with 3 mm thick steel plates, IC debonding does occur after yield at strains that ranged from 0.0044 to 0.0213. To demonstrate the effect of very high debonding strains, we will

assume in this analysis that the debonding strain is 0.02. The residual stress remains at $\varepsilon_{res} = 0.00067$ (Section 7.3.1.3(b)).

The flexural analysis is also depicted by Fig. 7.7 expect that the pivotal point is now at $(\varepsilon_{pivot})_{RC} = 0.020 + 0.00067 = 0.02067$ and the results are given in row 3 of Table 7.2. The reinforcing bars have now well and truly yielded and it is also interesting to note that the maximum strain in the concrete has almost achieved the crushing strain of 0.003. However, even with such a large pivotal strain of 0.02067, the concrete has not crushed which suggests that it will rarely crush prior to debonding in practice. The plate width required is 136 mm per meter width of slab. The extent of plating for flexure is shown in Fig. 7.8(g) and is the same as for the FRP plate in Fig. 7.8(c) except that the anchorage length has increased from 187 mm for the FRP plate to 331 mm for the steel plate.

(b) Shear capacity (CDC debonding)

As in Options 1 and 2 in Sections 7.3.2.2 and 7.3.2.3, the shear load to cause a critical diagonal crack is much larger than the applied shear so that CDC debonding will not occur.

(c) Plate extent (PE debonding)

It can be seen in Eq. 6.12, that because the steel plate is thicker than the FRP plates in Options 1 and 2 and because the Young's modulus of the steel plate is larger than that of the FRP plate, the moment to cause PE debonding reduces for the steel plate in comparison to that of the FRP plate. Hence, the steel plate will have to be terminated closer to the point of contraflexure. From Eq. 6.12, $M_{PE} = 12.2$ kNm which requires a half plated length of 1465 mm, that is 80% of the length of the sagging region as shown in Fig. 7.8(h). A comparison of the extent of plating required in Figs 7.8(d), (g) and (h) shows that PE debonding now controls the extent of steel plating which is in contrast to Option 1 shown in Figs 7.8 (c), (d) and (e) where PE debonding did not control the extent of FRP plating.

The 3 mm steel plate increased the flexural rigidity of the cracked section from 1.31×10^{12} Nmm^2 (Section 7.3.1.3(b)) to 2.42×10^{12} Nmm^2 which is an 85% increase as compared with the 41% increase with the FRP plates in Options 1 and 2.

7.3.2.5 Comparison of plating procedures

The three options to plating the sagging region only, in Sections 7.3.2.2 to 7.3.2.4, are compared in Table 7.3. In row 5, is the volume of plate material required which could be considered to be a measure of the material and handling costs; in row 6, this volume is given in terms of the volume in the first option in column 2. In row 7, is the surface area of the interface between the plate and the slab which can be considered to be a measure of the surface preparation required and also the amount of adhesive required; this is given in row 8 as a proportion of the interface area in column 2.

The hinge approach with FRP plates in column 2 in Table 7.3 can be compared with the anchorage approach with FRP in column 3. The hinge approach requires a greater cross-sectional area of plate than the anchorage approach, but the hinge approach requires a shorter length of plate than the anchorage approach. The outcome is that the anchorage approach needs a slightly greater volume of FRP and volume of adhesive and area of surface preparation.

Let us compare the hinge approach with FRP plates in column 2 with the hinge approach with steel plates in column 4. The volume of steel plates is about twice that required for FRP plates which suggests that the handling costs are greater.

However, the steel plates are probably still less expensive than FRP plates, but they do need more surface preparation such as sand blasting. The steel plates have a smaller interface area suggesting less concrete preparation and adhesive.

Table 7.3 Results of plating sagging region only

(1)	(2) Option 1	(3) Option 3	(4) Option 3
(1) Design approach	Hinge	Anchorage	Hinge
(2) Plate	1.2 mm FRP	1.2 mm FRP	3 mm steel
(3) b_p [/m]	200 mm	145 mm	140 mm
(4) L_p (length of plate)	2520 mm	4034 mm	2930 mm
(5) V_p [/m] (plate volume)	604,800 mm^3	701,900 mm^3	1,230,600 mm^3
(6) ratio of V_p	1	1.16	2.03
(7) A_{int} [/m] (interface area)	0.504 m^2	0.585 m^2	0.410 m^2
(8) ratio of A_{int}	1	1.16	0.81

The differences between all three options in Table 7.3 are not great, which suggests that other considerations such as durability, application and ductility may have a much greater influence on choosing the material and design procedure.

7.3.3 *Plating -ve region only (redistribution from unplated +ve region)*

In this example, we will assume that access is only available to plate the hogging regions of continuous slabs. We will assume that further increases in shrinkage after plating will be minimal and that FRP plates are the preferred option as well as unpropped construction. The hinge and anchorage approaches will be applied.

7.3.3.1 Strengthening option based on moment redistribution

(a) Moment redistribution

The FRP plated slab is shown in Fig. 7.9(a). We will assume that FRP plated regions cannot redistribute moment (Section 3.3.1). Therefore, a hinge can only form in the unplated sagging region. The question is how much can we increase the overall capacity of the slab.

The moment distribution in the unplated beam at failure is shown as curve A in Fig. 7.9(b). On loading the unplated beam and because the hogging moment capacity of 41 kNm is less than twice the sagging moment capacity of 31 kNm, a hinge will first form in the hogging region. The only way to prevent a hinge first forming in the hogging region after it has been plated with FRP is to plate the hogging region so that the strength of the plated hogging region is at least twice the strength of the sagging region, that is 62 kNm; this is shown as curve B in Fig. 7.9(b). Curve B represents the minimum strengthening option for the hogging region. If the hogging region were strengthened to less than the minimum requirement of 62 kNm, then a hinge would first form in the FRP plated hogging section whose rotational capacity would not be sufficient to allow the sagging region to reach its ultimate capacity. Hence plate debonding would occur before the theoretical overall capacity of the beam was achieved. Curve B is the minimum strengthening requirement which will achieve a static moment of 31+62 = 93 kNm which is a 29% increase over the unplated static moment capacity.

The strength of the hogging region can be increased above the minimum requirement of 62 kNm in Fig. 7.9(b), as making it stronger will ensure that the hinge first forms in the sagging region. The question is what is the maximum theoretical capacity. The neutral axis depth factor for the unplated sagging region is $k_u = 0.10$ (Section 7.3.1.3(b)) and for which, from Fig. 3.14, most national standards will allow

30% redistribution, which is what we will use here. For the sagging region to redistribute 30% of its moment, will require the elastic moment at the sagging region to be 31/0.7 = 44 kNm. This is one point on the elastic distribution curve C in Fig. 7.9(b) but it also fixes the curve as the maximum hogging moment capacity must be twice the sagging capacity, that is 88 kNm. The static moment capacity of curve C is 44+88 = 132 kNm. Moving curve C upwards to allow for the 30% redistribution from the sagging region gives curve D.

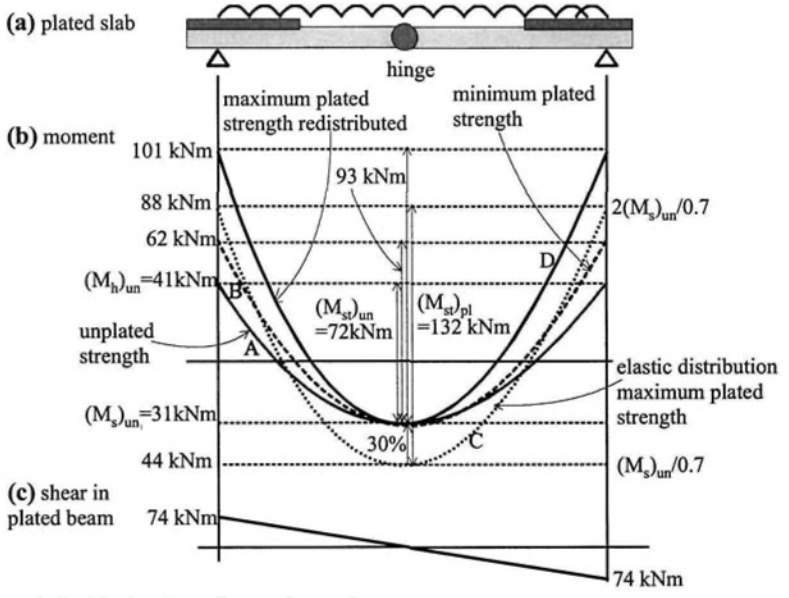

Figure 7.9 Plating hogging region only

Curve D in Fig. 7.9(b), where the hogging capacity is 101 kNm, represents the maximum strengthening that can occur. To verify this statement, let us consider what would happen if the hogging capacity had been increased from 101 kNm to say 122 kNm. The static moment is now 122+31 = 153 kNm, so that the elastic sagging moment is now 153/3 = 51 kNm. To go from the elastic sagging moment of 51 kNm to the sagging strength of 31 kNm requires (51-31)/31 = 65% moment redistribution in the sagging region, which is greater than its capacity of 30%.

The maximum theoretical increase in the static moment of the slab that can be achieved by plating is, therefore, 132-72 = 60 kNm, which is an 83% increase in the static capacity; this requires the hogging capacity to be increased by plating by 101-41 = 60 kNm, that is by 146%. This maximum increase of 83% can be compared with the minimum increase in strengthening of 29% which requires the hogging capacity to be increased by 88-41 = 47 kNm that is by 114%. In this example, we will increase the strength by the minimum requirement of 29% as at this stage of the design it is felt that it would be impractical to increase the hogging strength by 146% as will be discussed later.

(b) Applied loads

The plated static moment of 93 kNm in Fig. 7.9(b) requires a uniformly distributed load of 29.8 kN/m. As the dead load is 10.4 kN/m (Section 7.3.1.1(b)), this plating

option will allow an ultimate live load of 29.8-10.4 = 19.4 kN/m which is 65% of the total load and which is a 55% increase in the live load which may be considered to be substantial.

7.3.3.2 Option 4: Hinge approach, FRP plates in hogging region

(a) Flexural capacity (IC debonding)

The aim is to increase the hogging capacity from 41 kNm to 62 kNm using 1.2 mm thick carbon FRP plates and unpropped construction. The IC debonding strain is ε_{db} = 0.00267 (Section 7.3.1.4(b)) and the residual stress in the hogging section is ε_{res} = 0.00103 (Section 7.3.1.3(a)). The analysis is illustrated in Fig. 7.10 where for a specific depth of neutral axis the required force in the plate F_p is first established and then the moment in the cross-section determined; the neutral axis depth is varied until the required moment capacity is achieved. A detailed description of the analysis procedure is given in Section 7.3.2.2(a).

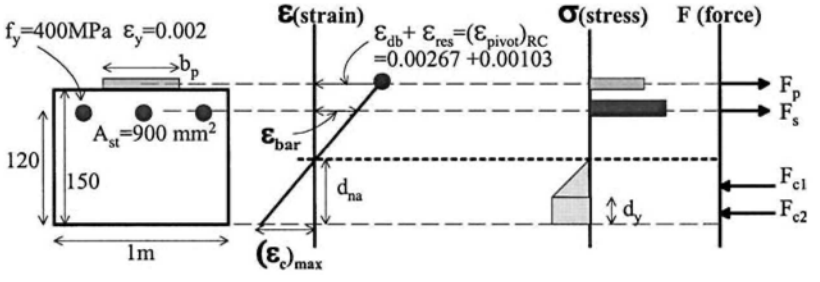

Figure 7.10 Flexural analysis of FRP plated slab in hogging region

The results of the analyses are given in row 1 in Table 7.4 where it can be seen that the reinforcing bars have yielded and the maximum strain in the concrete is well below its crushing strain. The width of plating required is 328 mm per meter width, say 330 mm, and this is required to increase the flexural capacity of the slab from 41 to 62 kNm per meter width in Fig. 7.9(b). Extrapolating this increase in strength would suggest that to increase the capacity to the maximum theoretically allowable of 101 kNm would require thicker plates and hence would be very inefficient and impractical.

Table 7.4 Plating hogging region only - unpropped

Details	$(\varepsilon_{pivot})_{RC}$	$k_u d$ [mm]	ε_{bar}	$(\varepsilon_c)_{max}$	d_y [mm]	F_p [kN]	b_p [mm]	M_{cap} [kNm]
1) FRP hinge	0.00370	36	0.00273	0.00117	5.3	168	328	62.0
2) FRP anch.	0.00570	31	0.00426	0.00149	10.1	164	183	62.1

The extent of plating required for flexural strengthening is illustrated in Fig. 7.11(c). The plate is extended to where the applied moment is equal to the moment capacity of the unplated section of 41 kNm as shown in Fig. 7.11(a) and extended a further distance of the effective length to ensure that it is fully anchored.

(b) Shear capacity (CDC debonding)

The total vertical shear force in the plated beam at failure varies from 43 kN to 74 kN in the hogging region as shown in Fig. 7.11(a). This shear force is considerably less

than the concrete shear capacity of the unplated slab from a national standard $(V_c)_{code}$ = 119 kN (Section 7.3.1.3(a)). Hence CDC debonding will not occur.

(c) Plate extent (PE debonding)

From Eq. 6.12, the moment at the plate end to cause PE debonding is M_{PE} = 38.8 kNm. This is the moment induced in the beam after plating. The ultimate live load to cause failure is 29.8-10.4 = 19.4 kN/m (Section 7.3.3.1(b)), which is 65% of the total load, and is shown as the *live load moment* in Fig. 7.11(a). It is this *live load moment* that occurs after plating which induces PE debonding and, hence, the plate should be terminated where M_{PE} is equal to this live load moment as shown in Fig. 7.11(a). The maximum live load moment is 0.65x62 = 40 kNm and, hence, for all intents and purposes PE debonding will not occur. From Eq. 7.2, the extent of plating required is 16mm. A comparison of Figs 7.11(c), (d) and (e), indicates that the extent of plating is governed by the flexural strengthening requirements.

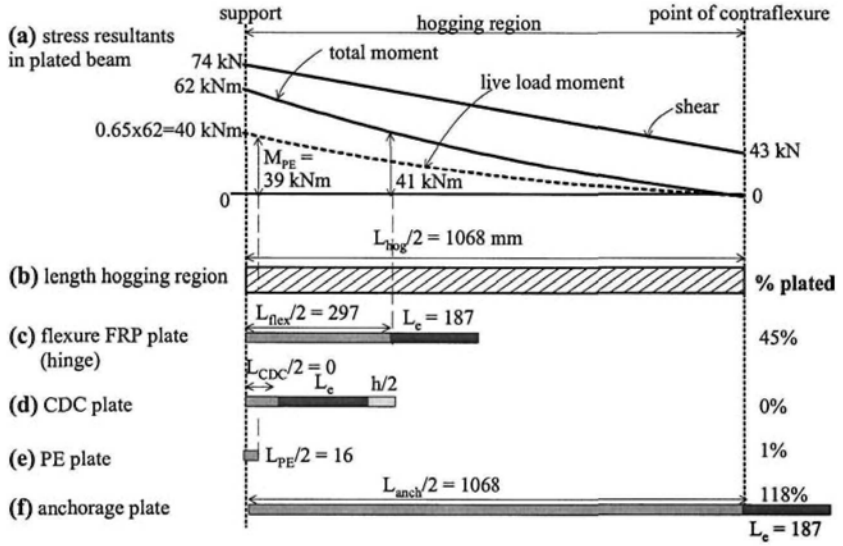

Figure 7.11 Extent of plating in hogging region – FRP plated slab

7.3.3.3 Option 5: Anchorage approach, FRP plates in hogging region

(a) Flexural capacity (IC debonding)

The aims are the same as in Section 7.3.3.2(a) except that the anchorage approach is now being applied, so that an IC debonding strain of 0.00467 (Section 7.3.1.4(b)) can be used with the residual strain of 0.00103 to give a pivotal strain of 0.00570 in Fig. 7.10. The results of the analyses are given in row 2 of Table 7.4. It can be seen that the use of an increased debonding strain has substantially increased the reinforcing bar strain when compared with the hinge approach in row 1 but has only a minor effect on the maximum concrete strain which is still well below its crushing capacity. The anchorage approach has reduced the width of plate required from 328 mm, in the hinge approach, to 183 mm, in the anchorage approach. Because of the narrower width of plate required in the anchorage approach, the anchorage approach is much more capable of achieving, or at least getting closer to, the theoretical maximum increase in the capacity of 101 kNm in Fig. 7.9 than the hinge approach.

(b) Shear capacity (CDC debonding)
The same conclusions as in Section 7.3.3.2(b); CDC debonding will not occur.

(c) Plate extent (PE debonding)
Plate end debonding is unlikely to occur because of the use of thin FRP plates, termination on a compression face, and termination adjacent to point of contraflexure as in Fig. 7.11(f).

7.3.3.4 Comparison of plating procedures
The amount of plating required in the hinge and anchorage approaches in Options 4 and 5 are compared in Table 7.5. The anchorage approach tends to require a larger volume of FRP and adhesive and a greater area of surface needs to be prepared. However the quantities we are dealing with are quite small as the hogging region itself is quite small.

Table 7.5 Results of plating hogging region only

(1)	(2) Option 4	(3) Option 5
1) Design approach	2) Hinge	3) Anchorage
2) Plate	1.2 mm FRP	1.2 mm FRP
3) b_p [/m]	330 mm	185 mm
4) L_p (length of plate)	968 mm	2510 mm
5) V_p [/m] (plate volume)	383,330 mm^3	557,220 mm^3
6) ratio of V_p	1	1.45
7) A_{int} [/m] (interface area)	0.319 m^2	0.464 m^2
8) ratio of A_{int}	1	1.45

7.3.4 ***Plating -ve and +ve regions (redistribution from -ve region)***
In the previous five options in Sections 7.3.2.2 to 7.3.2.4, 7.3.3.2 and 7.3.3.3, plating was deliberately restricted to one region, that is either the hogging region or the sagging region. This allowed a hinge to form in the unplated region so that the neutral axis depth factor approach in national standards (Section 3.3.1) could be used to control the amount of moment redistribution that could occur.

We will now look at plating both the hogging and sagging regions. In this example in this section, we will use steel plates in the hogging region where moment redistribution is required and FRP plates in the sagging region where it is not. We will design the steel plated regions so that the steel plates yield before debonding and make the assumption that these steel plated regions can be treated as ordinary RC sections where the neutral axis depth factor controls moment redistribution (Section 3.3.1). Then in Section 7.3.4.4 we will check, using the flexural rigidity approach (Section 3.3.2), whether the moment redistribution allowed using the neutral axis factor can be achieved.

7.3.4.1 Strengthening option based on moment redistribution
(a) Moment redistribution
The plated slab is shown in Fig. 7.12(a). It will be assumed that the use of FRP plates in the sagging region precludes the formation of a hinge in this region. Steel plates will be used in the hogging region and will be designed to yield before debonding and, hence, it will be assumed that hinges can form in the hogging regions and that the neutral axis depth approach for moment redistribution can be used.

In theory, virtually any amount of strengthening can be achieved by simply adding more and more plates to each region. The following suggesting is, therefore,

one of numerous solutions. The question is, what would be considered to be an efficient form of plating. As we are going to treat the steel plated hogging region as an RC section, then it may be a good idea to minimise the strengthening of the hogging regions so that they can still redistribute 30% of their elastic moment. Using Fig. 3.14 as a guide, we will assume that we can get 30% redistribution if the neutral axis depth factor $k_u = 0.2$. The analysis based on $k_u = 0.2$ is given in Section 7.3.4.2(a). From this analysis, the capacity of the steel plated hogging region is $(M_h)_{pl} = 61$ kNm which is shown in Fig. 7.12(b).

As the plated hogging capacity in Fig. 7.12(b) is $(M_h)_{pl} = 61$ kNm and as it is assumed that this plated hinge can redistribute by 30%, then the elastic moment at the hogging region is 61/0.7 = 87 kNm. This requires an elastic sagging moment of 87/2 = 44 kN and an elastic static moment of 87+44 = 131 kNm as shown in curve B. Allowing the hogging region to redistribute by 30% drops curve B to curve C where the maximum sagging strength is 70 kNm. Hence, plating both regions and using metal plates where moment redistribution is required increases the static moment by 82% from 72 kNm to 131 kNm. This large increase is feasible as the increase is shared fairly uniformly between the two regions; the hogging strength increasing by 49% from 41 kNm to 61 kNm and the sagging strength by 125% from 31 kNm to 70 kNm.

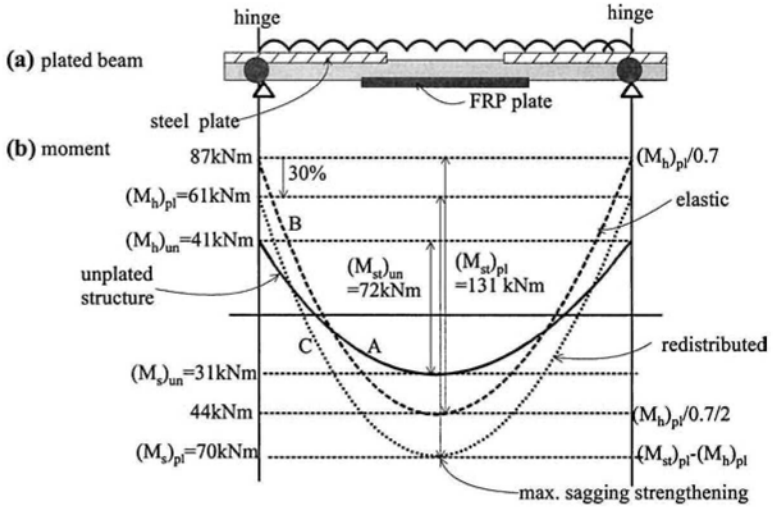

Figure 7.12 Plating hogging and sagging regions – hinge at hogging region

(b) Applied loads

A static moment of 131 kNm requires an ultimate uniformly distributed load of 41.9 kNm. As the ultimate dead load is assumed to be 10.4 kNm (Section 7.3.1.1(b)), the live load is 41.9-10.4 = 31.5 kNm which is 75% of the total load, hence, plating has increased the live load by 152%.

7.3.4.2 Option 6: Steel plating hogging region - hinge approach

(a) Flexural capacity (IC debonding)

The IC debonding strain and residual strain is shown in Fig. 7.13. We are specifically designing for a neutral axis depth of 0.2d to allow 30% redistribution. Hence d_{na} in

Fig. 7.13 is now fixed at 0.2x120 = 24 mm as shown. At this stage we do not know whether concrete crushing will precede plate debonding or vice versa so that both options need to be checked. If we assume debonding occurs first, then the strain profile in Fig. 7.13 goes through the debonding strain at point A and the fixed neutral axis depth at B; extrapolating this strain to the concrete compression face gives the maximum strain in the concrete of 0.00383 which is given in row 1 in Table 7.6. As the theoretical maximum concrete strain 0.00383 is larger than the concrete crushing strain of 0.003, this means that concrete crushing will precede plate debonding. Therefore, the strain profile needs to go through points C and B in Fig. 7.13.

Having now found the correct strain profile in Fig. 7.13, the stress profile is now known, bearing in mind the strain in the plate is the strain in the strain profile less the residual strain of 0.00103. From the stress profile, can be determined the force in the reinforcing bars F_s, and that in the concrete F_c; the latter can be determined using a standard rectangular or plastic stress block because the maximum compression strain is 0.003 although the elastic/plastic distribution shown will give almost identical results. As the longitudinal forces must sum to zero, this gives the force in the plate F_p that is required. As the stress in the plate is known, we can derive the area and width of plate required. The results of the analyses are given in row 2 in Table 7.6 and the extent of plating required in Fig. 7.14(c).

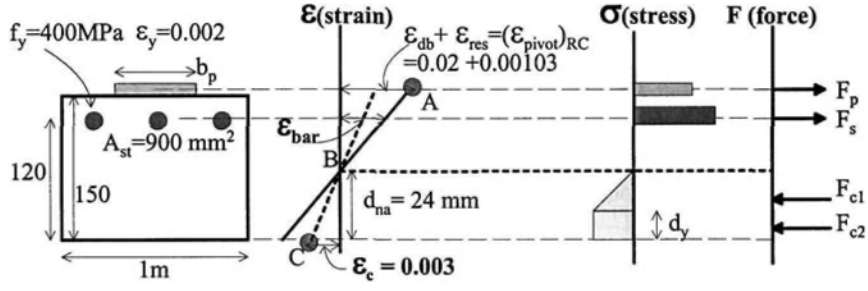

Figure 7.13 Flexural analysis of steel plated slab in hogging region

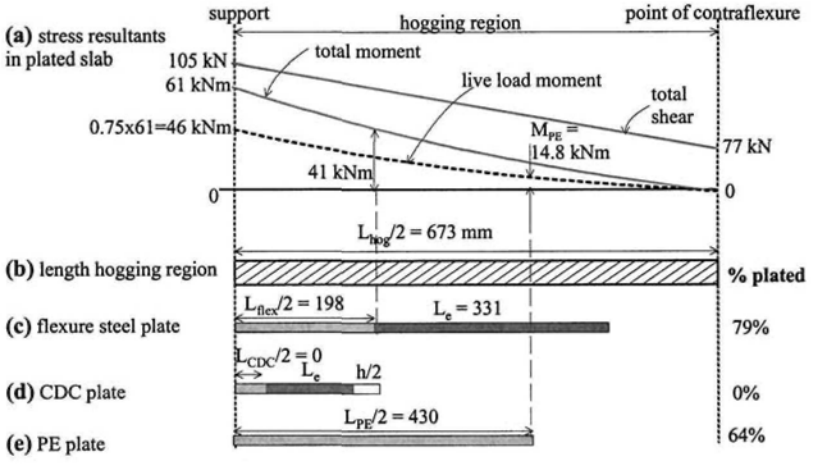

Figure 7.14 Extent of plating in hogging region – steel and FRP plated slab

Table 7.6 Steel plate hogging, FRP plate sagging

Details	$(\varepsilon_{pivot})_{RC}$	$k_u d$ [mm]	ε_{bar}	$(\varepsilon_c)_{max}$	d_y [mm]	F_p [kN]	b_p [mm]	M_{cap} [kNm]
1) Steel hog.	0.02103	24	-	0.00383	-	-	-	-
2) Steel hog.	ε_c=0.003	24	0.0121	0.003	N/A	152	169	61
3) FRP sag.	0.00334	39	0.00243	0.00117	5.7	301	588	70.0

(b) Shear capacity (CDC debonding)

The maximum shear load in the hogging region of 105 kN, as shown in Fig. 7.14(a), is less than the concrete shear capacity of $(V_c)_{code}$ = 119 kN of the unplated section (Section 7.3.1.3(a)). However, as the shear load is approaching the shear capacity of the unplated section, it may be worth determining the increase in the shear capacity due to plating. The simplest approach for estimating the effect of plating is the prestressed code approach in Section 5.2.2.2. For $P_{plate} = F_p$ = 152 kN (Table 7.6), the increase in the concrete component of the vertical shear capacity due to plating is $(V_{incr})_{pp}$ = 0.13(152) = 19 kN (Eq. 5.17), which is a 15% increase in $(V_c)_{code}$. From Eq. 5.18, the vertical shear load to cause CDC debonding is $V_{c\text{-}plate}$ = 119+19 = 138 kN, which is 31% greater than the maximum applied shear load in the hogging region. Hence, it is confirmed that CDC debonding will not occur.

(c) Plate extent (PE debonding)

From Eq. 6.12, M_{PE} = 14.8 kNm. The live load to cause PE debonding of 31.5 kNm is 75% of the total load (Section 7.3.4.1(b)). From Eq. 7.2, the extent of plating is 430 mm as shown in Fig. 7.14(e). Hence the flexural requirement in Fig. 7.14(c) just controls the extent of plating.

7.3.4.3 Option 7: FRP plating sagging region - hinge approach

(a) Flexural capacity (IC debonding)

It is required to increase the sagging capacity from 31 kNm to 70 kNm, as shown in Fig. 7.12(b), using 1.2 mm FRP plates with a pull-test debonding strain of ε_{db} = 0.00267 and on a beam with residual stresses of ε_{res} = 0.00067. The flexural analysis is illustrated in Fig. 7.7 and the steps described in Section 7.3.2.2(a). The results of the analysis are given in row 3 of Table 7.6. The width of FRP plate required is 588 mm per meter width of slab which is not unreasonable as the strength is being more than doubled. The extent of plating for flexure is shown in Fig. 7.15(c).

(b) Shear capacity (CDC debonding)

The vertical shear load within the sagging region, shown in Fig. 7.15(a), is well within the concrete vertical shear capacity of $(V_c)_{code}$ = 108 kNm so CDC debonding will not occur.

(c) Plate extent (PE debonding)

From Eq. 6.12, M_{PE} = 43.7 kNm. The total live load of 31.5 kN/m is 75% of the total load (Section 7.3.4.1(b)). From Eq. 7.2, the extent of plating is 747 mm, as shown in Fig. 7.15(e). It can be seen in Figs. 7.15(c) to (e) that the flexural strengthening requirement determines the extent of plating.

7.3.4.4 Moment redistribution based on flexural rigidity approach

Having designed the plated continuous beam for 30% redistribution from the steel plated hogging region to the FRP plated sagging region, it is now necessary to

determine whether the steel plated hogging region has the rotational capacity or ductility to shed 30% of its elastic moment. The *flexural rigidity approach* of Section 3.3.2 will be used. In the analysis, the sagging FRP region stays linear elastic, that is it follows the path O-A_s-B_s-C_s in Fig. 3.17, whereas the steel plated region moves along the path B_h - C_{deb}. The analysis is fully explained in Section 3.5.4, in which the flexural rigidity in the sagging region in Fig. 3.45(c) is that of O-Cs in Fig. 3.17, and that of the hogging region is the secant flexural rigidity of O-C_{dcb} in Fig. 3.17, that is the flexural rigidity at plate debonding.

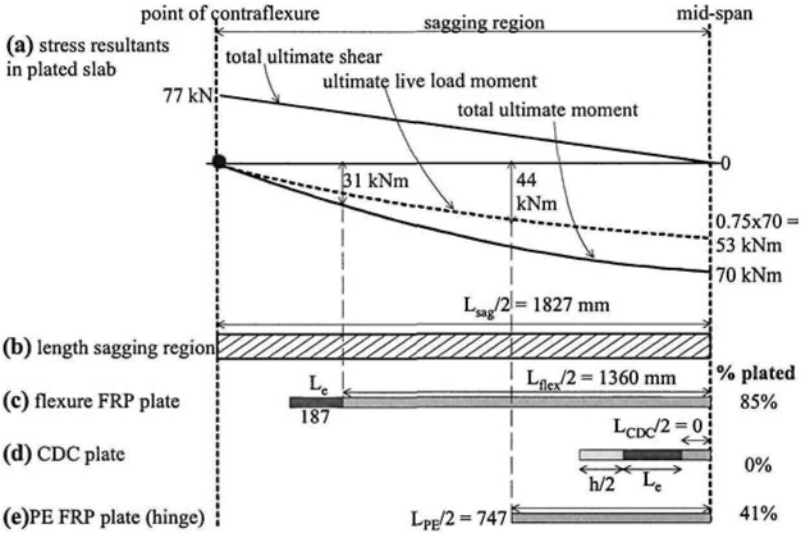

Figure 7.15 Extent of plating in sagging region – steel and FRP plated slab

For any magnitude of applied load, a stiffness analysis program was used to vary the length of the hogging region L_h in Fig. 3.45(c) until it coincided with the position of the point of contraflexure, from which the hogging moment M_h, sagging moment M_s and static moment $M_{static} = M_h + M_s$ is derived. Hence for this continuous beam with a uniformly distributed load, the percentage moment redistribution, %MR, is $(2/3\ M_{static}–M_h)/(2/3\ M_{static})$. The plate strain at debonding ε_{db} was varied; a flexural analysis, such as that depicted by Fig. 7.13, was performed for each debonding strain from which the curvature and moment and, hence, flexural rigidity could be determined for use in the *flexural rigidity approach* of the moment redistribution analysis. The results of the analyses are shown in Fig. 7.16. It can be seen that a debonding strain of about 0.011 is required to achieve 30% redistribution which steel plates can achieve as shown in Table 7.1.

7.3.5 Summary of all plated slab options

The various options for strengthening the slab are summarised in Table 7.7 where L_{pl} = length of plate required; A_{int} = surface area required; ΔM_{st} is the increase in the static moment due to plating. It can be seen that if both regions are plated, then large increases in the overall strength can be achieved particularly if FRP plates are combined with steel plates. The last column, which is the increase in the static

moment divided by the interface area, is an attempt at quantifying the efficiency. Plating the hogging region turns out to be the most efficient simply because the hogging region is shorter than the sagging region so that less plates are required.

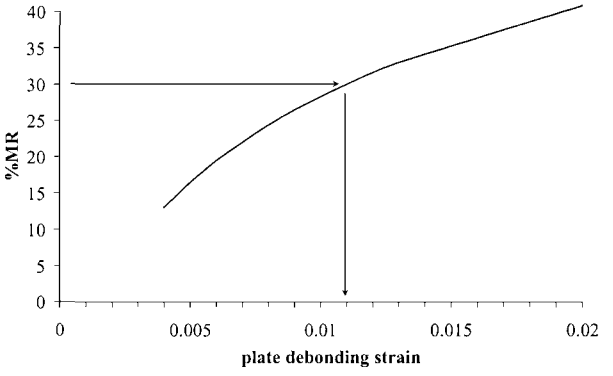

Figure 7.16 Variation in moment redistribution with plate debonding strain

Table 7.7 Results of retrofitting the slab

	Approach	b_p (mm)	$L_{pl}/2$ (mm)	t_p (mm)	$A_{int}/2$ (m^2)	ΔM_{st} /A_{int}
Option 1-3: plating sagging region only with redistribution from hogging ΔM_{static} = 16 kNm (22% increase)	Hinge	200	1260	1.2 FRP	0.274	63
	Anch.	145	2017	1.2 FRP	0.292	55
	Hinge	140	1465	3 steel	0.205	78
Option 4-5: plating hogging region only without redistribution from sagging ΔM_{static} = 21kNm (29% increase)	Hinge	330	484	1.2 FRP	0.160	131
	Anch.	185	1255	1.2 FRP	0.232	91
Option 6-7: plating both regions with redistribution from hogging ΔM_{static} = 59 kNm (82 % increase)	Hinge/hog	170	529	3 steel	0.090	
	Hinge/sag	590	1547	1.2 FRP	0.913	
	Total				1.003	59

7.4 Continuous beam structure with adhesively bonded plates

Section 7.3 dealt with slabs, so that retrofitting was restricted to adhesive bonding tension face plates. As slabs are relatively strong in shear, that is they are much more likely to fail in flexure than form a critical diagonal crack and fail in shear, CDC debonding was shown not to be a problem, which allowed us to concentrate on moment redistribution. Section 7.3 also dealt with residual stresses present prior to plating and their effect on IC debonding, and also on PE debonding and the additional curvature after plating that induces PE debonding.

Section 7.4 will now deal with adhesive bonding plates to RC beams. In contrast to Section 7.3 on slabs: we will assume the beams are propped prior to plating so that there are no residual stresses, which also means that the total applied load will now induce PE debonding; we will retrofit according to the elastic distribution of moment, so that there will be no moment redistribution; dealing with

beams, will allow us to plate the sides of beams as well as their tension faces; as most beams have stirrups, beams are much more likely to form critical diagonal cracks prior to flexural failure, so that CDC debonding can now become a problem and will be dealt with in detail.

The detailed beam specifications are first given. The hinge approach will be used throughout, as plates are adhesively bonded to the sides of the beam and the anchorage approach, as yet, cannot be applied to side plates. The first example uses FRP plates and these are compared with steel plates in the second example.

7.4.1 *Detailed beam specifications*

7.4.1.1 Beam structure

(a) Beam strength

The internal continuous beam is shown in Figs 7.17(a) and (d). We will assume that it is encastre and subjected to uniformly distributed loads. The beam has a hogging capacity of 339 kNm and a sagging capacity of 173 kNm, so that the distribution of moment at ultimate flexural failure is given by the *strength* curve in Fig. 7.17(b) where the static moment is 512 kNm. For all intents and purposes, the *elastic* distribution in Fig. 7.17(b) can be considered to be identical to the strength distribution as the moment redistribution is only 0.6%. Hence, the unplated beam has been designed without moment redistribution.

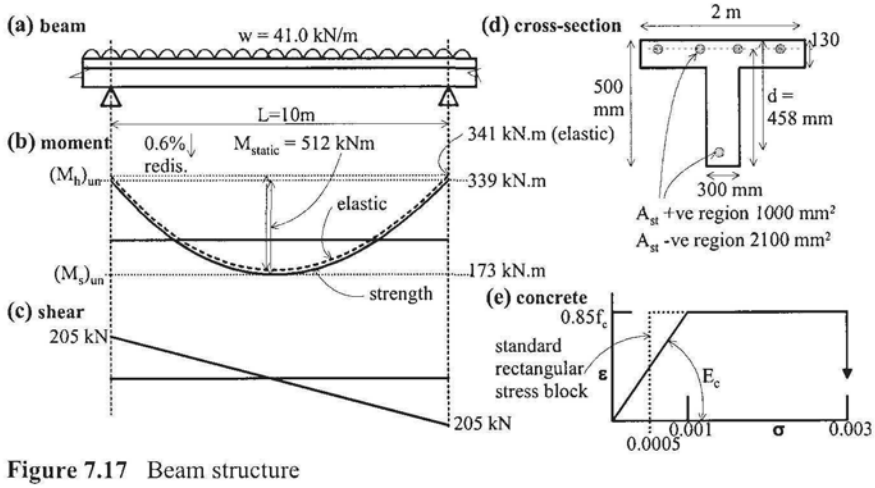

Figure 7.17 Beam structure

(b) Applied loads

The static moment is 512 kNm, which requires a uniformly distributed load of 41.0 kN/m. In the following calculations, there is now no need to break down the ultimate load into live and dead as we are assuming that the beam is propped prior to plating, so that all of the load acts after plating in the PE debonding analyses. Furthermore, as it is propped prior to plating, we can assume that there are no residual stresses to affect the IC debonding calculations, so that there is no need to determine the serviceability loads.

7.4.1.2 Reinforced concrete material properties
These are the same as for the slab in Section 7.3.1.2

7.4.1.3 Unplated beam mechanical properties
(a)Hogging section
Hogging moment capacity $(M_h)_{un}$ = 339 kNm; rigid plastic neutral axis depth as a proportion of the effective depth k_u = 0.29 which for most national standards would not allow much moment redistribution (Fig. 3.14); shear capacity from national standard $(V_c)_{code}$ = 134 kN; assume sufficient stirrups so that $V_s+(V_c)_{code}$ can resist any shear load required; $(I_{cracked})_{short}$ = 1848x10^6 mm^4; $(EI_{cracked})_{short}$ = 4.71x10^{13} Nmm^2.

(b) Sagging section
Sagging moment capacity $(M_s)_{un}$ = 173 kNm; rigid plastic neutral axis depth as a proportion of the effective depth k_u = 0.14 which would allow substantial moment redistribution if so required; shear capacity from national standard $(V_c)_{code}$ = 104 kN; assume sufficient stirrups so that $V_s+(V_c)_{code}$ can resist any shear load required; $(I_{cracked})_{short}$ = 1378x10^6 mm^4; $(EI_{cracked})_{short}$ = 3.51x10^{13} Nmm^2.

7.4.1.4 Plate material properties
These are the same as for the slab in Section 7.3.1.4.

7.4.2 *Hinge approach: FRP side plates in +ve and tension face plates in -ve regions*
7.4.2.1 Strengthening option
We will try and increase the static capacity by 30% from 512 kNm to 666 kNm. As we are maintaining the 2:1 elastic distribution ratio, this will mean increasing the hogging capacity by 30% from 339 kNm to 441 kNm and the sagging moment capacity by 30% from 173 kNm to 225 kNm. To achieve a static moment of 666 kNm, will require an applied load of 53.3 kN/m. As the elastic distribution of moment is being maintained, moment redistribution is not required so that FRP plates can be used anywhere.

7.4.2.2 Option 8: Hinge approach, FRP side plates in sagging region
(a) Flexural capacity (IC debonding)
It is required to increase the sagging capacity from 173 kNm to 225 kNm using 1.2 mm carbon FRP plates with a debonding strain of ε_{db} = 0.00267. As the debonding strain is usually much less than the fracture strain of the FRP plate, the pivotal point is taken as the debonding strain at the level of the bottom of the plate where the strain is the greatest, as shown in the flexural analysis in Fig. 7.18.

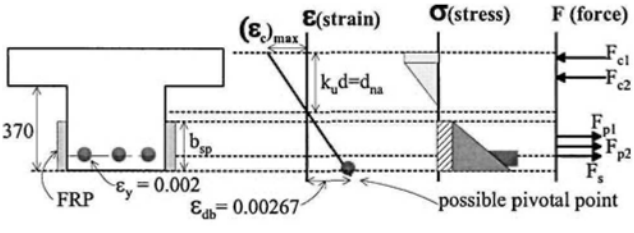

Figure 7.18 Flexural analysis of side FRP plated beam in sagging region

The results of varying the height of the plate, b_{sp} in Fig. 7.18 whilst maintaining the bottom of the plate at the level of the beam soffit, is shown in Table 7.8, where $\varepsilon_{p(top)}$ is the strain at the top level of the plate. A height of plate of 150 mm is required to achieve the moment capacity of 225 kNm which is shown in the row in bold in Table 7.8. The reinforcing bars have yielded but the maximum concrete strain is well below its crushing capacity. The strain at the top of the plate is 66% of the debonding strain. The extent of plating required for flexure is shown in Fig. 7.19(c).

Table 7.8 Results of varying depth of FRP side plate

b_{sp} [mm]	$k_u d$ [mm]	$\varepsilon_{p(top)}$	$(\varepsilon_c)_{max}$	ε_s	M_{cap} [kNm]
50	54.2	0.00237	0.00032	0.00242	198
100	56.6	0.00207	0.00034	0.00242	215
150	**58.5**	**0.00176**	**0.00035**	**0.00242**	**227**
200	60.1	0.00146	0.00036	0.00242	237
250	61.3	0.00115	0.00037	0.00241	243

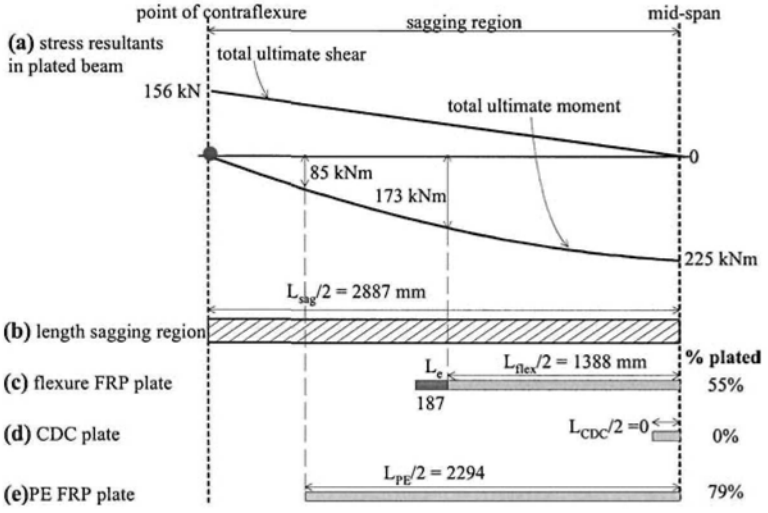

Figure 7.19 Extent of plating in sagging region – FRP side plated beam

(b) Shear capacity (CDC debonding)

The concrete shear capacity for the unplated section from national standards $(V_c)_{code}$ = 104 kN (Section 7.4.1.3(b)) is less than the maximum shear force in the sagging region of 156 kN as shown in Fig. 7.19(a). Hence there is a possibility of CDC debonding.

The results of the iterative CDC analysis are shown in Fig. 7.20 for varying focal point locations z from the point of contraflexure because the location of the CDC in the sagging region is not easily defined with a uniformly distributed load; a more detailed explanation of this type of analysis is described in Section 4.6.2 and Fig. 4.26. It can be seen in Fig. 7.20 that $(V_{dat})_{c\text{-}plate}$ is greater than $(V_{dat})_{applied}$ hence, CDC debonding will not occur in the plated structure. Furthermore, as $(V_{dat})_{c\text{-}unpl}$ is also greater that $(V_{dat})_{applied}$, the CDC analysis suggests that the formation of a CDC will not occur in the unplated beam. This is further demonstrated by comparing the

shear strength of the concrete component of the unplated beam from the CDC analysis, $V_{c\text{-}unpl}$ in Fig. 7.20 and $(V_{max})_{Lo}$, which is the distribution of shear due to the applied load. $V_{c\text{-}unpl}$ exceeds $(V_{max})_{Lo}$ everywhere confirming that a CDC will not occur in the unplated beam. It is interesting to note that $V_{c\text{-}unpl}$ increases near the point of contraflexure where the moment is small. This phenomenon is often indirectly allowed for in national standards by designing for the maximum shear at an effective depth d from the support; whether this should apply to points of contraflexure is debatable. It can be seen that $(V_c)_{code}$ = 104 kN, which is assumed to be constant over the entire sagging region, is less than the applied shear $(V_{max})_{Lo}$ near the point of contraflexure but greater than that near mid-span.

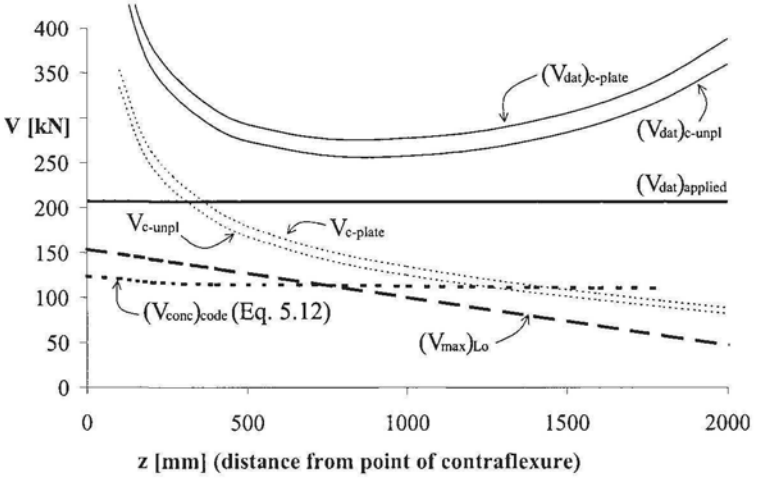

Figure 7.20 Results of CDC analysis for sagging region

The difference between $V_{c\text{-}plate}$ and $V_{c\text{-}unpl}$ in Fig. 7.20 is the increase in the concrete component of the shear capacity due to plating, which can be added to $(V_c)_{code}$ as in Eq. 5.12 to give $(V_{conc})_{code}$ in Fig. 7.20, which shows that CDC debonding would occur as $(V_{conc})_{code}$ is exceeded by $(V_{max})_{Lo}$ near the point of contraflexure. However, at an effective depth d (of approximately 500mm for this beam) from the point of contraflexure at z = 500 mm $(V_{conc})_{code} \approx (V_{max})_{Lo}$ so that CDC debonding may not occur.

To use the simplified *prestressed code approach* described in Section 5.2.2.2, P_{plate} is required. From Fig. 7.18 and Table 7.8, the strain distribution along the side plates is known so that P_{plate} = 128 kN. From Eq. 5.17 the increase in the concrete component of the shear capacity is $(V_{incr})_{pp}$ = 16 kN so that the vertical shear load to cause CDC debonding is 120 kN (Eq. 5.18), which is less than the maximum applied shear in the sagging region at the point of contraflexure (Fig. 7.20) but close to the applied shear at an effective depth from it.

For comparison, the increase in the shear capacity based on the passive prestress approach $(V_{incr})_{pp}$ is shown in Table 7.9 for the side plate depths b_{sp} given in Table 7.8. It can be seen that increasing the depth of a side plate is an effective way of increasing the CDC debonding resistance. In summary, based in particular on the more accurate iterative CDC analysis summarised in Fig. 7.20, CDC debonding will not occur as indicated by the extent of plating shown in Fig. 7.19(d).

Table 7.9 $(V_{incr})_{pp}$ with varying side plate depths

b_{sp} [mm]	P_{plate} [kN]	$(V_{incr})_{pp}$ [kN]	$V_{c\text{-}plate}$ [kN]	$V_{c\text{-}plate}/(V_c)_{code}$
0	0	0	104	1.0
50	48	6	110	1.06
100	91	11	115	1.11
150	**127**	**16**	**120**	**1.15**
200	158	20	124	1.19
250	183	23	127	1.22

(c) Plate extent (PE debonding)

Equation 6.10 gives the plate end debonding capacity for the side plates as 85.0 kNm. For this plated section: K = 0.81; $(EI)_{cr,pl} = 4.31 \times 10^{13}$ Nmm^2 which is a 23% increase over the unplated stiffness (Section 7.4.1.3(b)); $f_{cb} = 2.7$; $E_p = 160$ GPa; $t_{sp} = 1.2$ mm; and $d_{sp} = 362$ mm. Because this beam is propped prior to plating, all of the applied load acts on the plated section to induce PE debonding. Hence, the extent of plating is governed by the total moment as shown in Figs 7.19(a) and (e).

7.4.2.3 Option 9: Hinge approach, FRP tension face plates in hogging region

The aim is to increase the flexural capacity of the hogging region from 339 kNm to 441 kNm using 1.2 mm FRP plates on the tension face.

(a) Flexural capacity (IC debonding)

The flexural analysis is illustrated in Fig. 7.21 where the depth of the neutral axis was varied until the required moment capacity was achieved. When the depth of the neutral axis was $k_u d = 205$ mm in Fig. 7.21: the moment capacity was 449 kNm; this required a plate width of 600 mm; the strain in the reinforcing bars was 0.00229; and the maximum strain in the concrete was 0.00186. The extent of plating required is shown in Fig. 7.22(c).

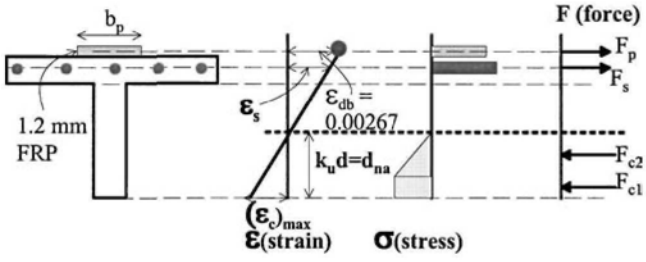

Figure 7.21 Flexural analysis of tension face plated beam in hogging region

(b) Shear capacity (CDC debonding)

The concrete shear capacity of the unplated section from national standards is $(V_c)_{code}$ = 134 kN (Section 7.4.1.3(a)) is less than the shear force in the hogging region as shown in Fig. 7.22. Hence there is a possibility of CDC debonding.

For convenience in the CDC analysis, the datum point will be taken at the point of contraflexure so that $M_{dat} = K_M = 0$, and $V_{dat} = 156$ kN from Fig. 7.22 and K_W is defined by Eq. 5.3, which varies depending on the orientation of the crack as illustrated in Fig. 5.3(c). In this calculation K_W can be taken as Eq. 4.17 and in this analysis the focal point is taken at the position of the support. From Eqs 5.1 and 5.5, the loads to cause cracking and crack sliding, respectively, are calculated using a

spreadsheet analysis and are given by the solid curves in Fig. 7.23 for the plated beam where P_{plate} = 128 kN based on the debonding strain shown in Fig. 7.21. Based on this analysis, $[(V_{dat})_{crit}]_{pl}$ = 112 kN, which is less than V_{dat} = 156 kN and hence, CDC debonding will occur prior to achieving the desired increase in flexural strength.

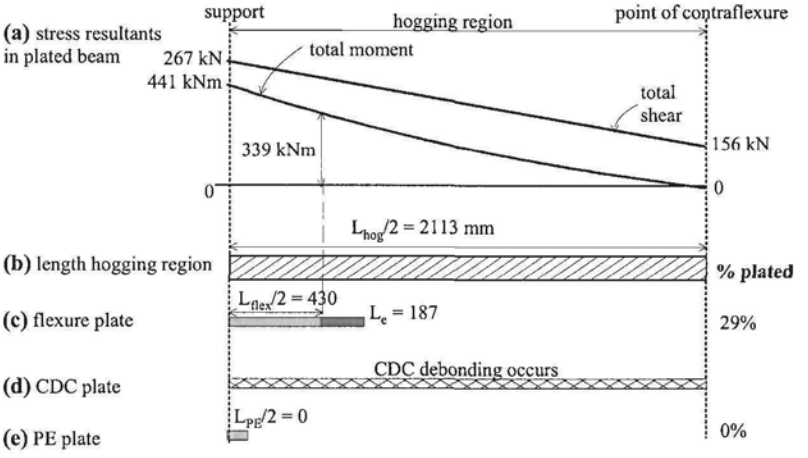

Figure 7.22 Extent of plating in hogging region – FRP tension face plated beam

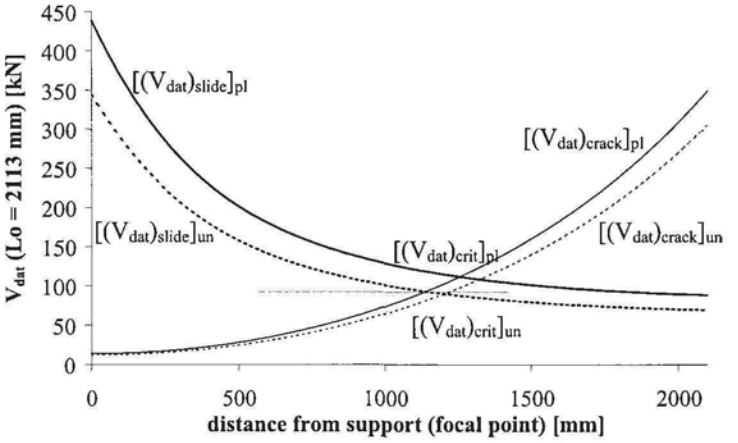

Figure 7.23 CDC analysis of FRP tension face plated beam in the hogging region

For the sake of comparison, Fig. 7.23 also shows the CDC analysis for the unplated beam, where it can be seen that $[(V_{dat})_{crit}]_{un}$ = 90 kN so that from Eq. 5.11 the increase in the concrete component of the shear capacity due to plating is $(\Delta V_{conc})_{pl}$ = 28 kN, which is a 20% increase in $(V_c)_{code}$ for the unplated beam given by national concrete standards. The increase in shear capacity is now compared with the direct approaches, which require the entire sagging region to be plated and fully anchored. Using the *mean approach* of Section 5.2.2.1 that assumes a crack inclination of 57° gives $(\Delta V_{conc})_{pl}$ = 28 kN using Eq. 5.16, which is the same as the increase predicted

using the iterative CDC analysis. From the *prestressed code approach* of Section 5.2.2.2, the increase in the concrete component of the shear capacity due to plating is 16.5 kN (Eq. 5.17), which is conservative compared to the other approaches.

In summary, all of the approaches demonstrated that the plating arrangement illustrated in Fig. 7.21 is not sufficient to increase the concrete component of the shear capacity of the beam in the hogging region to prevent CDC debonding. Hence, an alternative plating arrangement would need to be investigated to develop a valid solution.

(c) Plate extent (PE debonding)

The short term flexural rigidity of the cracked tension face plated beam is 5.87×10^{13} Nmm^2 which is 25% greater than that of the unplated section. From Eq. 6.12, the PE debonding capacity is 923 kNm which is much greater than the maximum moment capacity of 441 kN. Hence PE debonding will not occur.

As summarised in Figs 7.22(c) - (e), CDC debonding is restricting the use of this plating option. Other options must be investigated such as those described in the following sections.

7.4.3 *Hinge approach: steel side plates in +ve and –ve regions*

7.4.3.1 Strengthening option

In this example, we will determine the effect of adhesive bonding 3 mm steel plates over the full depth of the web and on both sides of the web. We will ignore moment redistribution and design for the elastic distribution of moment.

7.4.3.2 Option 10: Hinge approach, steel side plates in hogging region

(a) Flexural capacity (IC debonding)

The flexural analysis is illustrated in Fig. 7.24. Pivoting about the debonding strain of $\varepsilon_{db} = 0.02$ showed that the maximum concrete strain was greater than its crushing capacity of 0.003. Hence, the pivotal point was changed to that of the crushing strain. This gave a moment capacity of 403 kNm with a strain in the reinforcing bars of 0.0061 and that at the top of the plate of 0.0044. The extent of plating required is shown in Fig. 7.25(c).

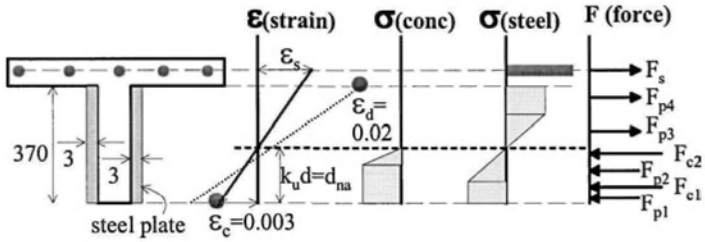

Figure 7.24 Flexural analysis of steel side plated beam in hogging region

(b) Shear capacity (CDC debonding)

As we are dealing with an elastic distribution of moment, the static moment is 1.5x403 = 605 kNm which requires an applied load of 48.4 kN/m. Hence the maximum shear force is 242 kN as shown in Fig. 7.25(a). The concrete shear capacity from a national standard is 134 kN (Section 7.4.1.3(b)) which is much less than the maximum applied shear so that there is a good chance that CDC debonding will occur.

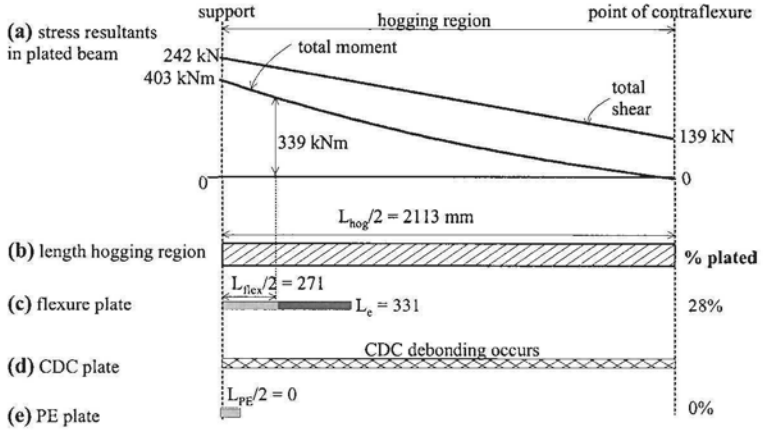

Figure 7.25 Extent of plating in hogging region – full depth steel plates

The CDC analysis procedure in Section 7.4.2.3(b) is used in this example and the results are summarised in Fig. 7.26. With P_{plate} = 666 kN, $[(V_{dat})_{crit}]_{pl}$ = 133 kN and is slightly less than V_{dat} = 139 kN, which was again taken at the point of contraflexure for convenience. Once again, CDC debonding is restricting the use of this plating option. The CDC analysis of the unplated beam is also shown in Fig. 7.26 and from this analysis, the increase in the concrete component of the shear capacity due to plating is found to be $(\Delta V_{conc})_{pl}$ = 54 kN, which is a 40% increase in $(V_c)_{code}$ of the unplated beam in the hogging region. Although the effectiveness of side plates in increasing $(V_c)_{code}$ is demonstrated in this example, it also shows the difficulty of preventing CDC debonding in the hogging region of continuous beams. One method of overcoming this difficulty is to bolt side plates, which is the topic of Section 7.5.

For comparison, the increase in the concrete component of the shear capacity of the beam in the hogging region due to plating is 50 kN using the *mean approach,* and 86 kN using the *prestressed code approach.*

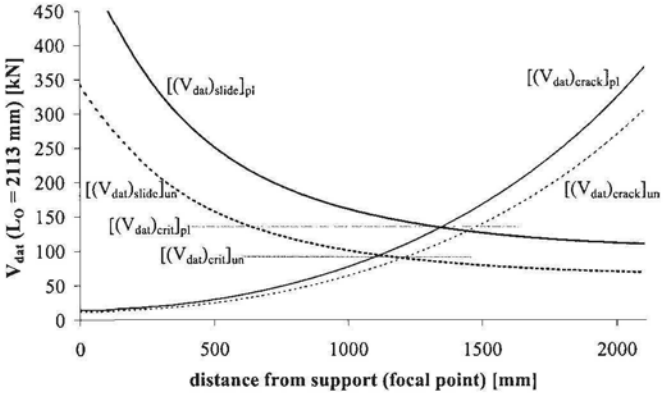

Figure 7.26 CDC analysis of full depth steel side plated beam in the hogging region

(c) Plate extent (PE debonding)
The short term flexural rigidity of the cracked tension face plated beam is 5.24×10^{13} Nmm^2. From Eq.6.10, the PE debonding capacity is 828 kNm which is much greater than the maximum moment capacity of 403 kN. Hence PE debonding will not occur.

As summarised in Figs 7.25(c) - (e), CDC debonding has once again restricted the use of this plating option in the hogging region.

7.4.3.3 Option 11: Hinge approach, steel side plates in sagging region
(a) Flexural capacity (IC debonding)
The flexural analysis is shown in Fig. 7.27. Pivoting about the debonding strain of ε_{db} = 0.02 gave a moment capacity of 277 kNm with a maximum concrete crushing strain of 0.00139. As we are dealing with an elastic distribution of moment, the maximum applied moment cannot be greater than half the maximum hogging moment (Section 7.4.3.2) of 403/2 = 202 kNm. Hence, the sagging flexural capacity is sufficient. The extent of plating is shown in Fig. 7.28(c).

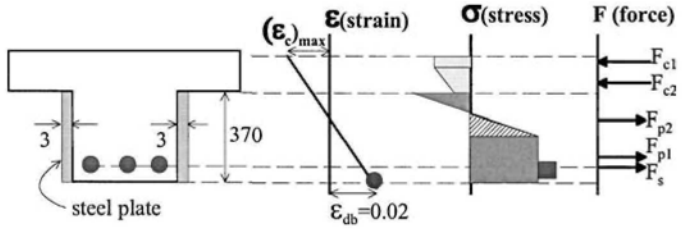

Figure 7.27 Flexural analysis of steel side plated beam in sagging region

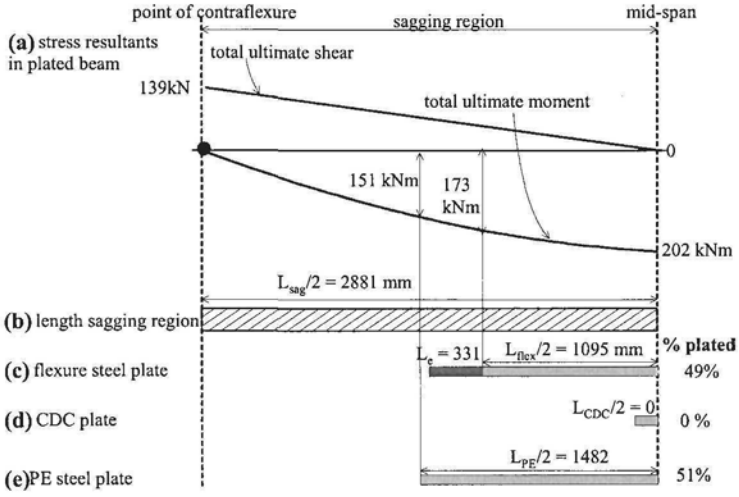

Figure 7.28 Extent of plating in sagging region – full depth steel plates

(b) Shear capacity (CDC debonding)
The CDC debonding analyses for this plating option in the sagging region is the same as that in Section 5.6.1 hence, it is not repeated here. The analyses using the indirect

CDC analysis and direct prestressed code approach demonstrated that CDC debonding will not occur. As the applied load is less in this example, the same conclusion can again be made.

(c) Plate extent (PE debonding)
The short term flexural rigidity of the cracked tension face plated beam is 5.24×10^{13} Nmm^2. From Eq. 6.10, the PE debonding capacity is 151 kNm which requires the extent of plating shown in Fig. 7.25(e).

From Figs 7.28(c) - (e) it can be seen that PE debonding governs the extent of plating for this option in the sagging region. Contrary to the hogging regions, CDC debonding was shown not to occur as the applied shear is less in the sagging region.

7.5 Continuous beam structure with bolted plates

7.5.1 *Detailed beam specifications*

In the retrofitting example of Option 10 in Section 7.4.3.2, it was found that plates could not be adhesively bonded to the hogging regions because of CDC debonding. To overcome this problem, plates will be bolted to these regions. The beam specifications are given in Section 7.4.1 and the properties of the plates are given in Section 7.3.1.4(c) for the steel plates, (d) for the aluminium plates and (e) for the prefabricated carbon/glass FRP plates.

7.5.2 Option 12: Side plates bolted to tension zone in hogging region

From Section 7.4.3.2, it is required to increase the flexural capacity to 403 kNm.

(a) Maximum flexural capacity
The analysis is illustrated in Fig. 7.29. The plate depths are fixed at 150 mm, as can be seen in Fig. 7.29(a), and the plate thickness is varied to achieve the required moment capacity. As the plates are bolted, IC debonding is no longer a problem, which leaves plate fracture and concrete crushing as possible pivotal points. As the strain capacity of steel and aluminium is vary large, the concrete crushing strain was chosen as the pivotal point in Fig. 7.29(b), and the maximum strain in the FRP plate checked to ensure that the FRP plate did not fracture prior to the concrete crushing. For a given plate thickness, the neutral axis depth d_{na} in Fig. 7.29(b) was varied until the longitudinal forces in Fig. 7.29(d) were in equilibrium. Then the resulting moment capacity was derived by taking moments of the forces in Fig. 7.29(d) about any convenient level. The plate thickness was varied until the required moment capacity was achieved. Figure 7.29(c) shows how the stress distributions are broken up into convenient shapes, such as triangles and rectangles, in which the resultant forces and their positions can be easily determined. For example, in the plate element, the stress distribution is broken into two rectangular elements and one triangular element, and the resultant forces from these three stress distributions are shown as F_{p1} to F_{p3} in Fig. 7.29(d).

Having obtained the required moment capacity in the analysis in Fig. 7.29, it is necessary to determine the stress resultants in the plate in Fig. 7.29(e) so that the bolts can be designed to transfer these stress resultants across the plate/beam interface. The sum of the plate forces F_{p1} to F_{p3} is equal to the resultant axial force in both plates P_{plate}, that is both side plates of combined thickness $2t_p$, and the moment of these plate forces about the plate centroid is equal to the moment in both plates M_{plate}.

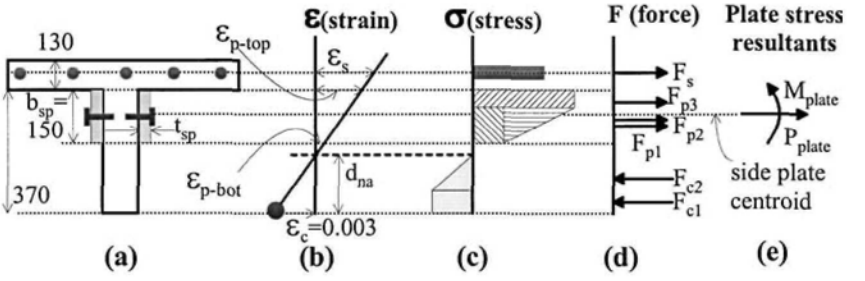

Figure 7.29 Flexural analysis of bolted side plated beams in sagging region

The results of the analyses are shown in Table 7.10. The required plate thicknesses vary from 10 mm for the steel plates to 25 mm for the carbon/glass FRP plate; the multiple 2 in the column for t_p is to remind the reader that in the analysis we are dealing with the combined thickness of plate and, therefore, the remaining values in Table 7.10 refer to a plate of thickness $2t_p$. These plates are much thicker than the 1 mm or 3 mm thick plates typically used in adhesive bonding. They need to be thicker to allow the bolts to bear against the plate to transfer the shear by dowel action and they also need to be thicker in order to resist buckling should the plate be extended into the compression zone which is not the case in this example. The strains in the reinforcing bars, ε_s in Table 7.10, show that they have yielded.

Table 7.10 Results of varying plate material

	t_{sp} mm	ε_s	$\varepsilon_{p\text{-}top}$	$\varepsilon_{p\text{-}bot}$	$(M_{cap})_{fi}$ [kNm]	ΔM_{cap} [kNm]	$(M_{cap})_{pi}$ [kNm]	P_{plate} [kN]	M_{plate} [kNm]
steel	2x10	0.0032	0.0020	0.0000	435	96	421	570	12
alum.	2x20	0.0037	0.0024	0.0002	424	85	411	486	10
FRP	2x25	0.0036	0.0024	0.0002	424	85	411	490	10

The strains at the bottom of the plate, $\varepsilon_{p\text{-}bot}$ in Table 7.10, are almost zero being close to the neutral axis. The strains at the top of the plate, $\varepsilon_{p\text{-}top}$ in Table 7.10, show that the top of the steel and aluminium plates have yielded and that the carbon/glass FRP plate is well below its fracture strain of 0.012. The moment capacities $(M_{cap})_{fi}$ are the moment capacities from the analyses illustrated in Fig. 7.29. This analysis assumes full interaction, that is the strain profile through the plate is the same as that through the RC beam as shown in Fig. 7.29(b). Because bolts require slip to resist shear, there is partial interaction and the true strain profile is illustrated in Fig. 3.33(b). It is recommended in Section 3.4.1.5 that the increase in strength due to plating, ΔM_{cap}, be reduced by 15% to allow for the reduction in strength due to partial interaction and this is shown as $(M_{cap})_{pi}$ in Table 7.10.

(b) Bolt shear connectors

Let us now determine the total shear force that has to be resisted by the bolts for the steel plate in Table 7.10 where P_{plate} = 570 kN and M_{plate} = 12 kNm; these are the stress resultants in both plates, that is the plates on either side of the RC beam as shown in Fig. 7.29(a). The derivation of the bolt shear forces is explained in Section 3.4.1.5 and illustrated Fig. 3.33(a) which is reproduced in Fig. 7.30(a) with the bolt forces for this steel plated example.

Figure 7.30(a) shows the hogging region on both sides of the position of maximum moment. The shear span lengths of 2113 mm were previously derived in Fig. 7.25(a). Because of the theoretically steep moment gradient in the hogging region, the extent of plating theoretically required is only 271mm as shown in Fig. 7.25(c); this is shown once again in Fig. 7.30(a) between the points A. Any length of plate can be chosen just as long as it is longer than 271 mm. For a comparison, the left plate has been chosen as just over 2 m long, with the distance from the position of maximum moment to the furthest bolts, which is the effective length of the plate, being 2 m. The right hand plate has an effective length of 1 m.

From Table 7.10, the axial longitudinal force P_{plate} on one shear span is 570 kN; this is the force in both plates on either side of the RC beam in that shear span. For the left shear span, the lever arm between the vertical transverse forces is 0.7x2 = 1.4 m. From Table 7.10, the moment M_{plate} = 12 kNm, therefore, the transverse force is 12/1.4 = 9 kN. Hence, the total bolt shear force in the left shear span is 570+(2x9) = 588 kN. This is the shear force transmitted by the bolts in both plates in a shear span. Therefore, the shear force per plate is 588/2 = 294 kN. If we assume that the bolt shear connectors have a shear capacity of 20 kN, then the number of bolts required is 294/20 = 14.7. Let us use 2 rows of bolts with 8 bolts per row. Then the longitudinal spacing would be 266 mm and with a transverse spacing of about 75 mm.

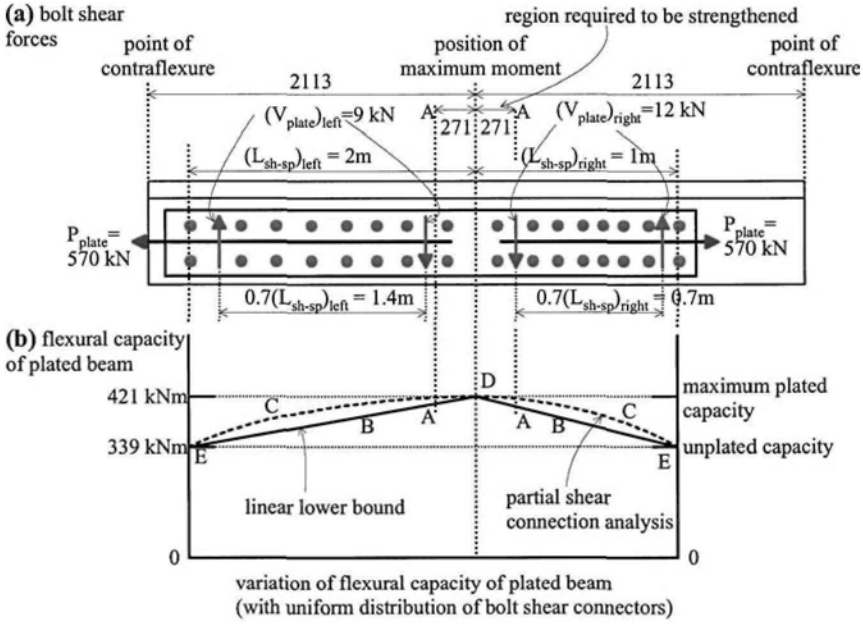

Figure 7.30 Dowel forces on bolt shear connectors

For the right hand shear span in Fig. 7.30, the total shear force is 570+(2x12/0.7) = 604 kN. This will require 604/2/20 = 15.1 bolts. Hence two rows of 8 bolts with a longitudinal spacing of 133mm. The total number of bolts required is 64. In this example, the transverse forces are relatively small compared with the longitudinal forces because the depth of the plate is quite shallow. This is not always

the case, as deeper plates can actually reduce the longitudinal force and attract more moment and hence increase the transverse force.

(c) Variation in flexural capacity

At the position of maximum moment, the moment capacity is that of the plated beam of 421 kNm from Table 7.10, which is shown as point D in Fig. 7.30. At the plate ends at point E, the moment capacity is that of the unplated beam of 339 kNm. Between these extremities, the moment capacity varies such as shown by the curves marked C. To determine the variation in curves C, partial shear connection theory has to be applied (Oehlers and Bradford 1995, 1999). However, a lower bound to the moment capacity is given by the linear variations marked B which can be used in design, just as long as there is a uniform distribution of the bolt shear connectors as shown in Fig. 7.30(a), otherwise, partial shear connection theory will have to be applied. It can be seen in Fig. 7.30(b) that extending the plates beyond the theoretical requirement of 271 mm given by the points A-A has ensured that the moment capacity at point A on curve B is greater than that required of 339 kNm.

7.5.3 Option 13: Deep side plates bolted in hogging region

In Option 12 in Section 7.5.2, shallow plates were used to strengthen the beam as this ensured that the plates remained in the tensile zone and, hence, buckling did not have to be considered. We will now plate the whole web, so that part of the plate goes into compression in order to illustrate the effect on the bolt shear connectors. We will ignore buckling although research has been published to position the bolts so that the plate does not buckle (Smith, Bradford and Oehlers 1999, 2000).

(a) Maximum flexural capacity

The flexural analysis is similar to that described in Section 7.5.2, the difference being that the side plates now extend to the compression face of the beam and hence, the compressive stresses in the plate must be considered as shown in Fig. 3.44. The flexural analysis has already been described in Section 3.5.3.1 and summarised in Table 3.5 and is not repeated here.

Comparing the full interaction results of the steel side plated beams in Tables 3.5 and 7.10, the 150 mm deep plate increased the moment capacity by 28%, whereas the 370 mm deep steel side plate increased the moment capacity by 59%. Furthermore, the curvature at failure for the 150 mm deep plate is $1.3\text{x}10^{-5}$ mm^{-1}, compared to $1.8\text{x}10^{-5}$ mm^{-1} for the 370 mm plate. Hence, the full depth steel plate is more effective in increasing the moment capacity of the beam and also improves the ductility.

It may be expected that the moment in the plates M_{plate} is bigger in the 370 mm deep side plates (190 kNm in Table 3.5) compared to that of the 150 mm deep plates (12 kNm in Table 7.10) because the moment capacity is bigger. However, it is interesting to note that the axial force in the plates P_{plate} is considerably less with the 370 mm deep side plates (220 kN in Table 3.5), because the resultant axial tensile and compressive forces in the plate (Fig. 3.44) tend to cancel each other out, compared with the 150 mm deep side plates (570 kN in Table 7.10). The influence this has on the number of bolt shear connectors required is described in the following section for the steel plated beam.

(b) Bolt shear connectors

From Table 3.5 for the 370 mm deep steel side plate, M_{plate} = 190 kNm and P_{plate} = 220 kN. For the sake of comparing the number of bolt shear connectors required with the 150 mm deep steel side plate, the same extent of plating shown in Fig. 7.30 will be used; that is, 2 m in the left shear span and 1 m in the right shear span.

The lever arm between vertical transverse forces in the left shear span is 1.4 m as shown in Fig. 7.29 and therefore, the transverse force is 190/1.4 = 136 kN. Hence, the total bolt shear force per plate in the left shear span is (220/2) + (2x136/2) = 246 kN. As in Section 7.5.2(b), a bolt shear connector shear capacity of 20 kN is assumed and therefore, the number of bolts required is 246/20 = 12.3. Hence, for strength requirements, 2 rows of 7 bolts per row are required, which is two bolts less than that required for the 150 mm deep plate in the left shear span.

Comparing with the right shear span, the total bolt shear force per plate is (220/2) + (2x190/0.7/2) = 381 kN. The total number of bolts required in the right shear span is 381/20 = 19.1, which can be arranged in 2 rows of 10 bolts per row, four more than that required for the right shear span of the 150 mm deep plate.

In summary, the total number of bolt shear connectors required in each arrangement is similar, with 68 for the 370 mm deep steel plates and 64 for the 150 mm deep steel plates, even though the moment capacity is increased significantly more using the 370 mm deep steel plate. Because the 370 mm deep steel plate extends into the compression region of the beam, the spacing of the bolts must also be designed to prevent buckling of the plate.

7.6 References

Ochlers, D. J. and Bradford, M. A. (1995)."Composite Steel and Concrete Structural Members: Fundamental Behaviour." Pergamon Press, Oxford.

Oehlers, D.J. and Bradford, M.A. (1999) "Elementary behaviour of Composite Steel and Concrete Structural Members". Butterworth Heinemann, Oxford, September.

Smith, S.T., Bradford, M.A. and Oehlers, D.J. (1999) "Local buckling of side-plated reinforced concrete beams. Part 1: Theoretical study. ASCE Structural division, Journal of Structural Engineering, June. 622-634.

Smith, S.T., Bradford M.A. and Oehlers, D.J. (2000) "Unilateral buckling of elastically restrained rectangular mild steel plates". Journal of Computational Mechanics, Vol.26, No.4, 317-324.

Index